Improving the Spatial Resolution of the Contour Method

Thesis

The Open University

Faculty of Mathematics, Computing & Technology

Department of Engineering and Innovation

Improving the spatial resolution of the contour method

by

Nida Naveed

2015

A THESIS SUMMITTED TO THE DEPARTMENT OF ENGINEERING AND INNOVATION OF THE OPEN UNIVERSITY UNITED KINGDOM FOR THE DEGREE OF DOCTOR OF PHILOSOPHY

DATE OF SUBMISSION : 25 AUGUST 2015
DATE OF AWARD : 28 JANUARY 2016

ProQuest LLC.
789 East Eisenhower Parkway
P.O. Box 1346
Ann Arbor, MI 48106 – 1346

Abstract

The contour method involves precise cutting of a body into two halves and provides a measured cross-sectional map of the residual stress acting normal to the cut surface. The method is being increasingly used to measure the residual stress field in critical engineering components that have high structural integrity requirements. Therefore, it is of paramount importance to improve the precision and accuracy of the method. The results of the method are critically affected by the cutting process, the deformation contour measurement accuracy and the data analysis procedure. The aim of the present thesis is to improve the reliability and accuracy of contour residual stress measurements by minimising errors and uncertainties that can be introduced during the cutting and data analysis steps of the technique.

The first part of this thesis covers the design of a test specimen to benchmark the quality of cutting for contour method measurement. The design allows sequential trial cuts on a nominally stress-free specimen. Two different materials have been tested: a high yield strength mild steel (EN3B) and an austenitic stainless steel (304L). An accompanying characterisation record sheet for each trial cut has been devised to quantify the cut surface quality and features. The most important parameters that can be used to demonstrate the quality of the contour cut have also been identified in order to help optimise the cutting process.

The second part of the thesis covers an investigation of important parameters that are used for contour stress measurements including surface deformation data collection spacing, deformation data smoothing and finite element mesh size. A simple approach for choosing initial parameters is developed based on an idealised cosine displacement function (giving a self-equilibrated one-dimensional residual stress profile). Guidelines are proposed to help the measurer select the most suitable choice of these parameters based on the estimated wavelength of the residual stress field. The outcomes of this research have successfully been applied to improve the spatial resolution and detailed characterisation of the residual stress field in three welded components.

Acknowledgement

I am greatly thankful to almighty Allah. He gave me the strength and power to make my dream come true and give me the opportunity to contribute a little in the vast field of residual stress research work.

I am truly and deeply thankful to my supervisors, Prof. John Bouchard and Dr. Jan Kowal for their valuable guidance, advice and support. I am particularly thankful to Dr. Foroogh Hosseinzadeh, who gave me great help, good advice and support during my research work.

I would like to thank to The Open University, Rolls Royce and the East Midlands Development Agency (EMDA) for financial support and for giving me the grant for this research.

I would like to thank Peter Ledgard for his high-skill workshop assistance, Stan Hiller and Gordon Imlach for their support and guidance to perform the experiments. I would like to thank all my friends, colleagues and all the Open University supporting staff. Also special thanks to Dr. Yeli Traore for his kind help during the work.

In the end, I am very gratefully thankful to my lovely parents Mr. and Mrs. Naseem Uddin, and my brothers and sisters, they always supported me in great ways. I am deeply thankful to my dearest husband Dr. Muhammad Naveed Anwar for his love, encouragement and his trust on my every decision. I am thankful to my sons (Faheel and Ahmed), they gave me remarkable strength to achieve my goals.

Preface

This thesis is submitted for the degree of Doctor of Philosophy of the Open University, United Kingdom. The work described in this thesis was performed in the Department of Engineering and Innovation, Faculty of Mathematics, Computing and Technology, between March 2011 and August 2015 under the supervision of Prof. Peter John Bouchard, Dr. Jan Kowal and Dr. Foroogh Hosseinzadeh.

It is entirely the author's own work except where clearly referenced. No portion of the work referred to in this thesis has been submitted in support of an application for another degree or qualification in this or any other university. Some of the results related of this work have been published in conference proceedings and as oral or poster presentation as listed below:

Conference paper

Naveed N, Hosseinzadeh F, Kowal J. Residual Stress Measurement in a Stainless Steel Clad Ferritic Plate Using the Contour Method. In: ASME 2013 Pressure Vessels and Piping Conference - Materials and Fabrication. Paris, France: American Society of Mechanical Engineers; 2013. p. V005T11A006.

Departmental reports

Naveed N. Measurement of residual stresses in electron beam welded ferritic plates using the contour method. The Open University, Milton Keynes, UK; 2012. Report No.: OU/MatsEng/029, Issue 1.

Hosseinzadeh F, **Naveed N**. Residual stress measurement in three pass groove welded plate using the contour method. The Open University, Milton Keynes, UK; 2013. Report No.: OU/MatsEng/042, Issue 1.

Naveed N. DMW-Creep: Residual stress measurement on a thin dissimilar metal electron beam welded plate using the contour method. The Open University, Milton Keynes, UK; 2014. Report No.: OU/MatsEng/065, Issue 1.

Posters

Naveed N. Optimisation of the contour method for measuring residual stresses. 2012; The Open University, Milton Keynes, UK.

Naveed N. Contour measurement on a three pass groove welded plate. 2012; The Open University, Milton Keynes, UK.

Naveed N. Improving the spatial resolution of the contour method for residual stress measurement. 2014; The Open University, Milton Keynes, UK.

Chapter 1 : Introduction

Residual stresses or locked–in stresses can be defined as those stresses existing in the body of material in the absence of any external loads (1,2). Basically any in-homogeneous plastic deformation caused by mechanical and thermal loading is the fundamental mechanism for the formation of residual stresses (3). Residual stresses develop in almost all fabrication and manufacturing processes. They can also originate as a result of in-service loading of manufactured components (4,5). The residual stresses are self-equilibrating throughout the volume of the material and have portions of non-uniform compressive and tensile stresses with zero force resultant. In some cases they possess considerably high magnitude with large stress gradients (6) that can have significant harmful effects on material durability. These effects include promoting, initiation and propagation of fatigue and stress corrosion cracking (7,8). Residual stresses can also result in premature failure when combined with service life loads (9). Stresses due to externally applied load can be easily calculated with a high degree of accuracy, but residual stresses cannot be accurately predicted by a simplified approach.

Welding is a thermo-mechanical process that generates high magnitude of residual stresses in engineering components (10–12). Advance welding techniques such as high energy density electron beam or laser welding (13) and over-lay cladding (14) are candidate fabrication methods for critical applications such as nuclear power plants. High energy density weld (HEDW) processes such

as electron beam welding (EB) is capable of providing high power density weld input levels with high penetration into a component (13). It produces a deep, narrow and parallel sided fusion zone with small thermal contraction (shrinkage) of the weld metal compared to conventional welding processes (15,16). However, these advanced welding techniques also have some major challenges. These challenges include short-length scale residual stress variations of high magnitude associated with the narrow fusion zone and sharp gradients arising from phase transformation effects that are difficult to measure and locate (14,17,18). High concentrated tensile stress regions can challenge the structural integrity of engineering components and have adverse effects on their performance.

It is important to obtain authentic and detailed configuration of these stresses for structural integrity assessments of engineering components. For nuclear and aerospace applications, residual stress predictions for advance welding procedures need to be validated using an appropriate measurement technique (9,19,20). The measurement technique used must be sufficiently refined to capture the stress field length scales of interest (21,22); that is the spatial resolution of the measurement volume and measurement density must be considered. Thus, it is important to have a good understanding about the capabilities of different measurement techniques.

There is a wide range of techniques available for the measurement of residual stress. These methodologies are broadly categorised as destructive, semi-destructive or non-destructive (4,5). Non-destructive techniques such as X-ray diffraction has limited penetration depth and is restricted to the surface and near-

surface measurement of residual stress (8). The neutron diffraction technique can measure the elastic strain associated with residual stresses for depths up to about 25 mm in steel with a spatial resolution of less than one mm (23). This technique can provide a full three dimensional map of the residual stress field throughout the volume of the component (24,25). However, the application of this technique has some additional limitations such as it is not suitable for surface measurements, it has limited penetration depth (26), it is sensitive to the material grain size and texture, its difficult to determine reliable stress free lattice parameter reference measurements (27) and its difficult to access a neutron source. Semi-destructive and destructive techniques, such as deep hole-drilling, layer removal, sectioning, slitting and the contour method are often used to measure type I residual stresses (continuum long-range). Destructive techniques are capable of measuring through-thickness residual stresses but most can only provide a one dimensional spatial profile of residual stresses. The incremental centre hole drilling method has a capability to provide near surface measurements up to the depth of about 1 mm, and measures the line distribution of uniaxial or biaxial in-plane direct stress components but does not provide any information for the stress component normal to the surface (28). The deep hole drilling technique provides three in-plane stress components (two direct and one shear) throughout the thickness of the component along the line (29,30). However, the spatial resolution of deep hole drilling is limited by the diameter of the trepanned core (31) and a minimum 5 mm trepanned diameter has been reported to be used (32). Other traditional relaxation techniques such as layer removal and slitting (crack compliance), commonly give a depth profile and provide a single component of stress.

Thus, there are limitations and advantages associated with each of the techniques, and they can only provide restricted information for some component of the residual stress tensor with limited spatial resolution. The contour method is a promising technique for the measurement of residual stresses in engineering components (33,34). The contour method is based on cutting the test component into two halves. The cut surfaces deform, owing to the relaxation of residual stresses. The deformation of the cut surfaces is measured and used to back calculate the two-dimensional map of original residual stresses acting normal to the plane of the cut (33). Earlier, this method used to provide only one stress component normal to the plane of the cut. Now, the capabilities of this method have been extended to measure multiple stress components by applying multiple cuts (35,36) and by combining with surface residual stress measurement techniques (37).

There are several assumptions associated with the contour method which may be violated during the implementation of the method and cause errors and uncertainty in the stress measurements (38,39). This research is particularly focused on improving the reliability and accuracy of residual stress results for the contour method by minimising errors and uncertainties that can be introduced during cutting and data analysis procedures. The outcomes of this research have successfully been applied to achieve precise and detailed characterisation of the residual stress field in two electron beam welded plates and in an over-lay clad plate.

1.1 Outline of the thesis

The outline of the thesis is as follows:

Chapter 2 comprises two parts. The first part of the chapter covers the underlying concept of residual stresses, and their origin and types. It also gives a review of various residual stress measurement techniques, which includes theory, limitations, advantages and disadvantages. The second part of the chapter provides a detailed literature review of the contour measurement method as this is the main focus of the thesis. It describes the principles, recent developments, and implementation steps of the method. At the end of this literature review chapter, section 2.11 describes the research 'needs and gaps' in the field. The aims of the present research are then defined, and the methodology to achieve these aims and objectives is explained.

Chapter 3 covers the design of a quality of cut benchmark specimen and provides experimental details for a programme of trial cuts that were conducted during this research. The chapter also presents the characterisation results sheets for each trial cut and assesses the study outcomes.

Chapter 4 investigates the important parameters for the contour method such as pitch of deformation measurement, data smoothing and finite element mesh size that have sufficient effects on contour measurement. At the end of this chapter, on the basis of the investigations, guidelines are proposed to select the most suitable choice of data analysis parameters.

Chapter 5 presents experimental residual stress measurements that implement the criteria proposed in chapters 3 and 4. The examples include residual stress measurement in two electron beam welded plates and a stainless steel clad ferritic plate, where short length scale fluctuations owing to phase transformation are expected to be present.

Chapter 6 covers discussions on the outcomes of this research. This chapter also presents the conclusions of the thesis followed by recommendations for future work.

Chapter 2 : Literature review

2.1 Introduction

The aim of this research is to improve the reliability and accuracy of residual stress measurements made by the contour method by minimising errors and uncertainties that can be introduced during the cutting and data analysis steps of the technique.

Residual stresses are introduced during the fabrication of almost all engineering components and structures (1,2), including critical engineering structures, for example reactor pressure vessels. The residual stresses interact with service loading and can promote degradation mechanisms, such as encouraging surface crack growth, increasing the rate of change of fatigue damage, stress corrosion, and under weld cracking (3). Therefore, reliable knowledge of residual stress measurement techniques is essential in order to provide reliable structural stability assessment of engineering structures, in particular for safety critical applications (19,40).

There is a wide range of techniques available for the measurement of residual stresses (41). These are broadly categorised as destructive, semi destructive and non-destructive (4,5). The contour method is a recently developed destructive technique (33). The method offers several advantages but in common with every other residual stress measuring technique, it also suffers from factors that affect its

accuracy and limit its spatial resolution. By recognising and addressing these factors, the contour results can be improved for a given specimen.

The beginning of this chapter presents a literature review on the nature, origin and types of residual stresses. Commonly used residual stress measurement techniques are explained together with their advantages and disadvantages. Particularly, the contour method is discussed extensively as this technique is the main focus of this research. This review is intended to provide an overview of the contour method, including theory, assumptions and experimental procedures. Further, it explores possible sources of errors and uncertainties in residual stress measurements using the contour method, particularly those related to the cutting and data analysis steps. This chapter also identifies the research gaps in the area of the contour method that are explored in this research. At the end of the chapter, the aims of the research and the methodology to achieve the objectives are discussed.

2.2 Residual stresses

Residual stresses arise from a misfit between different regions in a component following the removal of external loading, in the absence of thermal gradients, when the piece is stationary and in equilibrium with its surroundings (7,8). Residual stresses are generated by incompatible internal permanent strains, or non-uniform plastic flow (2). The mechanisms for creating residual stresses include; non-uniform plastic deformation, surface modifications (occurring either during manufacture or in service, for example by corrosion) and material phase, or

density, changes (4,23). Residual stresses can be introduced by mechanical, chemical and thermal processes. They can also be present in unprocessed raw materials and or result from in-service loading. Mechanical processes that can cause residual stresses include machining, drawing, extruding, shot peening, forging and bending (3). Chemical processes such as nitriding and carbonitriding introduce high compressive stresses in the treated region of a component. These processes can improve fatigue resistance properties and impact strength (42). However, they may increase brittleness within the treated layer (43). Thermal processes such as casting, welding and heat treatment involve large temperature variations and are major contributors to residual stress. Therefore it can be stated that, in the absence of a final annealing process, all materials used in manufactured components contain residual stresses.

The detrimental effects that residual stresses can have on the performance and life of engineering structures (9) are due to the fact that in some circumstances, they add to the duty loads applied to a material or component leading to early failure. As in the case of compressive residual stresses introduced by certain surface treatments, the effects can be beneficial. Whether the effect is beneficial or detrimental depends on the type (tensile or compressive), the magnitude and the distribution of stress, with respect to the applied load. Tensile residual stresses can have a detrimental effect on a material's structural integrity and strength (44). Examples include a reduced resistance to corrosion, an increased rate of creep damage, a higher rate of fatigue damage, a reduced load carrying capacity, more likelihood of internal failure, and a lower resistance to fracture

processes. On the other hand, compressive residual stresses can have positive effects, such as delaying failure and enhancing the fatigue resistance of structures. However, if the external loading is highly compressive, then compressive residual stresses would result in the material yielding under compression. For example, in the case of buckling, compressive residual stresses could reduce the load carrying capacity (12,44). Residual stresses have to be taken into account when assessing the integrity of engineering structures, especially for safety critical applications.

In the following section, the types of residual stress are described. Residual stresses can be categorised into three main groups according to the length scale of the factor that has caused them.

2.3 Types of residual stresses

Residual stresses are classified according to their origin or cause, according to the scale over which they self-equilibrate (3), and according to the measurement techniques by which they can be quantified (8,41). Residual stresses are classified into three categories:

(I) Macro residual stress (large scale)

(II) Micro residual stress (grain scale)

(III) Atomic scale.

In general, macroscopic residual stresses are developed over large distances, vary over several material grains, and extend to length scales in the order of

millimetres, or even centimetres and metres. The other two types of residual stresses arise over microscopic or atomic length scales in a material (2). For the assessment of structural integrity, detailed investigation of the macro residual stresses is necessary, because it is these stresses that have the greatest effect on structural durability (4). Therefore, in this work, particular focus is on the exploration of macro residual stresses.

Several different measurement techniques are available for characterising residual stresses in fabricated components. These techniques can be categorized into three groups: non-destructive, semi destructive and destructive (4,5). In the following section deep-hole drilling, neutron diffraction and X-ray diffraction techniques are chosen for detailed review because they are used in the present research for comparison with contour results.

2.4 Residual stress measurement techniques

Reliable prediction of residual stresses in engineering structures is not a trivial task, due to the inherent complexity of manufacturing processes such as welding. It is therefore necessary to validate such predictions with experimental data. It follows that it is essential to use reliable residual measurement techniques (20,45). There is a wide range of techniques available for residual stresses measurement in metals (41). *Figure 2-1* summarises the capabilities of various techniques in terms of their penetration depth and spatial resolution.

Destructive and semi-destructive techniques (46) are based on material removal, and the fact that stresses are partially relaxed at the location of the

created free surfaces. All destructive techniques are based on a common assumption that as the result of material removal all the internal stresses are relaxed elastically (47). This local stress relaxation results in redistribution of stresses in the immediate surrounding region. The strain or deformation caused by this relaxation of residual stresses is measured, thus providing the information that is used to back calculate the value of the original undisturbed distribution of residual stresses (5). These techniques can provide measurement of through thickness residual stresses in thick components. The most commonly used destructive and semi-destructive residual stress measurement techniques include incremental hole-drilling, deep-hole drilling, slitting, the ring core method, layer removal and the contour method.

Non-destructive techniques are based on measuring some of the properties related to stress, such as polarisation (photoelastic measurements), magnetostriction and Barkhausen noise (magnetic methods) (48), or the speed of sound (ultrasound) (49). The great advantage of using a non-destructive technique (50,51) is that it does not disturb the geometry of the component, so after measurements have been taken, the component can be re-used in service or could be used for material characterisation, or perhaps for further residual stress measurements using other techniques. Most of the non-destructive techniques are constrained to the measurement of surface and sub-surface residual stresses (see *Figure 2-1*). Diffraction is the most widely used non-destructive method, often used for measuring residual stresses in polycrystalline and fine grained materials (26). The commonly used non-destructive diffraction techniques include X-ray

diffraction, synchrotron diffraction and neutron diffraction. One of the disadvantages of these techniques is the restriction on the depth at which they can measure residual stresses. X-ray diffraction has a penetration depth of less than 30 µm in steel (23). The neutron diffraction technique can measure the elastic strain associated with residual stresses for depths up to about 25 mm in steel with a spatial resolution better than one millimetre (23).

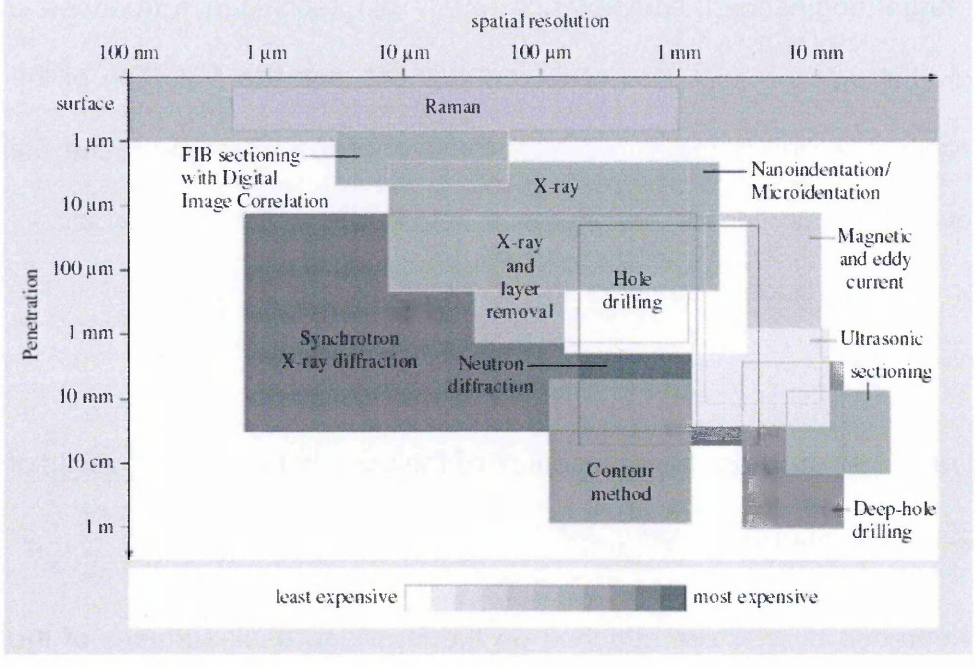

Figure 2-1: Represents the capabilities of various methods to measure residual stress deep into the specimen (penetration) vs. spatial resolution (23).

The choice of residual stress measurement method depends on various parameters. These parameters include; the type of residual stresses (macro stresses or micro stresses), the number of stress components to be measured, the length-scale of the residual stress distribution, the geometry of the part, the type of intervention (destructive or non-destructive), as well as time and cost factors (52).

Each residual stress measurement technique has its own advantages and disadvantages (23,53).

2.4.1 Deep hole-drilling method

The deep hole drilling method is a semi destructive mechanical strain relief technique (54) and that is capable of measuring through thickness residual stresses in large engineering components (30). This technique introduces a reference hole through the thickness of the component, and the distortion of the hole in the radial direction is measured after removal of the material around the reference hole. The distortion of the reference hole in the radial direction allows determination of the residual stresses in the plane normal to the axis of the reference hole.

The residual stress measurement procedure of the deep hole-drilling consists of four steps (55,56), as shown in *Figure 2-2*

- Two reference bushes are attached on the front and back surfaces of the component to avoid drill bell-mouthing and provide stress-free references.
- Then, a small reference hole is drilled through the sample using a gun drill where stresses are to be determined. Typically a nominal 3.175 mm diameter hole is drilled.
- This is followed by accurate measurement of the hole diameter. The diameter measurement is taken at different angular positions around the reference hole and equal intervals along the hole axis using an air probe system.

- In this step, a core of material coaxial to the reference hole is trepanned using an electric discharge machine. A typical core diameter is about 10 mm. Trepanning the column containing the reference hole releases residual stresses.
- Finally, the reference hole diameter is re-measured at the same angular positions and depths.

The change in diameter of the reference hole before and after trepanning is used to determine the radial distortion of the hole. Then, the residual stresses are obtained along the axis of the reference hole drilled through the component using the radial distortion of the hole (57). Commonly, three different reference hole diameters (i.e. 1.5mm, 3mm and 5mm) are used. The choice of reference diameter is depended upon the geometry of the component and the expected residual stress profile. The core diameter is selected on the basis of the diameter of the reference hole. For a 1.5 mm diameter reference hole a 5 mm diameter core is extracted, for a 3 mm reference hole a 10 mm core is extracted and for a 5 mm reference hole a 17 mm core is extracted (58). The spatial resolution of deep hole drilling is limited by the diameter of the trepanned core (31) and a minimum of 5 mm trepanned diameter has been reported to be used (29,59).

This technique provides a one dimensional profile of three in-plane (two direct and one shear) residual stress components (29,30). This technique can measure residual stresses up to a depth of 750 mm and it is suitable for laboratory or 'on-site' measurements (57,59). It can be applied to a wide range of materials, both metallic and non-metallic, and is applicable to both simple and complex

components (60,61). However, it is not applicable to components of less than 6 mm thickness (30,58).

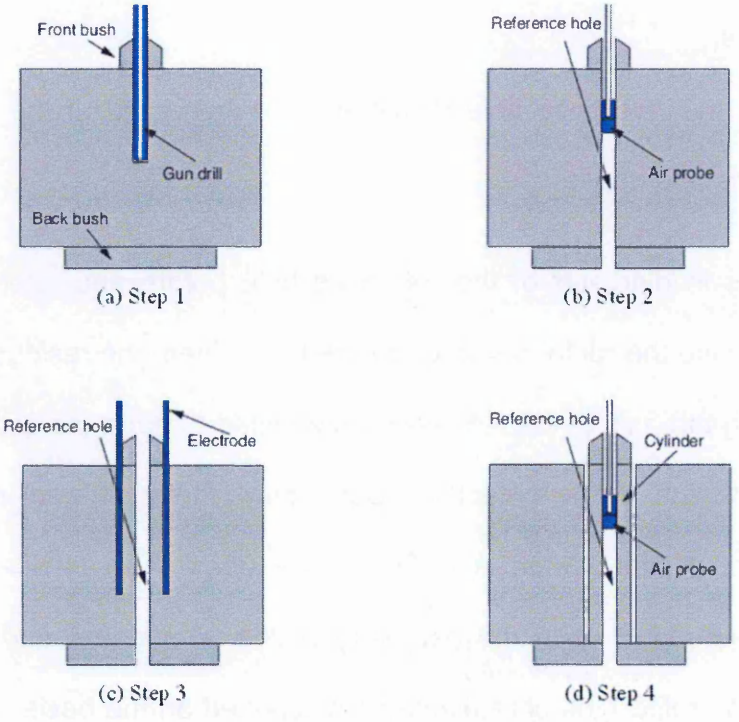

Figure 2-2: Schematic representation of the deep hole drilling technique (59)

The deep hole drilling technique is based on the assumption of elastic relaxation. However, plastic relaxation occurs during trepanning, when the technique is applied to measure large residual stresses (> 60 % of yield strength) (58). In order to avoid plasticity, trepanning is carried out in two steps. First, remove one cylinder (i.e. core) of material containing the same reference hole along its axis. It allows the partial stresses to relax elastically away from the yield surface. Then, a required core diameter can be removed containing the reference hole along its axis. The difference between the diameters before core extraction

and after core extraction allows calculating the initial residual stresses; details of the procedure are given in (61,62). As well as, the application of the technique also involves many uncertainties such as uncertainty associated with use of air probe for measurement of diameter, uncertainty related to the positioning the air-probe and uncertainty in material constants. All these uncertainties and its related errors, have been discussed in detail in (57).

2.4.2 Neutron diffraction technique

The neutron diffraction technique is based on Bragg's law (see *Figure 2-3*) that relates the atomic lattice spacing for crystallographic planes to a particular diffraction angle at which the peaks from these planes are observed (41,63). It can detect changes in the spacing of the lattice planes as a result of elastic deformations due to stress within polycrystalline material (26,63). The Bragg relationship, equation Eq 2-1, can be generalised to apply to multiple different crystal planes.

$$n\lambda = 2d_{hkl}sin\theta_{hkl} \qquad \text{Eq 2-1}$$

Where, the letter in subscripts h, k and l are the Miller indices that define the crystallographic planes. For example, {311} indicates the crystallographic planes, Miller's indices are h = 3, k = 1 and l = 1. θ_{hkl} represents the Bragg scattering angle, d_{hkl}indicates the atomic spacing, n is a positive interger, λ indicates the radiation wavelengths.

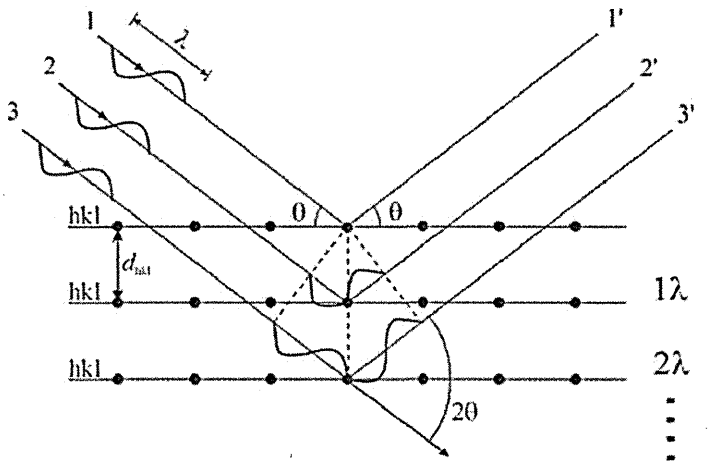

Figure 2-3: Illustration of Bragg's law for diffraction techniques (63).

Residual stresses are measured using the neutron diffraction technique by performing a lattice parameter measurement for a sample of stress-free material identical to that of the specimen being measured, measurement of the stressed material of the specimen, followed by data analysis for diffraction peak fitting and strain-stress calculations (64).

Stress free lattice parameter measurement

The accuracy of the neutron diffraction residual strain calculations is highly dependent on the accuracy of the stress-free lattice parameter, d_0. The stress free lattice parameter can be affected by changes in material composition and inter-granular strains (27). Highly accurate stress-free lattice parameters can be estimated using diffraction techniques (63,65) such as far-field (stress free) measurements, measurement on a stress-free powder or filing, cutting stress-free

cubes or combs from the test specimen studied and by applying a force/moment balance approach.

Lattice parameter and strain determination

The lattice parameter (d-spacing) can be determined by two diffraction methods, monochromatic 2θ strain scanning and time of flight (58). The choice of application of the diffraction method depends upon the diffraction instrument's neutron source. Currently, there are two types of neutron sources available for residual strain measurements; one is a spallation target and the other is a nuclear reactor (63,66). A spallation source produces an intense pulsed neutron beam, where each pulse contains neutrons with a wide range of wavelengths. A nuclear fission reactor provides a continuous source of neutrons, where a monochromator ensures that they are all within a narrow wavelength range (63,65).

The presence of residual stress in a sample causes a shift in the diffraction peak relative to that in a stress free sample. Lattice spacing can be determined by analysing the shifts in diffraction peaks and then strain can be calculated by using Eq 2-2.

$$\varepsilon = \frac{d_{hkl} - d_{0hkl}}{d_{ohkl}} = \frac{\Delta d_{hkl}}{d_{0hkl}} = \frac{sin\,\theta_{0hkl}}{sin\,\theta_{hkl}} \qquad \text{Eq 2-2}$$

Where, Δd_{hkl} is the change in lattice spacing, d_{0hkl} is a stress free lattice spacing and θ_{0hkl} is the angle at which the Bragg peak is observed from the stress free reference.

The time of flight approach for residual strain measurements is used for diffraction measurements at a spallation neutron source (63,65). It works on fundamentally the same principle as monochromatic strain scanning. In this approach, each measurement point provides information relative to the complete or partial diffraction spectrum. Then, measurement data can be analysed using multiple peak fitting by applying a profile refinement method (67).

Residual stress calculation

Once residual strains have been obtained by applying either type of the neutron diffraction method they can be converted into residual stresses. The classical Hooke's law (see Eq 2-3) and the material's diffraction elastic constants such as bulk Young's modulus and Poisson's ratio of isotropic materials can be used to determine the stresses from the strain (63).

$$\sigma_{xx}=\frac{E}{(1+v)(1-2v)}[(1-v)\varepsilon_{xx}+v(\varepsilon_{yy}+\varepsilon_{zz})]$$

$$\sigma_{yy}=\frac{E}{(1+v)(1-2v)}[(1-v)\varepsilon_{yy}+v(\varepsilon_{xx}+\varepsilon_{zz})]$$

$$\sigma_{zz}=\frac{E}{(1+v)(1-2v)}[(1-v)\varepsilon_{zz}+v(\varepsilon_{xx}+\varepsilon_{yy})] \quad \text{Eq 2-3}$$

Where, σ_{xx} represents the stress in its relevant direction, E is the crystallographic Young's modulus and v is Poisson's ratio for the material.

The neutron diffraction technique can measure the elastic strain associated with residual stresses for a depth up to 25 mm in steel with a spatial resolution of better

than one mm (23). This technique can provide a full three dimensional map of the residual stress field throughout the volume of the component (24,25). However, the application of this technique has some additional limitations such as: it is not suitable for surface measurements; it has limited penetration depth (26); it is sensitive to the material grain size and texture; it is difficult to determine reliable stress free lattice parameter reference measurements (27), and it is difficult (and expensive) to gain access to a neutron source.

2.4.3 X-ray diffraction method

The X-ray diffraction technique is commonly used for measuring residual stresses non-destructively. It is based on the principle that the crystalline lattice can be used like an atomic strain gauge. Based on Bragg's law and continuum mechanics using Hooke's law, residual stresses are derived from measuring changes in lattice spacing due to elastic strains (68). Equation 2-1 expresses Bragg's law. According to this the diffracted beam and the incident beam are symmetrical in relation to the lattice plane. Crystallographic planes are as shown in *Figure 2-3.*

By differentiating Bragg's equation:

$$\Delta\theta = -\frac{\Delta d}{do} tan\theta_0 \qquad \text{Eq 2-4}$$

Where $\Delta\theta$ is the change in the Bragg scattering angle, Δd is the change in the lattice plane spacing θo is the Bragg scattering angle and do is the lattice plane spacing.

$sin^2\psi$ Technique

X-ray diffraction measures stresses at the surface or near the surface (< 30 μm) (23). In order to measure the surface stress using X-ray diffraction a plane-stress condition is assumed to exist in the diffraction surface layer. The stress distribution is then described by principal stresses σ_{11} and σ_{22} in the plane of the surface and σ_{33} normal stress and shear stresses acting out of the plane of the surface are equal to zero (69), as shown in *Figure 2-4*. The strain component perpendicular to the surface, ε_{33}, exists as a result of Poisson's ratio contractions caused by the principal stresses. The strain in the sample surface at an angle ϕ from the principal stress σ_{11} is given by Eq 2-5:

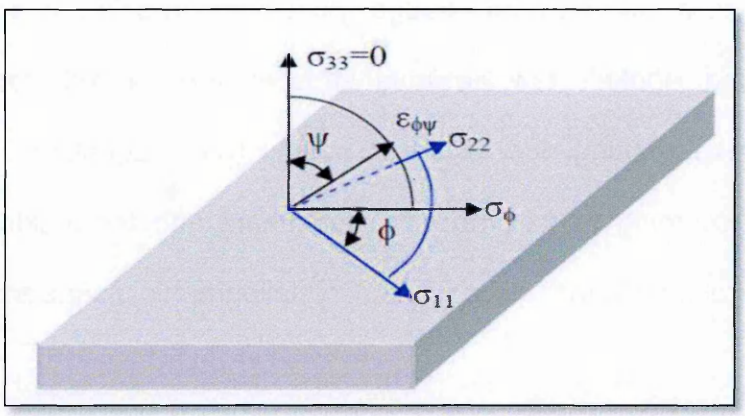

Figure 2-4: Schematic showing diffraction planes parallel to the surface and at an angle φ. Note σ_{11} and σ_{22} are both lie in the plane of the specimen surface (69).

$$\varepsilon_{\phi\psi} = \left(\frac{1+\upsilon}{E}\right)\sigma_{\phi}sin^2\psi - \left(\frac{\upsilon}{E}\right)(\sigma_{11} + \sigma_{22}) \qquad \text{Eq 2-5}$$

σ_ϕ is the surface stress in any direction defined by the angle ϕ, to the strain, $\varepsilon_{\phi\psi}$ in the direction of (ϕ,ψ) and the principal stresses in the surface. If $d_{\phi\psi}$ is the spacing between the lattice planes measured in the direction define by of ϕ and ψ, the strain can be expressed in term of changes in the spacing of the crystal lattice in Eq 2-6:

$$\varepsilon_{\phi\psi} = \frac{\Delta d}{do} = \frac{d_{\phi\psi} - do}{do} \qquad \text{Eq 2-6}$$

Where do is the stress free lattice spacing. Combining Eq 2-5 and Eq 2-6 and solving for $d_{\phi\psi}$:

$$d_{\phi\psi} = \left[\left(\frac{1+\upsilon}{E}\right)\sigma_\phi\, d_o\right] sin^2\psi - \left(\frac{\upsilon}{E}\right) d_o(\sigma_{11} + \sigma_{22}) + d_0 \qquad \text{Eq 2-7}$$

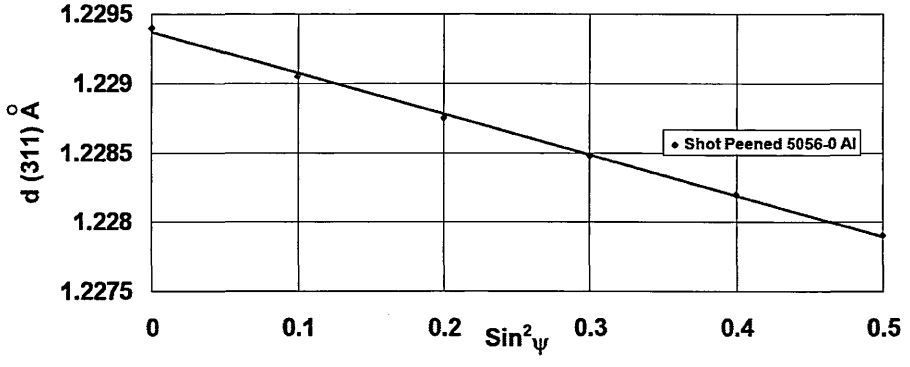

Figure 2-5: Example of a d vs. $sin^2\psi$ (Linear dependence of d (311) upon $sin^2\psi$ for shot peened 5056-0 aluminium) (69).

Eq 2-7 shows the relationship between lattice spacing and the biaxial stresses in the surface of the sample. The lattice spacing $d_{\phi\psi}$ is the linear function of $sin^2\psi$. Linear variation between d(311) with $sin^2\psi$ is shown in *Figure 2-5*, for the range of

ψ from 0 to 45° for shot peened 5056-O aluminium having a surface stress of -145MPa (69).

In the plot shown in *Figure 2-5* at $sin^2\psi = 0$ equals the unstressed lattice spacing, d_0 minus the Poisson's ratio contraction caused by the sum of the principal stresses:

$$d_{\phi 0} = d_o[1 - \left(\frac{\upsilon}{E}\right) d_o(\sigma_{11} + \sigma_{22})] \qquad \text{Eq 2-8}$$

The most commonly used method for stress determination is the $sin^2\psi$ method. A number of XRD measurements are made at different psi tilts (see *Figure 2-4*). The inter-planar spacing, or 2-theta peak position, is measured and plotted as a curve similar to that shown in *Figure 2-5.* The stress can then be calculated from such a plot by calculating the gradient of the line and with basic knowledge of the elastic properties of the material. This assumes a zero stress at $d = d_o$, where d is the intercept on the y-axis when $sin^2\psi = 0$ (69). The gradient of the line (see in *Figure 2-5*) is:

$$\frac{\partial d_{\phi\psi}}{\partial sin^2\psi} = (\frac{1+\upsilon}{E})\sigma_{\phi} d_o \qquad \text{Eq 2-9}$$

Thus, the stress is given by:

$$\sigma_{\phi} = \frac{E}{(1+\upsilon)} \frac{1}{do} \left(\frac{\partial d_{\phi\psi}}{\partial sin^2\psi}\right) \qquad \text{Eq 2-10}$$

The value of unstressed lattice spacing d_o is unknown. However, $d_{\phi 0}$in Eq 2-8 differs from d_o but not more then $\pm 0.1\%$, therefore σ_ϕ can be calculated approximately by substituting $d_{\phi 0}$ for d_o (70).

According to the state of the stress in the material, different relationships for the d vs. $sin^2\psi$ curves can be found (see *Figure 2-6*): normal stress, shear stresses and large variation in stress relation.

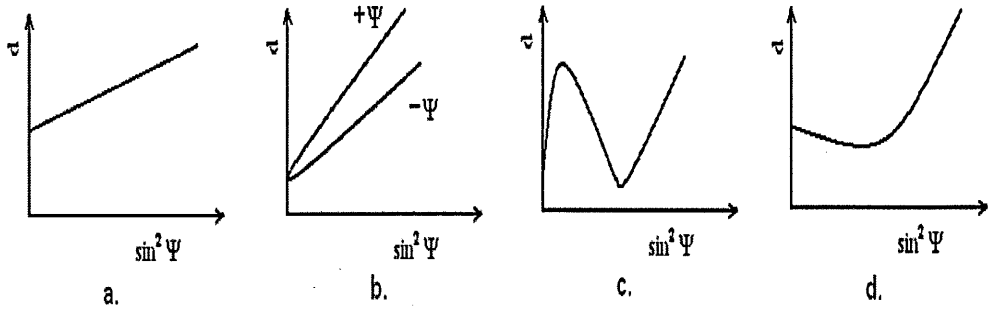

Figure 2-6: The d vs. $sin^2\psi$ relationships: a) normal stress only on the plane of the surface, b) presence of shear stress perpendicular to the surface, c) presence of large variations in stress, d) stress gradient perpendicular to the surface (69).

The next sub-section covers a critical comparison of the residual stress measurement techniques discussed in this chapter. It comprises brief comments on their capabilities to resolve residual stresses and limitations in terms of measured stress component, penetration depth and spatial resolution.

Critical comparison of residual stress techniques

X-ray diffraction can be used to measure type I, II and III stresses. However, it can only provide one dimensional (1D) in-plane stresses (69). It has a very limited penetration depth (23). This technique is sensitive to the material grain size and surface texture (69). The neutron diffraction technique can measure the elastic strain associated with residual stresses for depth of up to about 25 mm in steel with a spatial resolution of less than one millimetre (23). This technique can provide a full three dimensional map of the residual stress field throughout the volume of the component (24,25). It has a capability to measure tri-axial stress components. It can be used to measure type I and II stresses. However, the application of this technique has some additional limitations such as it is not suitable for surface measurements (26), it is sensitive to the material grain size and texture, it is difficult to make reliable stress free lattice parameter reference measurements (27) and its difficult to access a neutron source. This technique often does not measure reliable values of stresses within and around the weld region because of variations in the spatial resolution of the reference lattice constant (71). In addition to this, the neutron diffraction technique is not capable of measuring through-thickness residual stresses in large engineering components (i.e. where the thickness exceeds 50 mm or so).

Deep hole-drilling (DHD) method is a semi-destructive residual stress measurement technique. It is often used to measure type I residual stresses (continuum long-range). The deep hole drilling method is capable of measuring through-thickness residual stresses. It is less sensitive to the material type and can be applied on a wide range of materials and applicable to both simple and

complex components (60,61). The deep hole drilling technique provides three in-plane stress components (two direct and one shear) throughout the thickness of the component along the line (29,30). However, the spatial resolution of deep hole drilling is limited by the diameter of the trepanned core (31) and a minimum 5 mm trepanned diameter has been reported to be used (32). It can provide only a one-dimensional profile of residual stresses along the centre line of the drilled hole (29,30). This technique does not resolve the problem of reliable measurement of surface residual stresses. It is not applicable to components of less than 6 mm thickness (30,58). The DHD technique stress results can be compromised by plasticity, when the technique is applied to measure large residual stresses (>60 % of yield strength) (58).

Thus, all the above discussed residual stress measurement techniques have their own advantages and disadvantages and they have limited capabilities in terms of measured stress components, penetration depth and spatial resolution.

The following section describes the importance of welding and the challenges it poses for safety critical applications. In this thesis, components made using advanced welded processes (electron beam and overlay-cladding) are studied by applying the contour method of residual stress measurement. In the following section the characteristics of induced residual stresses in weldments made by these processes are described, their measurement challenges identified and the limitations of deep hole drilling and neutron diffraction methods discussed.

2.5 Welding and its consequences

Welding is a joining technique widely used in the fabrication of engineering structures (10). It is also extensively used in the fabrication of safety critical components such as pressure vessels and pipework in nuclear power plant (11). Despite its wide application, welding is a highly disruptive process. It involves intensive localised heating and cooling of the surfaces to be joined. Misfits are created through solidification of the molten metal, differential contraction, chemical diffusion, phase transformation and plasticity (12). This results in a complex, three dimensional residual stress field with high levels of stress in the welded joint (5).

Electron beam welded P91 plate

Ferritic martensitic steels are increasingly used in manufacturing of high integrity structural components such as main steam pipes, boilers, steam headers, turbine castings and super heater tubings of ultra-supercritical power plants and fossil fuelled power generating plants that sustain elevated temperatures (72,73). Ferritic martensitic steels containing 9-12 wt. % chromium offer a better high temperature creep resistance than the classical 2.25 Cr-1Mo grades. They are less susceptible to degradation through thermal fatigue due to having a lower coefficient of thermal expansion and higher thermal conductivity compared with stainless steel (74,75). However, P91 weldments (made by conventional welding process) in service operation can exhibit premature failure. The failure type falls into the category of 'type IV' cracking due to the position of the cracks. In this case, the weldments will be weakest due to formation of creep voids in the refined

(inter-critical) region of the HAZ of the weld (74,76). To improve long term creep properties, the earlier grades of 'type 91' steels are modified through small additions of niobium (Nb), vanadium (V) and nitrogen (N) (77,78). The modified P91 steels are used together with high energy electron beam welds to enhance the resistance to type IV cracking (79).

High energy density weld (HEDW) processes such as electron beam welding (EB) are capable of providing high penetration into a component (13). Autogenous EB welds produce excellent joint fits without introducing excessive heat and distortion. They have a deep, narrow and parallel sided fusion zone in the vicinity of the weld, due to the small thermal contraction in the weld metal compared to conventional welding processes such as arc welding (15,16). The small thermal contraction prevents excessive angular deformation, bowing, buckling and twisting of the component. High energy electron beam welds are less prone to type IV cracking and likewise less premature failure.

Dissimilar Electron Beam Welded Plate

The welding process is also used to join dissimilar metals, for example modified 9Cr-1Mo ferritic steels (that contain a low amount of carbon) and austenitic stainless steel. Such joints are often welded by gas tungsten arc or shielded metal arc processes with stainless steel or nickel based welding consumables. The combination of austenitic stainless steel and Mod.9Cr-1Mo ferritic steel can produce a strong joint and provide satisfactory service performance with a good combination of mechanical properties, formability and weldability (80,81).

Due to their high performance, these joints are widely used in high-temperature applications including nuclear power generating plants, chemical and petrochemical industries as well as conventional power systems (82). In the steam generator circuit of sodium cooled fast breeder reactors (SFRs), 316L(N) austenitic stainless steel pipes from intermediate heat exchangers are joined with modified 9Cr-1Mo ferritic steel (9Cr-1MoVNb) pipes of steam generators (83). On the other hand, when joining dissimilar metals the weld thermal cycle adversely affects the weld region, causing microstructural changes and large variations in physical, mechanical and chemical properties across the joint (84). These variations arise due to the metallurgical and physical incompatibility of the two metals, such as differences in melting temperature, differences in coefficient of thermal expansion and differences in thermal conductivity. The large difference in melting temperature between the two metals causes the segregation of high and low melting phases and hot cracking. The large difference in thermal conductivity of two metals causes uneven heat dissipation. The large difference in thermal expansion of the two metals leads to the formation of high residual stresses, reducing the joint strength and causing fatigue problems (85).

EB welding can reduce dissimilar metal joining problems to some extent and potentially produce satisfactory joints. The high energy density of EB welding produces a high heating and cooling rate that resolves the problem of the large difference in melting temperature between the two metals. The result of a low heat input per unit length of the EB welds is to form a low width to depth ratio weld and a small weld bead size. This minimises the mixing of dissimilar metals and controls

the dilution of the weld. Therefore, it limits the size of the brittle zone, reduces distortion and induces lower residual stresses. Electron beam welds have a high welding speed, excellent material properties and high yield strength compared with gas tungsten arc and friction welds (86,87). Hence, EB welding is recognized as a suitable technique for joining stainless steel to modified 9Cr-1Mo ferritic steel for high temperature applications.

There are also some disadvantages of the EB welding process. Because of the very high cooling rate, the molten material formed in the welding process rapidly solidifies and shrinks. This can cause many unwanted consequences such as material property changes, cracking within the weld, changes of shape and deformation in some materials, for example high carbon steel (17). Furthermore, the EB welding process produces a significant level of residual stresses in the direction of the weld (longitudinal direction). The magnitude of these stresses are considerable at the weld centre line and form a very fine steep gradient moving away from the weld line within a small region (18,88).

Stainless steel clad ferritic plate

The overlay-cladding process is a widely used technique in the nuclear industry to provide a protective barrier between corrosive environments and ferritic low alloy base metal in pipes, fittings, valves and pressure vessels. The reactor pressure vessel (RPV) of a light water reactor is made from ferritic low alloy steel with the inner surface clad using austenitic stainless steel to protect against crack initiation and growth by corrosion of ferritic steel exposed to reactor coolant water

conditions. These two materials have different mechanical and thermal properties. The low thermal conductivity of the austenitic cladding material shields the inner surface of the RPV against thermal shock loading and development of excessive transient thermal stresses. However, residual stresses are introduced into the clad itself and ferritic base material during the cladding application process (89,90). These stresses are modified by post weld heat treatment (PWHT). This is typically carried out in the temperature range of 605-620 °C, usually for at least 10 hours (45). Holding at the heat treatment temperature acts to relieve, but does not completely eliminate, high magnitude welding-induced stresses. When the temperature is decreased from the notionally "stress-free" heat treatment of the vessel, additional residual stresses are introduced. The final distribution of such stresses in the clad component depends on many factors such as: the cladding and base material physical and mechanical properties; the cladding thickness; the cladding (weld) procedure; the PWHT, and how it is applied to the vessel. When ferritic base material is clad with the layers of austenitic material, the peak tensile stresses normally occur in the cladding layer. The magnitude of these tensile stresses can reach the yield strength of the cladding material at room temperature (45,91). They can encourage surface crack growth through the cladding, increase the rate of fatigue damage and stress corrosion. In addition, there is a possibility of phase transformation in the ferritic base material that will result in a sharp variation of residual stresses within a short length scale and this can promote under clad cracking. All these effects can change fracture margins and contribute to brittle fracture (45).

Although EB and weld overlay cladding processes are promising manufacturing techniques for high integrity structural components, they can introduce short length residual stresses that are of potential concern. Therefore it is of paramount importance that the initial state of residual stress is well characterised. This will provide an important base to understand how the residual stresses interact with service loading when the manufactured components are in use.

In this research, the residual stress fields resulting in EB welded plates and an overlay-clad weldment are investigated. High stress gradients over very short distances associated with both of these weld types make it necessary to make stress measurements on as small and highly precise regions as possible. Thus, measurement spatial resolution is an important consideration for residual stress investigation of these components.

The limitations of the deep-hole drilling technique previously described make it less suited to resolving short length scale residual stress variations in thin section EB welds and in a thick clad plate. A thick cylindrical steel EB welded sample has been tested using the deep hole drilling method (62). But the spatial resolution of the residual stress measurement was limited by the 5 mm diameter trepanned core. The deep hole drilling method has also been applied to measure the residual stresses in a cladded component (90,92), but phase transformation effects were not captured in the stress results. The neutron diffraction measurement technique has sufficient spatial resolution and depth penetration for many cases. However, the application of this technique has some additional limitations: for example it is not suitable for near surface measurements (26), it is sensitive to the material

grain size and texture, and it can be difficult to obtain reliable stress free lattice parameter measurements (27). In addition to this, the neutron diffraction technique is not capable of measuring through-thickness residual stresses in large engineering components (i.e. where the thickness exceeds 40 mm or so). Residual stress measurement results for an EB welded plate using neutron diffraction have been reported in (18,94). However, reliable stress measurements were not achieved within and around the weld region because of variations in reference lattice constant measurements. This technique has also been employed to measure the residual stress field in a cladded component but phase transformation effects were not captured in the stress results (89,95) due to the use of a large gauge size.

2.6 The contour method

The contour method has emerged as a promising technique for the measurement of residual stresses in engineering components. This method was invented in 2000 by Mike Prime (33). It is based on cutting the test component of interest in two halves. The cut surfaces deform, owing to the relaxation of residual stresses. The deformations of the two cut surfaces are then measured, and used to back calculate the 2-dimensional map of original residual stresses normal to the plane of the cut (96). The contour method is capable of measuring through-thickness residual stresses. The contour method is relatively simple, inexpensive, and utilizes readily available equipment in workshops (97). It has been successfully validated by commonly used residual stress measurement techniques, such as neutron diffraction (98), slitting (99,100), synchrotron x-ray

diffraction (101,102) and sectioning (103). The method is useful to obtain detailed information of residual stresses introduced by various manufacturing processes such as welding (97,104–106), hammer peening (107), laser peening (108–110), cold expanded hole (111) and aluminium alloy forging (36). Nevertheless, like the other residual stress measuring techniques, the contour method also suffers from factors that impact on the accuracy and the spatial resolution of the method, and cause uncertainties in the measured stresses. The residual stress measurement results for an electron beam welded plate and a clad plate using the contour method have been reported in (89,112). However, reliable stress results were not achieved within and around the weld region because of the limited spatial resolution of the method. The reliability and accuracy of the contour method measurement results can be improved by minimising errors and uncertainties that can be introduced during cutting and data analysis procedures.

2.6.1 Theory of the contour method

The theory of the contour method is based on a variation of Bueckner's elastic superposition principle:

"If a cracked body subject to external loading, or prescribed displacements at the boundary, has forces applied to the crack surfaces to close the crack together, these forces must be equivalent to the stress distribution in an un-cracked body, of the same geometry, subject to the same external loading" (113).

To help explain this principle, a 3D illustration for a thick plate, in which the stress varies parabolically through the thickness of a plate, is shown in *Figure 2-7*.

In step 'A', the part containing residual stress is in an undisturbed state. In step 'B', the part is cut in half on the plane x = 0, and the newly cut surfaces are deformed due to the relaxation of the residual stresses. It is noted that only σ_x stress is represented in *Figure 2-7*, as the contour method only measures the stresses normal to the cut plane. In the present case, that normal stress is, σ_x. These deformations are measured over the entire cut surface and will be used in step 'C' to derive residual stresses. In step 'C', the deformed free surface, is forced back to its original configuration. Assuming elasticity, superimposing the partially relaxed stresses in step 'B', with the change in stresses from 'C', provides the original residual stress that existed in the part (96).

$$\sigma^{(A)}(x,y,z) = \sigma^{(B)}(x,y,z) + \sigma^{(c)}(x,y,z) \qquad \text{Eq 2-10}$$

Where, σ refers to the entire stress tensor, σ^A indicates the original stress, σ^B refers to the remaining stress and σ^c refers to the stress change (i.e. it indicates how much stress has relaxed from cut).

In the conventional contour method, because the stresses in step 'B' are not known, one cannot determine the original stresses throughout the body. However, it can be appreciated that, in step B, any 'in-plane' shear stresses on the plane of the cut (τ_{xy}, τ_{xz}), as well as the stress component normal to the cut surface (σ_x), will have zero stress value. Therefore, step 'C' can give those stresses along the plane of the cut.

$$\sigma_x^{(A)}(0,y,z) = \sigma_x^{(C)}(0,y,z)$$

$$\tau_{xy}{}^{(A)}(0,y,z) = \tau_{xy}{}^{(C)}(0,y,z)$$

$$\tau_{xz}{}^{(A)}(0,y,z) = \tau_{xz}{}^{(C)}(0,y,z) \qquad \text{Eq 2-11}$$

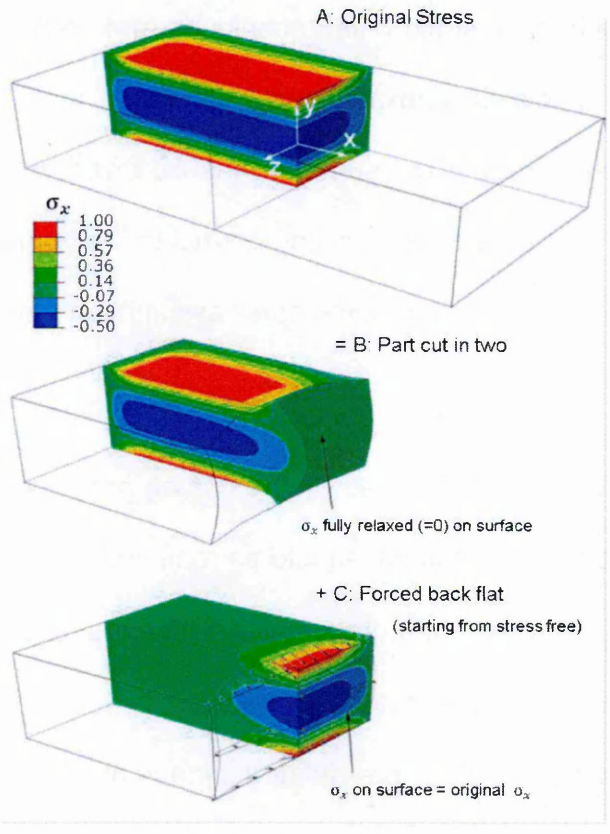

Figure 2-7: The contour method; Superposition principle for measuring residual stresses. Stresses are plotted on one quarter of the original body (96).

But, one can only measure the deformations normal to the cut face, in the x direction (shear deformations in transverse directions cannot be measured directly). Therefore, the cut surface is displaced back to the flat configuration in the x-direction only. The effects of shear stresses on displacements normal to the

plane of the cut are cancelled out by averaging the surface contours of opposing cut surfaces (96). This limits the contour method to measuring the direct residual stress component that is normal to the plane of the cut.

Similar to the mechanical strain relief techniques, the contour method is based on the assumption of elastic relaxation. It is assumed that any deviation from planarity, of the newly created cut surfaces has occurred solely because of the elastic relaxation of residual stresses, acting normal to the plane of the cut, prior to the cutting (33). However there are some other assumptions that are unique to the contour method.

- The width of any material removed by the cutting process should be constant and a minimal quantity of material should be removed.
- The cutting process must not induce any significant stress on the cut surface, thus not adding to the original residual stresses.
- Cutting must follow perfectly, a pre-defined surface profile.
- The cutting process should not induce plastic deformation.
- The cutting process must not recut the already cut surfaces

The sources of error regarding the cutting process are discussed later in this chapter. In the following section the experimental procedures of the contour method are explained.

2.7 Experimental procedure of the contour method

The experimental steps in undertaking the contour method of residual stress measurement are: constraining the test component, specimen cutting and surface contour measurement.

2.7.1 Constraining test component

Constraining the part is one of the most important experimental aspects of the contour method. During specimen cutting, the plane of the cut should be constrained from any movement as the stresses relax (33). Ideally the test component should be rigidly and symmetrically clamped at both sides of the cut. *Figure 2-8 (a)* and *(b)* shows two schematic clamping configurations. *Figure 2-8 (a)* represents finger clamp configuration, this clamping system is the most commonly used strategy in practice. During cutting, the clamping system provides vertical support to the specimen. However, there is a possibility that the specimen moves laterally if the support is not sufficient. *Figure 2-8 (b)* represents a rigid clamping strategy using fitted bolts. This system of clamping provides close control on opening and closure of the cut face during the cutting (114,115).

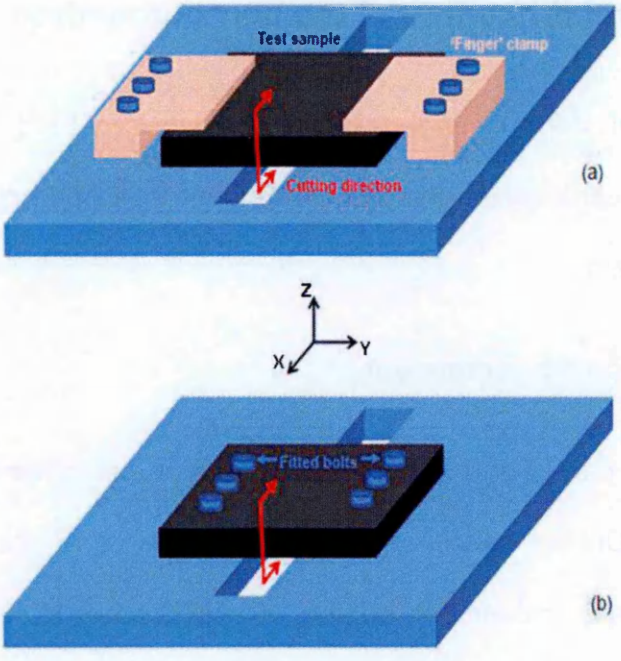

Figure 2-8: Illustration of symmetric clamping arrangements used for the contour method cutting by wire EDM (116).

Some novel approaches (117,118) have been used to try to obtain efficient constraint of specimens during the cutting process. One particular method creates restraint by leaving a ligament of uncut material, until the process of cutting along the remainder of the cut plane is complete. This self-restraint method of clamping is known as an embedded cutting configuration (116). This approach was applied in experiments recorded in chapters 3 and 5.

2.7.2 Specimen cutting

Specimen cutting is the most crucial step of the contour method. Wire Electric Discharge Machining (WEDM) has previously been identified as the best choice for the cutting step of the contour method (38,39,96). WEDM cutting is based on a

thermo-electric process, and it is performed by generating a series of electrical sparks between the EDM wire (electrode), and the component (119–121). It can be applied to all electrically conductive materials, irrespective of their hardness, material strength, shape and toughness. Also, WEDM is a non-contact machining process; there is no direct contact between the electrode and the work piece during cutting. In addition, due to its non-contact nature, there is no direct force, so no mechanical plasticity is introduced by the machining process. The absence of mechanical loads during cutting also eliminates the vibration problem that often occurs with other mechanical machining methods.

Throughout the cutting process, the component is submerged in a temperature controlled deionized water tank, in order to minimise thermal effects from the cutting process. As a consequence, the work piece and the wire are actually separated by a thin film of fluid. This thin film between the work piece and the wire is sufficient to prevent an electrical short circuit, and to compensate wire vibration during the machining process. During the electrical discharge machining, sparks, initiated by a high voltage, are generated in a small gap between the cutting wire and the work piece. This develops a channel of ionised-high temperature, electrically conductive, gas (plasma), and forms a localized region of high temperature (119–121). This heat results in localized melting and vaporisation of work piece material. The molten and vaporized material forms small deposits on the wire, and on the work piece surfaces. On cooling, the solidified material generates spherical debris particles, and these particles are carried away from the spark gap with dielectric liquid. The evacuation of eroded particles by the

pressurised fluid is called the flushing process. Pressurised water is injected from top and bottom nozzles. Efficient flushing and removal of metal particles (chips) from the thin film of fluid (in the working gap) can help to sustain a stable machining environment. A proportion of solidified material is immediately re-deposited on the work piece surfaces as a recast layer because it was not completely expelled by dielectric fluid flushing (122–124). During cooling and solidification of that layer, the microstructure and the material properties can be altered, both within the newly-formed layer and in the heat-affected zone (125). Thus, the quality of the cut surface is highly dependent on the cutting conditions (such as the cutting parameters, debris flushing and the nature of the dielectric fluid).

During the cutting process, the wire is continuously fed from a spool held between upper and lower guides. Hence always fresh wire is involved in the process. The straightness of the wire is adjusted by applying a tension force to the wire. Wire tension aims to reduce the wire vibration and deflection which could affect the quality of the cut surfaces. *Figure 2-9* illustrates the wire EDM process.

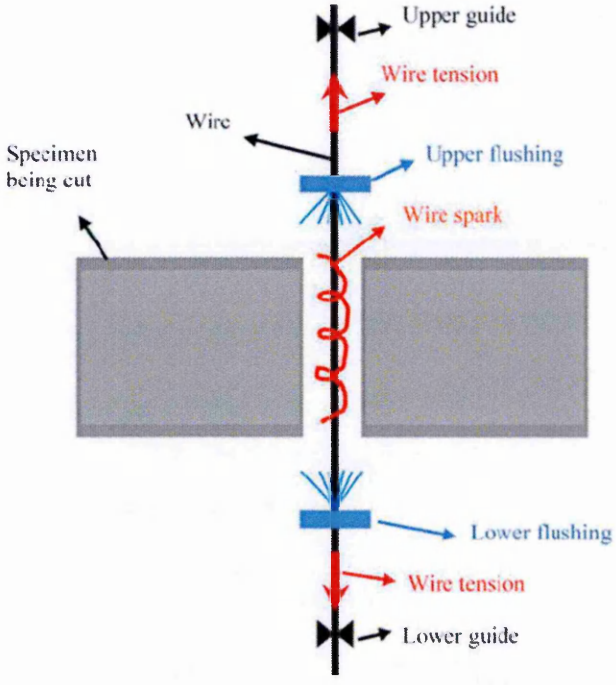

Figure 2-9:Through-thickness view showing the flushing and wire tension during WEDM process (39).

Figure 2-10 (a) shows a schematic representation of a test specimen undergoing cutting by wire EDM. The drawing and annotations help to explain the terminologies used throughout this thesis. Metal is removed by the wire slowly traversing, simultaneously in both horizontal and vertical directions, in the direction of the cut.

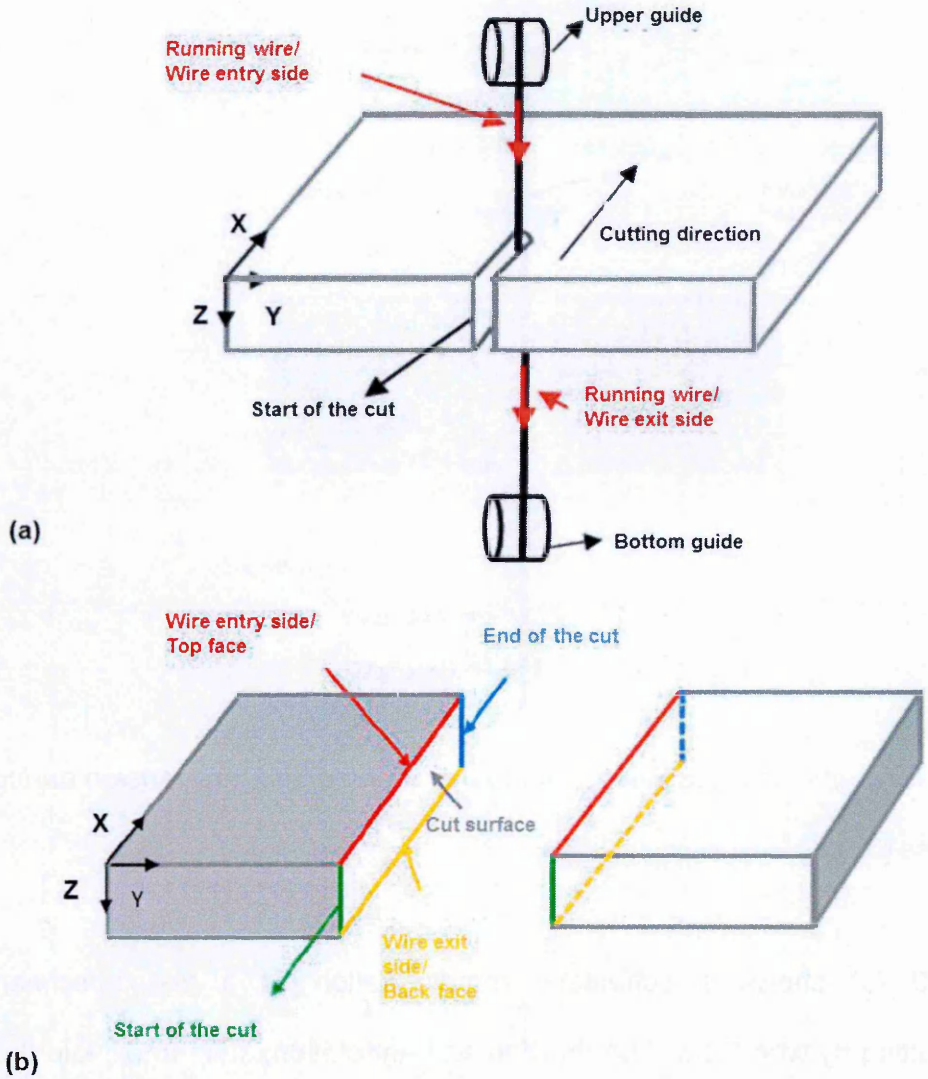

Figure 2-10: (a) Schematic representation of a test specimen being cut by WEDM and (b) labelled edges of cut parts (39).

In *Figure 2-10* (b) the 'start of the cut' refers to the location where the wire begins to cut the specimen, whilst moving in the horizontal direction. The 'end of the cut' refers to the location where the wire finishes cutting the specimen, whilst moving in the horizontal direction. The 'wire entry' refers to the top surface entry of the wire when it is moving in the vertical direction. The 'wire exit' refers to the

bottom surface exit of the wire when it is moving in the vertical direction. The 'wire contact length' is the segment of the wire that is enclosed by the specimen material, during cutting, and is therefore always of a length equivalent to the thickness of the specimen (39).

2.7.3 Surface contour measurement

After wire EDM cutting, the contours of the created cut surfaces are measured. Measuring the deviation from planarity of the cut surface, with high accuracy is important when using the contour method for residual stress measurement. A coordinate measuring machine (CMM) has the capability to register three spatial coordinates (displacements) for any point on a cut surface. CMMs can measure the cut surfaces using contact and non-contact devices, which include touch trigger probes, continuous scanning probes and optical system. The most common techniques for measuring the surface contours are reported in detail in (39). A CMM, with a fitted touch probe (see *Figure 2-11*) (126–128), is the most commonly used instrument for taking surface contour measurements (33). They are widely available in many engineering workshops.

The measurement of surface displacement is used to quantify the residual stress values. Before conducting the CMM measurements, the cut surface must be clean and dry, and free of any dirt, dust and oil. Any dirt particles on the sample surface can affect the measurement data and can cause error in the contour method stress results. Since the touch probe sampling rate is about one measurement point per second the measurement process can take several hours.

Therefore, temperature stability is important, so the contour cut surface is measured in a temperature controlled room and should be isolated from thermal fluctuation (96,129). Furthermore, whilst measuring, the touch probe cannot provide measurement very close (< 0.5 mm) to the edges of the sample (129). Also, the touch probe makes contact with the measuring surface, and some local deformation occurs due to the low but finite contact force. These limitations can be overcome by using an entirely non-contact method such as laser sensors (130).

Due to faster acquisition of measurement points using laser sensors, they are more suitable for measurement of large engineering components. As such the thermal fluctuation, if there is any, is less of an issue. They have a capability to measure the cut surface with better resolution and high accuracy. However, laser sensors cannot exactly capture the outline of the cut surface perimeter because of finite diameter of the laser beam, which is typically at least 50 μm (39).

The two CMM systems are installed at the Open University, one is the Mitutoyo Crysta Plus 574 CMM equipped with a Renishaw motorised head, PH10M and the other one is a laser CMM system comprising a Zeiss Eclipse CMM to which a Micro-Epsilon triangulating laser probe is fitted. The touch probe system has a resolution of 0.5 μm and the laser sensor has a resolution of 0.15 μm at its maximum sample rate of 20,000 per second and without averaging (129).

Figure 2-11: Touch probe CMM at the Open University, Materials Engineering Laboratory

2.8 Data analysis

Data processing should not change the underlying features of surface deformation. To process the contour data, for the calculation of residual stresses using the contour method, several data analysis steps are involved. These steps include (39,130);

- aligning the contour data of the opposing cut surfaces
- Interpolating the two data sets into a common grid
- extrapolating to the perimeter
- averaging the two sets of data points

- removing noise and outliers
- flattening
- smoothing the cleaned and averaged data

The following sections describe these steps in more detail.

Aligning the data sets

The two cut surface deformation data sets are measured in two different coordinate systems. These data sets must be aligned on the same coordinate system, so that all the points in both data sets are coincident with each other, in the same manner as the material points were in the single component prior to the cutting. The mating cut surfaces appear as mirror images of each other. In this situation, one of the *x-z* coordinate directions needs translation and rotation, so that both cut surfaces exactly overlay each other and the corresponding data points on each mating surface can be aligned. This data set alignment is facilitated by measuring the perimeter of both cut parts. Note that deformation measurement points are y coordinates and the points on the surface are on x-z plane.

Interpolating in a common grid

For several reasons, the data points of both cut surfaces cannot always be overlaid exactly on top of each other. Reasons include; uncertainty in the uniform lateral movement of the CMM or in the movement of stages of the laser sensors, alignment of the cut surfaces and the defined local coordinates. So, in this case, it is necessary to linearly interpolate the data sets of each cut surface onto a

common grid, with the same approximate density, as the original measured data points (39,130).

Extrapolating to the perimeter

The surface contour measurement method (CMMs and laser sensors) cannot exactly capture the displacement approaching the outline of the cut surface perimeter. Therefore, extrapolation is required to replace any missing data points, usually situated around the perimeter of the cut surface. This extrapolation is necessary because displacements must be applied to all the nodes on the cut surface in the FE model (39,130). Often reconstructed near surface residual stresses are unreliable and may not be reported.

Averaging of the two data sets

Once the measured surface data sets are aligned and on the same grid, they should be averaged point by point on the *x*-*z* grid to provide a single set of deformation data. This step is one of the most significant steps in the data processing because it can eliminate several potential sources of error, such as the effects of shear stresses and asymmetric cutting artefacts resulting from the cutting process (38,39,96).

Filtering

Noise and outliers can appear in the surface measurement data. They can be caused by factors such as, the roughness on the WEDM cut surface, a cutting fault such as WEDM wire breakage, or an error in the surface contour

measurement process, such as the CMM probe slipping at the edges of the cut surface. If the overall form of the surface is to be preserved, it is essential to eliminate these outliers. They can cause significant errors in the calculated stress values because for the contour method, stress calculation is dependent on surface displacement profiles (39,96,130).

Data smoothing

The averaged and cleaned displacement data set must be smoothed before its use as boundary conditions in an FE model for elastic stress analysis. Data smoothing is required, because any variations within the contour cut surface data, resulting from WEDM cutting irregularities or measurement errors, can be amplified in the stress results.

Surface data can be smoothed using different methods. Examples include bivariate spline smoothing, Fourier series and polynomial smoothing. The Fourier series method cannot always capture all the important features of the cut surfaces (130). The most commonly used smoothing technique when using the contour method is bivariate spline fitting, or two dimensional (2D) cubic splines (130). This technique, commonly used in previous contour measurement studies has led to the publication of very reliable results (94,131,132). When using 2D cubic splines, piecewise polynomials are joined at given locations called 'knots' which define the domain of each polynomial. The smoothing process is achieved by minimising the uncertainty in the calculated stress results, or error in the data point and the fit. The amount of smoothing and the density of knot spacing can affect the resulting

stresses. Too small a knot spacing would under-smooth the measured data. On the other hand, too large a knot spacing would over-smooth the measured data.

For too small a knot spacing, the roughness of the cut surface can be incorporated into the final smooth surface contour data, and for too large a knot spacing, the final smooth surface contour data would not capture all underlying surface deformation features. In both cases, the uncertainty in the calculated stresses would be increased. Hence, determining the optimum knot spacing, in order to obtain the best fit of the measured data, is essential to minimise uncertainty in the stress results.

Different approaches can be applied to determine the optimum smoothing parameter or 'knot spacing'. Commonly, it can be achieved by fitting the measured displacement data to cubic splines with a variety of knot spacings. The suitability of the knot spacing is evaluated by comparing the spline fits to the raw data (averaged from both cut surfaces) (106,132,133). Another approach to determine the optimum knot spacing, involves incrementally increasing the knot spacing, fitting the data for each knot spacing and then performing a finite element analysis for each increment to determine the stresses. The uncertainty in the calculated stresses at a given node is estimated by taking the standard deviation of the new stress and the stress from the previous, course fit. The standard deviation can be calculated from Eq 2-12

$$\partial\sigma(i,j) = \frac{1}{\sqrt{2}}|\sigma(i,j) - \sigma(i,j-1)| \qquad \text{Eq 2-12}$$

Where, $\sigma(i,j)$ represents the stress at node i for the smoothing spline solution j, and $j-1$ refers to the previous, course smoothing spline solution. An averaged uncertainty in the calculated stresses can then be calculated. The optimum knot spacing will always relate to the lowest average stress uncertainty using the root-mean-square (RMS) of all the nodal uncertainties from Eq 2-13 (130).

$$(avg)\ \partial\sigma(j) = \frac{1}{\sqrt{n}}\sqrt{\sum_{i=1}^{n}[\partial\sigma(i,j)]^2} \qquad \text{Eq 2-13}$$

2.9 Residual stress back calculation (FE modelling)

For the contour method stress calculation, linear elastic finite element (FE) analysis is performed using a standard FE code such as ABAQUS. The contour cut has to be symmetric therefore only one of the cut halves is used to create a three dimensional finite element model. The model is created by using the measured perimeter of the cut part. Ideally the cut surface should be modelled with a deformed face and then forced back to a flat surface. However in practice, the measured deformations resulting from stress relaxation are very small in comparison to the size of the components being measured and the analysis is elastic. Therefore, for convenience, the cut surface is modelled as having a flat (undeformed) cut face. The FE model of the specimen is meshed and the elastic material properties of the specimen are defined.

The contour method is based on an elastic superposition principle. The material behaviour is assumed to have isotropic linearly elastic properties, defined by the values of Young modulus and Poisson's ratio. However, when applying the

contour method on engineering components made from dissimilar-materials, for example a clad plate or a dissimilar metals welded plate, it is important to apply the appropriate material properties for each material of the component. In the present study, finite element analyses were performed on specimens with dissimilar materials, and these are covered in Chapters 5.

Conventionally, the finite element model is meshed using brick elements, with either linear shape function hexahedral 8-node elements, or quadratic shape function hexahedral 20-node elements. The next step is to apply the smoothed data, in the form of displacement boundary conditions, on the FE nodes of the model, with reverse sign (i.e. the displacement contour is applied in the opposite direction). Then, additional boundary conditions are applied to FE model to prevent rigid body motion (see *Figure 2-12*) (134). Finally, residual stresses are obtained by performing a linear elastic finite element analysis.

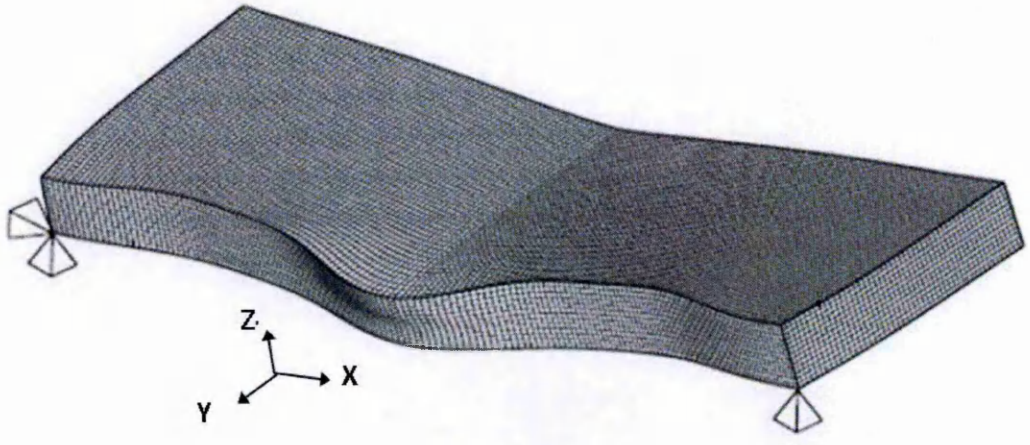

Figure 2-12: A deformed 3-dimensional linear FE model showing additional constraint to prevent rigid body motion (134).

2.10 Cutting errors in the contour method

The contour method is based on cutting the test components into two halves. The cut surfaces deform, owing to the relaxation of residual stresses. When a component of residual stress normal to the plane of the cut is relieved, both cut surfaces will deform either towards or away from each other, depending on whether the stress is compressive or tensile. The cutting should be performed by fulfilling the cutting criteria mentioned in section 2.6.1. There is a potential for geometric changes to occur on the cut surface contours in the result of any violation of the cutting assumptions leading to deformation artefacts and the introduction of error and uncertainty in the residual stress measurements (33,38).

These discontinuities can be classed as symmetric (since the surfaces are mirror images of one another) and anti-symmetric (38). Examples of each are shown in *Figure 2-13*.

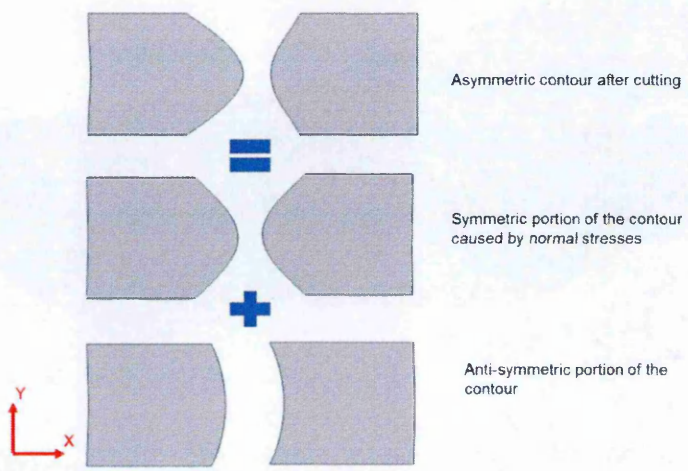

Figure 2-13: Asymmetric contours can be divided into symmetric and anti-symmetric portions (38).

In general, not all of the distortion of a cut surface will be symmetric, for example owing to shear stresses, asymmetrical constraint of the specimen during cutting, or use of curved or crooked cuts (see example in *Figure 2-14*). Consequently, the effect of cutting artefacts on the residual stress measurement depends on whether they are symmetric (38) or anti-symmetric (38,135).

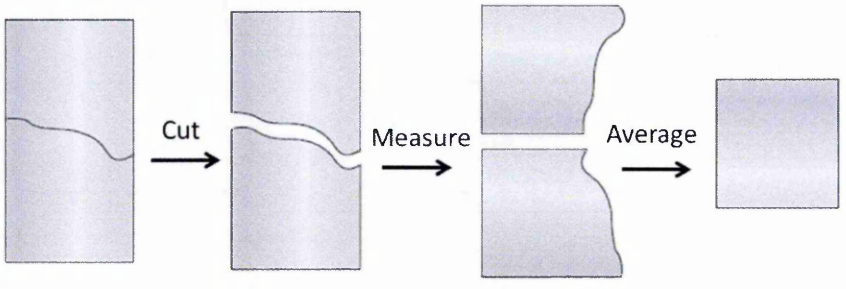

Figure 2-14: The effect of a crooked cut goes away when the two surfaces contours are averaged (96)

Errors related to anti-symmetric cutting artefacts are of less concern because they can be removed by averaging the data obtained from contours of both cut surfaces, for example see *Figure 2-14*. In contrast, symmetric cutting artefacts can cause significant errors because these errors cannot be removed by averaging the contours of the cut surfaces. Symmetric errors can be divided into two groups; symmetric errors independent of the stress magnitude and related to cutting artefacts (an important focus of the present thesis) and those dependent on the stress magnitude. Symmetric errors dependent on the stress magnitude can be further categorised as either elastic bulging or plasticity errors or both combined.

Examples of errors in residual stress measurements that can be introduced by non-ideal conditions in the cutting process are shown in *Figure 2-15.*

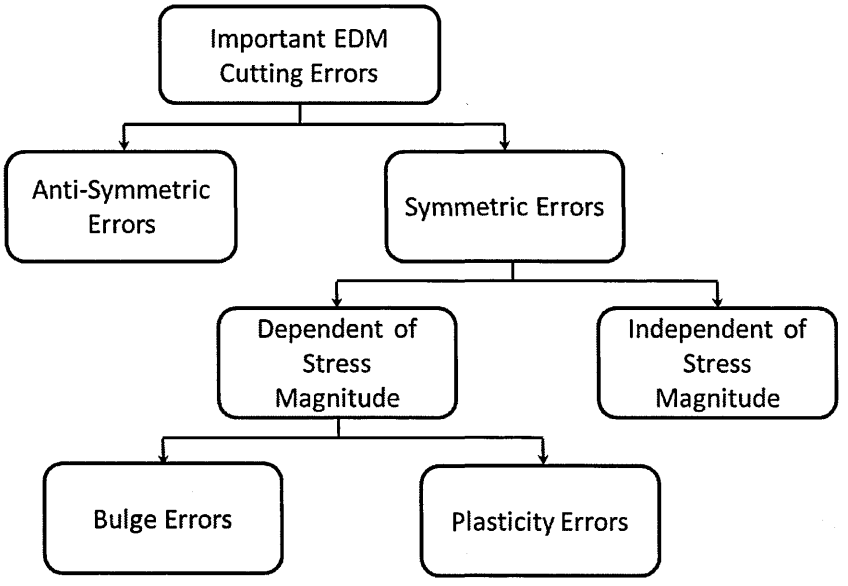

Figure 2-15: Errors that may be introduced by the contour method cutting process:

Symmetric error independent of the stress magnitude

Ideally a cut in a stress-free body should produce well defined surface profile that is both parts of the cut should match exactly and represent perfect flat mating surfaces. *Figure 2-16* represents the perfect flat surface in the absence of residual stresses. Any distortion on the stress free cut surfaces can be categorised as cutting artefacts.

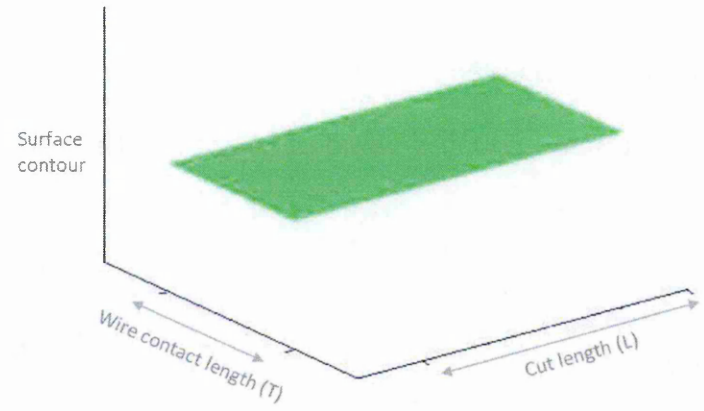

Figure 2-16: Schematic drawing of perfectly flat cut surface in the absence of residual stress *(39)*

Cutting artefacts cause uncertainty and error in the measured residual stresses (38). Therefore, it is of prime importance to understand the factors that contribute to the introduction of cutting artefacts.

The WEDM cutting process produces surfaces with an underlying level of roughness which imposes a fundamental limit on the residual stress length scale resolution of the contour method (39). Surface roughness can be quantified by the vertical deviations of a real surface from its ideal form, and can be represented by various parameters. Three roughness parameters, *Sq* (the root-mean-square), *Sa* (the arithmetic mean) of the absolute height, and RSm (the mean width of the roughness profile element) are universally recognised and most widely used (136).

Root mean square roughness, Sq

This is a 3D parameter expanded from the roughness (2D) parameter *Rq*. It can be defined as the root mean squared value of $Z(x,y)$ in the measured area (as shown in *Figure 2-17*).

$$Sq = \sqrt{\frac{1}{A}\iint_A Z^2(x,y)\,dxdy} \qquad \text{Eq 2-14}$$

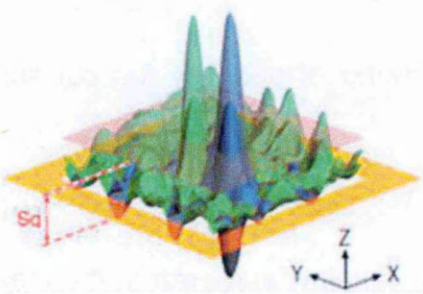

Figure 2-17: Root mean square roughness parameter (136).

Arithmetic means of the absolute height, Sa

This is a 3D parameter expanded from the roughness (2D) parameter *Ra*. It can be defined as the average of the absolute values of $Z(x,y)$ in the measured area as show in *Figure 2-18*.

$$Sa = \frac{1}{A}\iint_A \left|Z(x,y)\right| dxdy \qquad \text{Eq 2-15}$$

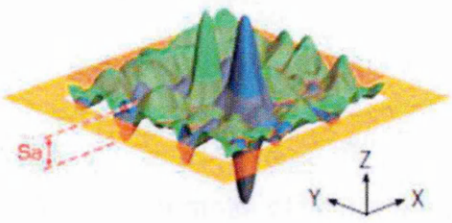

Figure 2-18: Arithmetic mean of the absolute height(136).

Mean width of the roughness profile elements, RSm

The RSm can be defined as the mean of the width of the profile curve elements, in a sampling length (as shown in *Figure 2-19*) (137), where m is the number of profile elements on the roughness profile and X_{si} represents the width of the profile of the curve elements, i represents elements from 1 to m.

$$RSm = \frac{1}{m}\sum_{i=1}^{m} X_{si} \qquad \text{Eq 2-16}$$

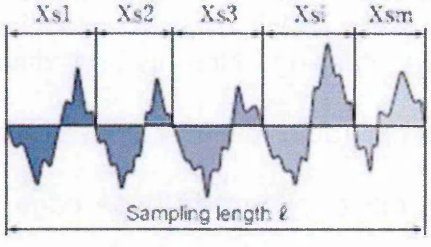

Figure 2-19: Mean width of the surface profile element (137).

Roughness of the WEDM cut surfaces can be affected by WEDM cutting parameters, flushing conditions, and wire diameters and material type. A smaller

diameter of WEDM wire is recommended to improve the surface finish. However, too small a wire diameter will increase the risk of wire breakage, and can increase the cutting duration. To obtain the best results, brass is the recommended material for WEDM (96). However, there is little information available in the open literature to help make the best material choice for WEDM machining for contour measurements. Previously, tungsten or zinc coated brass wires have been used to perform contour cuts, although a lower quality of the cuts has been reported (138,139).

In addition to this the cutting process can introduce discontinuities such as flared edges, steps, waviness and surface bowing (39,140). Flared edges are often seen at wire entry and exit locations, and at the start and end of the cut (i.e. at transition locations). Flared edges can be defined as high deformations caused by transient effects at wire entry and exit, and the cut start and end, across the edges of the test specimen. At these transition locations flushing is more dispersed. This is because the diameter of the flushing nozzles is few millimetres and at these locations the injected liquid only partly covers the specimen and causes non-uniform distribution of the flushing. Non-uniform distribution of flushing can produce wire vibration and high deformation at these locations. Another possibility is that the electric field is least uniform at these edge locations. High electrical energy increases the discharged pulse (141,142) which results in high erosion rate along the edges and causes a high value in displacement variations. One assumption of the cutting step of the contour method is that a constant width of material is removed. However, maintaining an even width is not often possible

near to the edges of the cut, thus resulting in errors when measuring stress magnitudes that exist close to edges. For this reason, practitioners of the contour method often do not report stresses in these regions. To deal with this issue and to produce reliable near surface stress results, sacrificial layers of similar material properties as the specimen can be attached at the top and bottom faces of the specimen along the plane of the cut as well as at the start and at the end of the cut (143). Recently, some success has been reported in getting the precise stress results near to the surface by using sacrificial layers for complex geometry (144).

Sharp variations in apparent deformation across the width of the component are called a "step". These cutting artefacts are commonly seen on the cut surface where the cut was performed on a work-piece that has non-uniform thickness (i.e. a sharply changing wire contact length). Changes in the wire contact length can cause instability of the cutting conditions. These cutting artefacts can be avoided by creating a uniform cross-section along the cut length using sacrificial layers.

Periodic variations of surface displacement measurements, normally along the cut direction, are termed waviness. This can be caused by local cutting irregularities such as, wire vibration and wire drift. These cutting artefacts can be avoided by increasing the wire tension.

Sometimes the cut surface is curved. This feature can be categorised as either a "convex bowed" or a "concave bowed" form of cut (see in *Figure 2-20*). In case of the convex bowed form, more material is removed close to the top and bottom, or at the start and end of the cut. The concave bowed form occurs when more

material is removed at the mid thickness of the cut. These features can occur due to wire vibration and wire bending during cutting. This is a symmetric cutting artefact, and so cannot be cancelled out by averaging data from the surface contours. Wire instability can occur during the cutting process for several reasons. The electrical spark applies several variable forces along and upon the wire such as electrostatic and electrodynamics forces (145). In addition to this, the flushing pressure, and the formation and evacuation process of debris can also cause wire instabilities. These artefacts can be minimised by adopting appropriate settings for the WEDM cutting.

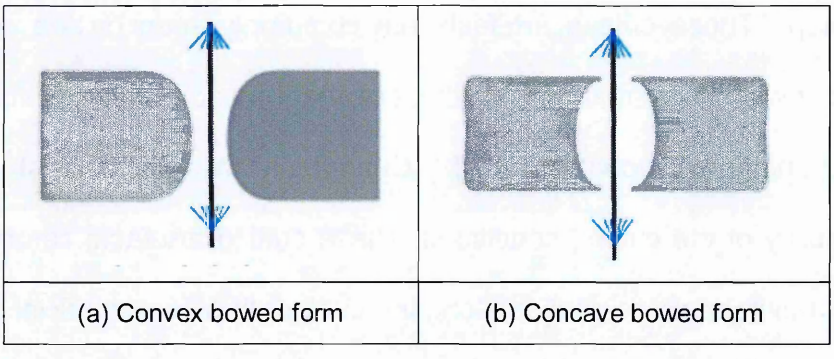

(a) Convex bowed form	(b) Concave bowed form

Figure 2-20: Schematically illustrates the through thickness view of the convex and concave bowed form of the cut surfaces (39).

Figure 2-21(a) and (b) schematically represents the different types of artefacts that can be observed in the result of cutting process performed on a stress free test specimen (39). Some of these cutting artefacts are investigated in chapter 3 of this thesis.

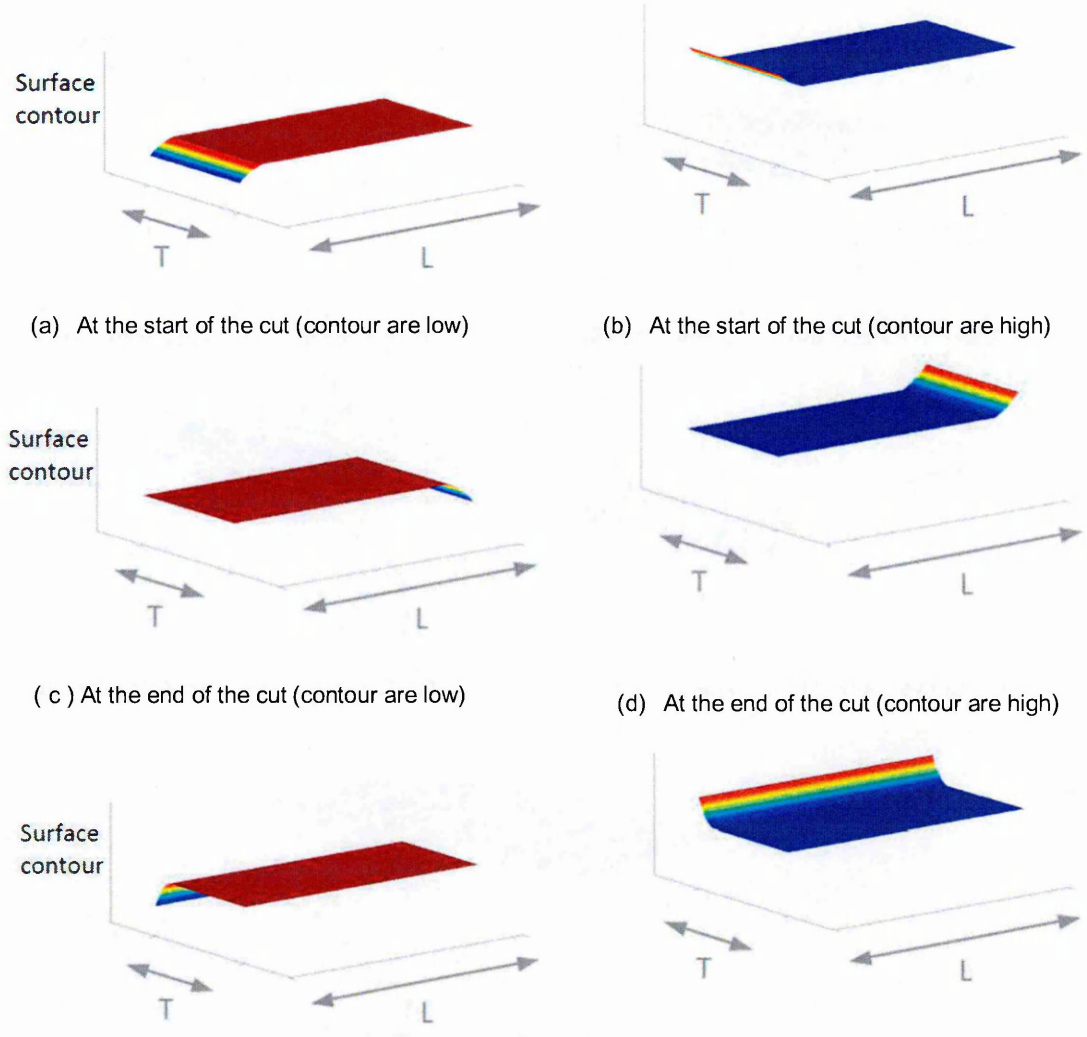

Figure 2-21(a): Schematically represents the different types of artefacts that can be observed in the result of cutting process performed on a stress free test specimen (39).

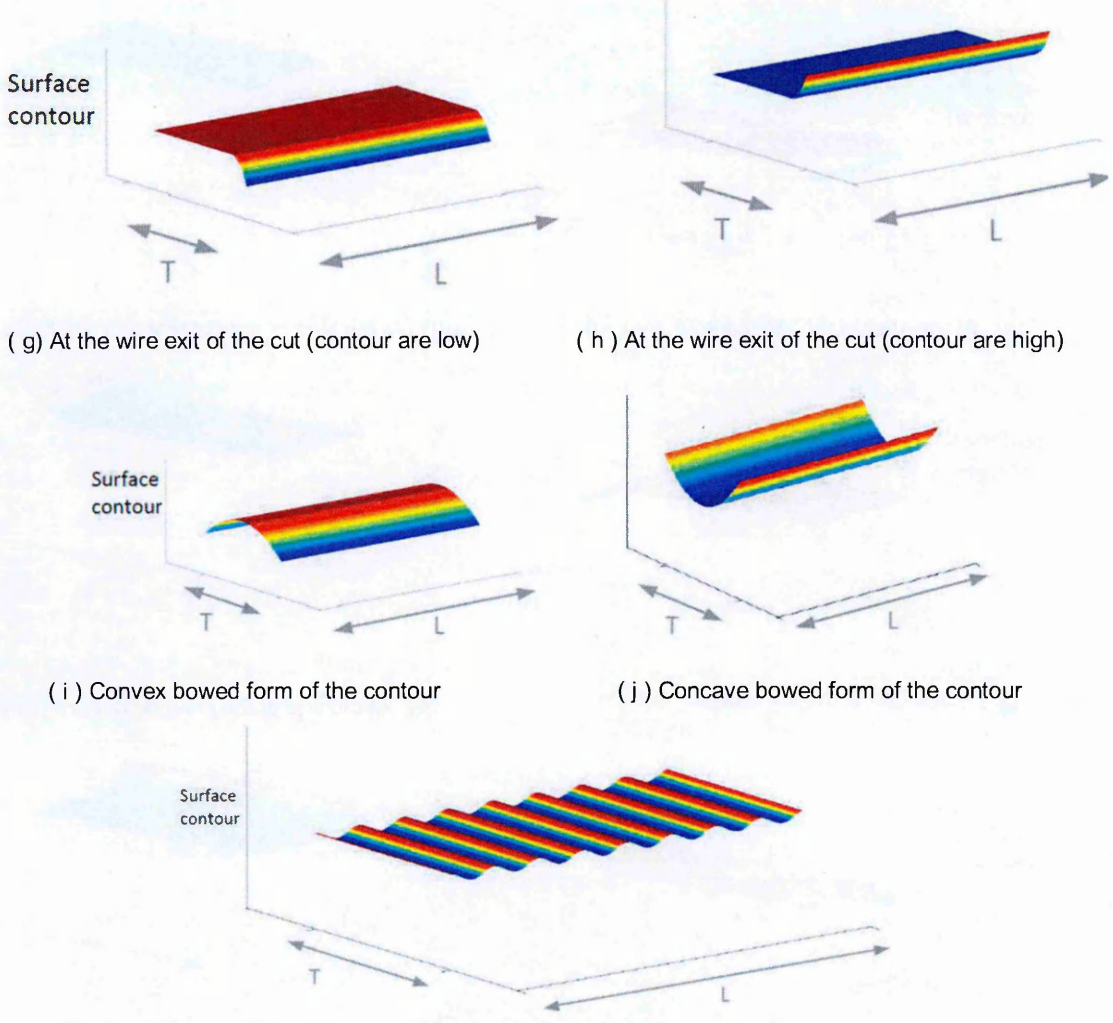

(g) At the wire exit of the cut (contour are low)

(h) At the wire exit of the cut (contour are high)

(i) Convex bowed form of the contour

(j) Concave bowed form of the contour

(k) Wavy form of the contour

Figure 2-21(b): Schematically represents the different types of artefacts that can be observed in the result of cutting process performed on a stress free test specimen *(39)*.

The quality of the cut surface can be improved by adopting the optimum setting of WEDM cutting conditions. The WEDM cutting parameters, and the cutting conditions, are machine specific, with each machine offering a library, of different, established cut settings. These cut settings are highly dependent on the properties of each specimen, such as specimen geometry and material type. The optimum

settings, for specific properties of the specimen, can be determined by undertaking stress-free trial cuts (135,143), carried out by skilled WEDM practitioners.

Moreover, the symmetric errors can be corrected by performing an initial test cut on a stress free material, so that in effect, all features of the cut surface represents cutting effects. Therefore, the expected form of the cut surface would be perfectly flat. Any non-planer shape present on the surface of the cut could then be identified as an artefact of the WEDM cutting process (33). These errors can be subtracted from the measured surface contour of the actual cut. In order to follow best practice, this stress free test cut can be performed on stress free portions of the same material of the same thickness, cut off at a small distance from the original cut surface on the actual test specimen (33,139,147).

Symmetric errors dependent of stress magnitude

Symmetric errors dependent on stress magnitude can cause two additional types of errors: elastic bulging and plasticity. These errors are briefly discussed in the following section.

Bulge Error

Bulge error happens when the cutting proceeds, so that whilst the material is being relaxed, the material at the cut tip will deform and stretch elastically, due to stress relaxation on the cut face and redistribution of the residual stresses in the remaining ligament. This in turn reduces, or increases, the original width, *'W'*, of the cut as shown in *Figure 2-22*. However, the physical width of the cut remains notionally constant (i.e. the wire diameter). This means that less (or more) material

is removed from the width of the cut, when compared to the original state of the material at the start of the cutting process. This leads to a variation in the width of the cut, resulting in a non-uniform cut width along the cut length. This causes deviation from the critical assumptions of the contour method; that material points are returned to their original configuration, and that a constant cut width is removed during the cutting process (38), hence leading to possible inaccuracies in the calculated stress. The incidence of bulge error primarily depends on the redistributed stress state at the tip of the cut. Secure clamping of the test component, on both sides of the cut, is believed to reduce this error. This error also depends on the cut slot width, so the occurrences of bulge error can also be lessened by narrowing the width of the cut. Larger bulging errors are more likely at the start and end of the cut. The bulge error can be estimated and corrected using an iterative FE analysis proposed by the Prime et al. (38). In this approach the calculated stress profile (affected by elastic bulging) is used as an initial residual stress field. Then, two dimensional finite element simulations of sequentially cutting a slot into the component of interest are performed to estimate the bulge error. The elements along the slot are removed sequentially in order to simulate the cutting process. The displacements are recorded for each step to estimate the errors. Consequently the bulge error is used to correct the measured surface contour. The corrected surface contours are then used to calculate the stresses. This process is iterated until the stress converges (38).

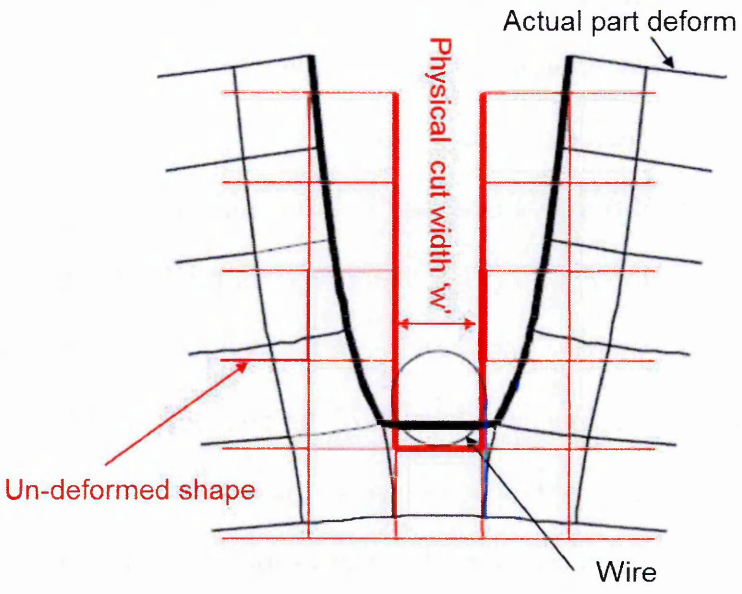

Figure 2-22: Demonstration of the bulging effect during the cutting process with assumed tensile stress relaxation (38).

Plasticity induced error

The second type of stress dependent error is related to plasticity at the cut tip. Plastic deformation during contour cutting is a deviation from one of the contour method assumptions i.e. that the stress relaxation is elastic during the cutting process. The level of plasticity induced is highly dependent on the stress field at the cut tip.

The stress field at the cut tip can be characterised by the stress intensity factor (SIF). Any attempt to reduce the severity of stress at the cut tip helps to reduce the risk of plasticity (38,116,118).

Recently, a novel cutting strategy has been developed to minimise the risk of plasticity induced errors, when using the contour method for residual stress

measurement (116). This new developed approach is based on the concept of linear elastic fracture mechanics. During the cutting process, the residual stresses in the cut portion are relaxed, due to the newly created cut surfaces and this causes redistribution of residual stresses in the remaining ligament and a stress concentration zone at the cut tip (118). Moreover, as the cut length increases, the stress concentration zone becomes more intense and may result in local yielding, which in turn may induce plasticity at the tip of the cut. Both the stress field and the plastic zone at the cut tip are directly related to the stress intensity factor (SIF) and yield stress. Therefore, any measure that can reduce the SIF at the cut tip during the cutting process will reduce the risk of plasticity induced error in the contour method (116,118).

2.11 Needs and gaps

The contour method is a powerful technique that can provide a two dimensional map of residual stress using equipment available in most workshops. The contour method is capable of measuring through-thickness residual stresses. However, the technique is still young and requires further development to improve its accuracy and reliability. All steps in the contour method (33,148) contribute some errors and uncertainty in the measured stresses. In order to achieve high-precision measurements, appropriate knowledge to perform each step has to be acquired. The above literature review explains the sources of uncertainty in the contour results.

Previously, errors related to the cutting step that are dependent on stress magnitude, such as bulge error (38) and plasticity error (116), have been addressed. Other limited studies address errors related to the cutting step that are independent of the stress magnitude where cutting artefacts are present in the surface contour data (131,140,143). The errors that are introduced from data processing (129,140) are also estimated. In order to minimise the error related to the cutting process, cutting conditions can be optimised by performing trial cuts on a stress free part of the test component (135,143,149), or on another piece of similar stress free material (38). However, performing the trial cuts will involve many variables, as the wire EDM cutting process contains a large number of electrical parameters. Moreover, the setting of these parameters can change depending on material type and geometric configurations of the specimen. Furthermore, performing a trial cut is itself a time consuming process.

The literature review reveals that there is currently no systematic approach to assess the quality of cut surfaces and evaluate stress errors introduced due to cutting artefacts. This chapter also identified a gap in the literature regarding the lack of provision of appropriate guidelines for selecting surface deformation measurement spacing, data smoothing parameters ('knot spacing' for example in cubic spline smooting) and finite element mesh size in contour data analysis. In this thesis these gaps are addressed.

2.12 Aims of the research

There are major issues that must be addressed to minimise error and uncertainty in the contour method measurement process. This research investigates the WEDM cutting process, surface deformation collection and data analysis steps. There are two particular aims:

- To develop benchmark test specimens for conducting contour trial cuts and develop criteria for characterising and quantifying the quality of the cut surfaces.
- To improve the spatial resolution of the contour method.

These additions to knowledge regarding the measurement of residual stress using the contour method will be a significant contribution to this important and worthy field of research.

2.13 Methodology

To achieve the first aim of the study, a benchmark test specimen was designed and a systematic approach applied to performing cutting trials and assessing the quality of the cut. Specimens nominally free of initial residual stress were chosen. Two materials were tested, a high yield strength mild steel (EN3B) and an austenitic stainless steel (304L). The form of the cut surfaces is presented and compared by means of graphical representations, alongside quantitative values of surface contour variations, magnitudes of inferred residual stresses and three

dimensional roughness measurements. The outcomes of this benchmark study are discussed in detail in chapter 3.

To achieve the second aim of the study, data analysis parameters were investigated by considering an idealised surface deformation profile and assessing how effectively the form of the profile is captured using different sets of measurement spacing and knot spacing intervals. The quality of fit was evaluated by calculating the error relative to the idealised profile. On the basis of this investigation, guidelines are provided to help contour method measurement practitioners select a suitable surface measurement density, knot spacing to smooth the deformation data and finite element mesh size for improving the spatial resolution of contour measurements.

Finally the developed advances in the contour method were implemented to measure residual stresses in case study welds:

- An electron beam welded plate made from modified P91 steel.
- An electron beam weld joining dissimilar metal plates (P91:304SS).
- A ferritic steel plate clad with layers of stainless steel.

Chapter 3 : Benchmark study to characterise the wire EDM contour cut

3.1 Introduction

The contour method involves cutting a specimen into two halves and provides a full cross-sectional map of the residual stress normal to the cut surface (33,148). The cutting process is the first and most important step of the contour method. Any error in this step can adversely affect all the subsequent steps of the method. Wire Electric Discharge Machining (WEDM) is the best choice cutting process for the contour method (5,35). Any deviation from the ideal contour cutting criteria (discussed in the section 2.6.1 of chapter 2), can cause inaccuracy and uncertainty in the contour stress results. Therefore, the most appropriate cutting conditions must be selected in order to minimise undesirable cutting effects and to obtain the best surface finish. To date, the extent, nature and causes of undesirable effects have not been fully investigated, and there is no commercial or published guidance available on how to select good cutting conditions for contour stress measurement. This chapter describes the tasks done in this project to address this deficiency in knowledge, including:

- Designing benchmark test specimens that are easy to manufacture and which are suitable for conducting a series of contour trial cuts on any WEDM machine to test the effects of changing process parameters.
- Investigate the quality of the contour cut surface and developing the criteria to characterise and quantify the quality of the cut surfaces.

- Designing experimental record (characteristic) sheets and identifying the most important parameters that are believed to have an influence on the quality of the cut surface.

This chapter also covers investigation of the following sub-areas:

- The issues arising from how the specimen is restrained during the cutting process.
- The reproducibility of a 'good' surface finish when using WEDMs.
- The merits of using different diameters of wires, based on a common wire material.
- Use of the standard factory set of cutting parameters for the best surface contour cut when using three different WEDMs: an Agie Charmilles FI 440 CCS EDM, a FANUC ROBOCUT α-OiB / OiB5 EDM, and a FANUC ROBOCUT α-C600iA EDM.
- The relative performance of the three WEDM machines in terms of giving the best surface cut, from a contour residual stress measurement point of view.

For this experimental evaluation, specimens nominally free of initial residual stress were chosen for several series of cutting trials. By performing a cut on stress-free material, the expected ideal cut surface should be perfectly flat. Any deviation from this can then be identified as an artefact of the WEDM cutting process (38). In this benchmark study, one sample thickness and two materials were tested. The two materials chosen were high yield strength mild steel (EN3B) and an austenitic stainless steel (304L), on the basis that they are widely used in

industrial applications. The form of the cut surfaces was presented and compared by means of graphical representations, alongside the quantitative values of surface contour variations, magnitudes of inferred residual stresses and three dimensional roughness measurements.

The work consisted of two broad experiments. The first experimental design included four series of cuts where the remote end of the specimen was clamped, and the end to be cut was left unclamped, hence *unrestrained* cutting conditions were used. Particular attention was given to maintaining the optimum control, and repeatability of the cutting conditions for each trial cut. In order to initiate the experiment, a standard set of WEDM cutting parameters (as recommended by the machine manufacturer) were used to perform the cuts without any manual intervention.

Following the results of the first experiment, a second experiment was designed, again with just the remote end of the specimen clamped. However for this experiment local constraint was provided at the ends of the specimen to be cut, hence this time *restrained* cutting conditions were used. This extra support, in the form of restraining ligaments of material, was provided at the start of the cuts, to help control the quality of the cuts, and to minimise the WEDM cutting artefacts found in results from the first experiment. This second experiment again included four series of cuts. Restraining ligaments of material were created by starting the cut from pilot holes located a small distance from one side of the test specimen. Two different ligament lengths were compared to see which offered the better restraint during cutting. In addition to this, some modifications were made in the setting of the WEDM cutting parameters based on previous cut results. The

second experiment also investigated the effect of wire diameter (two sizes) on the quality of the cut surfaces.

3.2 Test materials

The material specification for a high yield strength mild steel (EN3B) and an austenitic stainless steel (304L) are given in Table 3-1 and Table 3-2.

	C	Mn	S	P	Si	Cr	N
Mild Steel (En3B) – Wt.%	0.13-0.18	0.7-0.9	0.05	0.05	0.1-0.4	-	-
Stainless Steel (304L) – Wt.%	0.03	2	0.03	0.045	1	18-20	8 to 10.5

Table 3-1: The chemical composition for a high yield strength mild steel (EN3B) (150) and an austenitic stainless steel (304L) (151) - (remaining Fe - weight in percentage).

	Young's modulus (GPa)	Poisson's ratio	Yield strength (MPa)
Mild Steel (En3B)	210	0.3	370
Stainless Steel (304L)	180	0.3	241

Table 3-2: The material properties for the test materials at room temperature.

3.3 Specimen preparation

Each specimen was machined (using conventional cutting tools) into rectangular bars 245 mm long, 50 mm wide and 25 mm thick. Full details about specimen preparation are shown in *Figure 3-3*. The top and bottom surfaces of the

specimens were milled to get flat parallel sided surfaces to ensure "near perfect" flushing conditions, when bringing the WEDM flushing nozzles immediately adjacent to the specimen surfaces. The specimens were specifically designed to be fixed at one end, using M10 bolts fitted directly to the machine baseplate as illustrated in the photograph shown in *Figure 3-1.*

Figure 3-1: Photograph of the specimens

In order to eliminate machining stresses the specimens were stress relieved using appropriate heat treatments according to their material type. The mild steel (EN3B) specimens were placed in a vacuum furnace at 600 °C for about an hour. The stainless steel (304L) specimens were placed in a vacuum furnace at 1050°C for about an hour, and then air cooled.

In order to make sure they were close to a nominal stress-free state after heat treatment, the surface residual stresses were measured on the mild steel specimens (the surface residual stresses could not be measured on the stainless steel specimens due to limitation of the used instrument) using an XSTRESS 3000 X-ray diffractometer (Stresstech Oy, VALAKOSKI, Finland), fitted with a 3 mm

diameter collimator. The X-ray radiation source was Cr K-α, with a wavelength of 2.2897 Å at 270 W power and 10 mA current. The position of the peak arising from the {211} diffracting plane was at a 2θ angle of approximately 156.1°. The $\sin^2\psi$ technique (152) was applied using 10 scans with a range of - 45° ≤ ψ ≤ 45° psi angles, in order to determine the error margins for each stress measurement. These measurements were conducted for ten points on the top and back face of the specimens, along the plane of each cut. *Figure 3-2* shows the specimen being measured for surface residual stresses, using X-ray diffraction. The surface residual stress measurements showed compressive and tensile stresses within a range of 15 to 20 MPa for the mild steel specimens. It suggested that the mild steel specimens did not contain any surface residual stresses large enough to affect the quality of the cut surfaces.

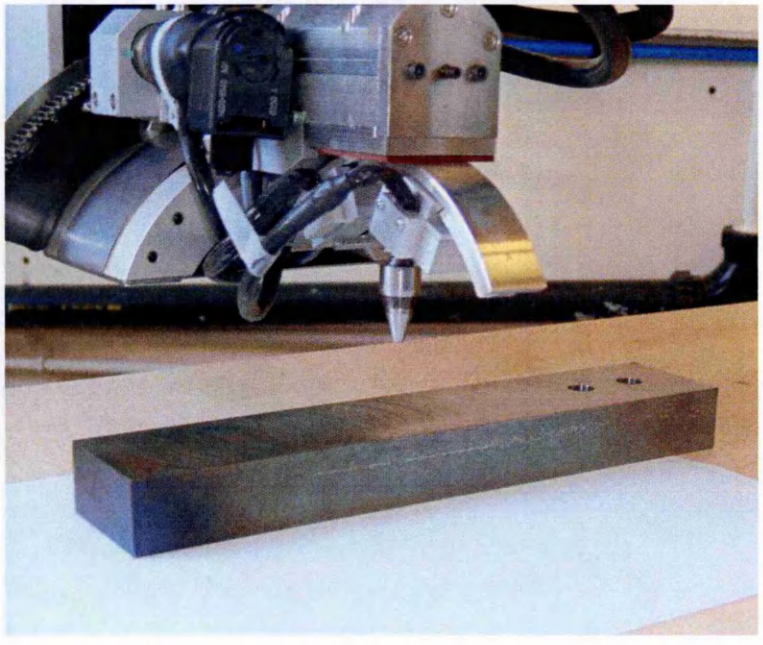

Figure 3-2: Specimen being measured for the surface residual stresses using X-ray diffraction.

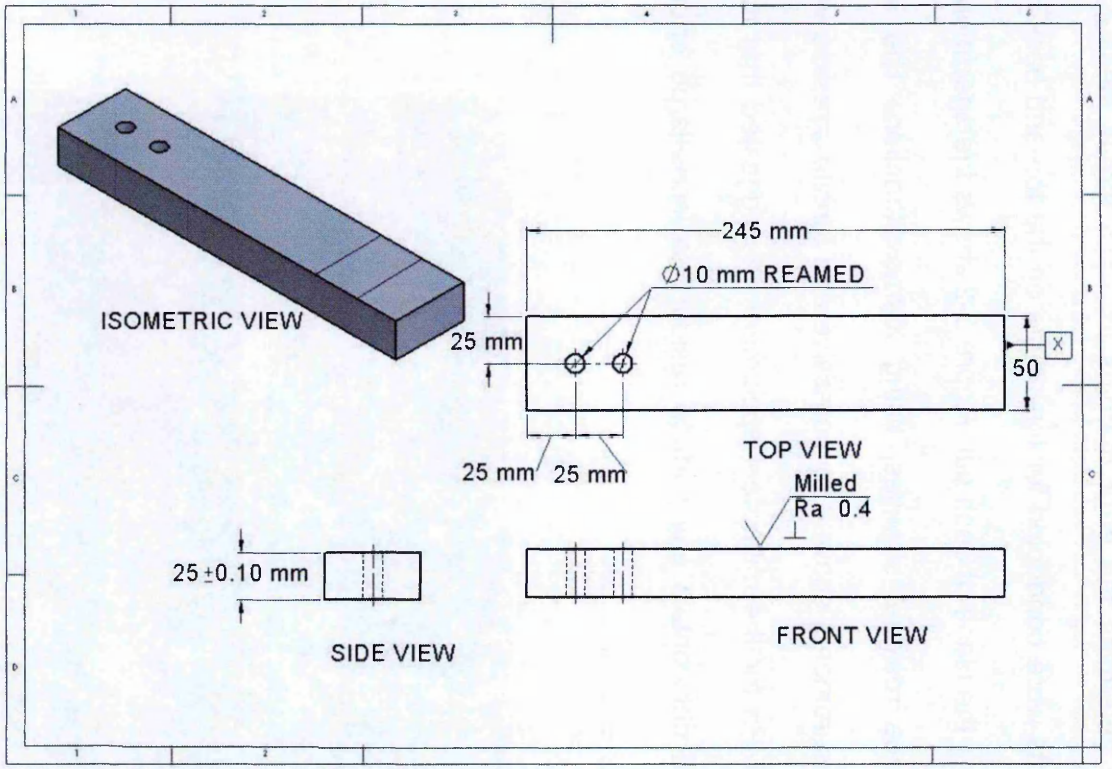

Figure 3-3: Illustrates the details of specimen preparations.

3.4 Experimental conditions

Transverse cuts were made using 50 mm wide specimens (therefore having 25 mm thick Z-axis cuts). As described in section 3.3, two M10 bolts were used to fix the specimens directly to the machine baseplate. The bottom face of each specimen was laid in line with the top surface plane of the baseplate, so that optimum alignment of the bottom flushing nozzles was ensured. The material used for the wire was standard brass. Both flushing nozzles were placed within 0.2 mm of the specimens' surfaces (the clearances were measured and adjusted using feeler gauges). The WEDM bath temperature was maintained at 20 °C. A flushing pressure of 14 bar / 1.4 MPa was used as a default setting. Prior to the cut, the specimens were allowed to reach thermal equilibrium with the deionised water in the EDM tank. After EDM cutting, the cut pieces were removed immediately from the tank to minimise the risk of corrosion.

3.5 Referencing and cataloguing of the cut samples

Unique names were assigned to each specimen and each cut surface. For example, the first cut of the first series (on the mild steel specimen) was named as "MS-A-1", where 'MS' represents material of the specimen, 'A' represents the bar reference letter, and '1' represents the number of the cut. Furthermore, the surfaces of the cut were specified as RS (right side) and LS (left side). Hence, the two examples for the designations are shown here as MS-A-1-RS and MS-A-1-LS respectively. Table 3-3 gives details of all the trial WEDM contour cuts performed.

	No.	Cut ID	Specimen Material	Specimen number	Cut number	Cut description
Unrestrained cuts	1	MS-A-1	MS	A	1	Cut on mild steel-Agie
	2	MS-A-2	MS	A	2	Repeat cut-Agie
	3	MS-A-3	MS	A	3	Cut in opposite direction-Agie
	4	MS-B-1	MS	B	1	Cut on mild steel-Fanuc1
	5	MS-B-2	MS	B	2	Repeat cut-Fanuc1
	6	SS-A-1	SS	A	1	Cut on stainless steel-Agie
	7	SS-A-2	SS	A	2	Repeat cut-Agie
	8	SS-B-1	SS	B	1	Cut on stainless steel-Fanuc2
	9	SS-B-2	SS	B	2	Repeat cut-Fanuc2
Restrained cuts	1	MS-C-1	MS	C	1	Cut on mild steel-Agie-S5
	2	MS-C-2	MS	C	2	Cut on mild steel-Agie-S3 A=0.2, TAC=0.1
	3	MS-C-3	MS	C	3	Cut on mild steel-Agie-S3 A=0.1, TAC=0.05
	4	SS-C-1	SS	C	1	Cut on stainless steel-Agie-S5
	5	SS-C-2	SS	C	2	Cut on stainless steel-Agie-S3 A=0.2, TAC=0.1
	6	SS-C-3	SS	C	3	Cut on stainless steel-Agie-S3 A=0.1, TAC=0.05
	7	MS-B-4	MS	B	4	Cut on mild steel-Agie-S5 5 mm ligament length
	8	MS-C-4	MS	C	4	Cut on mild steel-Agie-S5 Similar stiffness
	9	SS-A-5	SS	A	5	Cut on stainless steel-Agie-S5 5 mm ligament length
	10	SS-C-4	SS	C	4	Cut on stainless steel-Agie-S5 Similar stiffness

Table 3-3: Details of all the WEDM trial contour cuts performed in this study.

3.6 Cleaning of the cut surfaces

The cut surfaces were inspected by eye, and on a low magnification microscope to try to identify any defects such as step changes caused by inclusions during WEDM cutting. Then, the cut surfaces were cleaned using a rubber eraser and an air duster.

3.7 Measurement of the cut surfaces

3.7.1 3D displacement measurements

The cut parts were left in a temperature-controlled metrology laboratory for a minimum of six hours to reach thermal equilibrium with the laboratory environment. The three dimensional (3D) topography of each surface cut was measured using a Mitutoyo Crysta plus 547 CMM fitted with a 3 mm diameter Renishaw PH10M touch trigger probe. The three spatial coordinates of each point, on a 0.5 mm square grid pattern on the cut surfaces were measured. The perimeters of the surfaces were also measured, for use in FE modelling.

3.7.2 3D roughness measurements

Three dimensional (3D) surface roughness measurements were taken over both mating surfaces of each cut, using a confocal microscope. Roughness parameters, S_q (the root-mean-square), S_a (the arithmetic mean) of the absolute height, and RSm (the mean width of the roughness profile element), were used in the analysis. These parameters are universally recognised and widely used (136). These measurements were conducted over 8 mm square patches, in nine specific

locations on each cut surface. The locations of all the 8 mm square patches are identified in *Figure 3-4*. The mean values of each of the three roughness parameters were calculated for each cut surface. This procedure for the 3D roughness measurements was performed for the first five cuts. Each cut surface had very similar roughness values over an 8 mm patch, in the nine specific locations. Therefore, for simplicity, the roughness measurements were performed only for centre patch for all remaining cuts.

3.8 Surface evaluation criteria

Each cut surface was evaluated on the basis of the following criteria:

- Whole surface topography of both parts of the cuts was examined using 3D mapping methods, in order to get an overall assessment for the quality of the cut, and to identify any symmetric features.
- The 'contour' surface profiles for each individual cut part, and the averaged displacements of both mating surfaces, were analysed using 'thick' line profiles. For each thick line profile, five displacement measurement line profiles were extracted across a 2 mm width. The mean values of the five measurement points were then calculated. Displacement values for the thick line profiles were extracted along the wire direction, and along the cutting direction, at the positions of X_{ST}, X_0, X_{FN} and Z_{EN}, Z_0, Z_{EX} respectively. The thick line profile designations (X_{ST}, X_0, X_{FN} and Z_{EN}, Z_0, Z_{EX}), and their locations, are defined in *Figure 3-4*. Where, ST and FN represent the cut start and finish positions, and EN and EX represent wire entry and exist positions.

The maximum and minimum displacement values along the X_0 and Z_0 thick line profiles were considered, so that the maximum and minimum height variations of the contour profiles could be calculated.

- The 3D surface roughness parameters, S_q , S_a and RSm, metrics at the defined reference positions, were recorded for each part of the cut surfaces. The details about the locations for taking the measurements on the cut parts are given in *Figure 3-4.*

3D linear elastic FE analyses for average displacement data points, using the ABAQUS FE code, were performed in order to estimate apparent stresses associated with the cut that would contribute to a contour measurement. For building the 3D model, one half of the cut was built first, by extruding the measurements of the perimeters of that half of the cut. For the stress analyses of each cut surface, the cut face was meshed with 0.5 mm × 0.5 mm linear hexahedral elements (type C3D8R). The averaged topographic measurements for each cut were inverted with respect to the height (Y) coordinate, and these data were used as the boundary conditions in the FE model. Finally, elastic FE analyses were performed to obtain the stress distribution associated with the cut. This map was used to assess the errors in stress across the cut surface introduced by the cutting process. In order to understand it clearly, only three colours were chosen within the range of ±20% of yield strength to represent the stress map and the exceeding values from the range were represented in black and grey colours. The stress values exceeding from ±20% of yield strength were of concern, and were minimised in order to make a good quality of the contour cut.

- The stress maps for each cut were analysed using thick stress line profiles in the same way as was used for the contour maps.
- The root mean square (RMS) deviation for both the displacement and the stress data points were calculated to quantify the RMS variations for each cut.

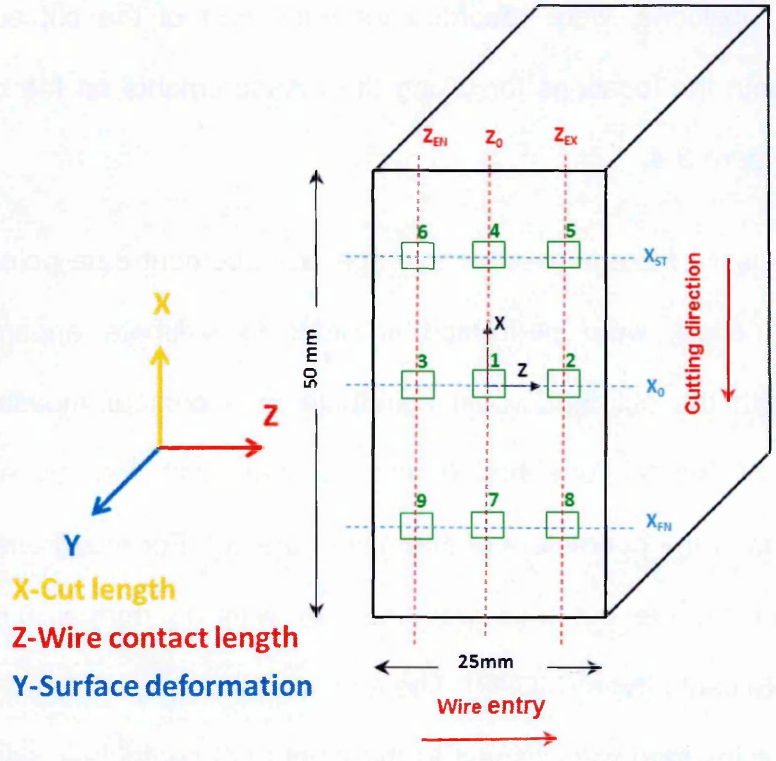

Figure 3-4: Shows the positions of lines (X_{FN}, X_0, X_{ST} along the thickness of the specimen and Z_{EN}, Z_0, Z_{EX} along the cut length) and also shows nine different locations for 3D roughness measurements (8 mm square area was considered for the each patch) on the cut parts, X-axis 'cutting direction', Y-axis 'out of plane', Z-axis in the direction of wire feed. The origin is at the centre of the block.

For brevity and clarity, and to differentiate between the two surfaces that are created during each cutting operation, the following terminology is introduced. The

cut surface that is part of the remaining portion of material, still clamped to the WEDM machine after the cut has been completed, is referred to as the *clamped side* of the cut; the other surface, which is now on the piece of material removed from the specimen, is referred to as the *free side* of the cut.

3.9 Layout of the characteristic sheet

In this study sequential trial cuts were performed and the quality of the cuts were characterised and quantified using the approach described in section 3.8. All of this information was then gathered in one place and summarised in the form of an experimental record (characteristic) sheet for each cut. An example is given in *Figure 3-7*.

The characteristic sheets contained the following information

Specimen details; information about specimen material type, reference number and the location of the cut.

WEDM cutting information; information about the WEDM cutting details such as machine type, wire diameter and material type, cutting conditions and WEDM cutting parameters, see Appendix A.

Metrology information; details about the cut surface measurements such as the instrument specification and its parameters.

Cut surface results; surface quality results which include displacement profiles for both sides of the cut, the averaged displacement profile, stress profile,

and two dimensional displacement and stress maps. These results are also mentioned in the 'surface quality metrics' (table) in numerals.

3.10 The first experiment - unrestrained cutting conditions

The first experiment involved making cuts on two different materials: high yield strength mild steel (EN3B); and austenitic stainless steel (304L), each with unrestrained cutting conditions.

3.10.1 Cutting strategy

Rectangular specimens with dimensions 245 mm long, 50 mm wide and 25 mm thick, were used for the experiment. The cuts were undertaken with a cut length of up to 50 mm and a wire contact length of 25 mm.

Details about the cutting strategy for the unrestrained cuts are shown in *Figure* 3-5. The cuts were conducted on three different WEDM cutting machines, installed at the Materials Engineering Laboratory of the Open University, using a standard wire diameter of 0.25 mm. The machine manufacturers' recommended cutting parameters were used (without any manual intervention).

The first experiment comprised four series of cuts. During EDM cutting, one end of the specimen was clamped, whilst 25 mm thick slices were removed from the free end. Each new cut was positioned 25 mm away from the previous cut plane, in order to maintain the surface finish quality and surface integrity of each surface, and to prevent one cut from influencing another. *Figure 3-6* shows annotated photographs of various stages of the first experiment.

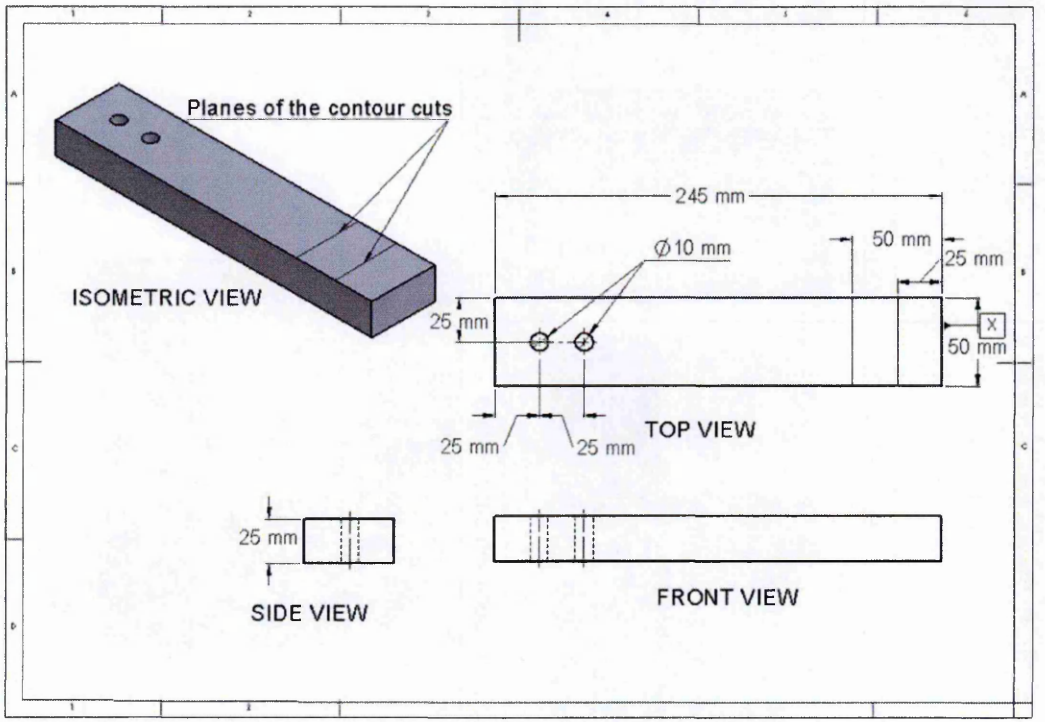

Figure 3-5: Represents the details about the cutting strategy were adopted for unrestrained cuts.

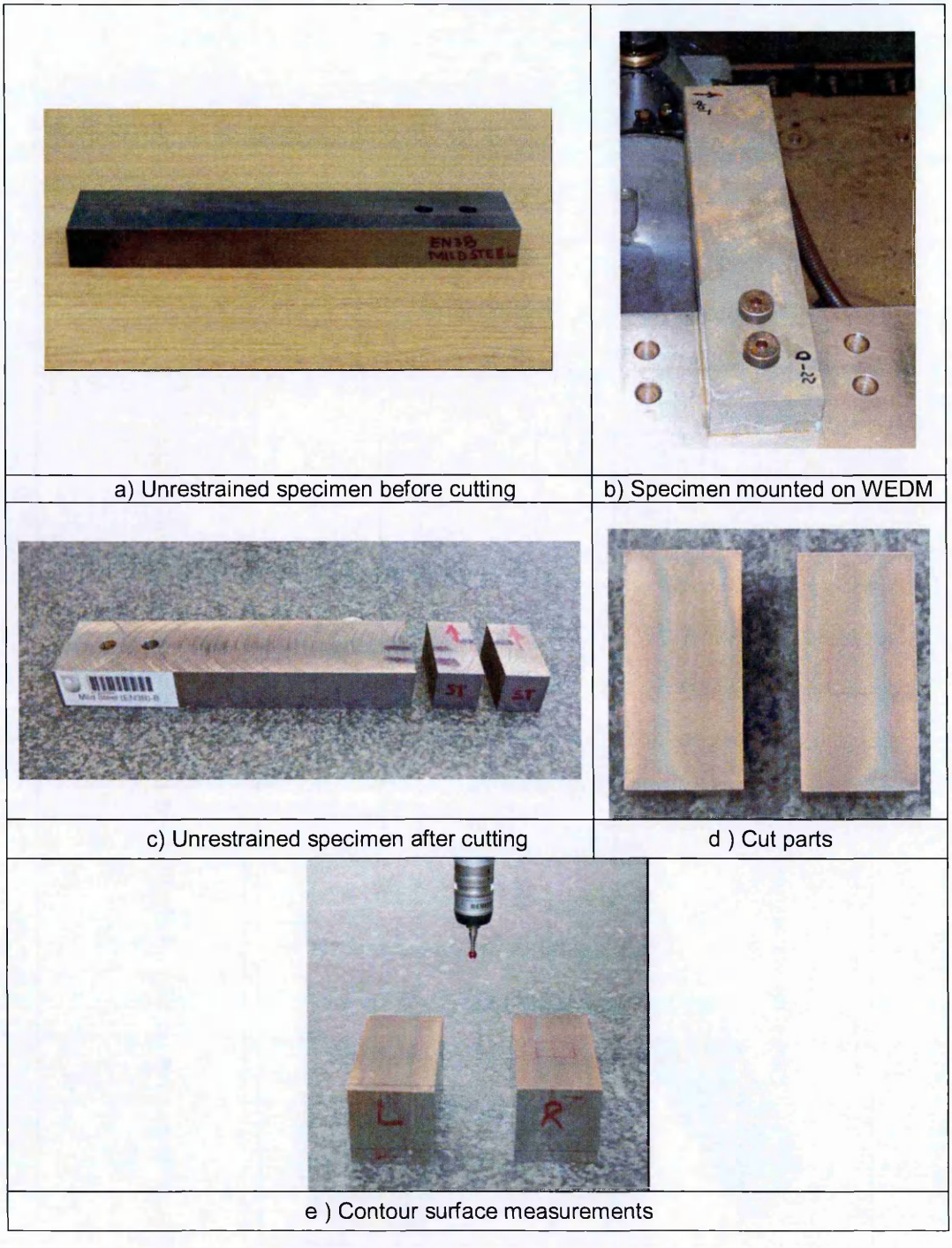

a) Unrestrained specimen before cutting

b) Specimen mounted on WEDM

c) Unrestrained specimen after cutting

d) Cut parts

e) Contour surface measurements

Figure 3-6: Photographs showing various stages of the first experiment.

3.10.2 Methodology for the first experiment

Unrestrained cuts – series 1

This series of cuts was performed on a benchmark mild steel specimen named as MS-A, using an Agie Charmilles FI 440 CCS WEDM. The following three cuts were carried out:

- The first cut was performed using a standard set of WEDM cutting parameters (designated S5 on the machine), with a 0.25 mm WEDM wire diameter. There was no manual intervention.
- The second cut was performed as a repeat of the first cut, using all the same cutting conditions, as a means of measuring the repeatability of the process.
- The third cut was performed with the cutting wire moving in the opposite direction to the first cut. All the other cutting conditions were a repeat of those used on the first cut. This cut was performed in order to explore the effect of electro-magnetic forces during cutting.

Unrestrained cuts – series 2

The second series of unrestrained cuts was performed on the same benchmark mild steel material, but on a different specimen than the first, this time named as MS-B. This specimen differs from the first series, in that the cuts were carried out using a FANUC ROBOCUT α-OiB / OiB5 WEDM. Two cuts were made:

- The first cut was performed using a standard set of WEDM cutting parameters (designated C1 on the machine), using a 0.25 mm WEDM wire diameter.

- The second cut was performed as a repeat of the first, using all the same cutting conditions as the first cut, as a means of measuring the repeatability of the process.

Unrestrained cuts – series 3

The third series of the first experiment was performed on a benchmark stainless steel (304L) specimen, named as SS-A. These cuts were performed using the Agie Charmilles WEDM. Two cuts were made:

- The first cut was performed using a standard set of WEDM cutting parameters (designated S5 on the machine) using a 0.25 mm WEDM wire diameter. There was no manual intervention.
- The second cut was performed as a repeat of the first, using all the same cutting conditions, as a means of measuring the repeatability of the process.

Unrestrained cuts – series 4

The fourth series of unrestrained cuts was performed on the same benchmark stainless steel (304L) material as before, but on a different specimen, this time named as SS-B. These cuts differed from series 3 in that they were made using a FANUC ROBOCUT α-C600iA WEDM. Two cuts were made:

- The first cut was performed using a standard set of the WEDM cutting parameters (designated C1 on the machine) using a 0.25 mm WEDM wire diameter.

- The second cut was performed as a repeat of the first, using all the same cutting conditions as the first cut, as a means of measuring the repeatability of the process.

3.10.3 Results of the first experiment for unrestrained cuts

During the first experiment, all unrestrained cuts were performed with the intention to evaluate the quality of the cut from a contour measurement point of view. The quality of the cuts was assessed by comparing selected characteristics of both clamped and free sides of the cuts, based on relevant measurements and calculations. Characterisation sheets represent in *Figure 3-7* to *Figure 3-15*, capture salient features of the unrestrained cuts on the benchmark mild steel and stainless steel specimens.

Specimen details							
Specimen reference				MS-A-1			
Specimen material				Mild Steel (EN3B)			
Cut length, m, thickness, n				(50 x 25) mm			
Cantilever dimensions, p, q				(25 x 195) mm			
Specimen top and bottom surfaces were milled flat surfaces. Vacuum heat treatment performed to relieve internal stresses.							
WEDM information							
Cut date				31st July, 2013			
Machine type				Agie Charmillies FI440ccS			
Wire material				Brass (LT25.WIR)			
Wire diameter				0.25 mm			
Cutting technology				LT25A.TEC			
WEDM bath temperature				20 °C			
Nozzles position, pressure				0.2 mm, 1.4 MPa			
The cut was performed with a standard S5 set of parameters and no manual intervention							
WEDM cutting parameters							
EL	10	PA	6	PM	3	Offset	0.16
ST	1	M	3	S	10	V	80
FF	100	B	7	A	0.6	TAC	0.3
Aj	41	S	10	WS	12	WB	1.6
Inj	14	Rate	3.5	IAL	10		
Metrology information							
CMM				Mitutoyo Crysta plus 547 CMM			
Spacing		(0.5 x 0.5) mm		**Probe dia.**		3 mm	
Roughness instrument				Leica 3DCM			
Resolution		12		**Overlap area**		10%	
Threshold		10 %		**Z-Scan value**		200 µm	

Cut MS-A-1 was performed on a mild steel sample with a standard S5 set of parameters using Agie machine.

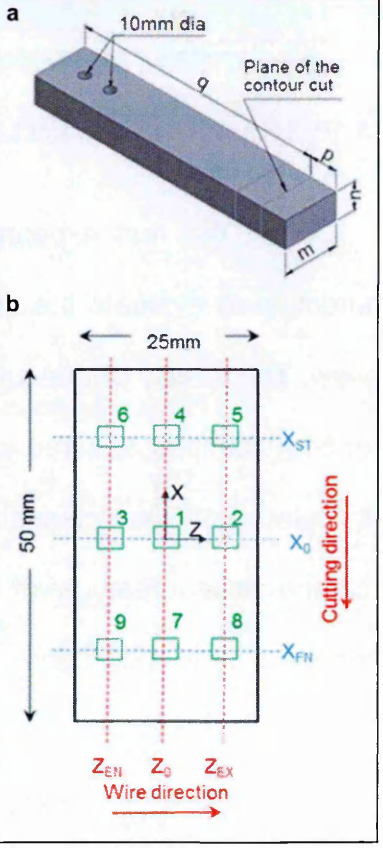

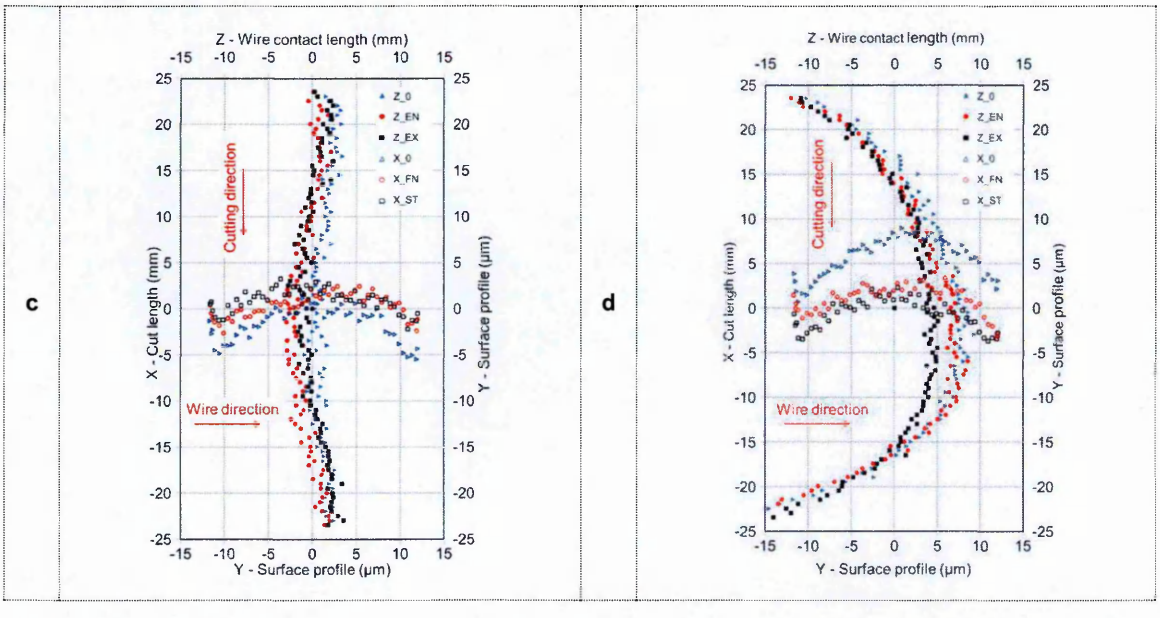

Figure 3-7: The MS-A-1 cut surface data and displacement profiles for clamped (c) and free sides (d).

Surface quality metrics				
	X (cutting direction)	Z (wire direction)	X (cutting direction)	Z (wire direction)
	Clamped side displacement, Fig c, µm		Free side displacement, Fig d, µm	
Min	-1.0	-5.5	-17.0	1.0
Max	3.5	2.0	9.0	10.0
Rsm	130	150	110.0	130.0
Sq, Sa	3.4 ±0.16, 2.6 ±0.08		3.7 ±0.44, 2.9 ±0.39	
	Averaged displacement, Figs e and g, µm		Stress error, Figs f and h, MPa (%yield)	
Min	-8.0	-2.0	-66.0 (18.0)	-69.0 (19.0)
Max	5.0	5.0	124.0 (34.0)	106.0 (28.0)
RMS	3.0		59 (16)	

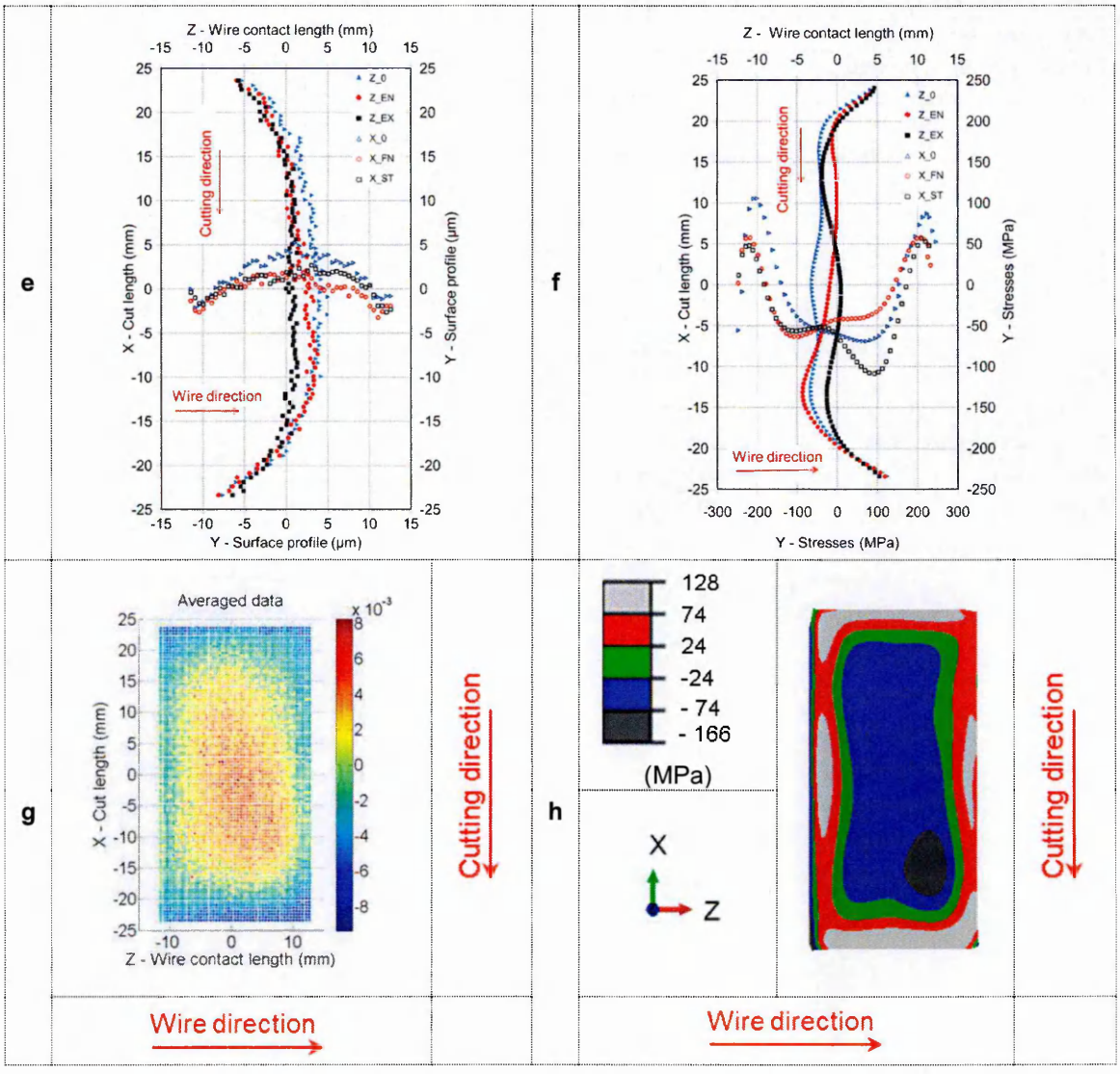

Figure 3-7 cont: The MS-A-1 cut surface quality metrics, profiles of averaged displacement (e) and stress (f), maps of averaged displacement (g) and stress (h).

Specimen details							
Specimen reference			MS-A-2				
Specimen material			Mild Steel (EN3B)				
Cut length, m, thickness, n			(50 x 25) mm				
Cantilever dimensions, p, q			(25 x 170) mm				
Specimen top and bottom surfaces were milled flat surfaces. Vacuum heat treatment performed to relieve internal stresses.							
WEDM information							
Cut date			31st July, 2013				
Machine type			Agie Charmillies FI440ccS				
Wire material			Brass (LT25.WIR)				
Wire diameter			0.25 mm				
Cutting technology			LT25A.TEC				
WEDM bath temperature			20 °C				
Nozzles position, pressure			0.2 mm, 1.4 MPa				
The cut was performed with a standard S5 set of parameters and no manual intervention							
WEDM cutting parameters							
EL	10	PA	6	PM	3	Offset	0.16
ST	1	M	3	S	10	V	80
FF	100	B	7	A	0.6	TAC	0.3
Aj	41	S	10	WS	12	WB	1.6
Inj	14	Rate	3.5	IAL	10		
Metrology information							
CMM			Mitutoyo Crysta plus 547 CMM				
Spacing		(0.5 x 0.5) mm	**Probe dia.**		3 mm		
Roughness instrument			Leica 3DCM				
Resolution		12	**Overlap area**		10%		
Threshold		10 %	**Z-Scan value**		200 µm		

Cut MS-A-2 was performed on a mild steel sample as a repeated cut of MS-A-1.

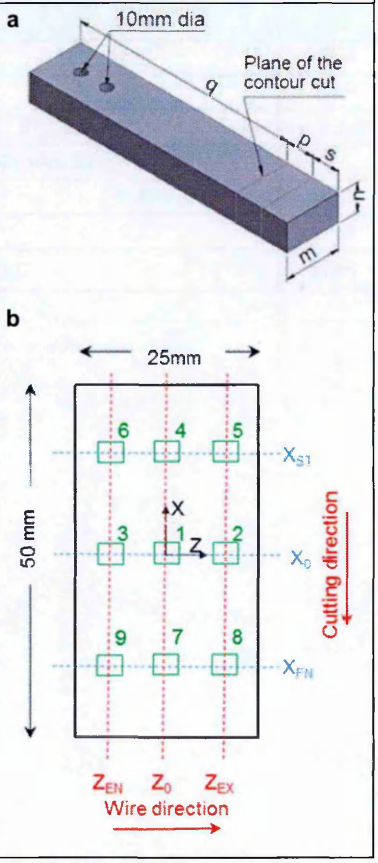

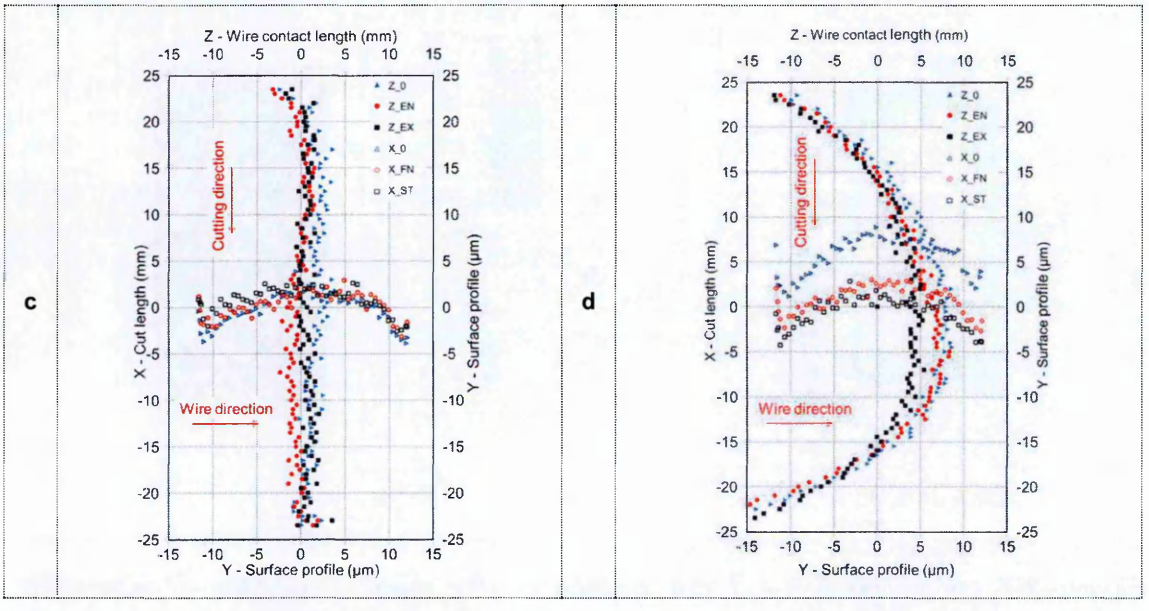

Figure 3-8: The MS-A-2 cut surfac data and displacement profiles for clamped (c) and free sides (d).

Surface quality metrics				
	X (cutting direction)	Z (wire direction)	X (cutting direction)	Z (wire direction)
	Clamped side displacement, Fig c, µm		Free side displacement, Fig d, µm	
Min	-2.5	-4.0	-17.0	1.0
Max	3.5	4.0	9.0	9.0
Rsm	130	150	120.0	130.0
Sq, Sa	3.3, 2.6		3.4 ±0.20, 2.6 ±0.16	
	Averaged displacement, Figs e and g, µm		Stress error, Figs f and h, MPa (%yield)	
Min	-9.0	-1.0	-76.0 (21.0)	-69.0 (18.0)
Max	5.0	6.0	119.0 (32.0)	91.0 (25.0)
RMS	3.6		60.0 (16.0)	

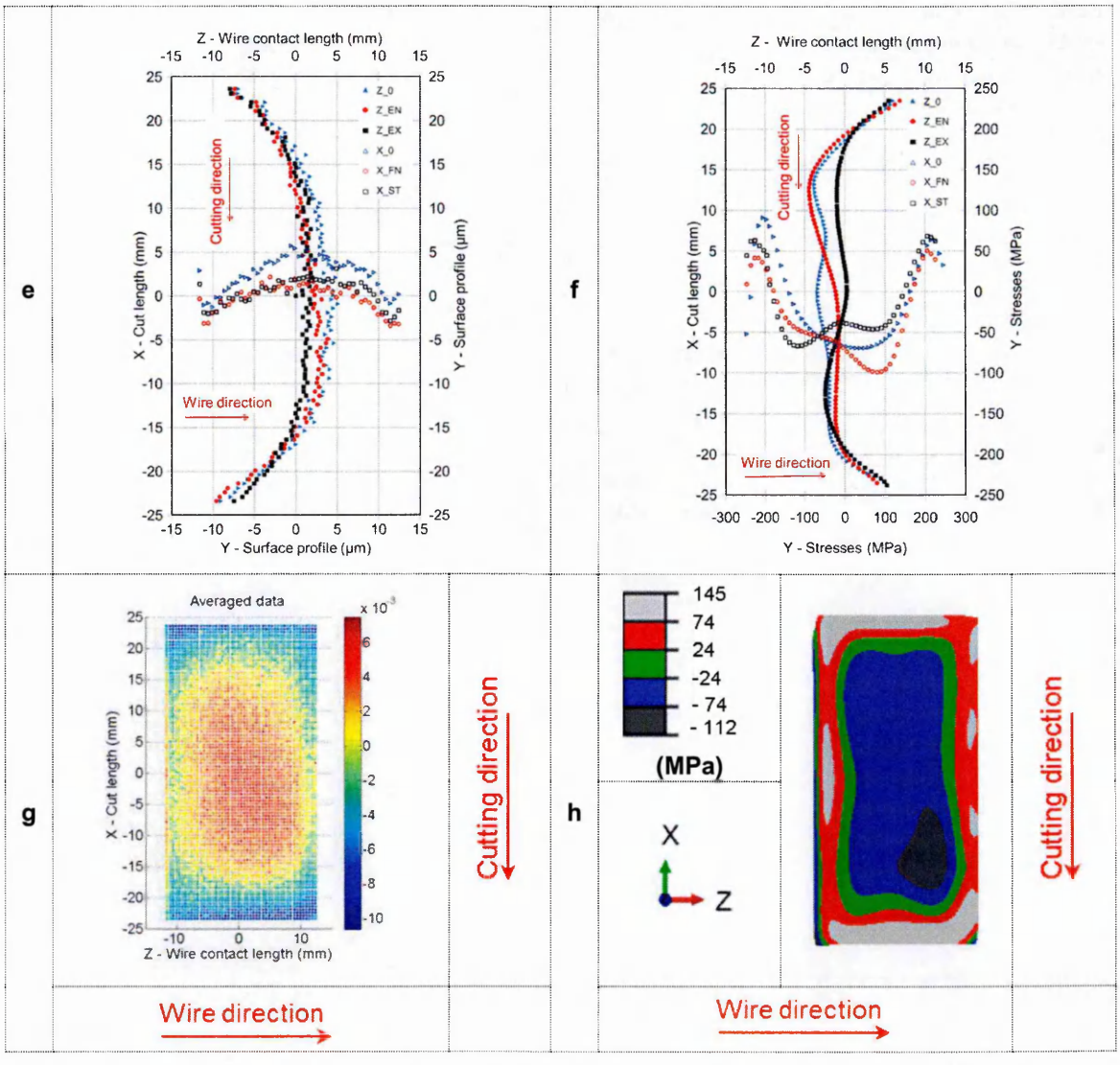

Figure 3-8 cont.: The MS-A-2 cut surface quality metrics, profiles of averaged displacement (e) and stress (f), maps of averaged displacement (g) and stress (h).

Specimen details							
Specimen reference				MS-A-3			
Specimen material				Mild Steel (EN3B)			
Cut length, m, thickness, n				(50 x 25) mm			
Cantilever dimensions, p, q				(25 x 119) mm			
Specimen top and bottom surfaces were milled flat surfaces. Vacuum heat treatment performed to relieve internal stresses.							
WEDM information							
Cut date				12^{th} Dec, 2013			
Machine type				Agie Charmillies FI440ccS			
Wire material				Brass (LT25.WIR)			
Wire diameter				0.25 mm			
Cutting technology				LT25A.TEC			
WEDM bath temperature				20 °C			
Nozzles position, pressure				0.2 mm, 1.4 MPa			
The cut was performed with a standard S5 set of parameters and no manual intervention							
WEDM cutting parameters							
EL	10	PA	6	PM	3	Offset	0.16
ST	1	M	3	S	10	V	80
FF	100	B	7	A	0.6	TAC	0.3
Aj	41	S	10	WS	12	WB	1.6
Inj	14	Rate	3.5	IAL	10		
Metrology information							
CMM				Mitutoyo Crysta plus 547 CMM			
Spacing		(0.5 x 0.5) mm		**Probe dia.**		3 mm	
Roughness instrument				Leica 3DCM			
Resolution		12		**Overlap area**		10%	
Threshold		10 %		**Z-Scan value**		200 µm	

Cut MS-A-3 was performed in the opposit direction to the MS-A-1 cut.

a

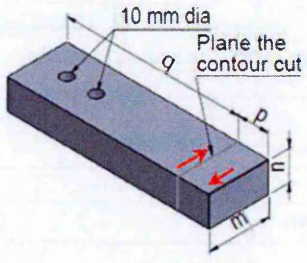

b

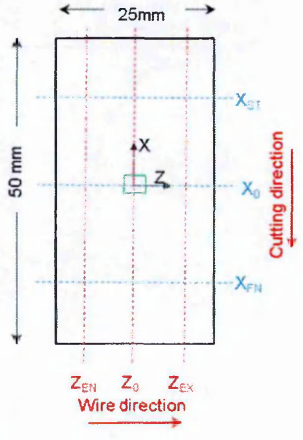

c

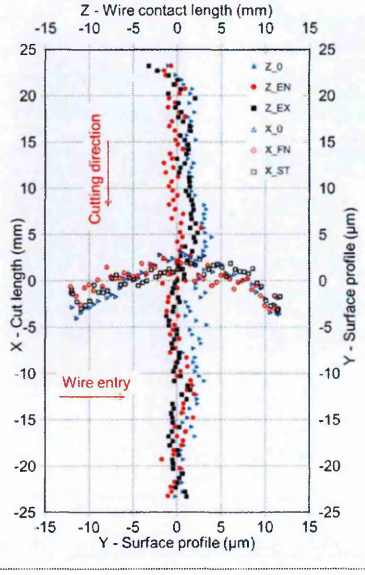

d

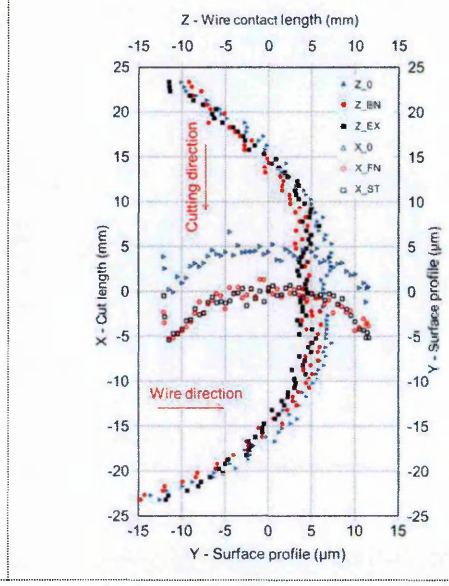

Figure 3-9: The MS-A-3 cut surface data and displacement profiles for clamped (c) and free sides (d).

Surface quality metrics				
	X (cutting direction)	Z (wire direction)	X (cutting direction)	Z (wire direction)
	Clamped side displacement, Fig c, µm		Free side displacement, Fig d, µm	
Min	-2.0	-4.0	-13.6	-1.0
Max	4.0	3.0	7.3	7.0
Rsm	145.0	130.0	126.0	134.0
Sq, Sa	3.3, 2.5		3.3, 2.5	
	Averaged displacement, Figs e and g, µm		Stress error, Figs f and h, MPa (%yield)	
Min	-6.0	-2.0	-77.0 (21.0)	-55.0 (15.0)
Max	5.0	5.0	97.0 (26.0)	104.0 (28.0)
RMS	3.5		55.5 (15.0)	

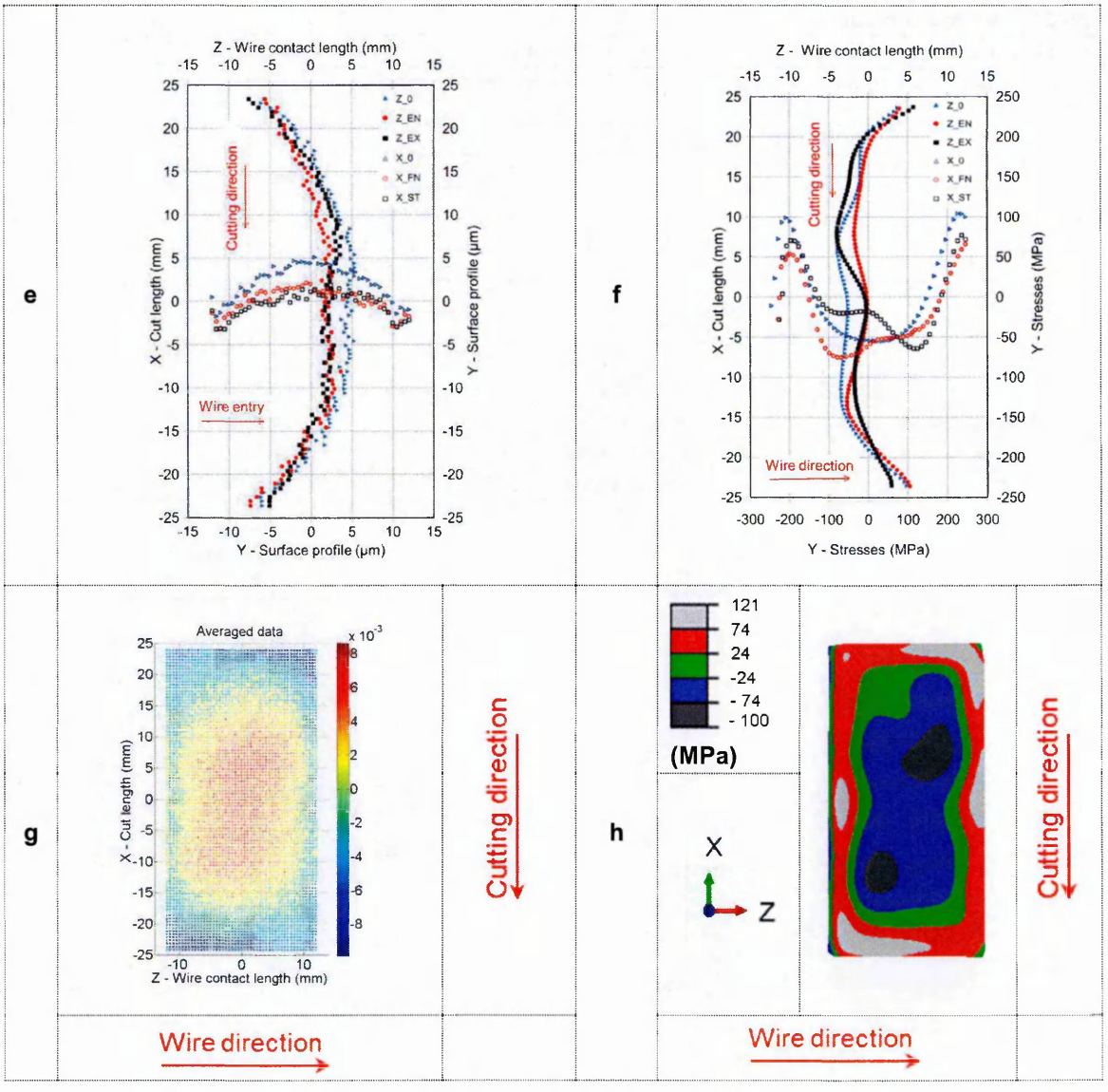

Figure 3-9 cont: The MS-A-3 cut surface quality metrics, profiles of averaged displacement (e) and stress (f), maps of averaged displacement (g) and stress (h).

Specimen details							
Specimen reference			MS-B-1				
Specimen material			Mild Steel (EN3B)				
Cut length, m, thickness, n			(50 x 25) mm				
Cantilever dimensions, p, q			(25 x 220) mm				
Specimen top and bottom surfaces were milled flat surfaces. Vacuum heat treatment performed to relieve internal stresses.							
WEDM information							
Cut date			14th Aug, 2013				
Machine type			Fanuc OiB5 EDM				
Wire material			Brass (LT25.WIR)				
Wire diameter			0.25 mm				
Cutting technology			LT25A.TEC				
WEDM bath temperature			20 °C				
Nozzles position, pressure			0.2 mm, 1.4 MPa				
The cut was performed with a standard C1 set of parameters and no manual intervention.							
WEDM cutting parameters							
PM	1	WP1A	6	FC	0		
VS	1	WP2A	2	SPD	3.23		
VM	6	T	1700	OVR	100		
OFF	14.4	WF	10				
SV	30	FR	10				
Metrology information							
CMM			Mitutoyo Crysta plus 547 CMM				
Spacing	(0.5 x 0.5) mm		**Probe dia.**	3 mm			
Roughness instrument			Leica 3DCM				
Resolution	12		**Overlap area**	10%			
Threshold	10 %		**Z-Scan value**	200 µm			

Cut MS-B-1 was performed on a mild steel sample with a standard C1 set of parameters using Fanuc1 WEDM.

a

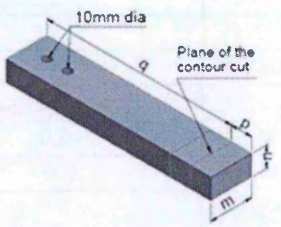

b

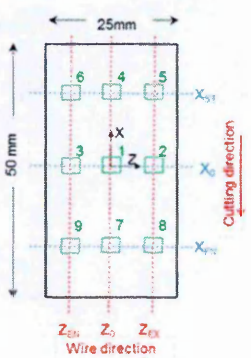

c

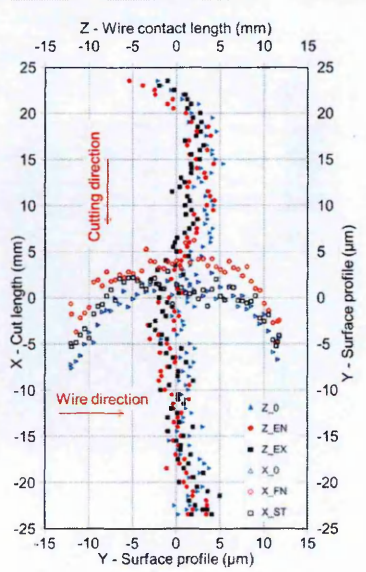

d

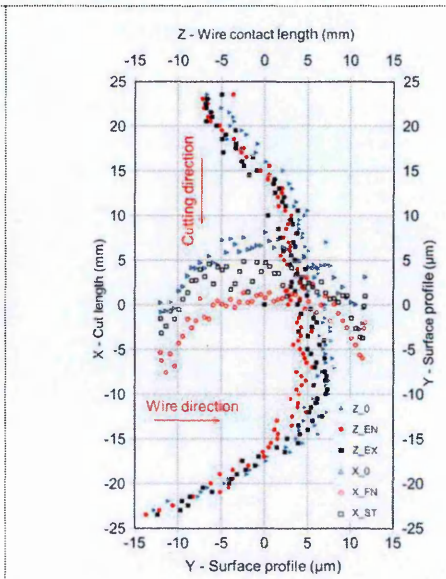

Figure 3-10: The MS-B-1 cut surface data and displacement profiles for clamped (c) and free sides (d).

Surface quality metrics				
	X (cutting direction)	Z (wire direction)	X (cutting direction)	Z (wire direction)
	Clamped side displacement, Fig c, µm		Free side displacement, Fig d, µm	
Min	-2.0	-7.5	-13.5	-3.0
Max	5.0	3.0	8.5	8.0
Rsm	150.0	140.0	135.0	150.0
Sq, Sa	4.5 ±0.11, 3.5 ±0.10		4.6 ±0.22, 3.6 ±0.19	
	Averaged displacement, Figs e and g, µm		Stress error, Figs f and h, MPa (%yield)	
Min	-7.0	-4.5	-52.0 (14)	-63.5 (17)
Max	5.0	4.5	153.0 (41)	157 (42)
SRMS	3.3		71 (19)	

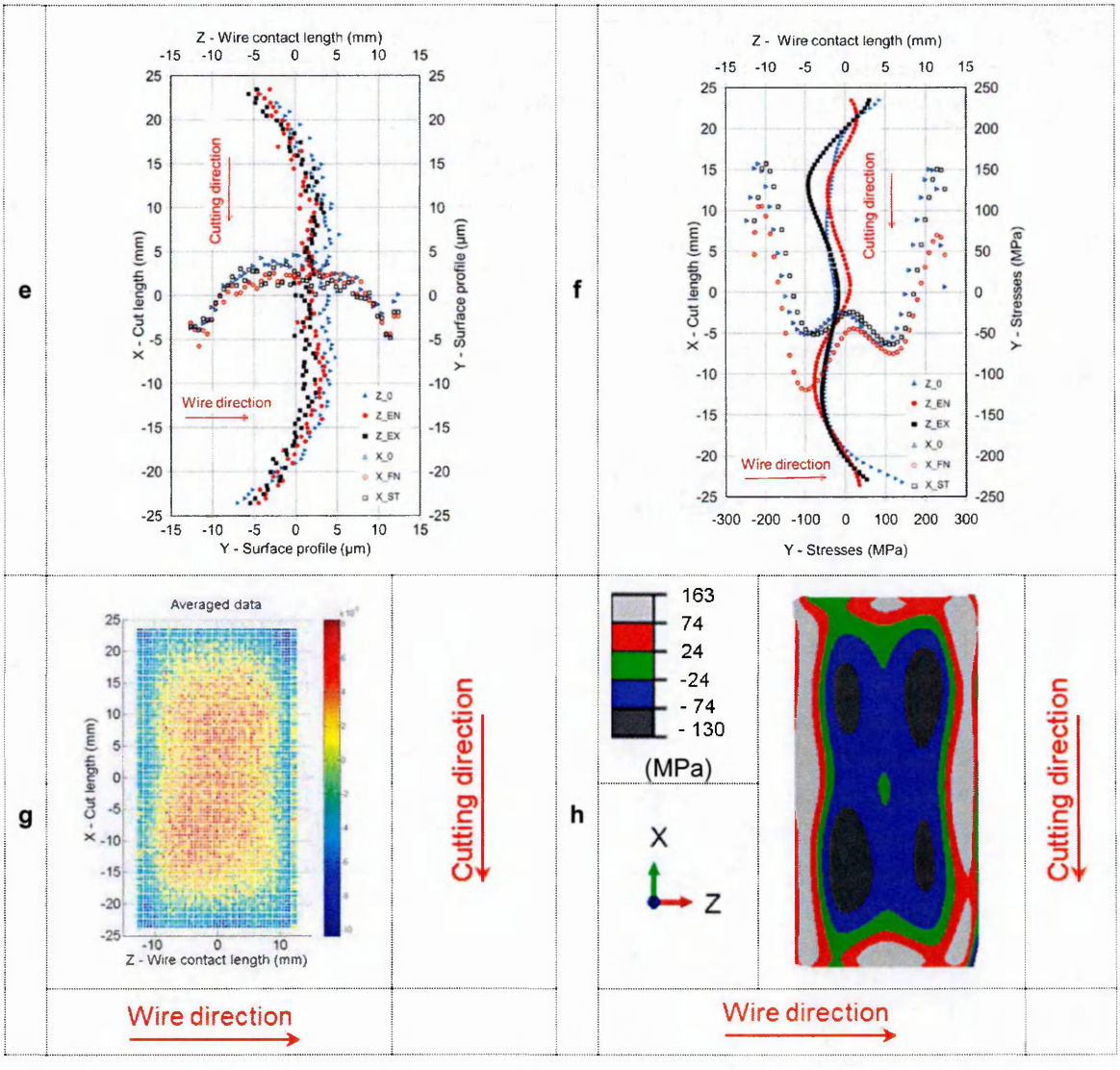

Figure 3-10 cont: The MS-B-1 cut surface quality metrics, profiles of averaged displacement (e) and stress (f), maps of averaged displacement (g) and stress (h).

Specimen details							
Specimen reference	MS-B-2						
Specimen material	Mild Steel (EN3B)						
Cut length, m, thickness, n	(50 x 25) mm						
Cantilever dimensions, p, q	(25 x 195) mm						
Specimen top and bottom surfaces were milled flat surfaces. Vacuum heat treatment performed to relieve internal stresses.							
WEDM information							
Cut date	14th Aug, 2013						
Machine type	Fanuc OiB5 EDM						
Wire material	Brass (LT25.WIR)						
Wire diameter	0.25 mm						
Cutting technology	LT25A.TEC						
WEDM bath temperature	20 °C						
Nozzles position, pressure	0.2 mm, 1.4 MPa						
The cut was performed with a standard C1 set of parameters and no manual intervention.							
WEDM cutting parameters							
PM	1	WP1A	6	FC	0		
VS	1	WP2A	2	SPD	3.23		
VM	6	T	1700	OVR	100		
OFF	14.4	WF	10				
SV	30	FR	10				
Metrology information							
CMM	Mitutoyo Crysta plus 547 CMM						
Spacing	(0.5 x 0.5) mm		**Probe dia.**	3 mm			
Roughness instrument	Leica 3DCM						
Resolution	12		**Overlap area**	10%			
Threshold	10 %		**Z-Scan value**	200 µm			

Cut MS-B-2 was performed on a mild steel sample as a repeated cut of MS-B-1.

a

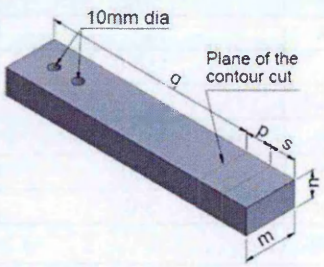

b

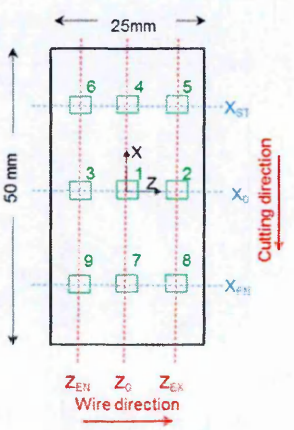

c

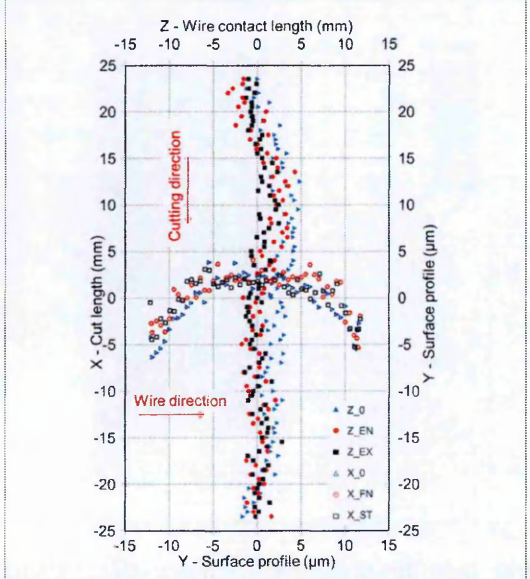

d

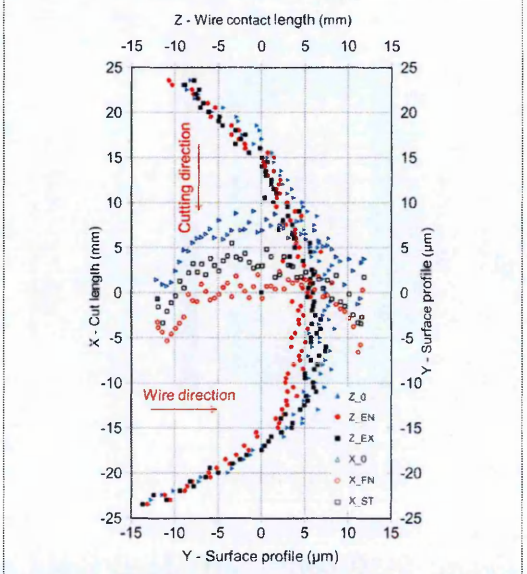

Figure 3-11: The MS-B-2 cut data and displacement profiles for clamped (c) and free sides (d).

Surface quality metrics				
	X (cutting direction)	Z (wire direction)	X (cutting direction)	Z (wire direction)
	Clamped side displacement, Fig c, µm		Free side displacement, Fig d, µm	
Min	- 2.0	-6.0	- 13.0	- 1.0
Max	5.0	4.0	9.0	8.5
Rsm	131.0	164.0	130.0	150.0
Sq, Sa	4.5, 3.5		4.5 ±0.14, 3.5 ±0.14	
	Averaged displacement, Figs e and g, µm		Stress error, Figs f and h, MPa (%yield)	
Min	- 8.0	- 4.0	- 60.0(16.0)	- 82.0 (22.0)
Max	5.5	5.5	141.0 (38.0)	136.0 (37.0)
RMS	3.6		70.0 (19.0)	

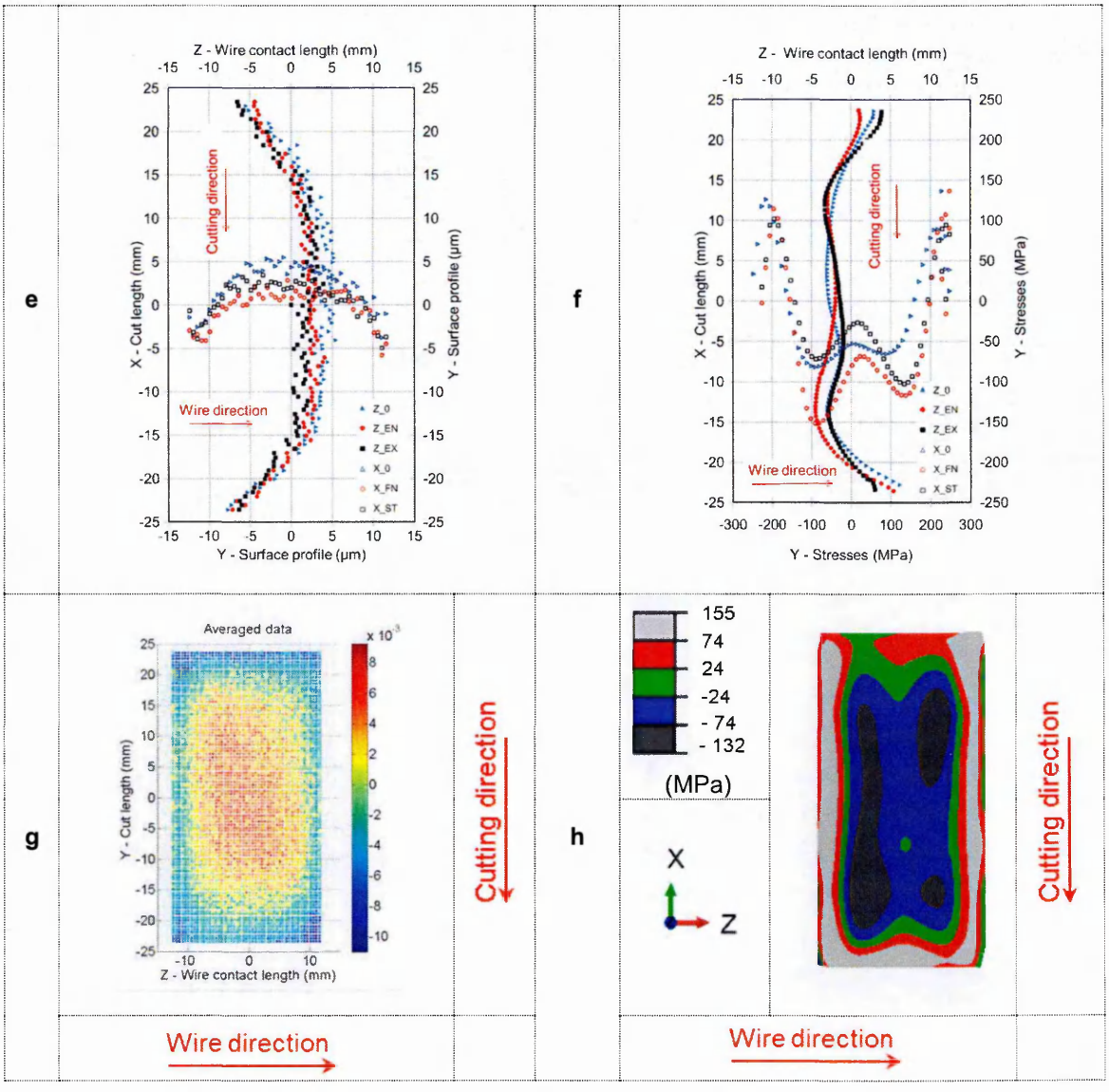

Figure 3-11 cont: The MS-B-2 cut surface quality metrics, profiles of averaged displacement (e) and stress (f), maps of averaged displacement (g) and stress (h).

Specimen details							
Specimen reference			SS-A-1				
Specimen material			Stainless Steel (304L)				
Cut length, m, thickness, n			(50 x 25) mm				
Cantilever dimensions, p, q			(25 x 195) mm				
Specimen top and bottom surfaces were milled flat surfaces. Vacuum heat treatment performed to relieve internal stresses.							
WEDM information							
Cut date			22nd Oct, 2013				
Machine type			Agie Charmillies FI440ccs				
Wire material			Brass (LT25.WIR)				
Wire diameter			0.25 mm				
Cutting technology			LT25A.TEC				
WEDM bath temperature			20 °C				
Nozzles position, pressure			0.2 mm, 1.4 MPa				
The cut was performed with a standard S5 set of parameters and no manual intervention							
WEDM cutting parameters							
EL	10	PA	6	PM	3	Offset	0.16
ST	1	M	3	S	10	V	80
FF	100	B	7	A	0.6	TAC	0.3
Aj	41	S	10	WS	12	WB	1.6
Inj	14	Rate	3.5	IAL	10		
Metrology information							
CMM			Mitutoyo Crysta plus 547 CMM				
Spacing	(0.5 x 0.5) mm		**Probe dia.**	3 mm			
Roughness instrument			Leica 3DCM				
Resolution	12		**Overlap area**	10%			
Threshold	10 %		**Z-Scan value**	200 µm			

Cut SS-A-1 was performed on a stainless steel sample with a standard S5 set of parameters using Agie machine.

a

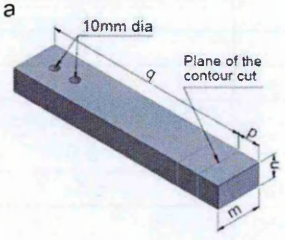

b

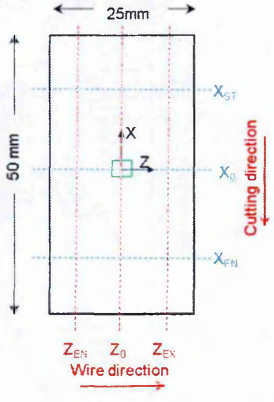

c

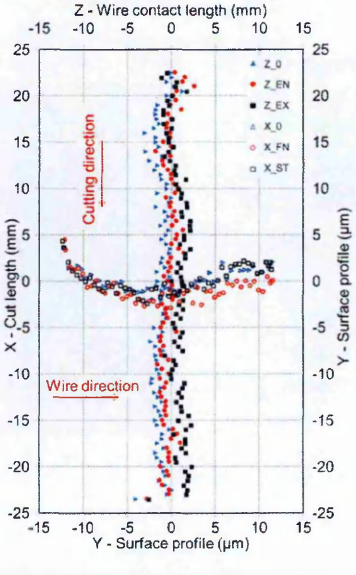

d

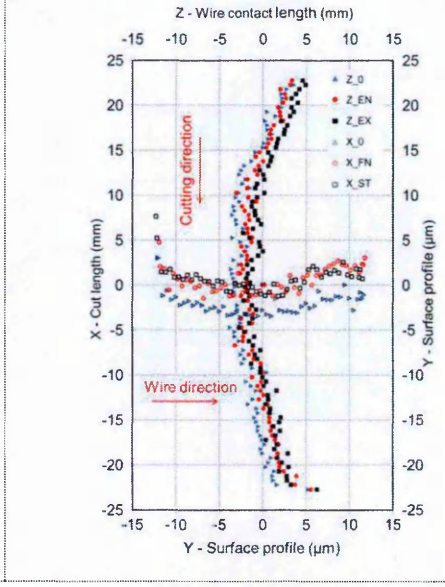

Figure 3-12: The SS-A-1 cut surface data and displacement profiles for clamped (c) and free sides (d).

Surface quality metrics				
	X (cutting direction)	Z (wire direction)	X (cutting direction)	Z (wire direction)
	Clamped side displacement, Fig c, µm		Free side displacement, Fig d, µm	
Min	-4.0	-2.0	-4.0	-4.0
Max	1.0	3.5	5.0	3.0
Rsm	120.0	150.0	130.0	150.0
Sq, Sa	3.4, 2.6		3.3, 2.5	
	Averaged displacement, Figs e and g, µm		Stress error, Figs f and h, MPa (%yield)	
Min	-2.0	-3.0	-39.0 (16.0)	-124.0 (51.0)
Max	3.0	3.5	43.0 (18.0)	30.0 (12.0)
RMS	2.0		33.0 (14.0)	

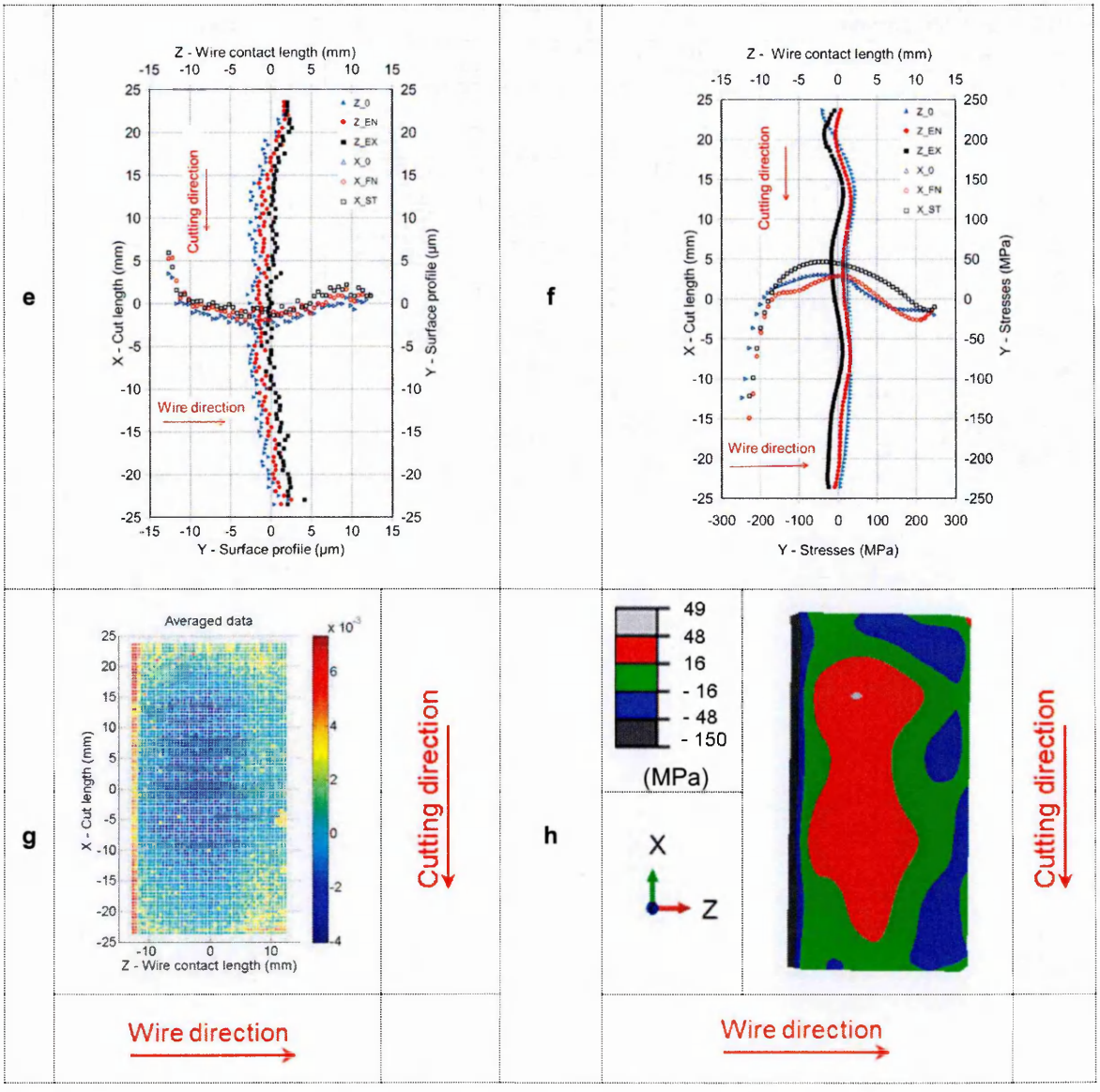

Figure 3-12 cont: The SS-A-1 cut surface quality metrics, profiles of averaged displacement (e) and stress (f), maps of averaged displacement (g) and stress (h).

Specimen details							
Specimen reference				SS-A-2			
Specimen material				Stainless Steel (304L)			
Cut length, m, thickness, n				(50 x 25) mm			
Cantilever dimensions, p, q				(25 x 170) mm			
Specimen top and bottom surfaces were milled flat surfaces. Vacuum heat treatment performed to relieve internal stresses.							
WEDM information							
Cut date				22nd Oct, 2013			
Machine type				Agie Charmillies FI440ccs			
Wire material				Brass (LT25.WIR)			
Wire diameter				0.25 mm			
Cutting technology				LT25A.TEC			
WEDM bath temperature				20 °C			
Nozzles position, pressure				0.2 mm, 1.4 MPa			
The cut was performed with a standard S5 set of parameters and no manual intervention							
WEDM cutting parameters							
EL	10	PA	6	PM	3	Offset	0.16
ST	1	M	3	S	10	V	80
FF	100	B	7	A	0.6	TAC	0.3
Aj	41	S	10	WS	12	WB	1.6
Inj	14	Rate	3.5	IAL	10		
Metrology information							
CMM				Mitutoyo Crysta plus 547 CMM			
Spacing		(0.5 x 0.5) mm		**Probe dia.**		3 mm	
Roughness instrument				Leica 3DCM			
Resolution		12		**Overlap area**		10%	
Threshold		10 %		**Z-Scan value**		200 µm	

Cut SS-A-2 was performed on a stainless steel sample as a repeated cut of SS-A-1.

A

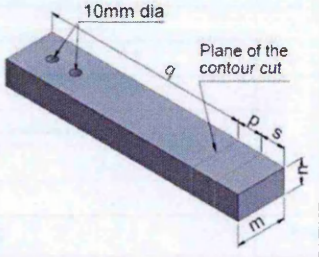

B

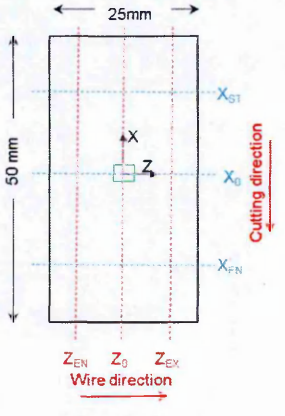

c

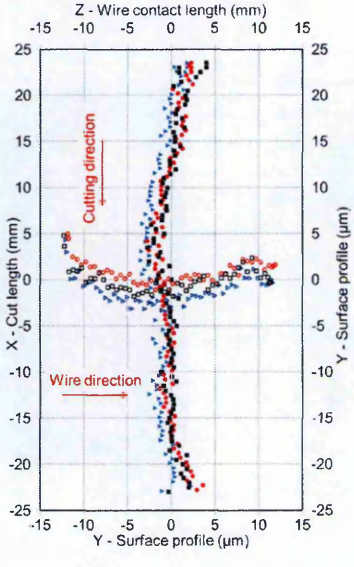

d

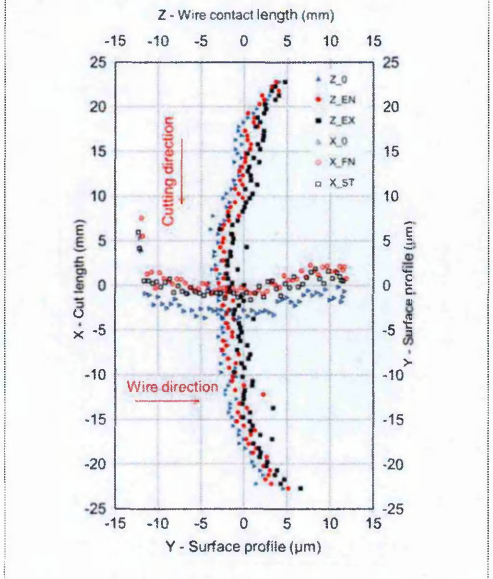

Figure 3-13: The SS-A-2 cut surface data and displacement profiles for clamped (c) and free sides (d).

Surface quality metrics				
	X (cutting direction)	Z (wire direction)	X (cutting direction)	Z (wire direction)
	Clamped side displacement, Fig c, µm		Free side displacement, Fig d, µm	
Min	-3.5	-3.0	-4.0	-4.0
Max	2.0	4.0	5.0	5.0
Rsm	134.0	125.0	110.0	170.0
Sq, Sa	3.5, 2.7		3.3, 2.6	
	Averaged displacement, Figs e and g, µm		Stress error, Figs f and h, MPa (%yield)	
Min	-4.0	-4.0	-17.0 (7.0)	-160.0 (66.0)
Max	2.0	5.5	54.0 (22.0)	46.0 (19.0)
RMS	2.3		37.0 (15.0)	

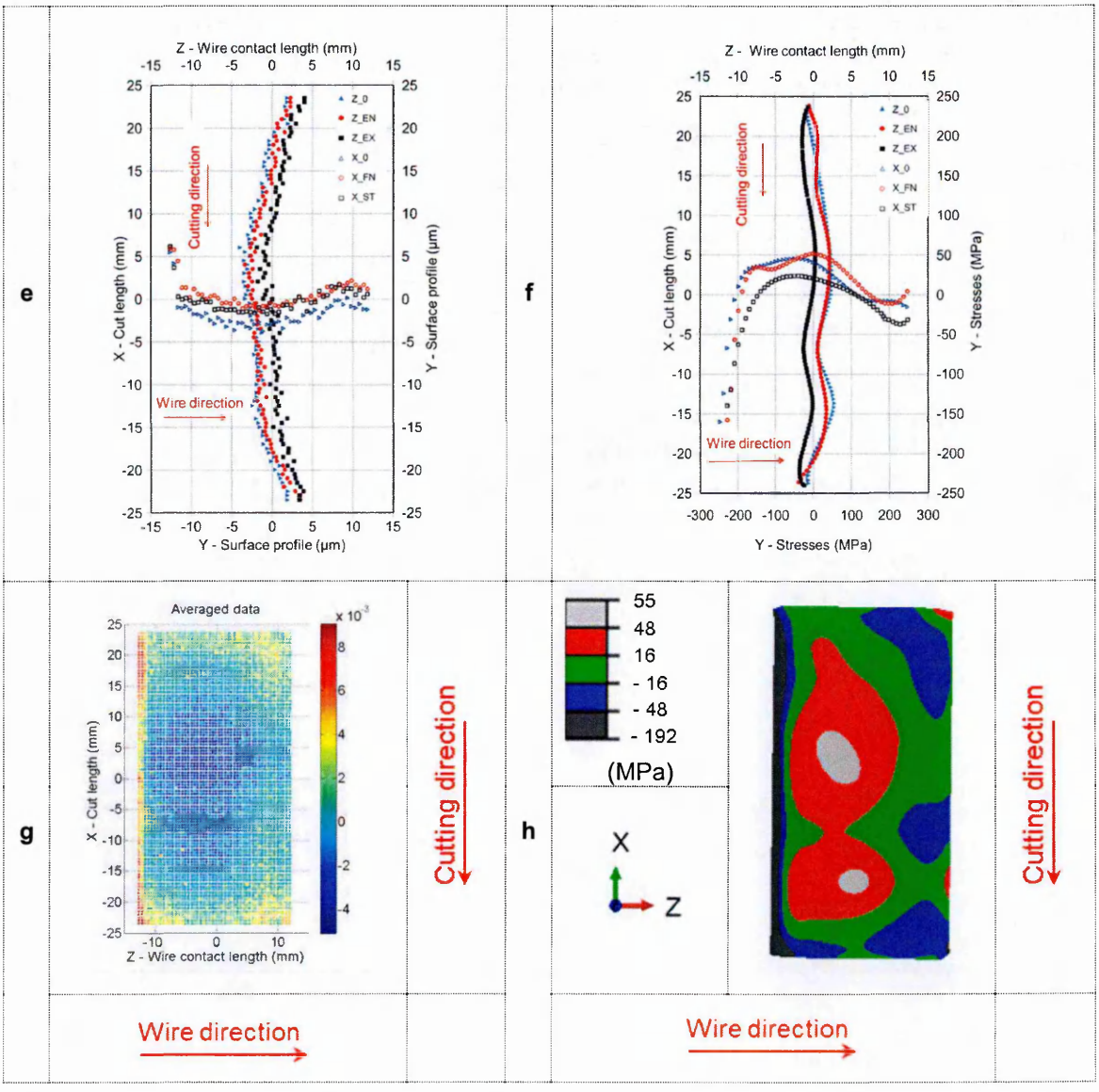

Figure 3-13 cont: The SS-A-2 cut surface quality metrics, profiles of averaged displacement (e) and stress (f), maps of averaged displacement (g) and stress (h).

Specimen details							
Specimen reference			SS-B-1				
Specimen material			Stainless Steel (304L)				
Cut length, m, thickness, n			(50 x 25) mm				
Cantilever dimensions, p, q			(25 x 220) mm				
Specimen top and bottom surfaces were milled flat surfaces. Vacuum heat treatment performed to relieve internal stresses.							
WEDM information							
Cut date			9th Oct, 2013				
Machine type			FanucC600iA EDM				
Wire material			Brass (LT25.WIR)				
Wire diameter			0.25 mm				
Cutting technology			LT25A.TEC				
WEDM bath temperature			20 °C				
Nozzles position, pressure			0.2 mm, 1.4 MPa				
The cut was performed with a standard C1 set of parameters and no manual intervention.							
WEDM cutting parameters							
PM	1	WP1A	6	FC	0		
VS	1	WP2A	2	SPD	3.23		
VM	6	T	1700	OVR	100		
OFF	14.4	WF	10				
SV	30	FR	10				
Metrology information							
CMM			Mitutoyo Crysta plus 547 CMM				
Spacing		(0.5 x 0.5) mm		**Probe dia.**	3 mm		
Roughness instrument			Leica 3DCM				
Resolution		12		**Overlap area**	10%		
Threshold		10 %		**Z-Scan value**	200 µm		

Cut SS-B-1 was performed on a stainless steel using Fanuc2 machine.

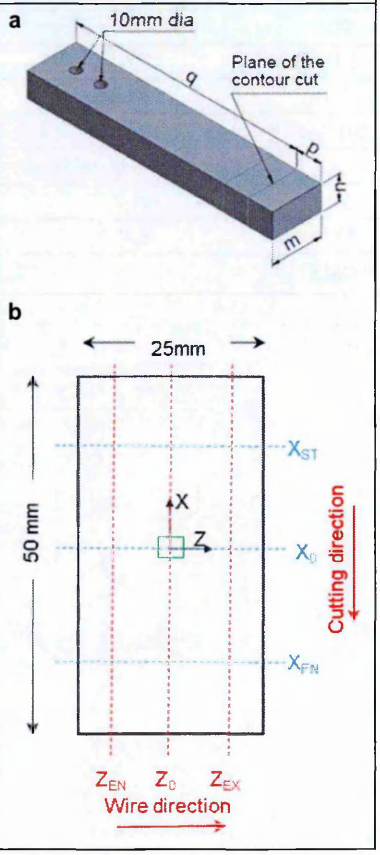

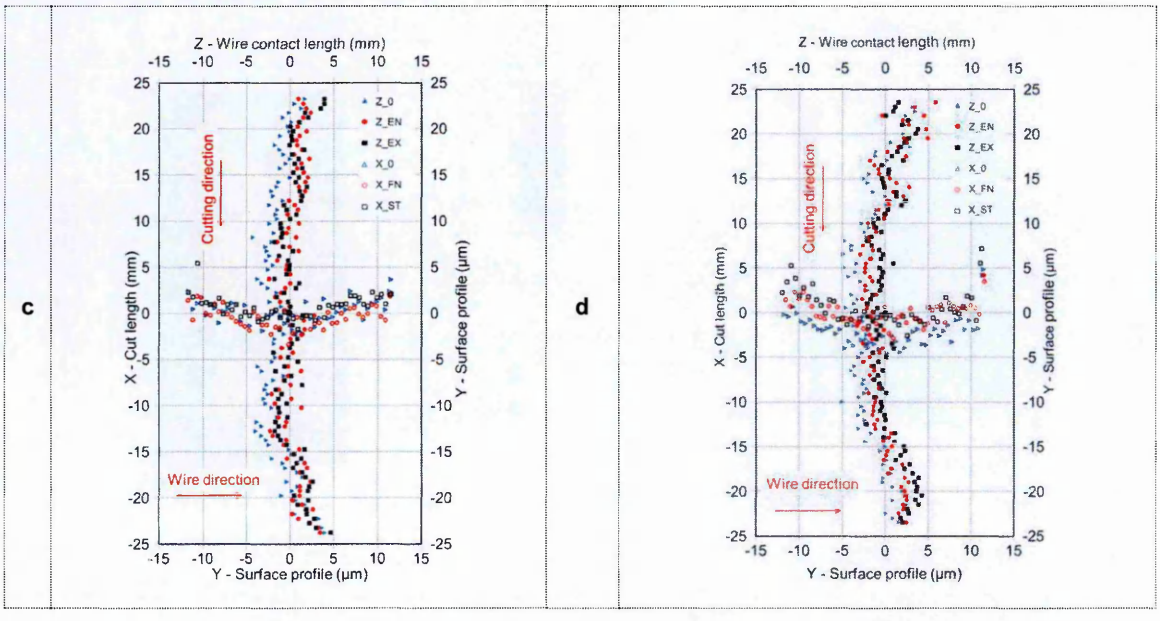

Figure 3-14: The SS-B-1 cut surface data and displacement profiles for clamped (c) and free sides (d).

Surface quality metrics				
	X (cutting direction)	Z (wire direction)	X (cutting direction)	Z (wire direction)
	Clamped side displacement, Fig c, µm		Free side displacement, Fig d, µm	
Min	-4.0	-2.0	-5.0	-4.5
Max	4.0	4.0	6.0	5.0
Rsm	150.0	130.0	160.0	150.0
Sq, Sa	4.7, 3.7		4.8, 3.8	
	Averaged displacement, Figs e and g, µm		Stress error, Figs f and h, MPa (%yield)	
Min	-4.0	-3.0	-73.0 (30.0)	-130.0 (54.0)
Max	3.5	4.0	67 (28.0)	22 (9.0)
RMS	2.0		33.0 (14.0)	

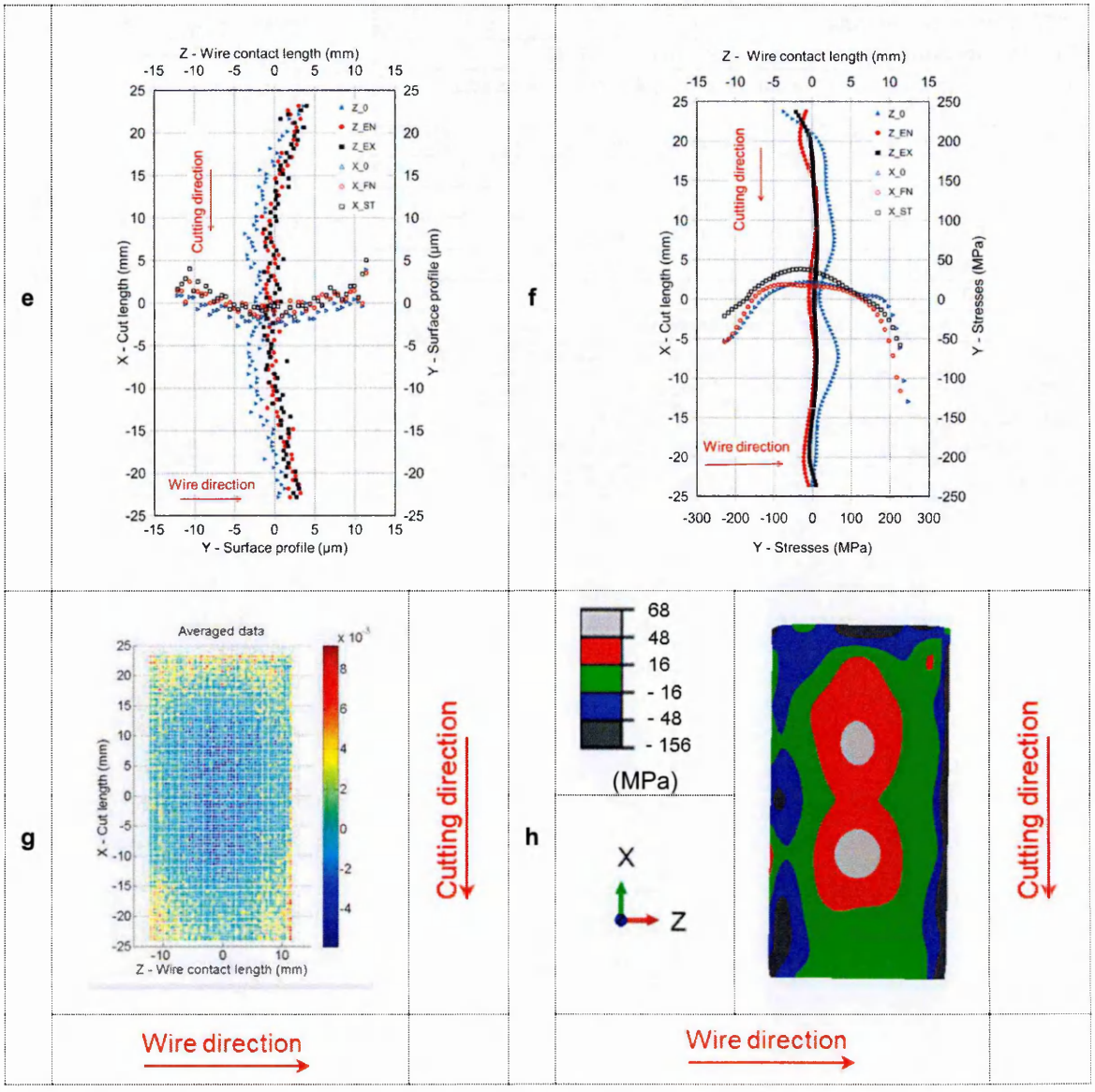

Figure 3-14 cont: The SS-B-1 cut surface quality metrics, profiles of averaged displacement (e) and stress (f), maps of averaged displacement (g) and stress (h).

Specimen details							
Specimen reference				SS-B-2			
Specimen material				Stainless Steel (304L)			
Cut length, m, thickness, n				(50 x 25) mm			
Cantilever dimensions, p, q				(25 x 195) mm			
Specimen top and bottom surfaces were milled flat surfaces. Vacuum heat treatment performed to relieve internal stresses.							
WEDM information							
Cut date				9th Oct, 2013			
Machine type				FanucC600iA EDM			
Wire material				Brass (LT25.WIR)			
Wire diameter				0.25 mm			
Cutting technology				LT25A.TEC			
WEDM bath temperature				20 °C			
Nozzles position, pressure				0.2 mm, 1.4 MPa			
The cut was performed with a standard C1 set of parameters and no manual intervention.							
WEDM cutting parameters							
PM	1	WP1A	6	FC	0		
VS	1	WP2A	2	SPD	3.23		
VM	6	T	1700	OVR	100		
OFF	14.4	WF	10				
SV	30	FR	10				
Metrology information							
CMM				Mitutoyo Crysta plus 547 CMM			
Spacing		(0.5 x 0.5) mm		**Probe dia.**	3 mm		
Roughness instrument				Leica 3DCM			
Resolution		12		**Overlap area**	10%		
Threshold		10 %		**Z-Scan value**	200 µm		

Cut SS-B-2 was performed on a stainless steel sample as a repeated cut of SS-B-1.

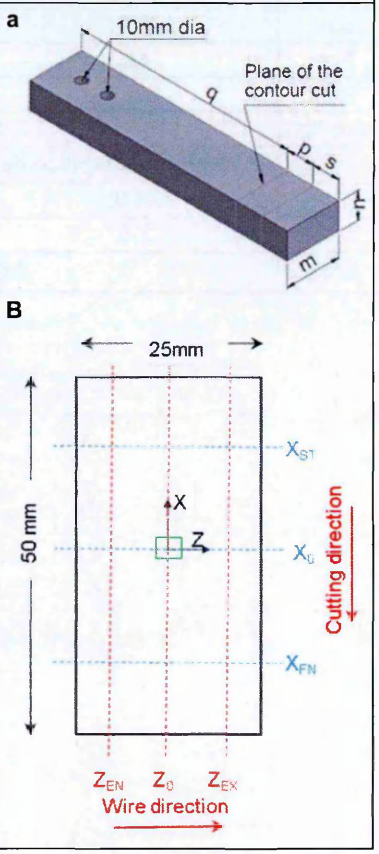

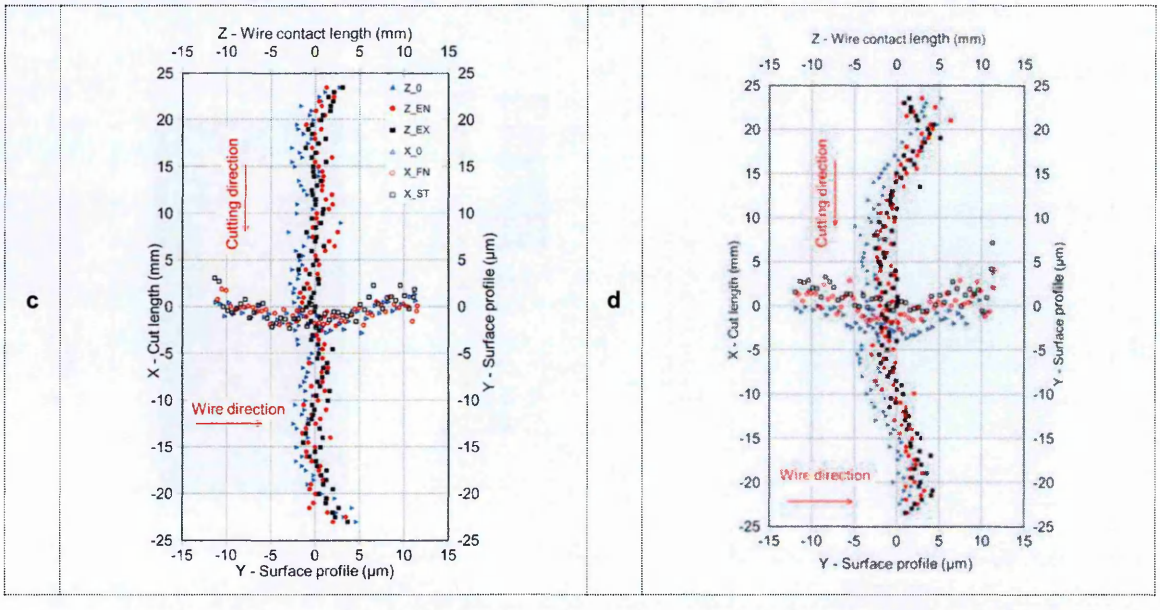

Figure 3-15: The SS-B-2 cut surface data and displacement profiles for clamped (c) and free sides (d).

Surface quality metrics				
	X (cutting direction)	Z (wire direction)	X (cutting direction)	Z (wire direction)
	Clamped side displacement, Fig c, µm		Free side displacement, Fig d, µm	
Min	- 3.0	- 3.0	- 5.0	- 4.0
Max	4.5	1.0	5.0	4.0
Rsm	153	155	120.0	150.0
Sq, Sa	4.4, 3.5		4.8, 3.7	
	Averaged displacement, Figs e and g, µm		Stress error, Figs f and h, MPa (%yield)	
Min	- 3.0	- 3.0	- 67.0 (28)	- 80.0 (33.0)
Max	4.0	2.5	65.0 (26)	44.0 (18.0)
RMS	2.0		31.0 (13.0)	

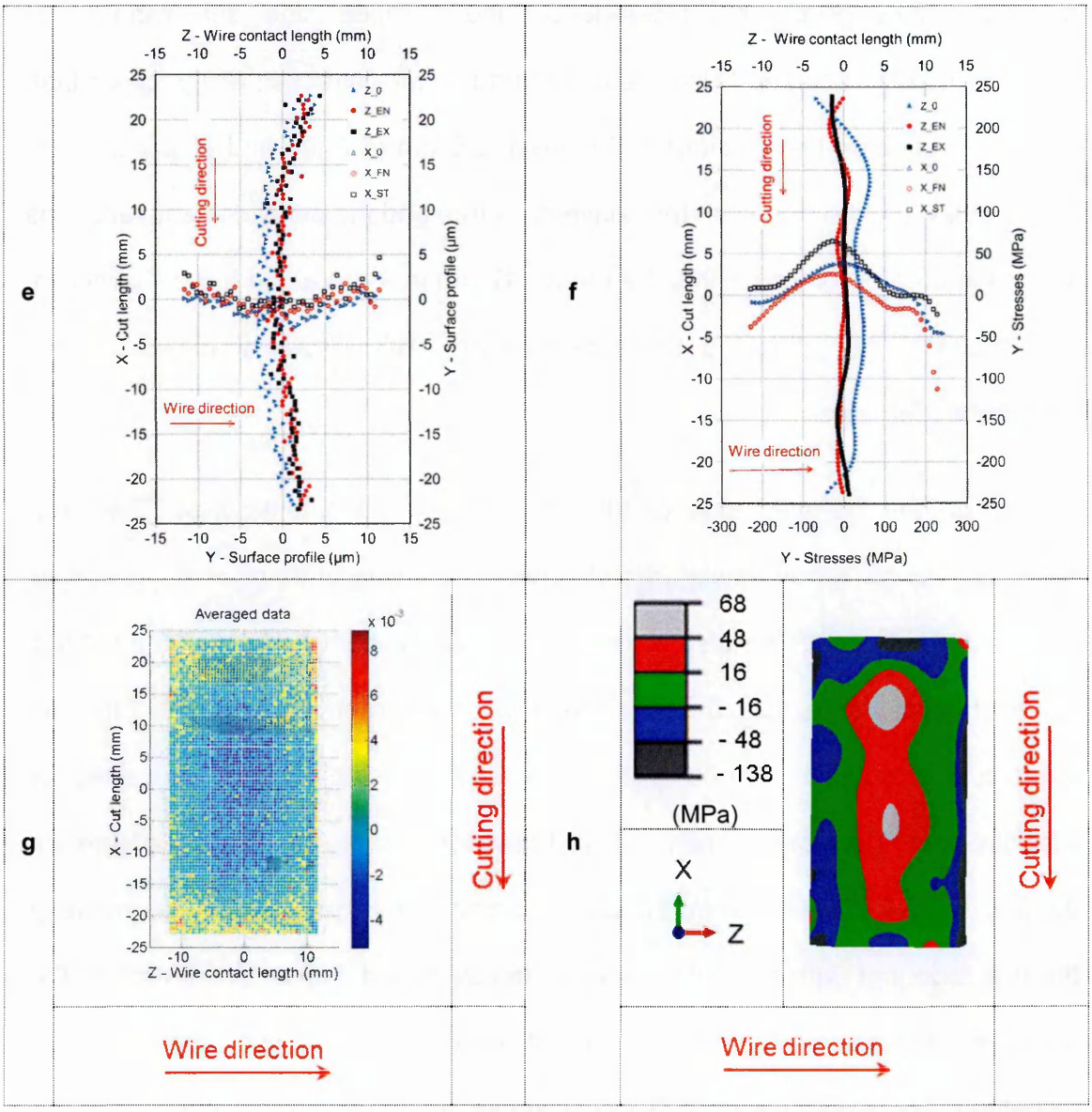

Figure 3-15 cont: The SS-B-2 cut surface quality metrics profiles of averaged displacement (e) and stress (f), maps of averaged displacement (g) and stress (h).

Series 1 (MS-A-1, MS-A-2 and MS-A-3) results and findings

Results from the first series of unrestrained cuts performed on mild steel specimen MS-A using the Agie WEDM are labelled MS-A-1, MS-A-2 and MS-A-3 in *Figure 3-7* to *Figure 3-9*.

Figure 3-7 shows the variation in measured displacements on both the clamped and free sides of the cut MS-A-1. On the clamped side, the variation in displacement is observed to be greater along the wire direction (Z-direction) than in the cut direction (X-direction) that is from -5.5 µm to 2 µm and -1 µm to 3 µm respectively. On the free side, the converse is true and the displacement variations are much greater varying within the range -17 µm to 9 µm along the cut direction, and 1 µm to 10 µm along the wire direction. This shows that the cut has asymmetric features.

Also on the clamped side of the cut, large displacements associated with features such as "flared edges", are observed at the wire entry position, as well as at the start of the cut. The displacement profile of the clamped side of the cut is a convex bowed shape along the wire direction. However, on the free side of the cut, these cutting artefacts are observed both along the cutting direction and along the wire direction. The bowed cutting artefacts are found to be significantly greater on the free side of the cut than on the clamped side. Consequently, it is the profile of the free side that dominates the shape of the averaged displacement profile. The averaged displacement profile was used to produce a stress map using FE modelling. The stress map shows larger stress gradient along the direction of the cut than along the wire direction. The stress profile also shows high values of

compressive stress approaching the wire entry edge of the specimen. It shall refer to this as the "flared edge effect" which is produced by wire entry into the sample.

Maps of the averaged displacements and stresses from the cut are represented in sub-panels (g) and (h) of the characterisation sheet represents in *Figure 3-7*. The averaged displacement map for the cut has positive values for displacements at the middle of the cut, and negative values for those along the edges. The corresponding stress map for the cut surface therefore shows compressive stresses at the middle of the cut surface and tensile stresses along the edges.

Three-dimensional surface roughness measurements were taken over each cut surface using a confocal microscope. The measurement details are also tabulated in the characterisation sheet. Values of S_q and S_a for the clamped side are 3.4 ± 0.16 µm and 2.6 ± 0.08 µm, and for the free side 3.7 ± 0.39 µm and 2.9 ± 0.44 µm respectively. The S_q and S_a values for the clamped side were found to have slightly lower values indicating a less rough surface than the free cut side.

The root mean squared (RMS) values for stress and displacement variations across the area of the cut surface were also calculated and are listed in the characterisation sheet, that is a stress of 59 MPa (16 % of yield strength) and displacement of 3 µm respectively.

Thus, the cut surfaces are not flat but possess many topographical features that do not cancel out after averaging the profiles of both sides. These 'symmetric' deformation features can introduce high apparent stress variations in a contour measurement.

The cut MS–A-2 was performed to quantify the repeatability of the cutting process. Hence, it was performed under conditions as close as possible to those used for the first cut MS-A-1. Displacement values for the clamped side range from – 2.5 µm to 3.5 µm along the cutting direction, and -4 µm to 4 µm along the wire direction. These variations are slightly higher than those found after the MS-A-1 cut. On the free side, no significant difference was found between displacement variations in the cuts, as shown in the surface quality metrics characterisation sheets, compare *Figure 3-7* and *Figure 3-8*.

The pattern that was observed on results from the first cut, where the clamped side showed less height variation than the free side, was also seen on the second cut surface. Moreover, in the second cut, the convex bowed shape of the surface, and the "flared edges effect" was observed, just as was seen on the first cut. No significant difference was found, in the RMS values for displacement and stress variations, between either of the cuts. Hence, the second cut MS-A-2 contains very similar surface features as the first cut MS-A-1. It is confirmed therefore, that there is high precision in repeatability performance, and in the reproducibility of surface finish using the Agie WEDM cutting machine.

Both cuts possessed large differences between the displacement variations on the free and clamped sides of the cuts. So, cut MS-A-3 was performed in order to assess any contribution that the cutting direction may have in forming the displacement variations. Therefore, for the cut MS-A-3, the direction of cutting was the opposite of that used in the first two cuts. The cut MS-A-3 results are shown in characterisation sheet, *Figure 3-9*, from which again it can be observed that the clamped side shows less height variation than the free side. This is similar to the

first two cuts. Moreover, in the third cut, as seen in the previous cuts, the convex bowed shape of the surface and the "flared edges effect" are also observed.

In conclusion, the series 1 cutting trials show that surface deformation characteristics in a mild steel sample can be reproduced using an Agie WEDM and that formation of a more highly bowed surface contour on the "free" side of a cut is unrelated to the cutting direction.

Series 2 (MS-B-1 and MS-B-2) results and findings

Results from the second series of unrestrained cuts performed on mild steel benchmark specimen MS-B using the FANUC ROBOCUT α-OiB/OiB5 WEDM (FANUC1) and are labelled MS-B-1 and MS-B-2 in characterisation sheets, *Figure* 3-10 and *Figure 3-11*.

The cut MS–B-1 was performed under conditions as close as possible to those used for the first series of cuts but using a different WEDM machine (FANUC1). Displacement values for the clamped side, ranged from - 2 μm to 5 μm along the cutting direction, and - 7.5 μm to 3 μm along the wire direction, see *Figure 3-10*. These variations are greater than those resulting from the first series of cuts. Hence, higher apparent stress variations are introduced. The surface roughness metrics are also significantly poorer for this cut than for series 1; S_a of 3.5 μm compared with 2.5 μm on the clamped side. On the free side of the cut MS-B-1, displacement variations (giving a bowed shape) are similar to those seen in the first series of cuts. And again the clamped side shows less height variation than the free side. A "flared edges effect" is also observed, just as was seen on the first series of cuts. Although the RMS values for displacement from both series of cuts

are similar, an inspection of the data plots in the characterisation sheets shows that the Fanuc1 WEDM produced an inferior surface quality.

So, in conclusion, cut MS-B-1 produced surfaces with similar features to series 1 cuts but with inferior roughness metrics and symmetric profiles contributing to higher apparent residual stress variations. This evidence indicates that the Agie WEDM machine used to perform the first series of cuts, gave a better quality of cut surfaces than the FANUC1 WEDM from a contour residual stress measurement perspective.

The cut MS-B-2 was performed to quantify the repeatability of the cutting process using the FANUC1 WEDM machine. The form that was observed on cut MS-B-2 displayed similar surface features as were seen on cut MS-B-1. Thus a good reproducibility of surface finish was achieved with the FANUC1 WEDM.

Series 3 (SS-A-1 and SS-A-2) results and findings

Results from the third series of unrestrained cuts performed on stainless steel benchmark specimen SS-A using the Agie WEDM are labelled SS-A-1 and SS-A-2 in characterisation sheets represent in *Figure 3-12* and *Figure 3-13.*

The SS-A-1 cut was performed under conditions as close as possible to those used for all previous cuts. For brevity and clarity, key metrics characterising surface features of the stainless steel cut SS-A-1 are shown in tabular form, with comparative results from mild steel cut MS-A-1. Note that both cuts were produced using the same WEDM machine. Table 3-4 shows the comparison of the quality of both the cut surfaces.

	MS-A-1		SS-A-1	
	X	Z	X	Z
Clamped side disp. (µm)	4.5	7.5	5.0	5.5
Free side disp. (µm)	26.0	11.0	9.0	7.0
Averaged disp. (µm)	13.0	7.0	5.0	6.5
Stress error-RMS (% yield) (MPa)	59.0 (16.0)		33.0 (14.0)	
	Clamped side	**Free side**	**Clamped side**	**Free side**
3D Surface roughness Sq, Sa (µm)	3.4, 2.6	3.7, 2.9	3.4, 2.6	3.3, 2.5

Table 3-4: A comparison of the quality of the cuts MS-A-1 and SS-A-1

Table 3-4 shows that the cut SS-A-1 has less displacement variation and lower surface roughness in comparison to the mild steel cut MS-A-1. However, it contains many symmetric features, such as flared edges at the wire entry side and a bowed form of the surface profiles just as were seen in the MS-A-1 cut surface. But interestingly in this case, the bowed form is concave (the opposite to all the mild steel cuts where the bowed form was convex). Due to the improvement in displacement variation, smaller stress errors were obtained for cut SS-A-1 compared with cut MS-A-1. This indicates that the WEDM machine used gave a better cut surface quality for the stainless steel specimen, than for the mild steel specimen. However, in this experiment the topography of the cut surface SS-A-1 ought to be free from symmetric surface features.

The cut SS-A-2 was performed in order to quantify the repeatability of the cutting process used for the stainless steel specimen. The cut resulted in the same form of surface topography as was seen in cut SS-A-1 (compare *Figure 3-12* and

Figure 3-13). Thus a good reproducibility of surface finish was achieved with the Agie WEDM for the stainless steel benchmark sample.

Series 4 (SS-B-1 and SS-B-2) results and findings

Results from the fourth series of unrestrained cuts performed on stainless steel specimen SS-B, using a FANUC 600iA WEDM (FANUC2) are labelled SS-B-1 and SS-B-2 in characterisation sheets, *Figure 3-14* and *Figure 3-15*.

The SS-B-1 cut was performed under conditions as close as possible to those used for the third series of the cuts (SS-A-1 and SS-A-2) but using the FANUC2 WEDM machine. Results for the quality of cut SS-B-1 are compared with cut SS-A-1 in Table 3-5.

	SS-A-1		**SS-B-1**	
	X	**Z**	**X**	**Z**
Clamped side disp. (µm)	5.0	5.5	8.0	6.0
Free side disp. (µm)	9.0	7.0	11.0	9.5
Averaged disp. (µm)	5.0	6.5	7.5	7.0
Stress error-RMS (% yield) (MPa)	33.0 (14.0)		33.0 (14.0)	
	Clamped side	**Free side**	**Clamped side**	**Free side**
3D Surface roughness Sq, Sa (µm)	3.4, 2.6	3.3, 2.5	4.7, 3.7	4.8, 3.8

Table 3-5: A comparison of the quality of the cuts SS-A-1 and SS-B-1.

The cut SS-B-1 results display poorer surface roughness metrics, and higher displacement variations and associated stress errors in comparison to results from cut SS-A-1. Cut SS-B-1 also possesses some surfaces features similar to cut SS-A-1, such as asymmetric features in both sides of the cut, where the clamped side

showed less height variation than the free side. Moreover, the surface displayed a concave bowed shape and the "flared edges effect" was also observed. Just as seen in the cut SS-A-1. Hence, the WEDM used to perform the cut SS-A-1 gave a better quality of surface finish compared to the machine used to perform cut SS-B -1.

SS-B-2 cut was performed to check the repeatability of the cutting process for the fourth series of cuts. This cut resulted in very similar surface features as was seen in cut SS-B-1 confirming good reproducibility of surface finish.

3.10.4 Discussion of first experiment results for unrestrained cuts

Results of this first experiment revealed the following features of the cuts:

- In all cut surface results, "flared edge effects" were commonly found along the wire entry side of the cuts. This is because during the WEDM process, the corners and edges of the work piece significantly deteriorate, possibly because this is where the electric field is least uniform. High electrical energy increases the discharged pulse (141,142) which results in a high erosion rate along the edges and causes a high value in displacement variations. In this research, for mild steel and stainless steel, the wire entry effects are found to be relatively similar. However, these effects are further investigated in section 3.11 by varying some of the electrical parameters of the WEDM and using two different WEDM wire diameters.
- High values of displacements across the edges of the cut surfaces result in the calculation of high values of stress in contour analysis for the respective

locations. These stresses can be compressive or tensile dependent on the displacement values.

- The 'bowed form' of the cut surfaces occurred in all the cuts. The formation of this cutting artefact is influenced by the WEDM cutting parameters, as well as the material type. On the mild steel specimens, a *convex* bowed form of the cut surfaces was found. On the stainless steel specimens, a *concave* bowed form of the cut surfaces was found. The severity of the bowing was greater in the mild steel specimens, than in the stainless steel. A suggested hypothesis to explain this effect is the higher degree of magnetisation that a mild steel material incurs, in response to the applied electro-magnetic field generated by the current pulses during WEDM cutting. The mild steel specimen concentrates a magnetic field within itself, and this affects the distribution of the magnetic flux density, during the flow of current through the brass cutting wire. So, because the magnetic permeability of mild steel is significantly higher, and more during the WEDM cutting, the wire cannot maintain an axisymmetric distribution of the magnetic flux, or a uniform current density around its axis. Therefore, looking at the wire in cross section, the magnetic flux density in the upper portion of the wire, is higher than that in the lower portion. Thus, the resultant electromagnetic force generated in the wire is magnetically attracted to, and directed towards, the mild steel work piece (153). This causes wire vibration, wire deflection (dislocation) and excessive material removal during the cut. These inaccuracies of the cutting process can be improved by reducing the effects of the electro-magnetic force induced during the cutting process of the mild steel specimen. These effects can be reduced by lowering the supply

current during the cutting processes (154). It may also be important to demagnetise steel components before cutting to minimise these effects, noting that this procedure is recommended practice for wire machining ferritic materials (155).

- Asymmetric features were found on both sides of all the cut surfaces. Features might be influenced by the specimen material type as well as clamping conditions during the cutting. It is quite possible that during cutting the free side (unclamped) moved, and so contributed to asymmetric features on the parts. Thus, it would be worthwhile investigating the cutting process whilst providing extra support to prevent any movement of the free side during cutting.
- All the cut surface features discussed above were observed on each side of the cut, as well as on the averaged surface profiles. Since these features are symmetric, they cannot be eliminated by averaging in the contour method deformation analysis. If caused by artefacts, symmetric features are highly undesirable on contour surfaces because they mimic the effects of residual stress, and thus introduce errors in its determination.
- The surface roughness values were not influenced by the type of material of the specimens. However, they were influenced by the use of different WEDM cutting machines, necessitating a change in WEDM cutting parameters for each machine used. Both the mild steel and stainless steel specimens resulted in similar surface roughness values when the cuts were performed using the same machine, suggesting that the material removal rates ought to also be the same for each material. The surface finish of the cuts can be improved by

optimisation of the WEDM cutting parameters, as well as by using a thinner wire diameter.

- This study confirmed the repeatability in performance, and the reproducibility of surface finish of the WEDMs.
- This study also determined the Agie Charmilles FI 440 CCS WEDM is the more suitable appliance for both the material types tested, and can give a better surface finish than the other two (FANUC) WEDM machines used.

3.11 The second experiment - restrained cutting conditions

Following the results of the first experiment (unrestrained cuts), the following modifications were made in the design of subsequent sets of experiments:

- The cuts were performed with restrained cutting conditions created by starting the cuts from pilot holes formed using an EDM hole drilling machine.
- Two different ligament lengths of material, between the pilot hole and edge of the specimen, were trialed in an attempt to introduce restraint during cutting.
- In addition to this, to reduce the effects of electromotive force (details are provided in section 3.10.4) during the cutting process, some modifications were also made in the electrical parameters of WEDM such as 'A (microsecond) - Energy duration of the pulse (voltage and current)' and 'TAC (microsecond) - Short A time'. These WEDM parameters are directly related to the energy of the spark. Decreasing A and TAC values decrease the energy of the spark. Reduction in energy of spark provides help to evacuate the eroded particles and can improve flushing conditions (156).

- The effects of using two different wire diameters, based on a common wire material, were also explored with an aim to improve the quality of the cut surface finish.

3.11.1 Cutting strategy

The same specimen design, specimen material types and Agie WEDM were used for this second experiment as were used in the first experiment. The experiment was composed of four series of cuts, giving ten cuts altogether. The cuts were started from pilot holes. The centre of the first pilot hole was placed 25 mm away from the free end of the cantilever specimen. A second pilot hole was drilled in line with the first, at a pitch of 25mm between centres. Details about specimen preparation for restrained cuts are given in *Figure 3-16*. During each cut one end of the specimen was clamped and cuts were performed using the same procedures as in the previous experiment. *Figure 3-17* shows annotated photographs of various stages of the second experiment.

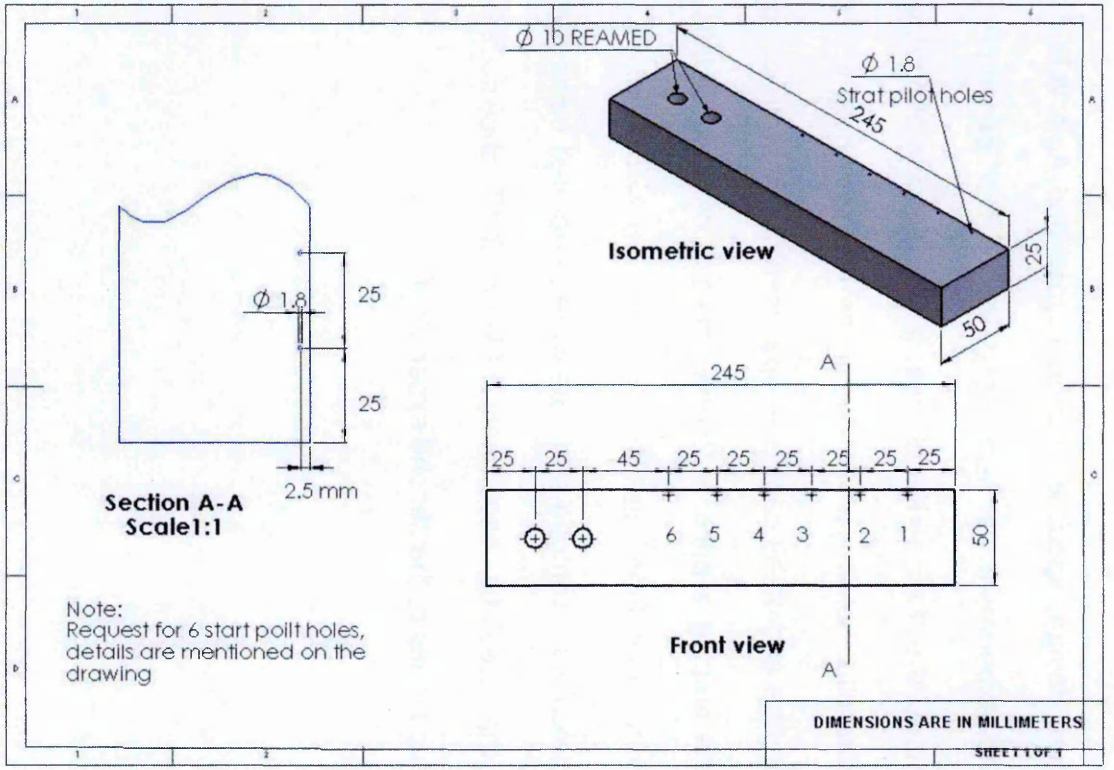

Figure 3-16: Represents the details of the specimen preparation for restrained cuts.

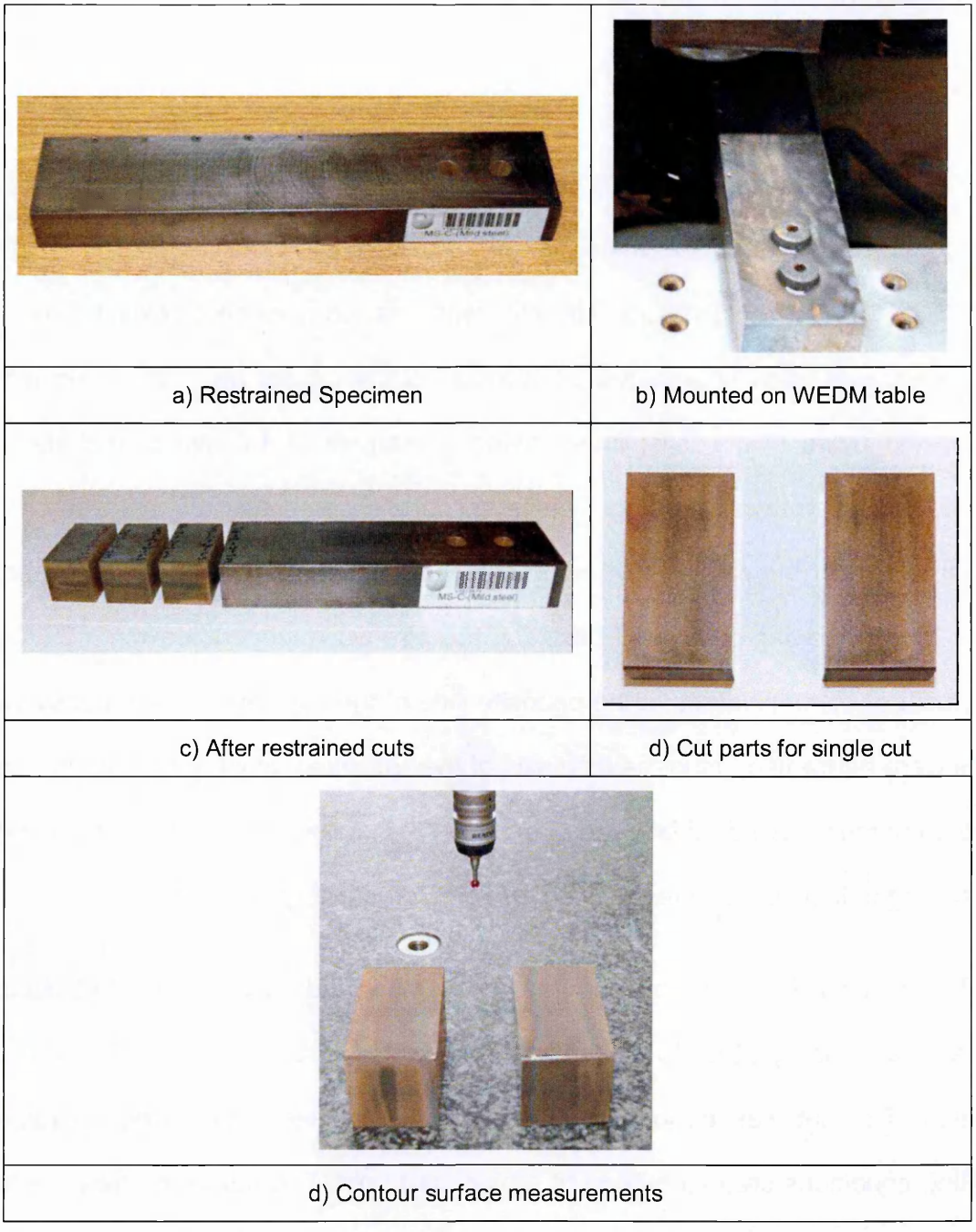

Figure 3-17: Photographs showing various stages of the second experiment.

3.11.2 Methodology for the second experiment

Restrained cuts – series 1

The first series of the second experiment-restrained cuts was performed on a benchmark mild steel specimen named as MS-C. It consisted of three cuts MS-C- 1, MS-C-2 and MS-C-3. The cuts were started from pilot holes 1.8 mm in diameter, with each hole centre positioned 2.5 millimetres away from one side, along the plane of the cuts, thus leaving a ligament of 1.6 mm of material, to provide constraint whilst cutting. The first pilot hole was placed 25 mm away from the free end of the cantilevered specimen. The spacing between each pilot hole was 25 mm. Having completed each cut, the wire was stopped, leaving a 2.5 mm ligament of material intact, at the opposite side of the specimen. Then, transverse cuts were performed along the long axis of the specimen, to intersect with the end of the contour cut and release the 25 mm piece. Details about the cutting strategy used for the first series of restrained cuts are shown in *Figure 3-18*.

The first cut MS-C-1 was performed using a standard set of WEDM cutting parameters (designated S5 on the machine) with A = 0.6 μs and TAC = 0.3 μs values. The cut was performed with 0.25 mm diameter wire using restrained cutting conditions created by use of a pilot start hole. The results of the cut were compared with those of the unrestrained cut MS-A-1, to evaluate the quality of the cut surface.

The second cut MS-C-2 was performed with a 0.1 mm diameter wire and a standard set of WEDM cutting parameters (designated S3 on the machine with

default A = 0.2 µs and TAC = 0.1 µs). This cut was performed to try and improve the quality of the cut surface by using a thinner wire diameter, than for cut MS-C-1.

The third cut MS-C-3 repeated the MS-C-2 but with reduced A = 0.1 µs and TAC = 0.05 µs values. The cut was performed using wire of 0.1 mm diameter. This cut was performed to assess the quality of the cut by using a smaller wire diameter, in addition to a further reduction in A and TAC values for the WEDM cutting parameters.

Restrained cuts – series 2

The second series of the second experiment for restrained cuts was performed using exactly the same cutting conditions as on the first series of restrained cuts, but with a change in material type of the specimen. A stainless steel specimen named as SS-C was used to perform the cuts. This series also comprised three cuts, the same as in the first series of restrained cuts. Details about the cutting strategy are shown in *Figure 3-18.*

Restrained cuts – series 3

The third series of the second experiment for restrained cuts was performed on mild steel specimens labelled MS-B-4 and MS-C-4.

The cut MS-B-4 was performed at 25 mm away from the free end of the mild steel MS-B specimen. It was started from 1.8 mm diameter pilot hole. The centre of the pilot hole was placed at 5.9 mm away from one edge of the specimen thus leaving a 5 mm ligament of material. The cut was performed all the way through the width of the specimen. The cut was performed using the standard set of

WEDM cutting parameters (designated S5 on the machine), and without any manual intervention. These cuts were performed using 0.25 mm wire diameter. The ligament length was increased from the 1.6 mm used on the first series restrained cut MS-C-1, to 5 mm, with the aim of providing additional support during the cut. *Figure 3-19* and *Figure 3-20* give details about the specimen preparation and the cutting strategy used to perform the cut MS-B-4.

The cut MS-C-4 was performed using the same cutting conditions as the cut MS-C-1 with the exception that the cut was performed approximately at mid length of the specimen, in order to provide a similar stiffness on both sides of the plane of the cut. Details about the cutting strategy used to perform the cut MS-C-4 are given in *Figure 3-20.*

Restrained cuts – series 4

The fourth series of the second experiment restrained cuts was performed on stainless steel specimens. It consisted of two cuts named as SS-A-5 and SS-C-4. using the same cutting conditions as for the third series of cuts MS-B-4 and MS-C-4 respectively.

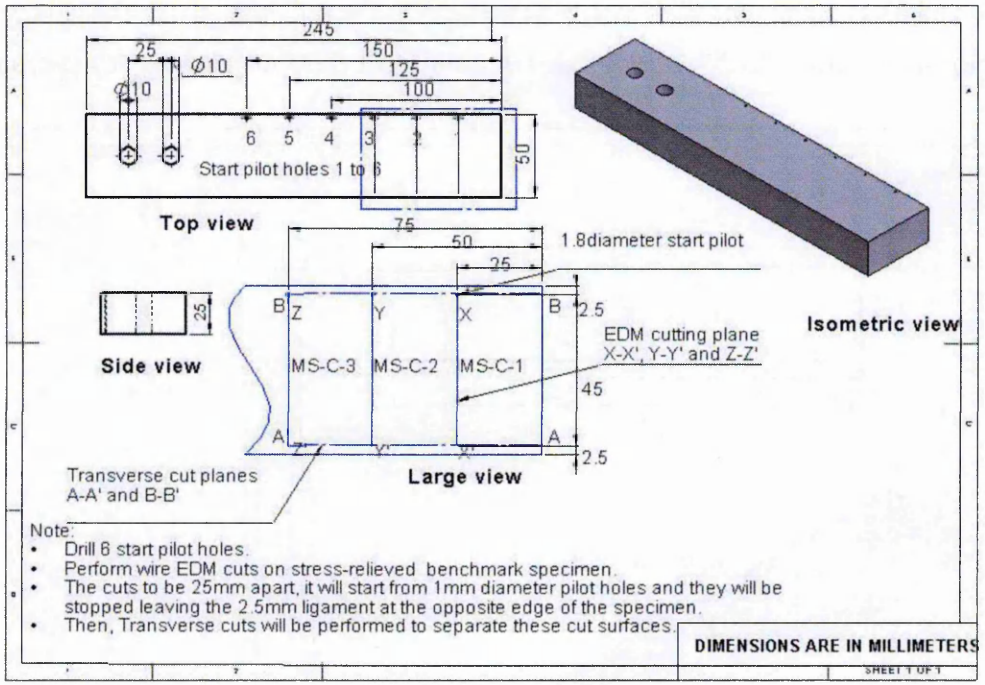

Figure 3-18: Represents the cutting strategy was used in the second experiment for the first and second series of restrained cuts.

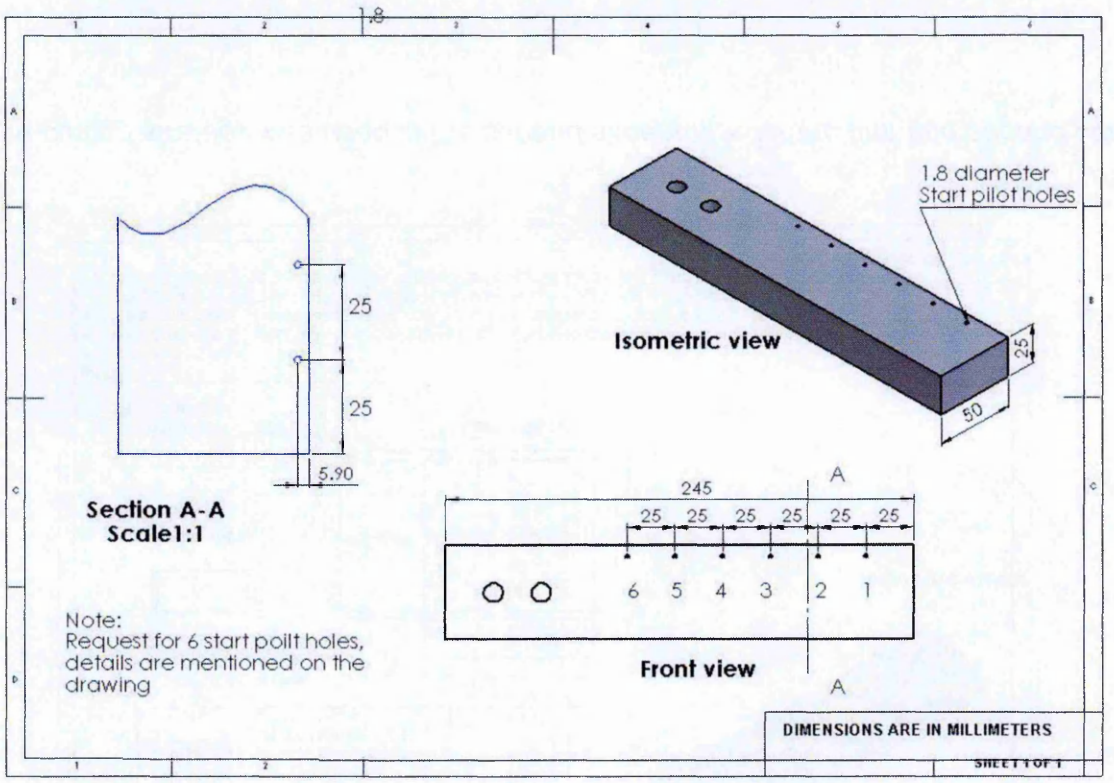

Figure 3-19: Represents the details for the specimen preparation in the second experiment for the third and fourth series of restrained cuts.

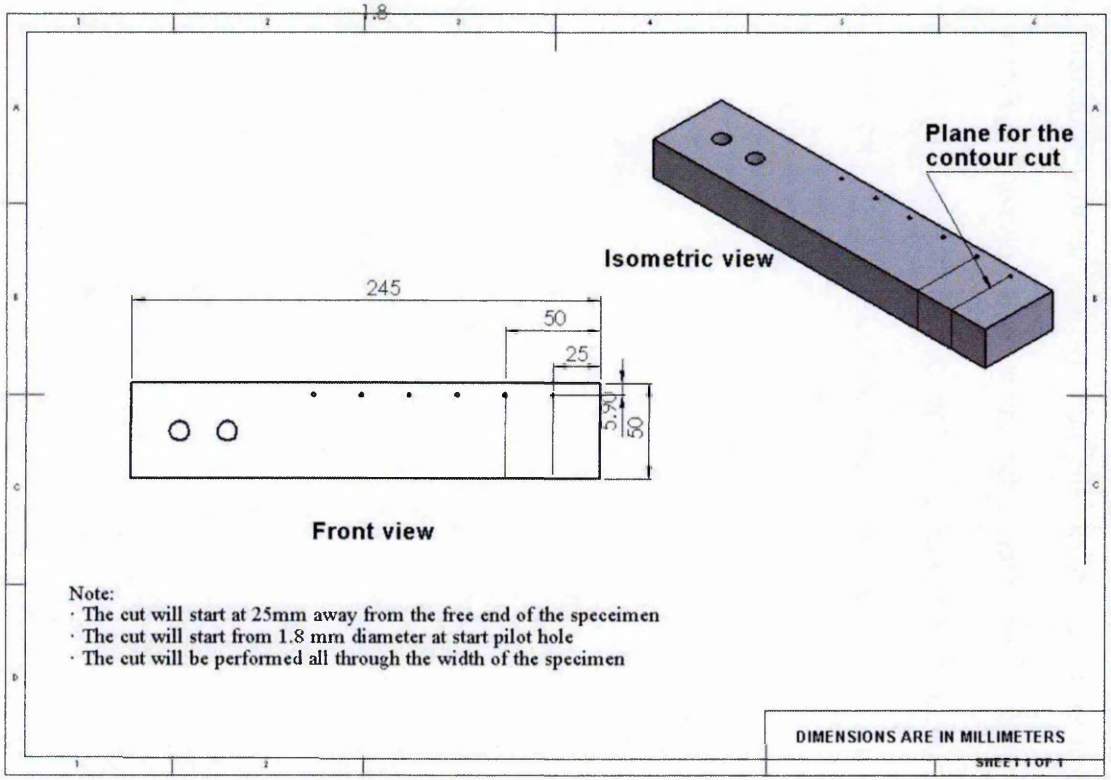

Figure 3-20: Represents the cutting strategy was adopted for the second experiment for the third and fourth series of restrained cuts.

3.11.3 Results of the second experiment for restrained cuts

The second experiment examined restrained cuts with the aim of improving the cut surface quality achieved in the first experiment that used unrestrained cutting conditions. The quality of the cuts was assessed by comparing key characteristics of the clamped and free sides of the cuts based upon measurements and calculations. Characterisation sheets for these cuts, shown in *Figure 3-21* to *Figure 3-30*, summarise key features of the cut surfaces. They are discussed below and comparisons made with the unrestrained results from the first experiment.

Specimen details							
Specimen reference				MS-C-1			
Specimen material				Mild Steel (EN3B)			
Cut length, m, thickness, n				(45 x 25) mm			
Cantilever dimensions, p, q				(25 x 220) mm			
Specimen top and bottom surfaces were milled flat surfaces. Vacuum heat treatment performed to relieve internal stresses.							
WEDM information							
Cut date				19^{th} Dec, 2013			
Machine type				Agie Charmilles FI440ccS			
Wire material				Brass (LT25.WIR)			
Wire diameter				0.25 mm			
Cutting technology				LT25A.TEC			
WEDM bath temperature				20 °C			
Nozzles position, pressure				0.2 mm, 0.8 MPa			
The cut was performed with a standard S5 set of parameters with no manual intervention							
WEDM cutting parameters							
EL	10	PA	6	PM	3	Offset	0.16
ST	1	M	3	S	10	V	80
FF	100	B	7	A	0.6	TAC	0.3
Aj	41	S	10	WS	12	WB	1.6
Inj	14	Rate	3.4	IAL	10		
Metrology information							
CMM				Mitutoyo Crysta plus 547 CMM			
Spacing		(0.5 x 0.5) mm		**Probe dia.**		3 mm	
Roughness instrument				Leica 3DCM			
Resolution		12		**Overlap area**		10%	
Threshold		10 %		**Z-Scan value**		200 µm	

Cut MS-C-1 was performed on restrained cutting conditions. The cut was performed with a standard S5 set of parameters with no manual intervention.

a

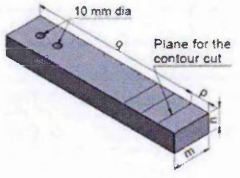

b

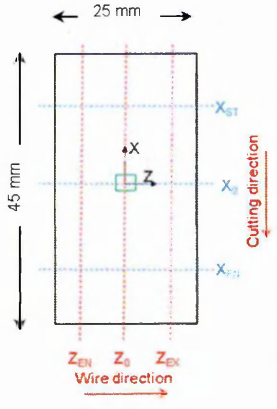

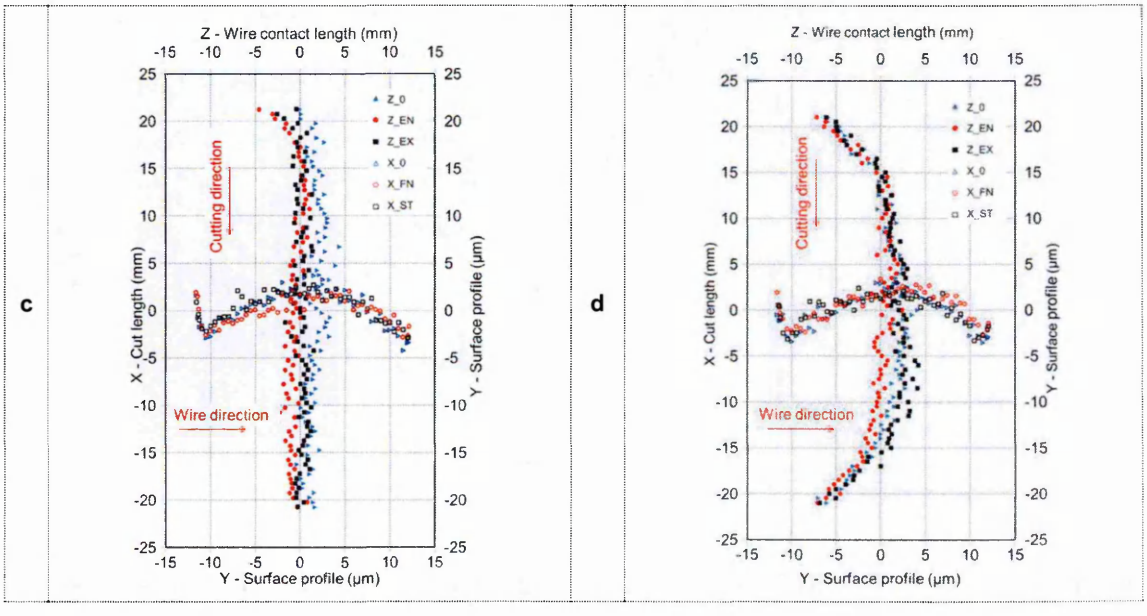

Figure 3-21: The MS-C-1 cut data and displacement profiles for clamped (c) and free sides (d).

Surface quality metrics				
	X (cutting direction)	Z (wire direction)	X (cutting direction)	Z (wire direction)
	Clamped side displacement, Fig c, µm		Free side displacement, Fig d, µm	
Min	0	-4.0	-7.0	-3.5
Max	4.0	3.5	4.0	3.0
Rsm	128.0	124.0	131.0	147.0
Sq, Sa	3.5, 2.6		3.7, 2.7	
	Averaged displacement, Figs e and g, µm		Stress error, Figs f and h, MPa (%yield)	
Min	-2.0	-3.0	-72.0 (19.0)	-91.0 (24.0)
Max	4.0	4.0	35.0 (9.5)	83.5 (22.0)
RMS	2.3		52.0 (14.0)	

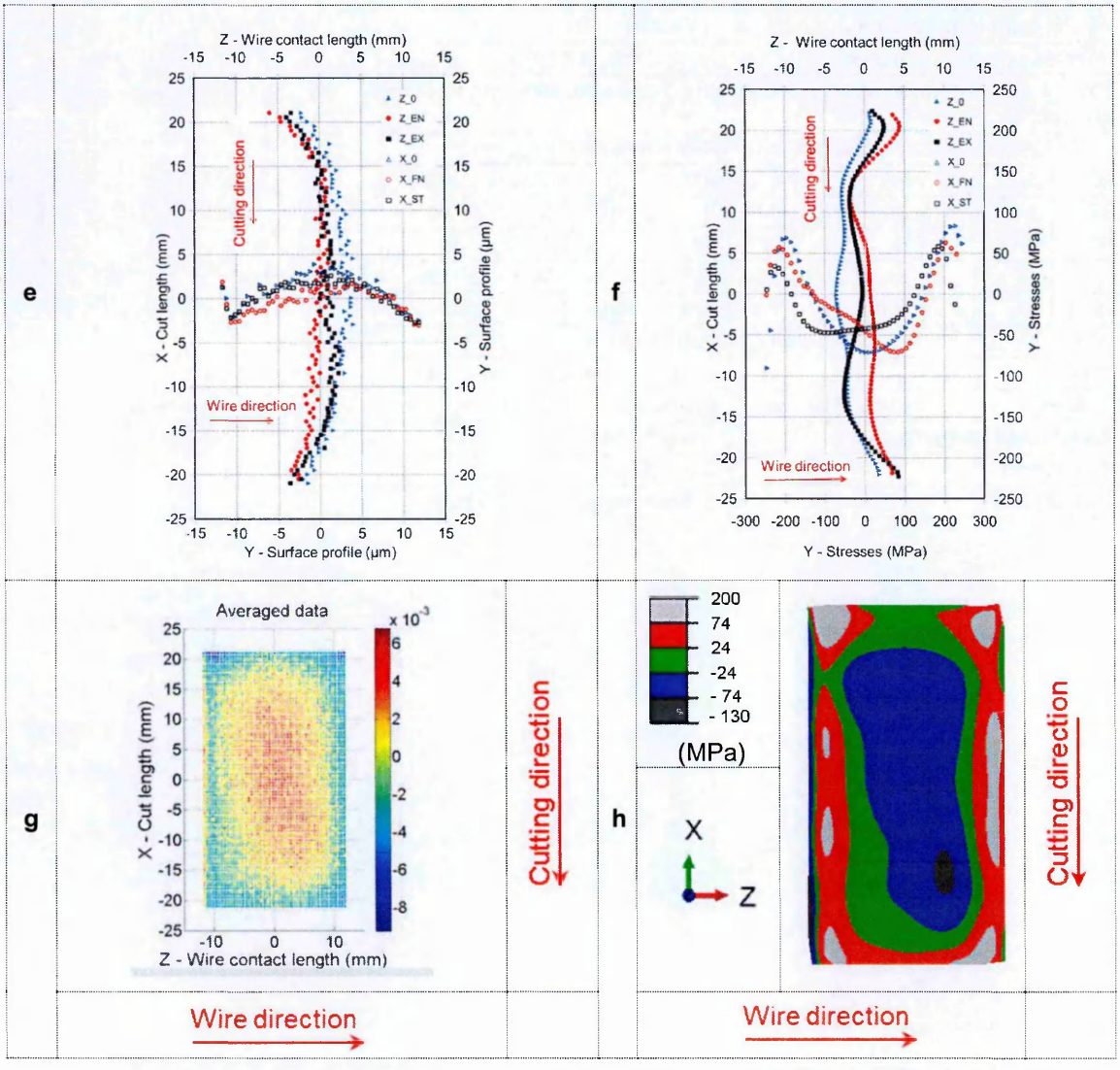

Figure 3-21 cont: The MS-C-1 cut surface quality metrics, profiles of averaged displacement (e) and stress (f), maps of averaged displacement (g) and stress (h).

Specimen details							
Specimen reference			MS-C-2				
Specimen material			Mild Steel (EN3B)				
Cut length, m, thickness, n			(45 x 25) mm				
Cantilever dimensions, p, q			(25 x 195) mm				
Specimen top and bottom surfaces were milled flat surfaces. Vacuum heat treatment performed to relieve internal stresses.							
WEDM information							
Cut date			19th Dec, 2013				
Machine type			Agie Charmilles FI440ccS				
Wire material			Brass (LT25.WIR)				
Wire diameter			0.1 mm				
Cutting technology			LT25A.TEC				
WEDM bath temperature			20 °C				
Nozzles position, pressure			0.2 mm, 0.1 MPa				
The cut was performed with a standard S3 set of parameters.							
WEDM cutting parameters							
EL	10	PA	6	PM	---	Offset	---
ST	1	M	37	S	5	V	60
FF	95	B	8.7	A	0.2	TAC	0.1
Aj	42	S	5	WS	10	WB	0.3
Inj	2	Rate	0.744	IAL	8		
Metrology information							
CMM			Mitutoyo Crysta plus 547 CMM				
Spacing	(0.5 x 0.5) mm		**Probe dia.**	3 mm			
Roughness instrument			Leica 3DCM				
Resolution	12		**Overlap area**	10%			
Threshold	10 %		**Z-Scan value**	200 µm			

Cut MS-C-2 was performed on restrained cutting conditions. The cut was performed with a standard S3 set of parameters using 0.1 mm wire diameter.

a

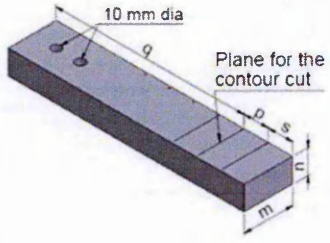

b

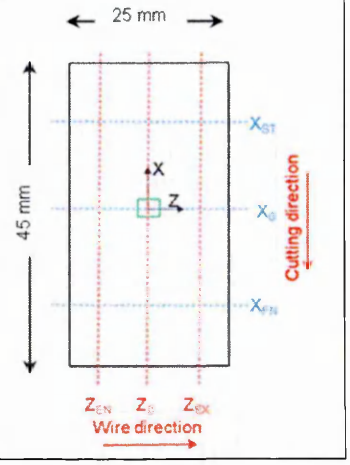

c

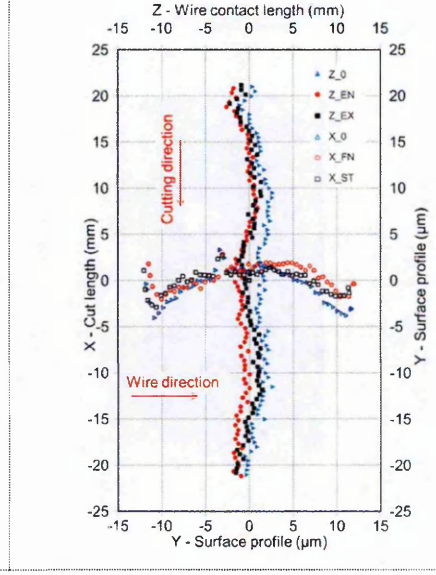

d

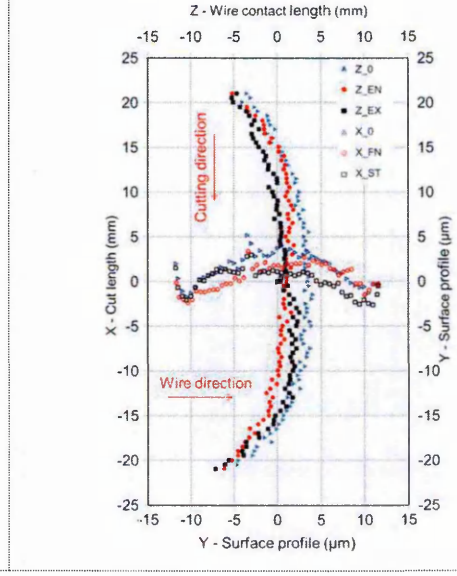

Figure 3-22: The MS-C-2 cut surface data and displacement profiles for clamped (c) and free sides (d).

Surface quality metrics				
	X (cutting direction)	Z (wire direction)	X (cutting direction)	Z (wire direction)
	Clamped side displacement, Fig c, µm		Free side displacement, Fig d, µm	
Min	-1.0	-4.0	-6.0	-2.0
Max	2.5	3.0	4.0	5.0
Rsm	131.0	121.0	133.0	122.0
Sq, Sa	2.5, 1.8		2.5, 1.8	
	Averaged displacement, Figs e and g, µm		Stress error, Figs f and h, MPa (%yield)	
Min	-3.0	-2.0	-62.0 (16.0)	-48.0 (13.0)
Max	3.0	2.0	40.0 (11.0)	87.0 (23.0)
RMS	2.0		47.0 (12.5)	

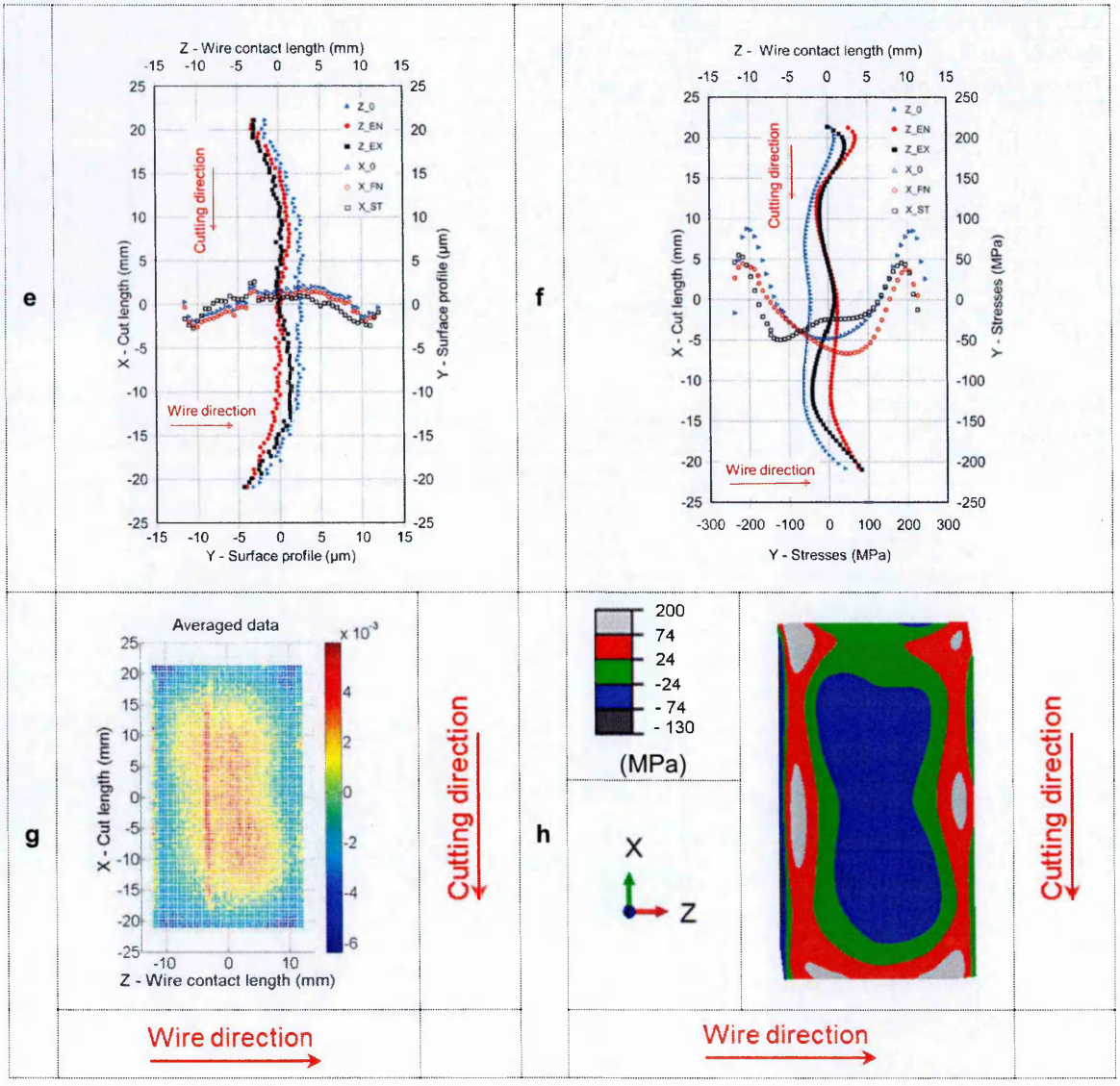

Figure 3-22 cont: The MS-C-2 cut surface quality metrics, profiles of averaged displacement (e) and stress (f), maps of averaged displacement (g) and stress (h).

Specimen details							
Specimen reference				MS-C-3			
Specimen material				Mild Steel (EN3B)			
Cut length, m, thickness, n				(45 x 25) mm			
Cantilever dimensions, p, q				(25 x 170) mm			
Specimen top and bottom surfaces were milled flat surfaces. Vacuum heat treatment performed to relieve internal stresses.							
WEDM information							
Cut date				19th Dec, 2013			
Machine type				Agie Charmillies FI440ccS			
Wire material				Brass (LT25.WIR)			
Wire diameter				0.1 mm			
Cutting technology				LT25A.TEC			
WEDM bath temperature				20 °C			
Nozzles position, pressure				0.2 mm, 0.1 MPa			
The cut was performed with a standard S3 set of parameters with reduced A and TAC.							
WEDM cutting parameters							
EL	10	PA	6	PM	---	Offset	---
ST	1	M	37	S	5	V	60
FF	95	B	8.7	A	0.1	TAC	0.05
Aj	42	S	5	WS	10	WB	0.3
Inj	2	Rate	0.47	IAL	8		
Metrology information							
CMM				Mitutoyo Crysta plus 547 CMM			
Spacing		(0.5 x 0.5) mm		**Probe dia.**		3 mm	
Roughness instrument				Leica 3DCM			
Resolution		12		**Overlap area**		10%	
Threshold		10 %		**Z-Scan value**		200 µm	

Cut MS-C-3 was performed on restrained cutting conditions . The cut was performed with a standard S3 set of parameters with some modifications and using 0.1 mm wire diameter.

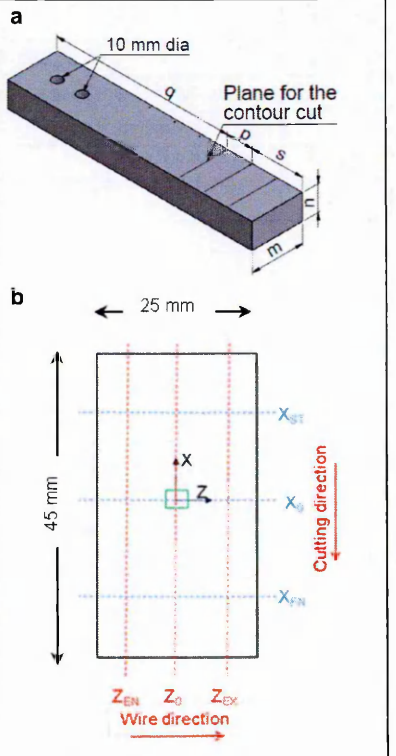

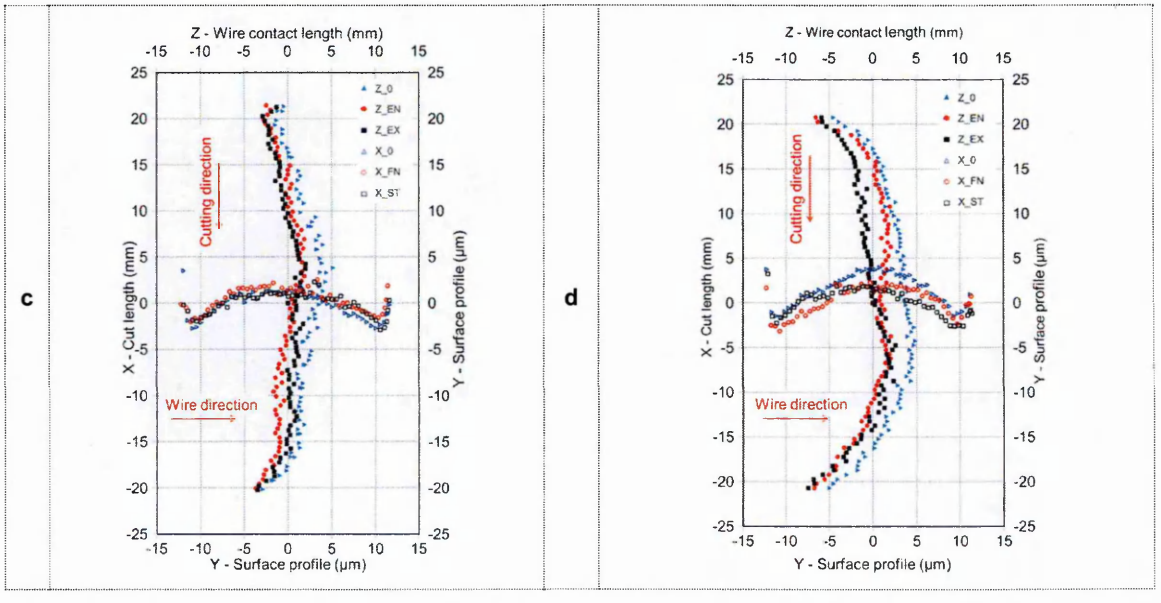

Figure 3-23: The MS-C-3 cut surface data and displacement profiles for clamped (c) and free sides (d).

Surface quality metrics				
	X (cutting direction)	Z (wire direction)	X (cutting direction)	Z (wire direction)
	Clamped side displacement, Fig c, µm		Free side displacement, Fig d, µm	
Min	-3.0	-3.0	-5.0	-2.0
Max	5.0	3.5	5.0	4.0
Rsm	120.0	130.0	102.0	131.0
Sq, Sa	2.3, 1.8		2.3, 1.8	
	Averaged displacement, Figs e and g, µm		Stress error, Figs f and h, MPa (%yield)	
Min	-3.5	-1.5	-88.0 (24.0)	-115.0 (31.0)
Max	4.0	4.0	52.0 (14.0)	69.0 (19.0)
RMS	2.3		54.0 (14.5)	

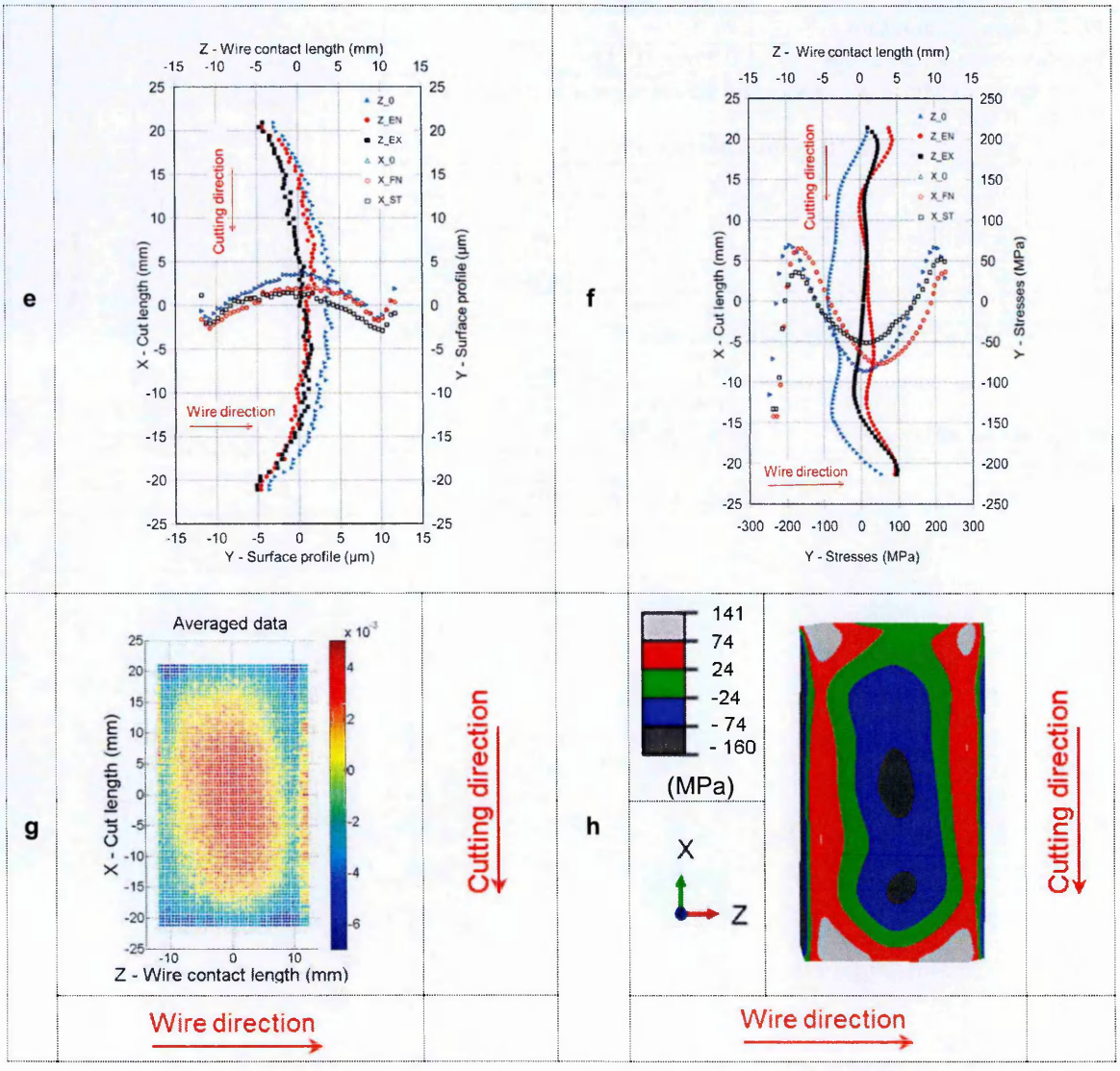

Figure 3-23 cont: The MS-C-3 cut surface quality metrics, profiles of averaged displacement (e) and stress (f), maps of averaged displacement (g) and stress (h).

Specimen details							
Specimen reference			SS-C-1				
Specimen material			Stainless steel (304L)				
Cut length, m, thickness, n			(45 x 25) mm				
Cantilever dimensions, p, q			(25 x 220) mm				
Specimen top and bottom surfaces were milled flat surfaces. Vacuum heat treatment performed to relieve internal stresses.							
WEDM information							
Cut date			20^{th} Dec, 2013				
Machine type			Agie Charmillies FI440ccS				
Wire material			Brass (LT25.WIR)				
Wire diameter			0.25 mm				
Cutting technology			LT25A.TEC				
WEDM bath temperature			20 °C				
Nozzles position, pressure			0.2 mm, 0.8 MPa				
The cut was performed with a standard S5 set of parameters with no manual intervention							
WEDM cutting parameters							
EL	10	PA	6	PM	3	Offset	0.16
ST	1	M	3	S	10	V	80
FF	100	B	7	A	0.6	TAC	0.3
Aj	41	S	10	WS	12	WB	1.6
Inj	14	Rate	3.4	IAL	10		
Metrology information							
CMM			Mitutoyo Crysta plus 547 CMM				
Spacing		(0.5 x 0.5) mm	**Probe dia.**		3 mm		
Roughness instrument			Leica 3DCM				
Resolution		12	**Overlap area**		10%		
Threshold		10 %	**Z-Scan value**		200 µm		

Cut SS-C-1 was performed on restrained cutting conditions . The cut was performed with a standard S5 set of parameters with no manual intervention.

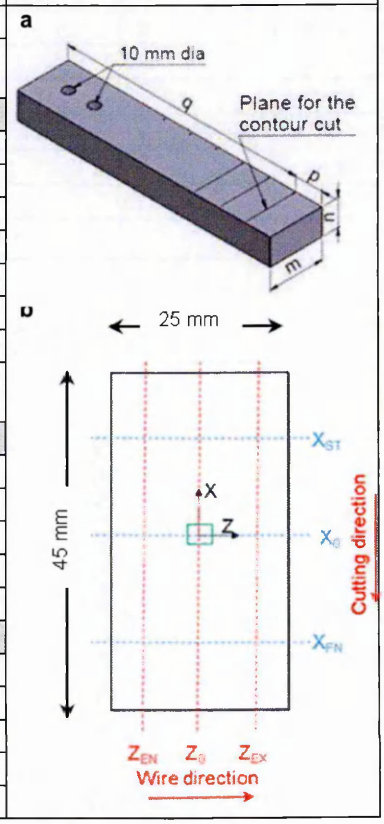

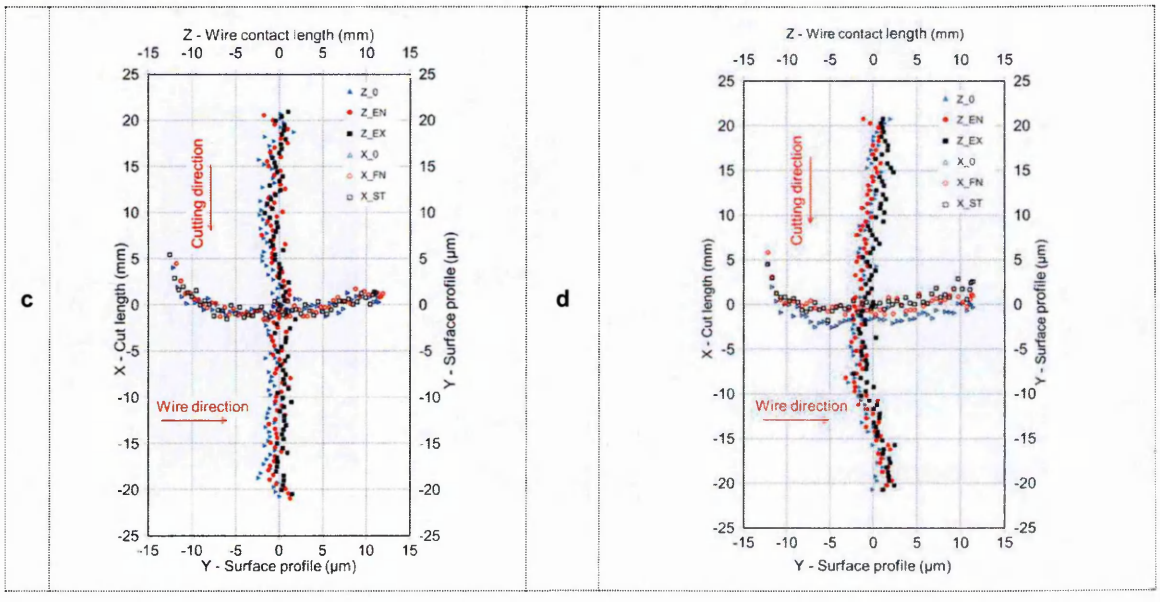

Figure 3-24: The SS-C-1 cut surface data and displacement profiles for clamped (c) and free sides (d).

Surface quality metrics				
	X (cutting direction)	Z (wire direction)	X (cutting direction)	Z (wire direction)
	Clamped side displacement, Fig c, µm		Free side displacement, Fig d, µm	
Min	-2.0	-1.0	-3.0	-2.5
Max	2.0	4.0	2.0	4.5
Rsm	127.0	151.0	125.0	135.0
Sq, Sa	3.0, 2.5		3.0, 2.5	
	Averaged displacement, Figs e and g, µm		Stress error, Figs f and h, MPa (%yield)	
Min	-2.0	-1.5	-20.0 (8.0)	-122.0 (50.0)
Max	1.0	3.0	24.0 (10.0)	30.0 (12.0)
RMS	1.5		33.0 (14.0)	

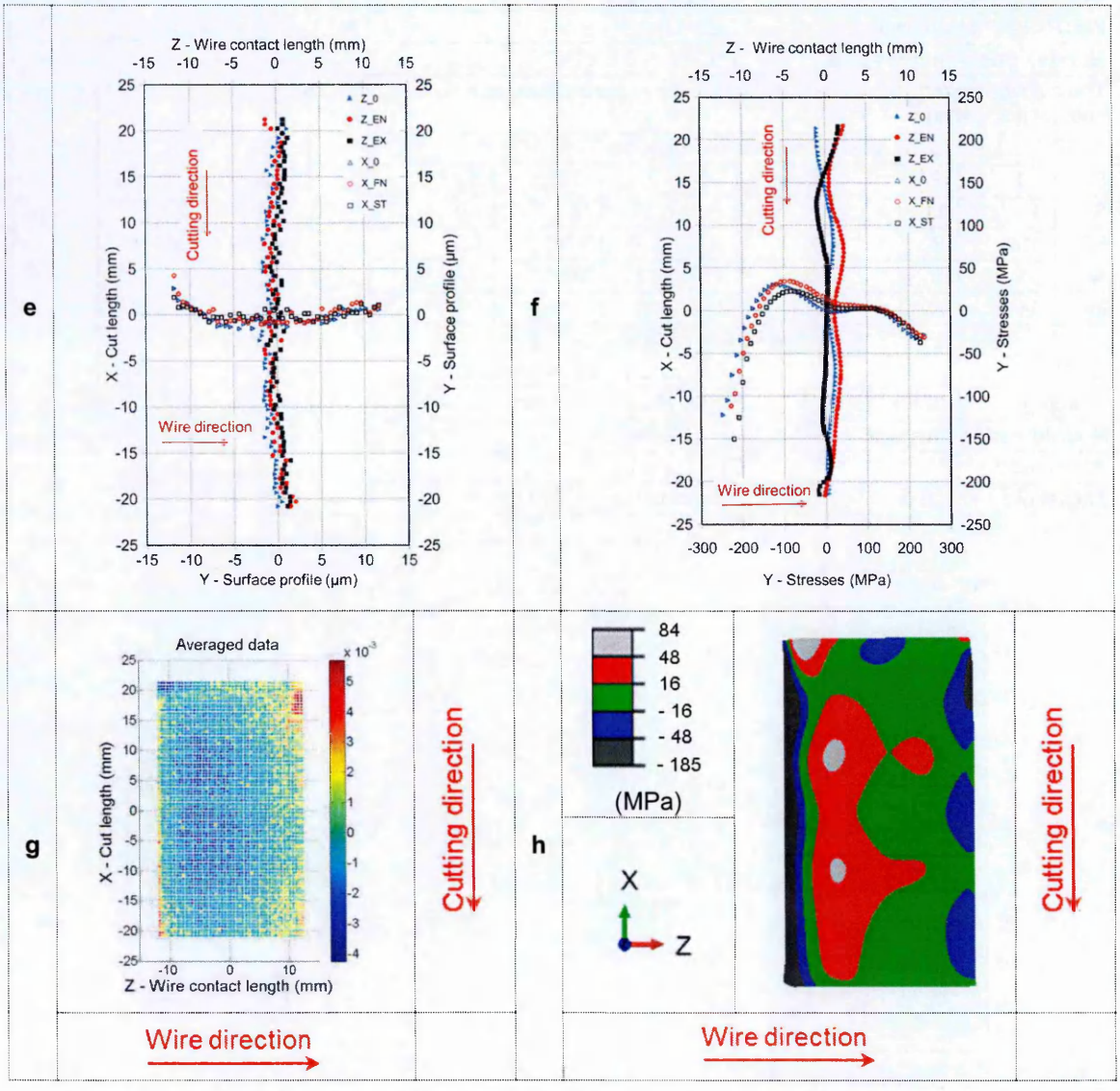

Figure 3-24 cont: The SS-C-1 cut surface quality metrics, profiles of averaged displacement (e) and stress (f), maps of averaged displacement (g) and stress (h).

Specimen details							
Specimen reference				SS-C-2			
Specimen material				Stainless steel (304L)			
Cut length, m, thickness, n				(45 x 25) mm			
Cantilever dimensions, p, q				(25 x 195) mm			
Specimen top and bottom surfaces were milled flat surfaces. Vacuum heat treatment performed to relieve internal stresses.							
WEDM information							
Cut date				20th Dec, 2013			
Machine type				Agie Charmillies FI440ccS			
Wire material				Brass (LT25.WIR)			
Wire diameter				0.1 mm			
Cutting technology				LT25A.TEC			
WEDM bath temperature				20 °C			
Nozzles position, pressure				0.2 mm, 0.1 MPa			
The cut was performed with a standard S3 set of parameters.							
WEDM cutting parameters							
EL	10	PA	6	PM	---	Offset	---
ST	1	M	37	S	5	V	60
FF	95	B	8.7	A	0.2	TAC	0.1
Aj	42	S	5	WS	10	WB	0.3
Inj	2	Rate	0.744	IAL	8		
Metrology information							
CMM				Mitutoyo Crysta plus 547 CMM			
Spacing		(0.5 x 0.5) mm		**Probe dia.**		3 mm	
Roughness instrument				Leica 3DCM			
Resolution		12		**Overlap area**		10%	
Threshold		10 %		**Z-Scan value**		200 µm	

Cut SS-C-2 was performed on restrained cutting conditions . The cut was performed with a standard S3 set of parameters using 0.1 mm wire diameter.

a

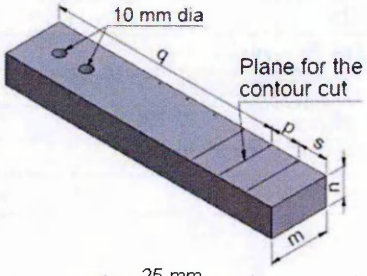

b

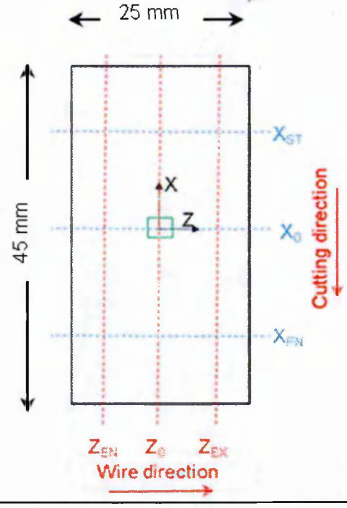

c

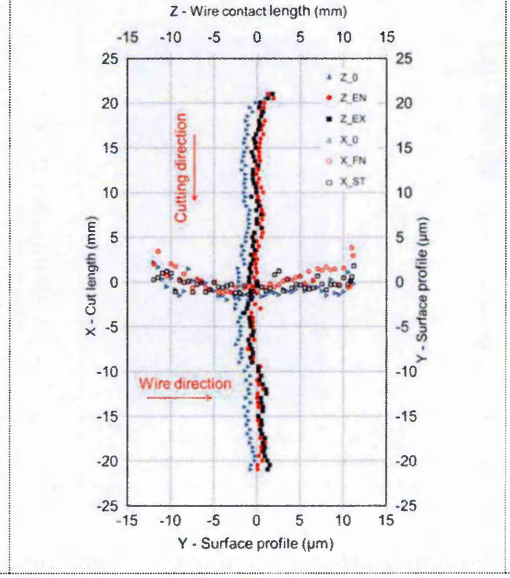

d

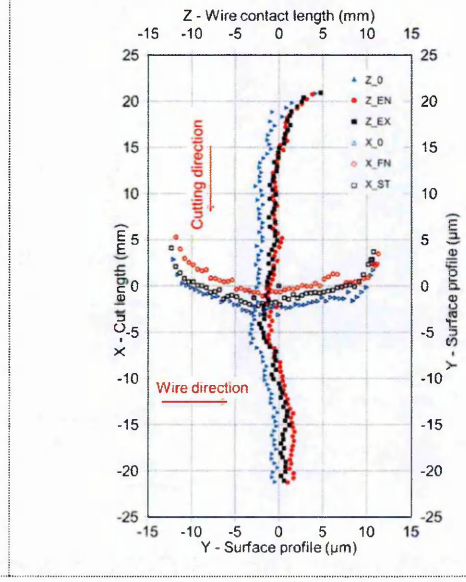

Figure 3-25: The SS-C-2 cut surface data and displacement profiles for clamped (c) and free sides (d).

Surface quality metrics				
	X (cutting direction)	Z (wire direction)	X (cutting direction)	Z (wire direction)
	Clamped side displacement, Fig c, µm		Free side displacement, Fig d, µm	
Min	-2.5	-2.0	-3.0	-3.0
Max	1.0	2.0	4.0	3.0
Rsm	126.0	129.0	125.0	116.0
Sq, Sa	1.9, 1.5		1.9, 1.5	
	Averaged displacement, Figs e and g, µm		Stress error, Figs f and h, MPa (%yield)	
Min	-2.0	-2.5	- 53.0 (22.0)	- 78.0 (19.0)
Max	3.0	3.0	47.0 (32.0)	44.5 (34.0)
RMS	1.9		37.0 (15.0)	

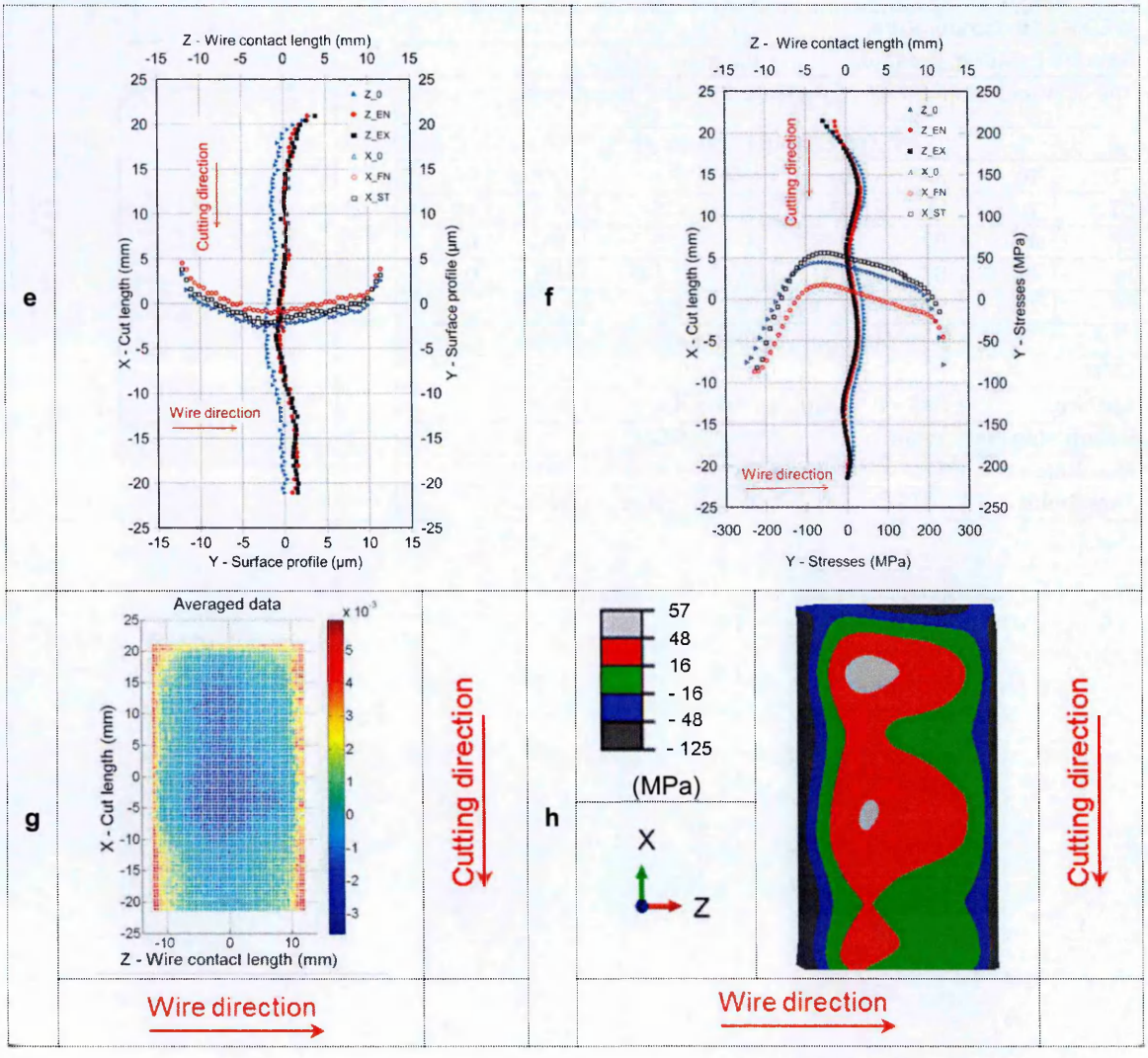

Figure 3-25 cont: The SS-C-2 cut surface quality metrics, profiles of averaged displacement (e) and stress (f), maps of averaged displacement (g) and stress (h).

Specimen details							
Specimen reference				SS-C-3			
Specimen material				Stainless steel (304L)			
Cut length, m, thickness, n				(45 x 25) mm			
Cantilever dimensions, p, q				(25 x 170) mm			
Specimen top and bottom surfaces were milled flat surfaces. Vacuum heat treatment performed to relieve internal stresses.							
WEDM information							
Cut date				20th Dec, 2013			
Machine type				Agie Charmillies FI440ccS			
Wire material				Brass (LT25.WIR)			
Wire diameter				0.1 mm			
Cutting technology				LT25A.TEC			
WEDM bath temperature				20 °C			
Nozzles position, pressure				0.2 mm, 0.1 MPa			
The cut was performed with a standard S3 set of parameters with reduced A and TAC.							
WEDM cutting parameters							
EL	10	PA	6	PM	---	Offset	---
ST	1	M	37	S	5	V	60
FF	95	B	8.7	A	0.1	TAC	0.05
Aj	42	S	5	WS	10	WB	0.3
Inj	2	Rate	0.47	IAL	8		
Metrology information							
CMM				Mitutoyo Crysta plus 547 CMM			
Spacing		(0.5 x 0.5) mm		**Probe dia.**		3 mm	
Roughness instrument				Leica 3DCM			
Resolution		12		**Overlap area**		10%	
Threshold		10 %		**Z-Scan value**		200 µm	

Cut SS-C-3 was performed on restrained cutting conditions . The cut was performed with a standard S3 set of parameters with some modifications and using 0.1 mm wire diameter.

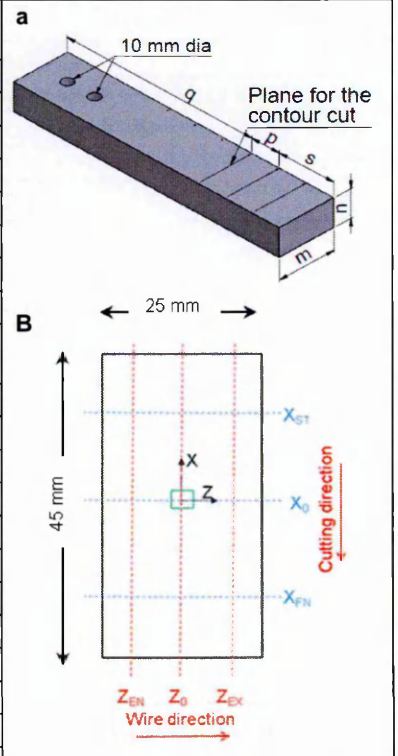

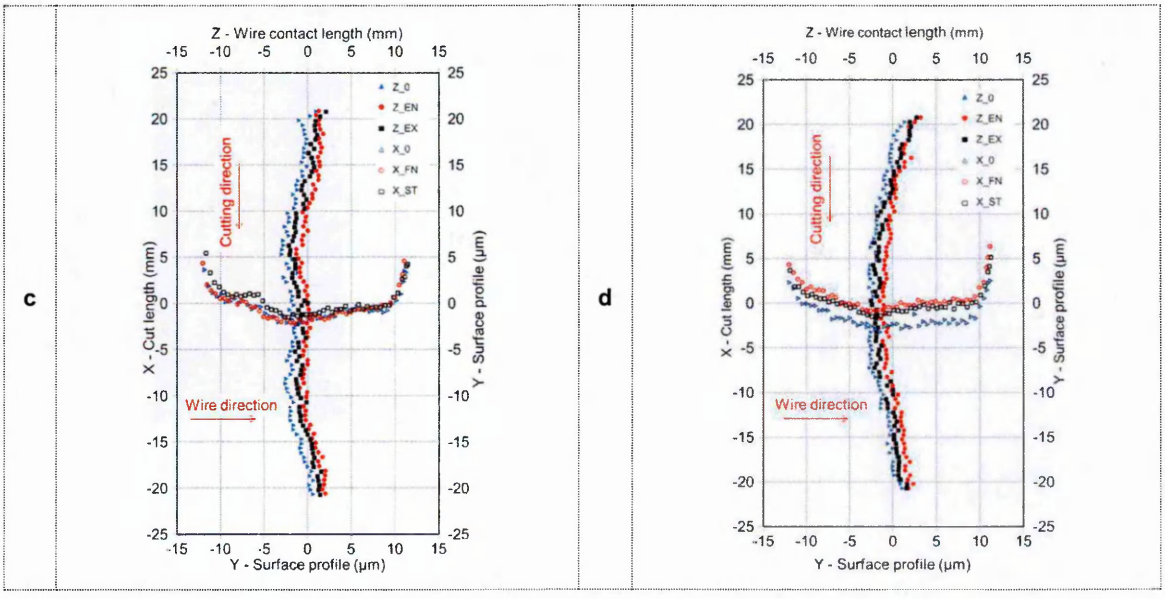

Figure 3-26: The SS-C-3 cut data and displacement profiles for clamped (c) and free sides (d).

Surface quality metrics				
	X (cutting direction)	Z (wire direction)	X (cutting direction)	Z (wire direction)
	Clamped side displacement, Fig c, µm		Free side displacement, Fig d, µm	
Min	- 3.0	- 2.0	-3.0	- 3.0
Max	1.0	3.5	3.0	2.5
Rsm	129.0	114.0	96.0	115.0
Sq, Sa	2.2, 1.7		2.1, 1.7	
	Averaged displacement, Figs e and g, µm		Stress error, Figs f and h, MPa (%yield)	
Min	- 2.0	- 3.0	- 8.0 (3.0)	-116.0 (48.0)
Max	2.0	3.0	43.0 (18.0)	29.0 (12.0)
RMS	2.0		39.0 (16.0)	

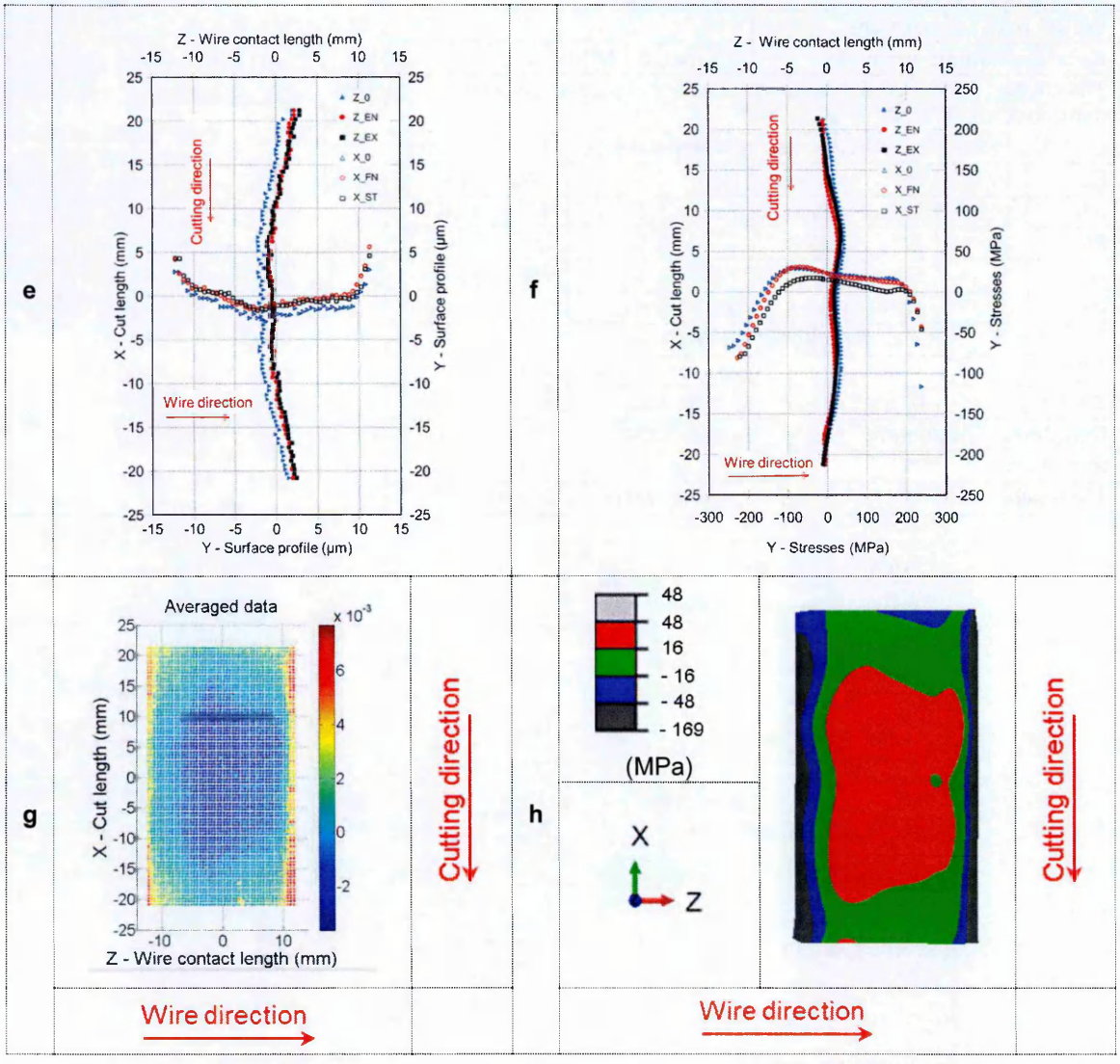

Figure 3-26: The SS-C-3 cut surface quality metrics, profiles of averaged displacement (e) and stress (f), maps of averaged displacement (g) and stress (h).

Specimen details							
Specimen reference				MS-B-4			
Specimen material				Mild steel (EN3B)			
Cut length, m, thickness, n				(42 x 25) mm			
Cantilever dimensions, p, q				(25 x 145) mm			
Specimen top and bottom surfaces were milled flat surfaces. Vacuum heat treatment performed to relieve internal stresses.							
WEDM information							
Cut date				01st Oct, 2014			
Machine type				Agie Charmillies FI440ccS			
Wire material				Brass (LT25.WIR)			
Wire diameter				0.25 mm			
Cutting technology				LT25A.TEC			
WEDM bath temperature				20 °C			
Nozzles position, pressure				0.2 mm, 0.8 MPa			
The cut was performed with a standard S5 set of parameters with no manual intervention							
WEDM cutting parameters							
EL	10	PA	6	PM	3	Offset	0.16
ST	1	M	3	S	10	V	80
FF	100	B	7	A	0.6	TAC	0.3
Aj	41	S	10	WS	12	WB	1.6
Inj	14	Rate	3.4	IAL	10		
Metrology information							
CMM				Mitutoyo Crysta plus 547 CMM			
Spacing		(0.5 x 0.5) mm		**Probe dia.**		3 mm	
Roughness instrument				Leica 3DCM			
Resolution		12		**Overlap area**		10%	
Threshold		10 %		**Z-Scan value**		200 µm	

Cut MS-B-4 was performed on restrained cutting conditions and was started from pilot hole placed at 5.9 mm away from one edge of the specimen.

a

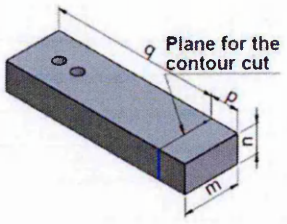

b

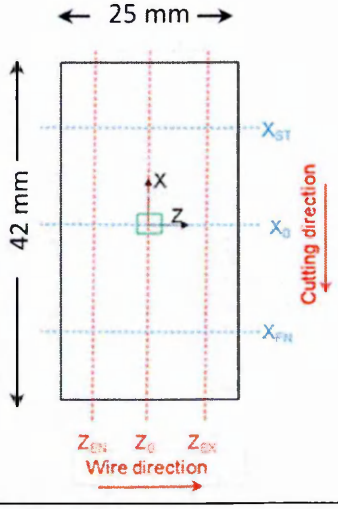

c

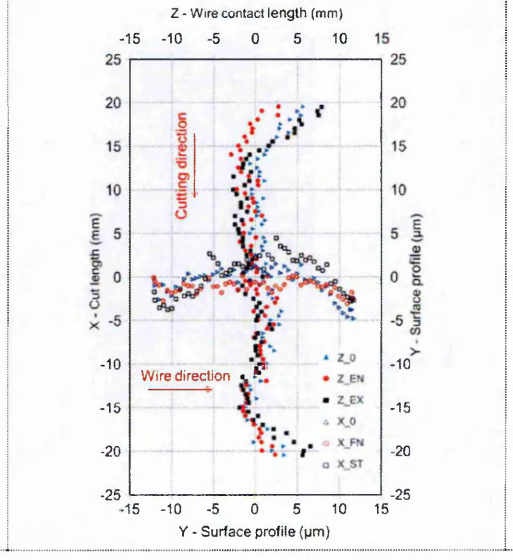

d

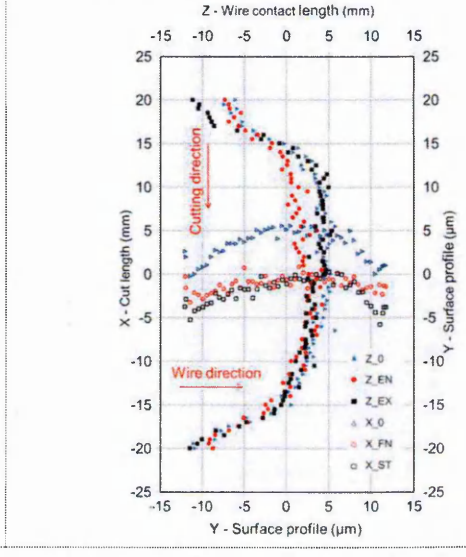

Figure 3-27: The MS-B-4 cut surface data and displacement profiles for clamped (c) and free sides (d).

Surface quality metrics				
	X (cutting direction)	Z (wire direction)	X (cutting direction)	Z (wire direction)
	Clamped side displacement, Fig c, µm		Free side displacement, Fig d, µm	
Min	- 4.8	- 1.2	- 11.0	- 0.2
Max	1.5	5.6	5.8	5.6
Rsm	X	X	135.0	136.0
Sq, Sa	X, X		3.6, 2.7	
	Averaged displacement, Figs e and g, µm		Stress error, Figs f and h, MPa (%yield)	
Min	- 4.0	- 2.0	- 46.0 (12.0)	- 71.0 (19.0)
Max	4.0	3.0	81.0 (22.0)	86.0 (23.0)
RMS	2.3		49 .0(13.0)	

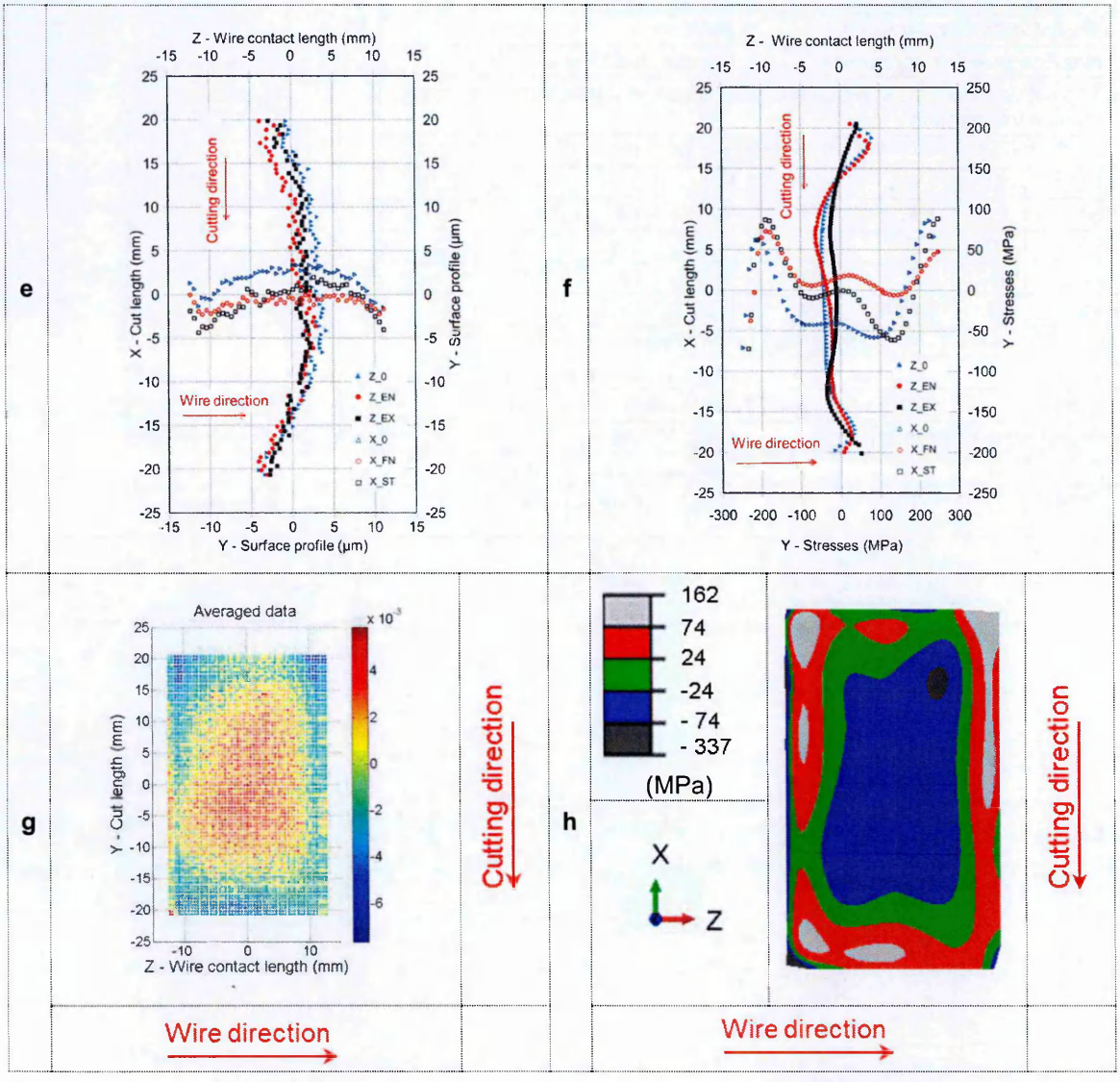

Figure 3-27 cont: The MS-B-4 cut surface quality metrics, profiles of averaged displacement (e) and stress (f), maps of averaged displacement (g) and stress (h).

Specimen details							
Specimen reference				MS-C-4			
Specimen material				Mild steel (EN3B)			
Cut length, m, thickness, n				(45 x 25) mm			
Cantilever dimensions, p, q				(50 x 120) mm			
Specimen top and bottom surfaces were milled flat surfaces. Vacuum heat treatment performed to relieve internal stresses.							
WEDM information							
Cut date				27th Aug, 2014			
Machine type				Agie Charmillies FI440ccS			
Wire material				Brass (LT25.WIR)			
Wire diameter				0.25 mm			
Cutting technology				LT25A.TEC			
WEDM bath temperature				20 °C			
Nozzles position, pressure				0.2 mm, 0.8 MPa			
The cut was performed with a standard S5 set of parameters with no manual intervention							
WEDM cutting parameters							
EL	10	PA	6	PM	3	Offset	0.16
ST	1	M	3	S	10	V	80
FF	100	B	7	A	0.6	TAC	0.3
Aj	41	S	10	WS	12	WB	1.6
Inj	14	Rate	3.4	IAL	10		
Metrology information							
CMM				Mitutoyo Crysta plus 547 CMM			
Spacing		(0.5 x 0.5) mm		**Probe dia.**		3 mm	
Roughness instrument				Leica 3DCM			
Resolution		12		**Overlap area**		10%	
Threshold		10 %		**Z-Scan value**		200 µm	

Cut MS-C-4 was performed on restrained cutting conditions with similar stiffness on both sides of the cut plane.

a

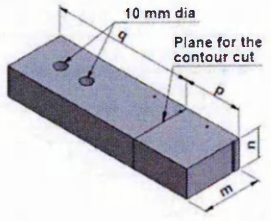

b

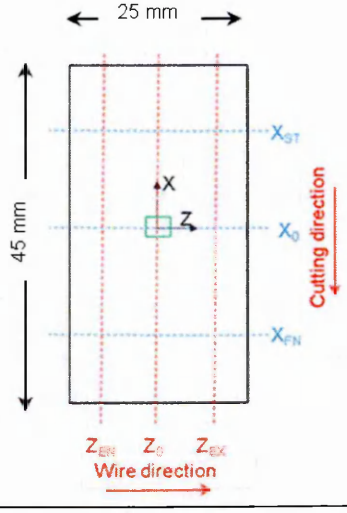

c

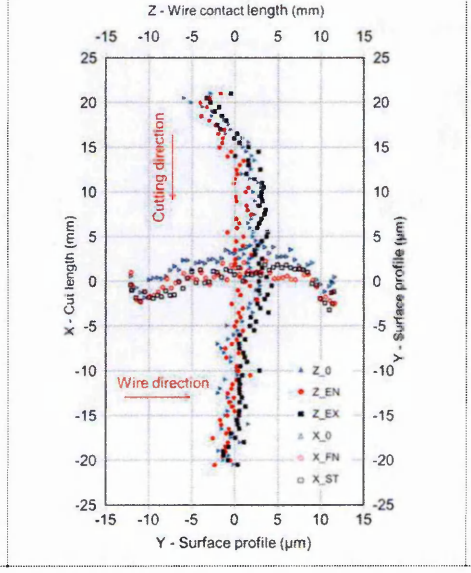

d

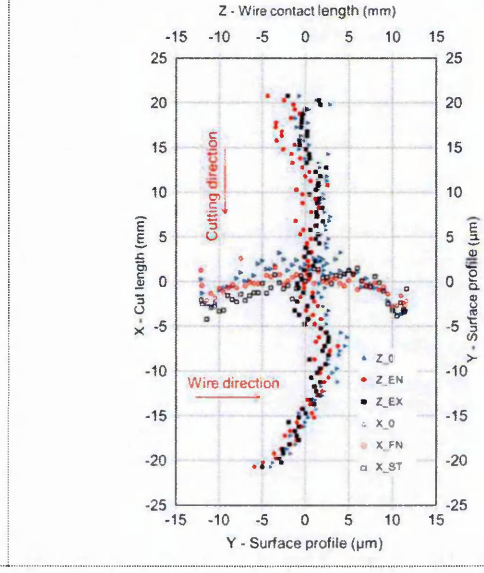

Figure 3-28: The MS-C-4 cut surface data and displacement profiles for clamped (c) and free sides (d).

Surface quality metrics				
	X (cutting direction)	Z (wire direction)	X (cutting direction)	Z (wire direction)
	Clamped side displacement, Fig c, µm		Free side displacement, Fig d, µm	
Min	- 6.0	- 1.8	- 4.0	- 3.6
Max	3.0	4.2	4.8	3.2
Rsm	115.0	148.0	125.0	142.0
Sq, Sa	3.3, 2.6		3.3, 2.5	
	Averaged displacement, Figs e and g, µm		Stress error, Figs f and h, MPa (%yield)	
Min	- 2.0	- 2.3	- 47.0 (12.0)	- 58.0 (15.0)
Max	3.2	3.7	36.0 (10.0)	86.0 (23.0)
RMS	2.0		43.0 (11.0)	

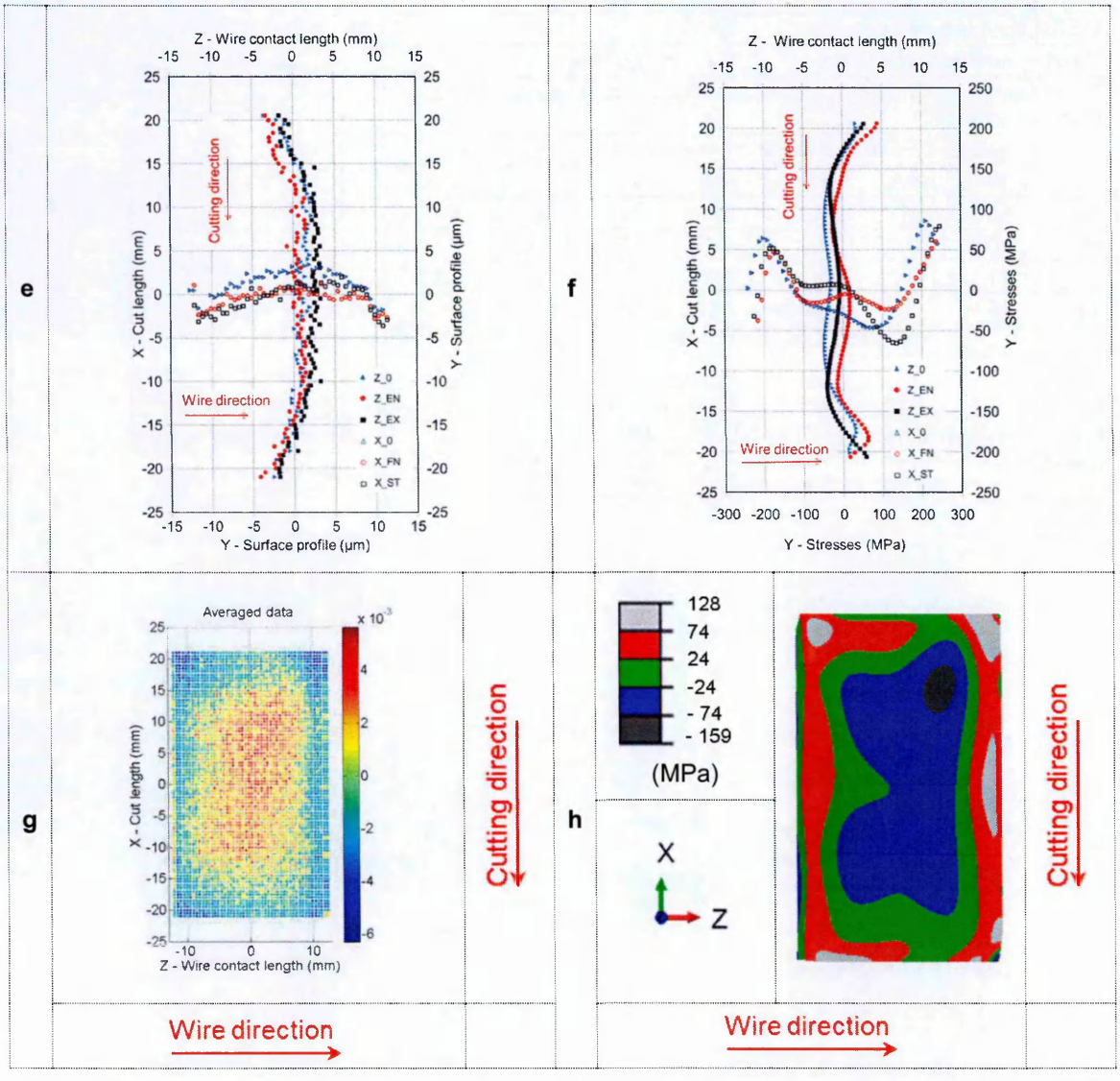

Figure 3-28 cont: The MS-C-4 cut surface quality metrics, profiles of averaged displacement (e) and stress (f), maps of averaged displacement (g) and stress (h).

Specimen details							
Specimen reference				SS-A-5			
Specimen material				Stainless steel (304L)			
Cut length, m, thickness, n				(42 x 25) mm			
Cantilever dimensions, p, q				(25 x 120) mm			
Specimen top and bottom surfaces were milled flat surfaces. Vacuum heat treatment performed to relieve internal stresses.							
WEDM information							
Cut date				01st Oct, 2014			
Machine type				Agie Charmillies FI440ccS			
Wire material				Brass (LT25.WIR)			
Wire diameter				0.25 mm			
Cutting technology				LT25A.TEC			
WEDM bath temperature				20 °C			
Nozzles position, pressure				0.2 mm, 0.8 MPa			
The cut was performed with a standard S5 set of parameters with no manual intervention							
WEDM cutting parameters							
EL	10	PA	6	PM	3	Offset	0.16
ST	1	M	3	S	10	V	80
FF	100	B	7	A	0.6	TAC	0.3
Aj	41	S	10	WS	12	WB	1.6
Inj	14	Rate	3.4	IAL	10		
Metrology information							
CMM				Mitutoyo Crysta plus 547 CMM			
Spacing		(0.5 x 0.5) mm		**Probe dia.**		3 mm	
Roughness instrument				Leica 3DCM			
Resolution		12		**Overlap area**		10%	
Threshold		10 %		**Z-Scan value**		200 µm	

Cut SS-A-5 was performed on restrained cutting conditions and was started from pilot hole placed at 5.9 mm away from one edge of the specimen.

a

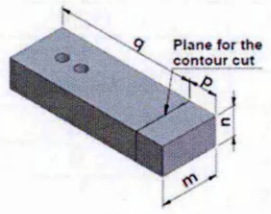

b

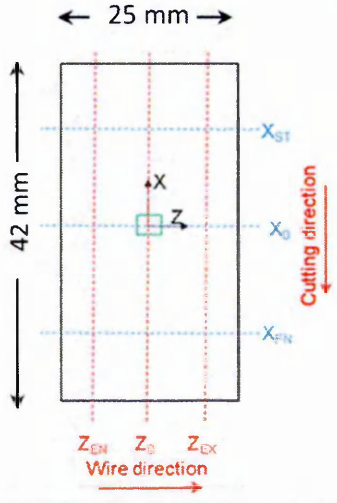

c

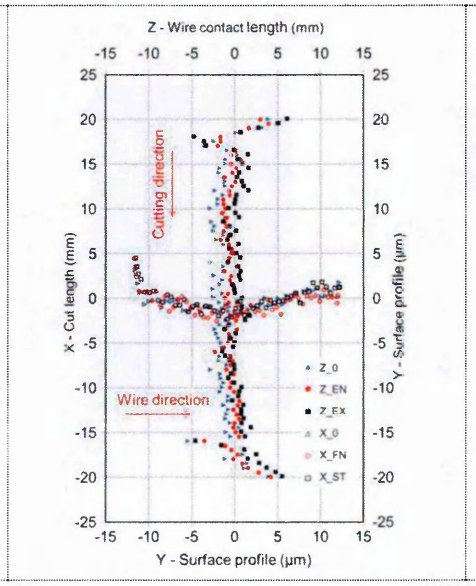

d

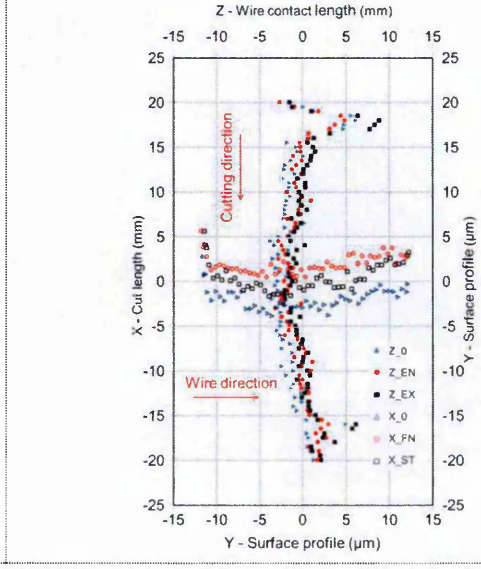

Figure 3-29: The SS-A-5 cut surface data and displacement profiles for clamped (c) and free sides (d).

Surface quality metrics				
	X (cutting direction)	Z (wire direction)	X (cutting direction)	Z (wire direction)
	Clamped side displacement, Fig c, µm		Free side displacement, Fig d, µm	
Min	- 5.5	- 1.8	- 3.7	- 4.5
Max	5.0	3.0	6.0	2.7
Rsm	112.0	142.0	140.0	131.0
Sq, Sa	3.4, 2.6		3.4, 2.6	
	Averaged displacement, Figs e and g, µm		Stress error, Figs f and h, MPa (%yield)	
Min	- 3.0	- 2.0	- 42.0 (17.0)	- 112.0 (46.0)
Max	1.6	1.2	49.0 (20.0)	39.0 (16.0)
RMS	1.9		41.0 (17.0)	

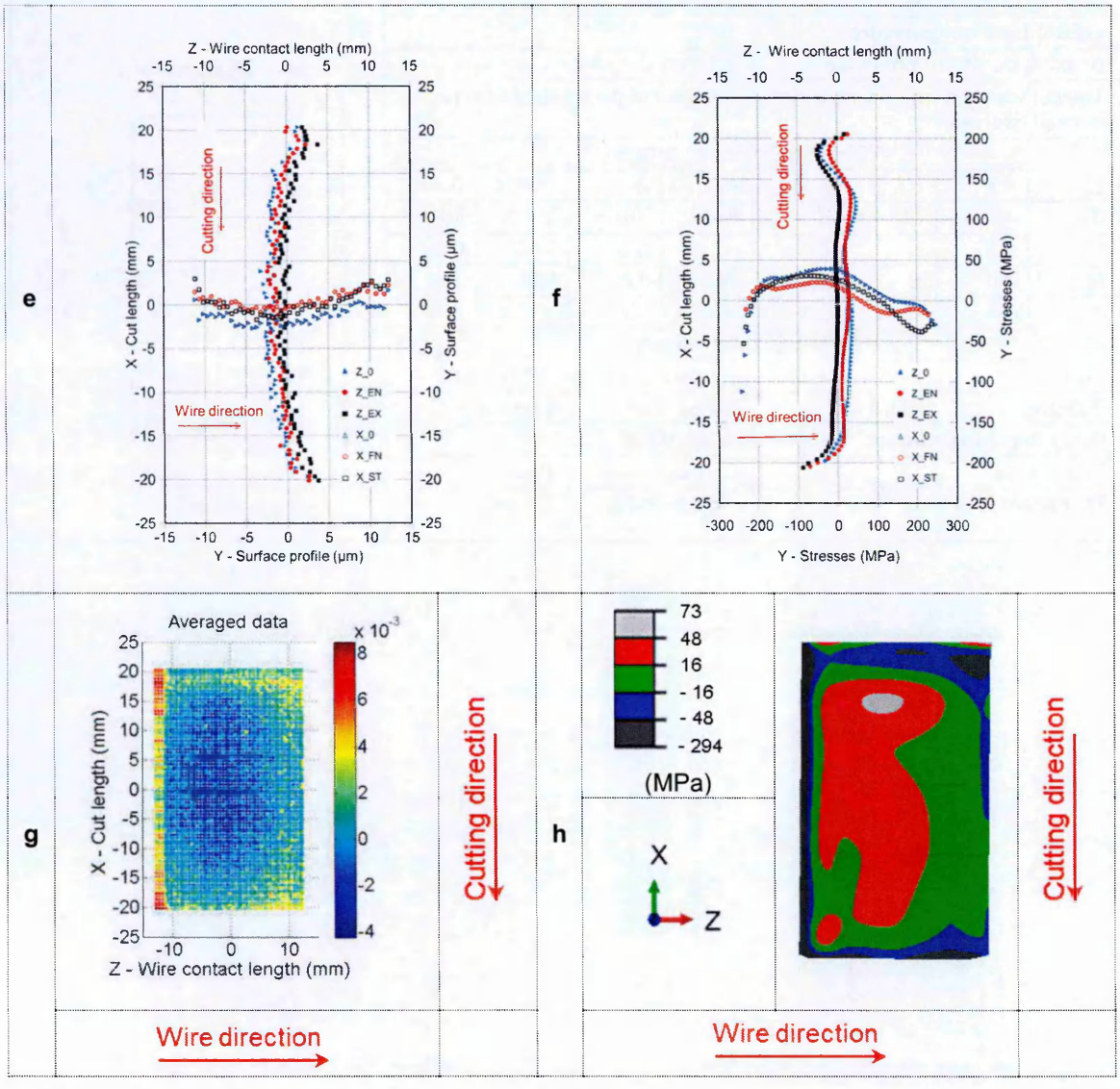

Figure 3-29 cont: The SS-A-5 cut surface quality metrics, profiles of averaged displacement (e) and stress (f), maps of averaged displacement (g) and stress (h).

Specimen details							
Specimen reference				SS-C-4			
Specimen material				Stainless steel (304L)			
Cut length, m, thickness, n				(45 x 25) mm			
Cantilever dimensions, p, q				(50 x 120) mm			
Specimen top and bottom surfaces were milled flat surfaces. Vacuum heat treatment performed to relieve internal stresses.							
WEDM information							
Cut date				27th Aug, 2014			
Machine type				Agie Charmillies FI440ccS			
Wire material				Brass (LT25.WIR)			
Wire diameter				0.25 mm			
Cutting technology				LT25A.TEC			
WEDM bath temperature				20 °C			
Nozzles position, pressure				0.2 mm, 0.8 MPa			
The cut was performed with a standard S5 set of parameters with no manual intervention							
WEDM cutting parameters							
EL	10	PA	6	PM	3	Offset	0.16
ST	1	M	3	S	10	V	80
FF	100	B	7	A	0.6	TAC	0.3
Aj	41	S	10	WS	12	WB	1.6
Inj	14	Rate	3.4	IAL	10		
Metrology information							
CMM				Mitutoyo Crysta plus 547 CMM			
Spacing		(0.5 x 0.5) mm		**Probe dia.**		3 mm	
Roughness instrument				Leica 3DCM			
Resolution		12		**Overlap area**		10%	
Threshold		10 %		**Z-Scan value**		200 µm	

Cut SS-C-4 was performed on restrained cutting conditions with similar stiffness on both sides of the cut plane

a

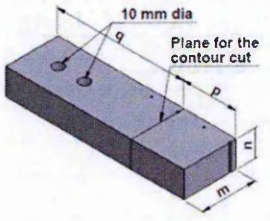

b

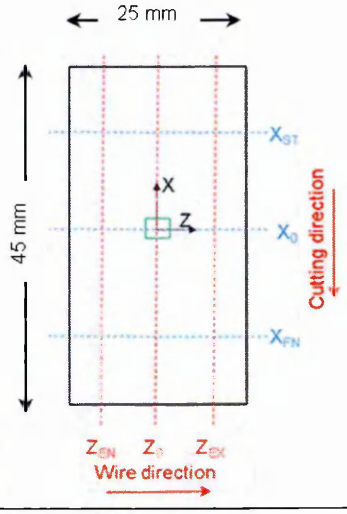

c

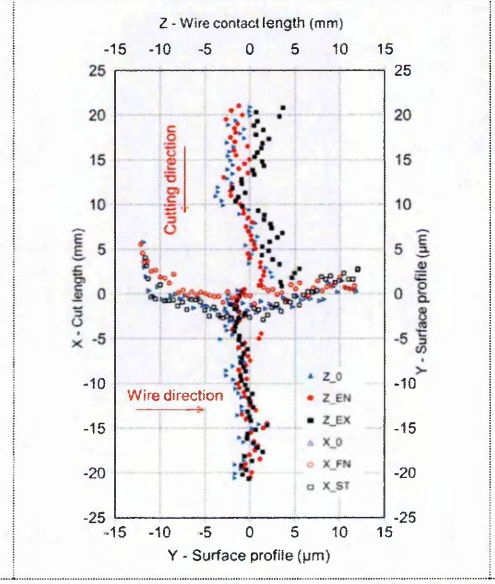

d

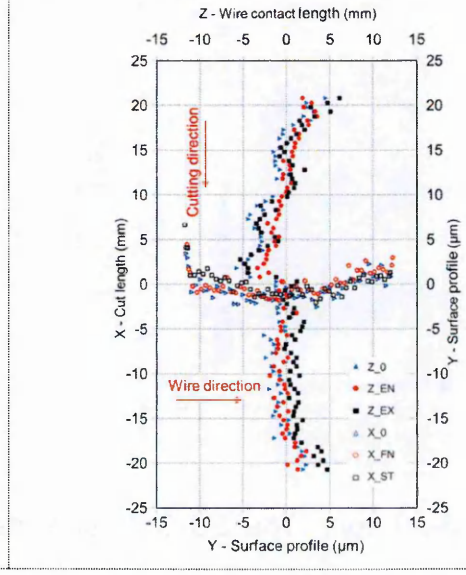

Figure 3-30: The SS-C-4 cut surface data and displacement profiles for clamped (c) and free sides (d).

Surface quality metrics				
	X (cutting direction)	Z (wire direction)	X (cutting direction)	Z (wire direction)
	Clamped side displacement, Fig c, µm		Free side displacement, Fig d, µm	
Min	- 3.7	- 3.0	- 6.0	- 2.6
Max	2.4	5.7	4.5	3.5
Rsm	121.0	174.0	140.0	150.0
Sq, Sa	3.6, 2.8		3.7, 3.0	
	Averaged displacement, Figs e and g, µm		Stress error, Figs f and h, MPa (%yield)	
Min	- 1.3	- 2.4	- 53.0 (22.0)	- 165.0 (69.0)
Max	3.2	4.8	57.0 (24.0)	34.0(14.0)
RMS	1.8		41.0 (17.0)	

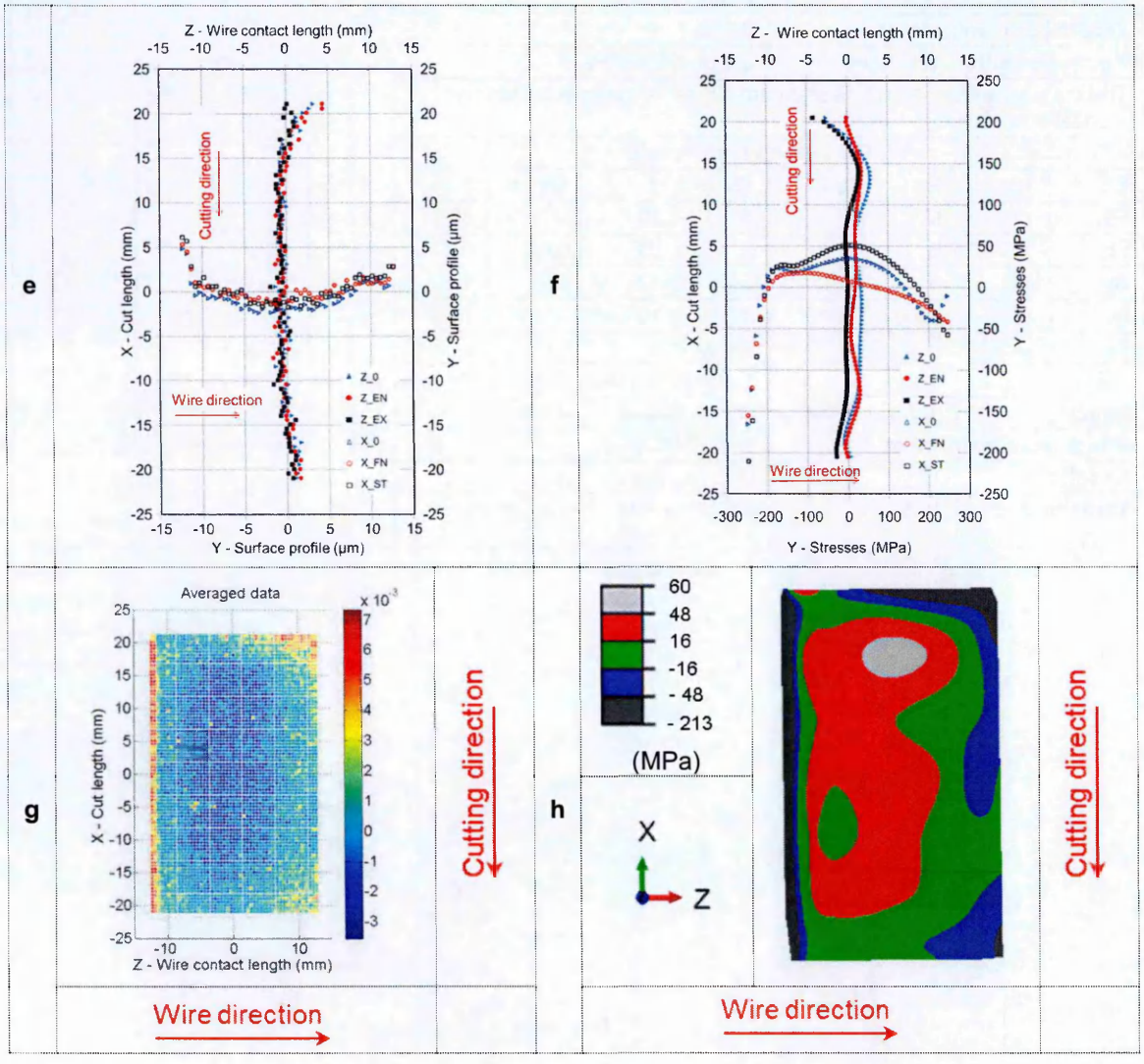

Figure 3-30 cont: The SS-C-4 cut surface quality metrics, profiles of averaged displacement (e) and stress (f), maps of averaged displacement (g) and stress (h).

Series 1 (MS-C-1, MS-C-2 and MS-C-3) results and findings

Table 3-6 shows a comparison of the quality of restrained cut MS-C-1 (*Figure* 3-21) and unrestrained cut MS-A-1 (*Figure 3-7*). The displacement variations in the free side of the cut MS-C-1 were considerably improved, in comparison to MS-A-1, by providing restraint along the plane of the cut. Furthermore, having the restraint also led to a reduction in the averaged displacement variations and stress errors for the cut MS-C-1. On the other hand, surface features such as flared edges at the wire entry side, the bowed form of the surface profiles, and asymmetry in both sides of the cuts, were seen in both MS-C-1 and MS-A-1. However, these features are reduced in MS-C-1 due to an improvement in the displacement variations of the free side of the cut.

	MS-A-1		**MS-C-1**	
	X	**Z**	**X**	**Z**
Clamped side disp. (µm)	4.5	7.5	4.0	7.5
Free side disp. (µm)	26.0	11.0	11.0	6.5
Averaged disp. (µm)	13.0	7.0	6.0	7.0
Stress error-RMS (% yield) (MPa)	59.0 (16.0)		52.0 (14.0)	
	Clamped side	**Free side**	**Clamped side**	**Free side**
3D Surface roughness Sq, Sa (µm)	3.4, 2.6	3.7, 2.9	3.5, 2.6	3.7, 2.7

Table 3-6: A comparison of quality of the cuts MS-A-1 and MS-C-1.

The cut MS-C-2 was performed using restrained cutting conditions with a 0.1 mm diameter wire (note MS-C-1 used 0.25 mm wire). Table 3-7 compares the quality of the cuts MS-C-2 and MS-C-1. The displacement variations in both sides

of the cut MS-C-2 (see *Figure 3-22*) were slightly reduced when compared to those in MS-C-1. Furthermore, averaged displacement variations and associated stresses were also reduced. However, flared edges at the wire entry side, the bowed form of the surface profiles and asymmetry in both sides of the cuts were seen in both MS-C-2 and MS-C-1. Conversely, less surface roughness was observed on cut MS-C-2 than on MS-C-1 because of the smaller wire diameter used. Slightly improved values were found in RMS variations for displacement and stress errors for the cut MS-C-2 when compared to MS-C-1.

	MS-C-1		**MS-C-2**		**MS-C-3**	
	X	**Z**	**X**	**Z**	**X**	**Z**
Clamped side displacement (µm)	4.0	7.5	3.5	7.0	8.0	6.5
Free side displacement (µm)	11.0	6.5	10.0	7.0	10.0	6.0
Averaged displacement (µm)	6.0	7.0	6.0	4.0	7.5	5.5
Stress error-RMS (% yield) (MPa)	52.0 (14.0)		47.0 (12.5)		54.0 (14.5)	
	Clamped side	**Free side**	**Clamped side**	**Free side**	**Clamped side**	**Free side**
3D Surface roughness Sq, Sa (µm)	3.5, 2.6	3.7, 2.7	2.5, 1.8	2.5, 1.8	2.3, 1.8	2.3, 1.8

Table 3-7: Surface quality metrics for the cuts MS-C-1, MS-C-2 and MS-C-3

The cut MS-C-3 (*Figure 3-23*) repeated MS-C-2 but with reduced values of cutting parameters A and TAC. From comparison Table 3-7 it is seen that the displacement variation for each side of the cut and the averaged displacements

from both sides of the cut were not improved. The associated stress errors were also found to be slightly larger than those from cut MS-C-2.

So, to summarize, the quality of the cut surface MS-C-1 was improved by providing the restraint along the plane of the cut in comparison to the unrestrained cut MS-A-1. The quality of cut MS-C-2 was further improved by reducing the wire diameter, A subsequent reduction in WEDM cutting parameters A (from 0.2 μs to 0.1 μs) and TAC (from 0.1 μs to 0.05 μs) for the 0.1 mm diameter wire gave no additional improvement. The surface topography of all three restrained cuts (MS-C-1, MS-C-2 and MS-C-3) exhibited similar surface features to the unrestrained cut surfaces.

Series 2 (SS-C-1, SS-C-2 and SS-C-3) results and findings

The cuts SS-C-1, SS-C-2 and SS-C-3 (*Figure 3-24* to *Figure 3-26*) were performed using a benchmark stainless steel specimen, under restrained cutting conditions. Table 3-8 compares the quality of cut SS-C-1 with the equivalent unrestrained cut SS-A-1 *(Figure 3-12*). For cut SS-C-1, the displacement variations were slightly reduced but not the apparent stresses, when compared to those in cut SS-A-1. This was due to the ligament restraint provided along the plane of the cut.

The results of cuts SS-C-2 and SS-C-3 showed no improvement in the quality of the cut surfaces from reducing the wire diameter to 0.1 mm (cut SS-C-2) and WEDM cutting parameters A (from 0.6 μs to 0.1 μs) and TAC (from 0.2 μs to 0.05 μs) for cut SS-C-3, as shown in the Table 3-9. The surface topography of all three

restrained cuts exhibited similar surface features to those seen on previous unrestrained cut surfaces.

	SS-C-1		SS-A-1	
	X	Z	X	Z
Clamped side disp. (µm)	4.0	5.0	5.0	5.5
Free side disp. (µm)	5.0	7.0	9.0	7.0
Averaged disp. (µm)	3.0	4.5	5.0	6.5
Stress error-RMS (% yield) (MPa)	33.0 (14.0)		33.0 (14.0)	
	Clamped side	Free side	Clamped side	Free side
3D Surface roughness Sq, Sa (µm)	3.0, 2.5	3.0, 2.5	3.4, 2.6	3.3, 2.5

Table 3-8: A comparison of the quality of the cuts SS-C-1 and SS-A-1.

	SS-C-1		SS-C-2		SS-C-3	
	X	Z	X	Z	X	Z
Clamped side displacement (µm)	4.0	5.0	3.5	4.0	4.0	5.5
Free side displacement (µm)	5.0	7.0	7.0	6.0	6.0	5.5
Averaged displacement (µm)	3.0	4.5	5.0	5.5	4.0	6.0
Stress error-RMS (% yield) (MPa)	33.0 (14.0)		37.0 (15.0)		39.0 (16.0)	
	Clamped side	Free side	Clamped side	Free side	Clamped side	Free side
3D Surface roughness Sq, Sa (µm)	3.0, 2.5	3.0, 2.5	1.9, 1.5	1.9, 1.5	2.2, 1.7	2.1, 1.7

Table 3-9: A comparison of the quality of the cuts SS-C-1, SS-C-2 and SS-C-3.

Series 3 (MS-B-4 and MS-C-4) results and findings

The cut MS-B-4 (*Figure 3-27*) was performed on a benchmark mild steel specimen using restrained cutting conditions as shown in *Figure 3-20,* notably the pilot hole ligament length was increased from those used on previous restrained cuts (from 1.6 mm to 5 mm), to provide added support during cutting. Table 3-10 compares the quality of cuts MS-B-4 and MS-C-1 (*Figure 3-21*). An improved quality of the cut surface was not achieved by increasing the ligament.

The following cut MS-C-4 (*Figure 3-28*) used the original ligament length (1.6 mm), and reduced the material stiffness mismatch across the cut plane (i.e. cantilever dimension p was increased from 25 mm to 50 mm). Table 3-10 compares the surface quality of the cut MS-C-4 with MS-B-4 and MS-C-1. For the cut MS-C-4, the displacement variations, and associated stress errors, were less than those found on cut MS-C-1. Moreover, the cut surface features such as asymmetry in both sides of the cut surfaces, and bowed form of the surface profile, were slightly improved compared to MS-C-1 cut. This suggests that the bowed deformation shape of the "free" side is related to the stiffness of material being cut away (note change in cantilever dimension, p, from 25 to 50 mm).

	MS-C-1		MS-B-4		MS-C-4	
	X	Z	X	Z	X	Z
Clamped side displacement (µm)	4.0	7.5	6.3	6.8	9.0	6.0
Free side displacement (µm)	11.0	6.5	16.8	5.8	8.8	6.8
Averaged displacement (µm)	6.0	7.0	8.0	5.0	5.2	6.0
Stress error-RMS (% yield) (MPa)	52.0 (14.0)		49.0 (13.0)		43.0 (11.0)	
	Clamped side	**Free side**	**Clamped side**	**Free side**	**Clamped side**	**Free side**
3D Surface roughness Sq, Sa (µm)	3.5, 2.6	3.7, 2.7	-	3.6, 2.7	3.3, 2.6	3.3, 2.5

Table 3-10: A comparison of the quality of the cuts MS-C-1, MS-B-4 and MS-C-4.

Series 4 (SS-A-5 and SS-C-4) results and findings

Similar to the third series of restrained cuts, SS-A-5 (*Figure 3-29*) was performed using extra ligament length and SS-C-4 (*Figure 3-30*) was performed with similar stiffness on both sides of the cut plane on benchmark stainless steel specimens.

The results in Table 3-11 confirm that, in both cases, the quality of the cut surfaces showed no improvement on the surface of the previous cut, SS-C-1 (*Figure 3-24*).

	SS-C-1		SS-A-5		SS-C-4	
	X	Z	X	Z	X	Z
Clamped side displacement (µm)	4.0	5.0	10.5	4.8	6.1	8.7
Free side displacement (µm)	5.0	7.0	9.7	7.2	10.5	6.1
Averaged displacement (µm)	3.0	4.5	4.6	3.2	4.5	7.2
Stress error-RMS (% yield) (MPa)	33.0 (14.0)		41.0 (17.0)		41.0 (17.0)	
	Clamped side	**Free side**	**Clamped side**	**Free side**	**Clamped side**	**Free side**
3D Surface roughness Sq, Sa (µm)	3.0, 2.5	3.0, 2.5	3.4, 2.6	3.4, 2.6	3.6, 2.8	3.7, 3.0

Table 3-11: shows the quality of the cut surfaces SS-A-5 and SS-C-4 compared with SS-C-1.

3.11.4 Discussion of the second experiment results for restrained cuts

Results from the second experiment for restrained cuts reveal the following features:

- The quality of the cut surfaces for both material types, mild steel and stainless steel specimens, were improved by providing a restraint along the plane of the cut compared to results from the unrestrained cuts. Specifically bowing of the free side of the cuts was reduced. This resulted in improved averaged displacement variations and a reduction of associated apparent stress errors.

- By reducing the wire diameter from 0.25 mm to 0.1 mm the quality of the cut surface was slightly improved on the mild steel specimen. But a reduction in WEDM cutting parameters (A from 0.2 μs to 0.1 μs, and TAC from 0.1 μs to 0.05 μs) for the 0.1 mm wire made little difference.
- For the stainless steel specimen, reducing the wire diameter from 0.25 mm to 0.1 mm improved the surface roughness but had no effect on the displacement errors. Likewise reduced values of electrical parameters such as A and TAC did not contribute to better quality of the cut surfaces.
- Thus both the mild steel and stainless steel cut surfaces displayed less surface roughness when a thinner wire diameter was used for the cutting process but little improvement in the artefacts contributing to apparent stress errors.
- Changing the ligament length from 1.6 mm to 5 mm (increasing restraint during cutting) did not improve the quality of the cut surface.
- A similar stiffness, on both sides of the plane of the cut, slightly improved the bowed displacement variation results in the mild steel cut surfaces, particularly on the unclamped side. However, the effects of these features can still be observed on the topography of the cut surfaces, and do contribute to stress errors.
- Flared edge effects at the wire entry sides were seen on the cut surfaces in all restrained cut results, as in previous unrestrained cuts results. These contribute to high stress errors along the cut surface edges and emphasise the importance of using sacrificial layers when near to surface stresses are of interest.

In summary, for mild steel, the MS-C-4 cut (*Figure 3-28*) gave a better surface finish compared to all other unrestrained and restrained cuts performed on the same material during the experiment. For this cut small values of averaged displacement variations were achieved ranging from -2 µm to 3.2 µm along the cutting direction, and -2.3 µm to 3.7 µm along the wire direction. However, the effects of the cut surface features such as asymmetry in both sides of the cut surfaces, and the bowed form of the surface profile were present on the topography of the cut surface. The stainless steel cut SS-C-1 (*Figure 3-24*) resulted in the best surface finish compared to all cuts that were performed during the experiment, and displayed very small values of averaged displacement variations ranging from -2 µm to 1 µm along the cutting direction, and -1.5 µm to 3 µm along the wire direction. Asymmetry and bowed form errors in the surface profile were generally small. However, "flared edge effects" at the wire entry side were seen on both of the cut surfaces, which contributed to the high values of apparent stress along the wire entry side. Table 3-13 provides a summary of the quality of the cuts that have been performed during the study.

3.12 Investigation for the cut surface features

The following studies were performed in order to further investigate the observed cutting features on the WEDM cut surfaces.

- A series of restrained cuts after performing a second heat treatment
- Incremental in-plane residual stress profiling using electro polishing on the WEDM surface and an X-ray diffractometer.
- A thin section reference cut adjacent to the WEDM cut surface.

3.12.1 Restrained cuts after performing second heat treatment

One possible interpretation of apparent residual stresses being identified by contour analysis of the benchmark cut deformation profiles is that, despite the heat treatment given to the specimen, there were real internal stresses present in the mild steel and stainless steel specimens. Therefore, one more restrained cuts series was designed for the mild steel specimen.

For the new restrained cuts series, a second reliable heat treatment was carried out, in order to remove any possible internal stresses within the mild steel specimens. Specimens named MS-B and MS-D were placed in a vacuum furnace at 600°C for about an hour to be stress relieved. Cuts were performed as given in *Table 3-12* repeating MS-C-4 and MS-C-1 because they represented a better surface quality compared to all of the previous cuts.

The results are shown in the surface quality metrics in *Figure 3-31* to *Figure 3-34*. The displacement variations along the wire direction and cutting direction were found to be same as achieved in previous restrained cuts. Moreover, in these cuts results the bowed form of the surface profiles and asymmetry in both sides of the cut surfaces were still found similar to the previous cuts. It is evident that there were no internal stresses present in the mild steel specimen. Thus all the cut surface features which are observed on the WEDM cut surfaces, are purely caused during the WEDM cutting process.

No.	Cut ID	Specimen Number	Cut Number	Cut descriptions
1	MS-B-5	B	5	Repeat cut of MS-C-4 Similar stiffness
2	MS-D-3	D	3	Repeat cut of MS-B-5 Similar stiffness
3	MS-D-1	D	1	Repeat cut of MS-C-1
4	MS-D-2	D	2	Repeat cut of MS-D-1

Table 3-12: Details of restrained WEDM contour cuts performed after second heat treatment.

Specimen details							
Specimen reference				MS-B-5			
Specimen material				Mild steel (EN3B)			
Cut length, m, thickness, n				(45 x 25) mm			
Cantilever dimensions, p, q				(45 x 95) mm			
Specimen top and bottom surfaces were milled flat surfaces. Vacuum heat treatment performed to relieve internal stresses.							
WEDM information							
Cut date				18th Nov, 2014			
Machine type				Agie Charmillies FI440ccS			
Wire material				Brass (LT25.WIR)			
Wire diameter				0.25 mm			
Cutting technology				LT25A.TEC			
WEDM bath temperature				20 °C			
Nozzles position, pressure				0.2 mm, 0.8 MPa			
The cut was performed with a standard S5 set of parameters with no manual intervention							
WEDM cutting parameters							
EL	10	PA	6	PM	3	Offset	0.16
ST	1	M	3	S	10	V	80
FF	100	B	7	A	0.6	TAC	0.3
Aj	41	S	10	WS	12	WB	1.6
Inj	14	Rate	3.4	IAL	10		
Metrology information							
CMM				Mitutoyo Crysta plus 547 CMM			
Spacing		(0.5 x 0.5) mm		**Probe dia.**		3 mm	
Roughness instrument				Leica 3DCM			
Resolution		12		**Overlap area**		10%	
Threshold		10 %		**Z-Scan value**		200 µm	

Cut MS-B-5 was performed on second heat treated specimen on restrained (similar stiffness) cutting conditions as the MS-C-4 cut.

a

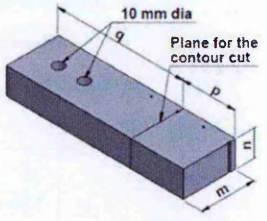

b

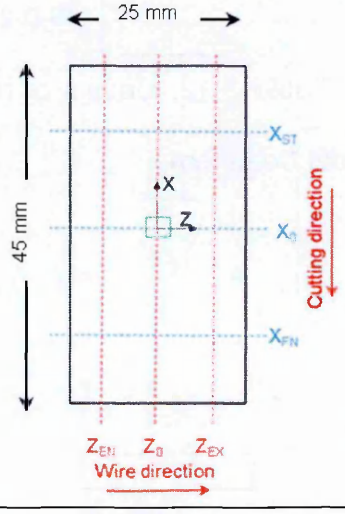

c

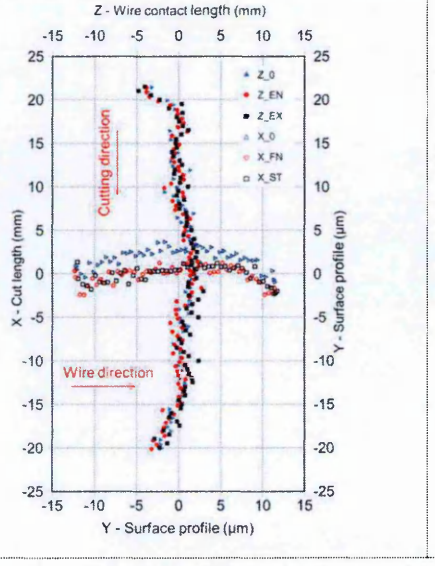

d

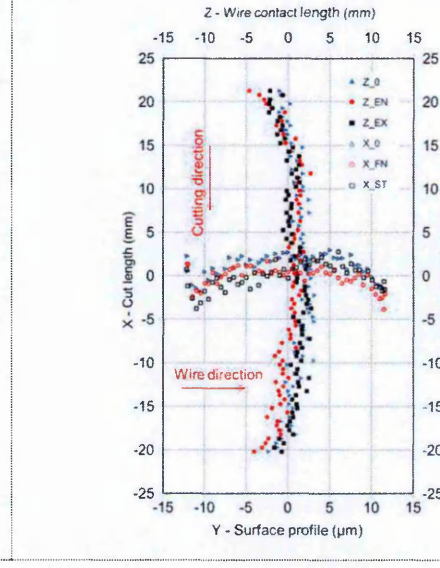

Figure 3-31: The MS-B-5 cut surface data and displacement profiles for clamped (c) and free sides (d).

Surface quality metrics				
	X (cutting direction)	Z (wire direction)	X (cutting direction)	Z (wire direction)
	Clamped side displacement, Fig c, µm		Free side displacement, Fig d, µm	
Min	- 3.6	- 1.4	- 2.3	- 1.8
Max	2.5	3.9	3.0	3.0
Rsm	127.0	143.0	135.0	145.0
Sq, Sa	3.4, 2.7		3.5, 2.6	
	Averaged displacement, Figs e and g, µm		Stress error, Figs f and h, MPa (%yield)	
Min	- 2.3	- 1.3	- 47.0 (12.0)	- 65.0 (17.0)
Max	3.0	3.0	31.0 (8.0)	51.0 (13.0)
RMS	1.8		39.0 (10.0)	

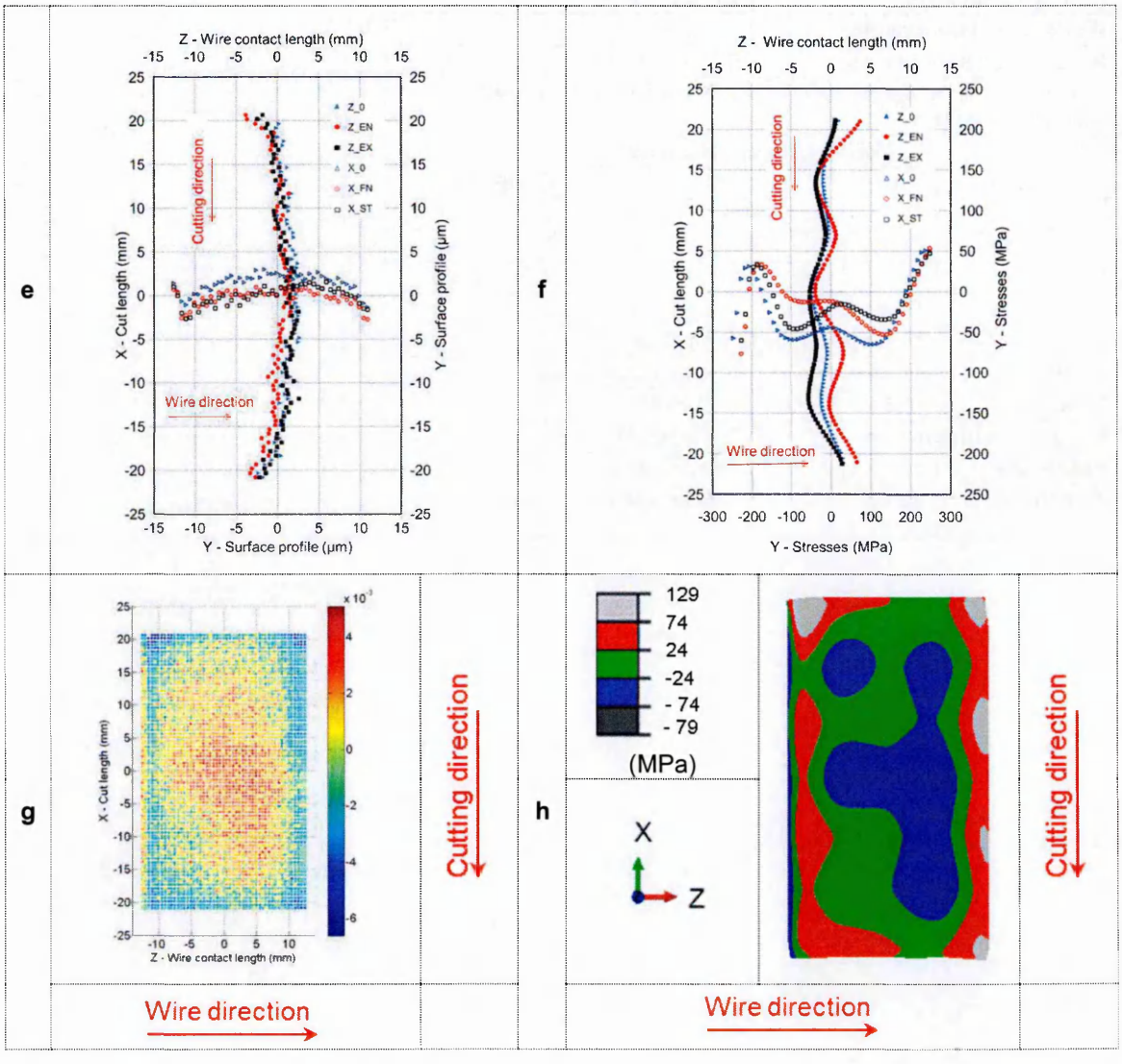

Figure 3-31 cont: The MS-B-5 cut surface quality metrics profiles of averaged displacement (e) and stress (f), maps of averaged displacement (g) and stress (h).

Specimen details							
Specimen reference				MS-D-3			
Specimen material				Mild steel (EN3B)			
Cut length, m, thickness, n				(45 x 25) mm			
Cantilever dimensions, p, q				(45 x 125) mm			
Specimen top and bottom surfaces were milled flat surfaces. Vacuum heat treatment performed to relieve internal stresses.							
WEDM information							
Cut date				5^{th} Feb, 2015			
Machine type				Agie Charmillies FI440ccS			
Wire material				Brass (LT25.WIR)			
Wire diameter				0.25 mm			
Cutting technology				LT25A.TEC			
WEDM bath temperature				20 °C			
Nozzles position, pressure				0.2 mm, 0.8 MPa			
The cut was performed with a standard S5 set of parameters with no manual intervention							
WEDM cutting parameters							
EL	10	PA	6	PM	3	Offset	0.16
ST	1	M	3	S	10	V	80
FF	100	B	7	A	0.6	TAC	0.3
Aj	41	S	10	WS	12	WB	1.6
Inj	14	Rate	3.4	IAL	10		
Metrology information							
CMM				Mitutoyo Crysta plus 547 CMM			
Spacing		(0.5 x 0.5) mm		**Probe dia.**		3 mm	
Roughness instrument				Leica 3DCM			
Resolution		12		**Overlap area**		10%	
Threshold		10 %		**Z-Scan value**		200 µm	

Cut MS-D-3 was performed on second heat treated specimen on restrained (similar stiffness) cutting conditions as repeat cut of the MS-B-5.

a

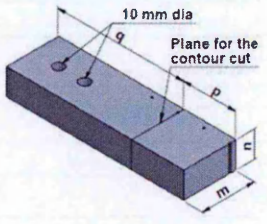

b

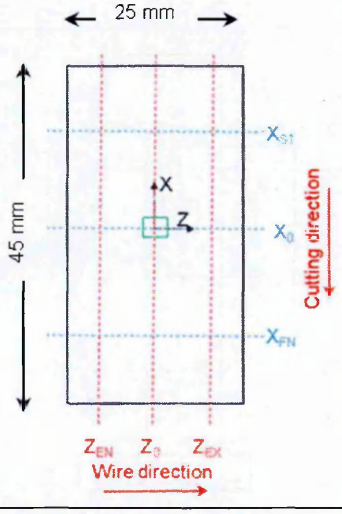

c

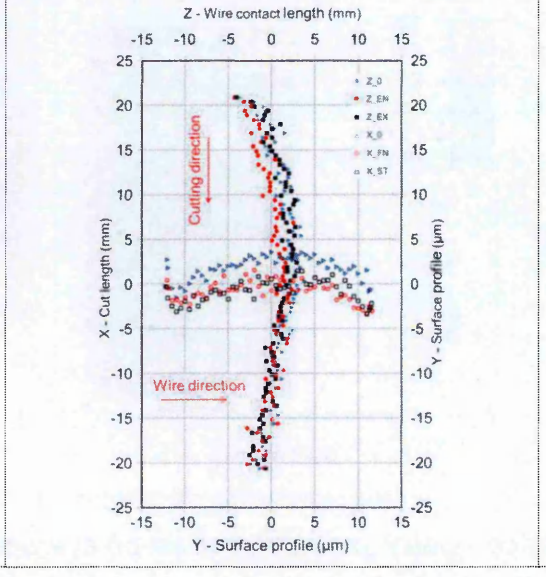

d

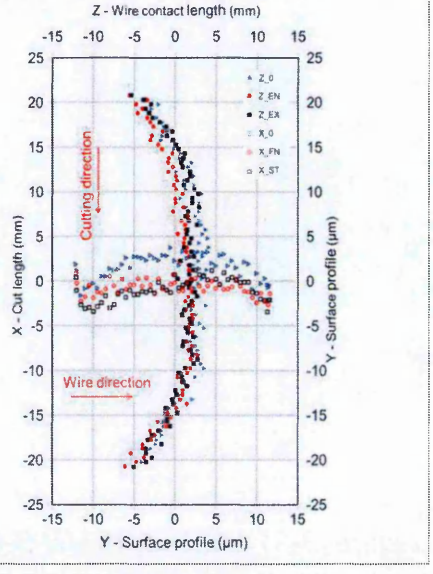

Figure 3-32: The MS-D-3 cut surface data and displacement profiles for clamped (c) and free sides (d).

Surface quality metrics				
	X (cutting direction)	Z (wire direction)	X (cutting direction)	Z (wire direction)
	Clamped side displacement, Fig c, µm		Free side displacement, Fig d, µm	
Min	- 3.7	- 1.5	- 6.0	- 1.6
Max	3.7	3.6	4.0	3.7
Rsm	126.0	145.0	125.0	140.0
Sq, Sa	3.3, 2.8		3.4, 2.7	
	Averaged displacement, Figs e and g, µm		Stress error, Figs f and h, MPa (%yield)	
Min	- 4.5	- 1.0	- 47.0 (12.0)	- 74.0 (20.0)
Max	3.5	3.3	66.0 (18.0)	50.0 (13.0)
RMS	2.0		43.0 (11.5)	

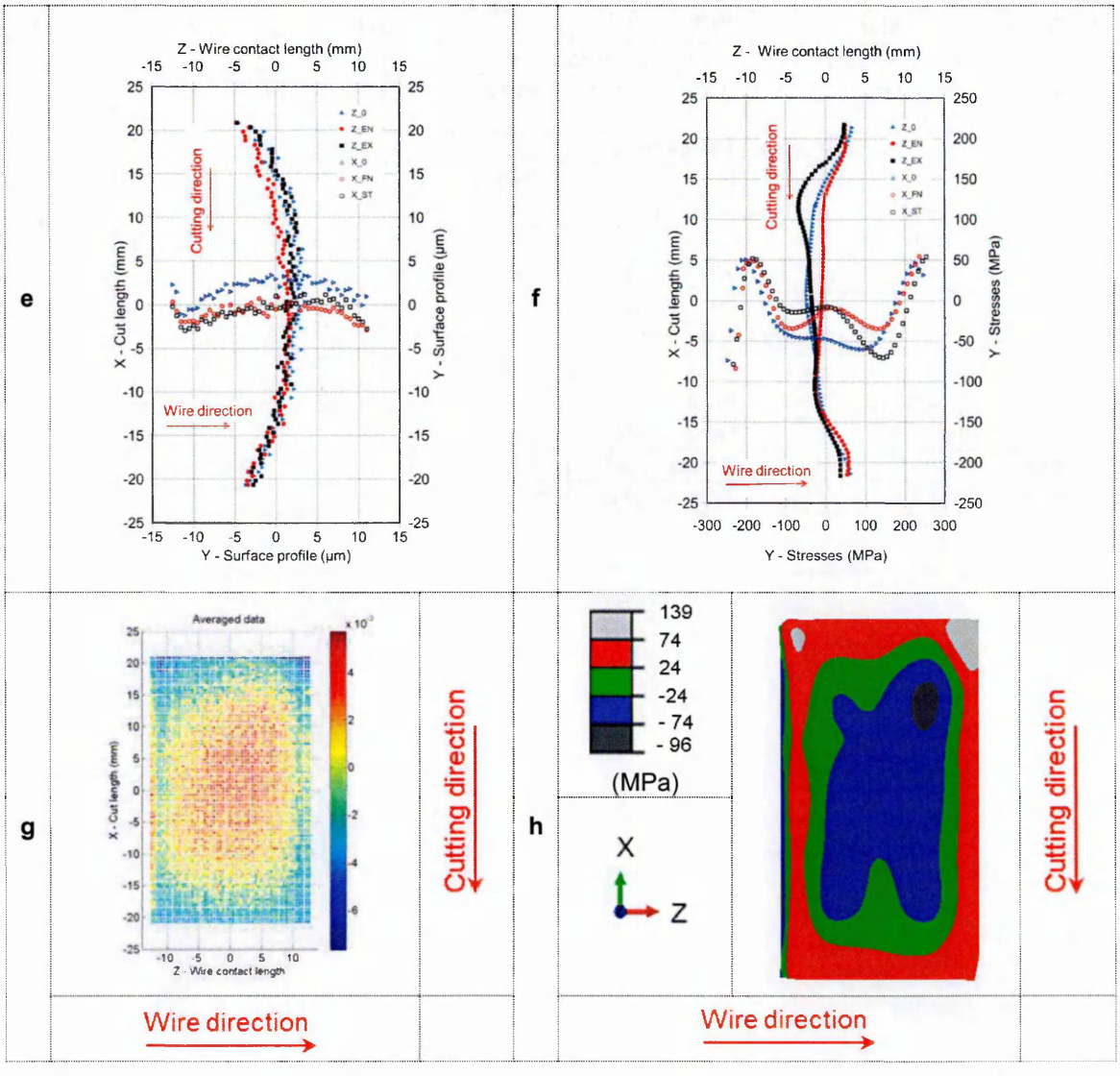

Figure 3-32 cont: The MS-B-5 cut surface quality metrics profiles of averaged displacement (e) and stress (f), maps of averaged displacement (g) and stress (h).

Specimen details							
Specimen reference			MS-D-1				
Specimen material			Mild Steel (EN3B)				
Cut length, m, thickness, n			(45 x 25) mm				
Cantilever dimensions, p, q			(25 x 220) mm				
Specimen top and bottom surfaces were milled flat surfaces. Vacuum heat treatment performed to relieve internal stresses.							
WEDM information							
Cut date			18th Jan, 2015				
Machine type			Agie Charmillies FI440ccS				
Wire material			Brass (LT25.WIR)				
Wire diameter			0.25 mm				
Cutting technology			LT25A.TEC				
WEDM bath temperature			20 °C				
Nozzles position, pressure			0.2 mm, 0.8 MPa				
The cut was performed with a standard S5 set of parameters with no manual intervention							
WEDM cutting parameters							
EL	10	PA	6	PM	3	Offset	0.16
ST	1	M	3	S	10	V	80
FF	100	B	7	A	0.6	TAC	0.3
Aj	41	S	10	WS	12	WB	1.6
Inj	14	Rate	3.4	IAL	10		
Metrology information							
CMM			Mitutoyo Crysta plus 547 CMM				
Spacing		(0.5 x 0.5) mm		**Probe dia.**		3 mm	
Roughness instrument			Leica 3DCM				
Resolution		12		**Overlap area**		10%	
Threshold		10 %		**Z-Scan value**		200 µm	

Cut MS-D-1 was performed on MS-D specimen after second heat treatment. The cut was performed on same cutting conditions as MS-C-1.

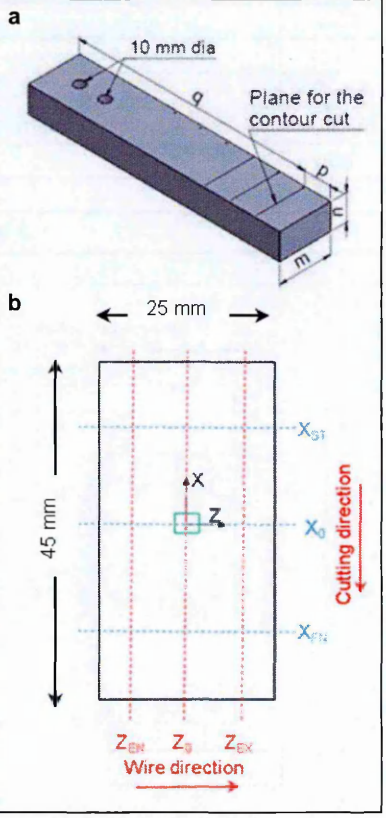

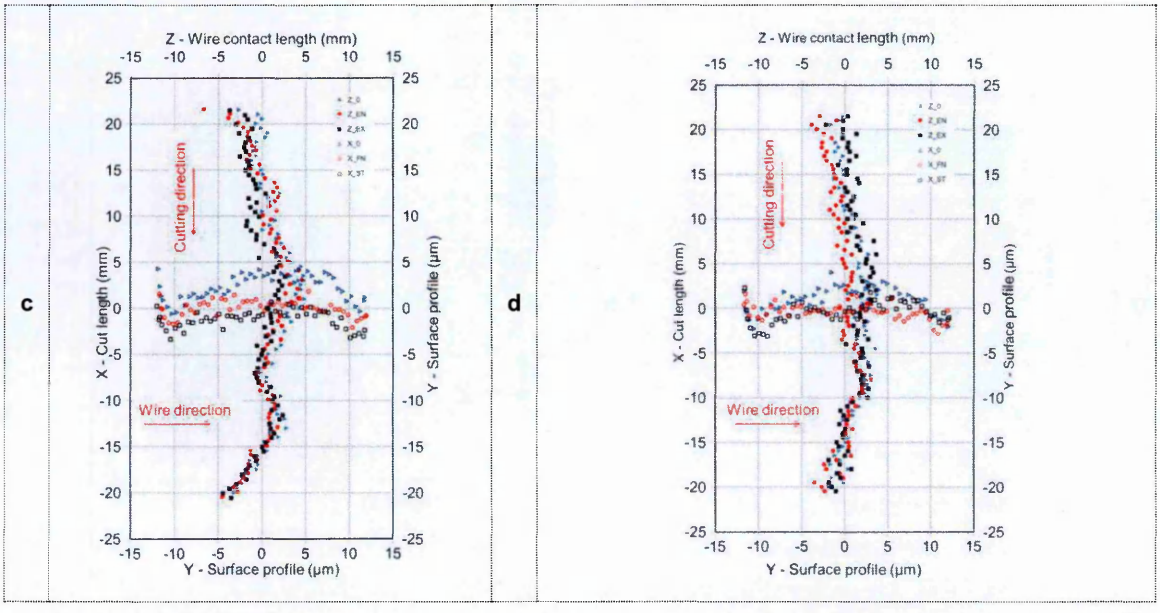

Figure 3-33: The MS-D-1 cut surface data and displacement profiles for clamped (c) and free sides (d).

Surface quality metrics				
	X (cutting direction)	Z (wire direction)	X (cutting direction)	Z (wire direction)
	Clamped side displacement, Fig c, µm		Free side displacement, Fig d, µm	
Min	-4.5	- 0.5	- 2.0	- 2.2
Max	4.8	5.6	3.7	4.0
Rsm	125.0	130.0	126.0	137.0
Sq, Sa	3.3, 2.6		3.2, 2.5	
	Averaged displacement, Figs e and g, µm		Stress error, Figs f and h, MPa (%yield)	
Min	- 3.6	- 1.0	- 50.0 (13.0)	- 97.0 (26.0)
Max	4.2	3.7	44.0 (11.0)	55.0 (15.0)
RMS	2.0		44.0 (12.0)	

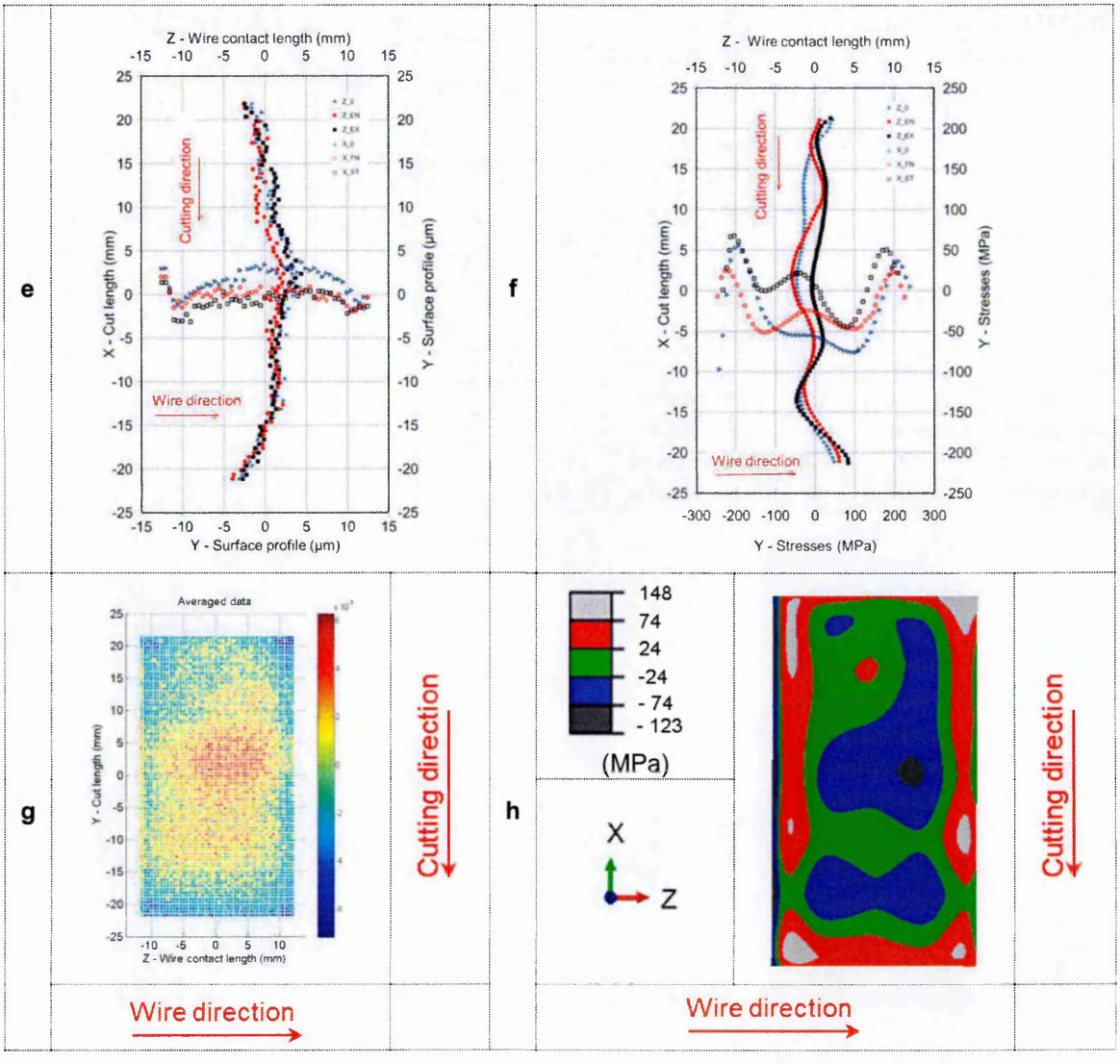

Figure 3-33 cont: The MS-D-1 cut surface quality metrics, profiles of averaged displacement (e) and stress (f), maps of averaged displacement (g) and stress (h).

Specimen details							
Specimen reference			MS-D-2				
Specimen material			Mild Steel (EN3B)				
Cut length, m, thickness, n			(45 x 25) mm				
Cantilever dimensions, p, q			(25 x 195) mm				
Specimen top and bottom surfaces were milled flat surfaces. Vacuum heat treatment performed to relieve internal stresses.							
WEDM information							
Cut date			5th Feb, 2015				
Machine type			Agie Charmillies FI440ccS				
Wire material			Brass (LT25.WIR)				
Wire diameter			0.25 mm				
Cutting technology			LT25A.TEC				
WEDM bath temperature			20 °C				
Nozzles position, pressure			0.2 mm, 0.8 MPa				
The cut was performed with a standard S5 set of parameters with no manual intervention							
WEDM cutting parameters							
EL	10	PA	6	PM	3	Offset	0.16
ST	1	M	3	S	10	V	80
FF	100	B	7	A	0.6	TAC	0.3
Aj	41	S	10	WS	12	WB	1.6
Inj	14	Rate	3.4	IAL	10		
Metrology information							
CMM			Mitutoyo Crysta plus 547 CMM				
Spacing	(0.5 x 0.5) mm		**Probe dia.**	3 mm			
Roughness instrument			Leica 3DCM				
Resolution	12		**Overlap area**	10%			
Threshold	10 %		**Z-Scan value**	200 µm			

Cut MS-D-2 was performed on MS-D specimen after second heat treatment. The cut was performed on same cutting conditions as MS-D-1.

a

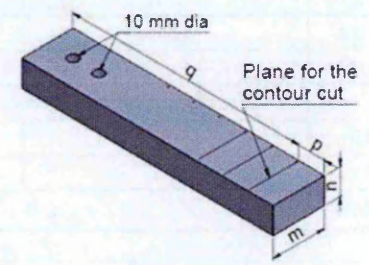

b

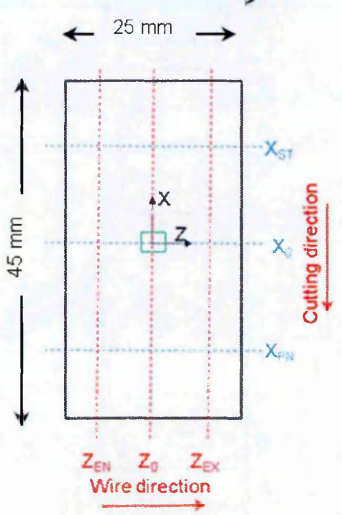

c

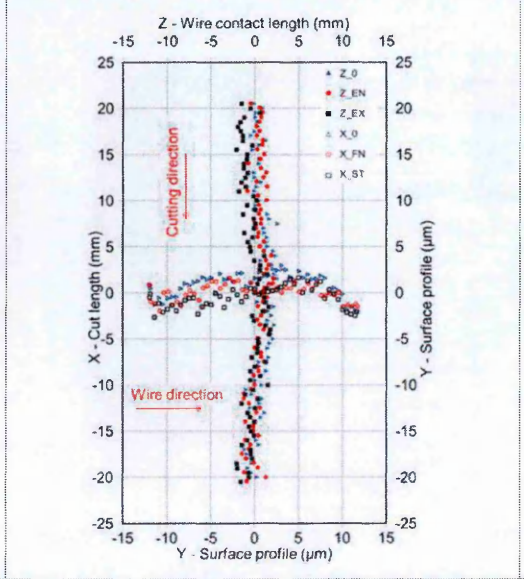

d

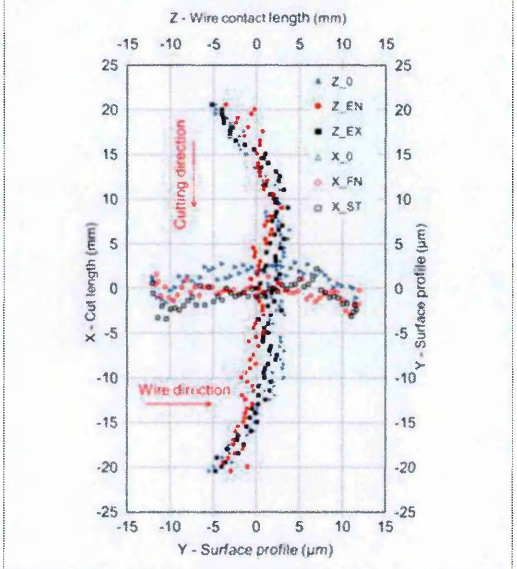

Figure 3-34: The MS-D-2 cut surface data and displacement profiles for clamped (c) and free sides (d).

Surface quality metrics				
	X (cutting direction)	Z (wire direction)	X (cutting direction)	Z (wire direction)
	Clamped side displacement, Fig c, µm		Free side displacement, Fig d, µm	
Min	-1.5	- 2.0	- 5.4	- 1.6
Max	3.1	3.0	3.8	2.9
Rsm	3.4	2.6	3.2	2.5
Sq, Sa	130.0, 145.0		135.0, 150.0	
	Averaged displacement, Figs e and g, µm		Stress error, Figs f and h, MPa (%yield)	
Min	- 3.4	- 1.6	-36.0 (10.0)	-53.0 (14.0)
Max	2.8	2.8	63.0 (17.0)	66.0 (18.0)
RMS	1.9		46.0 (10.0)	

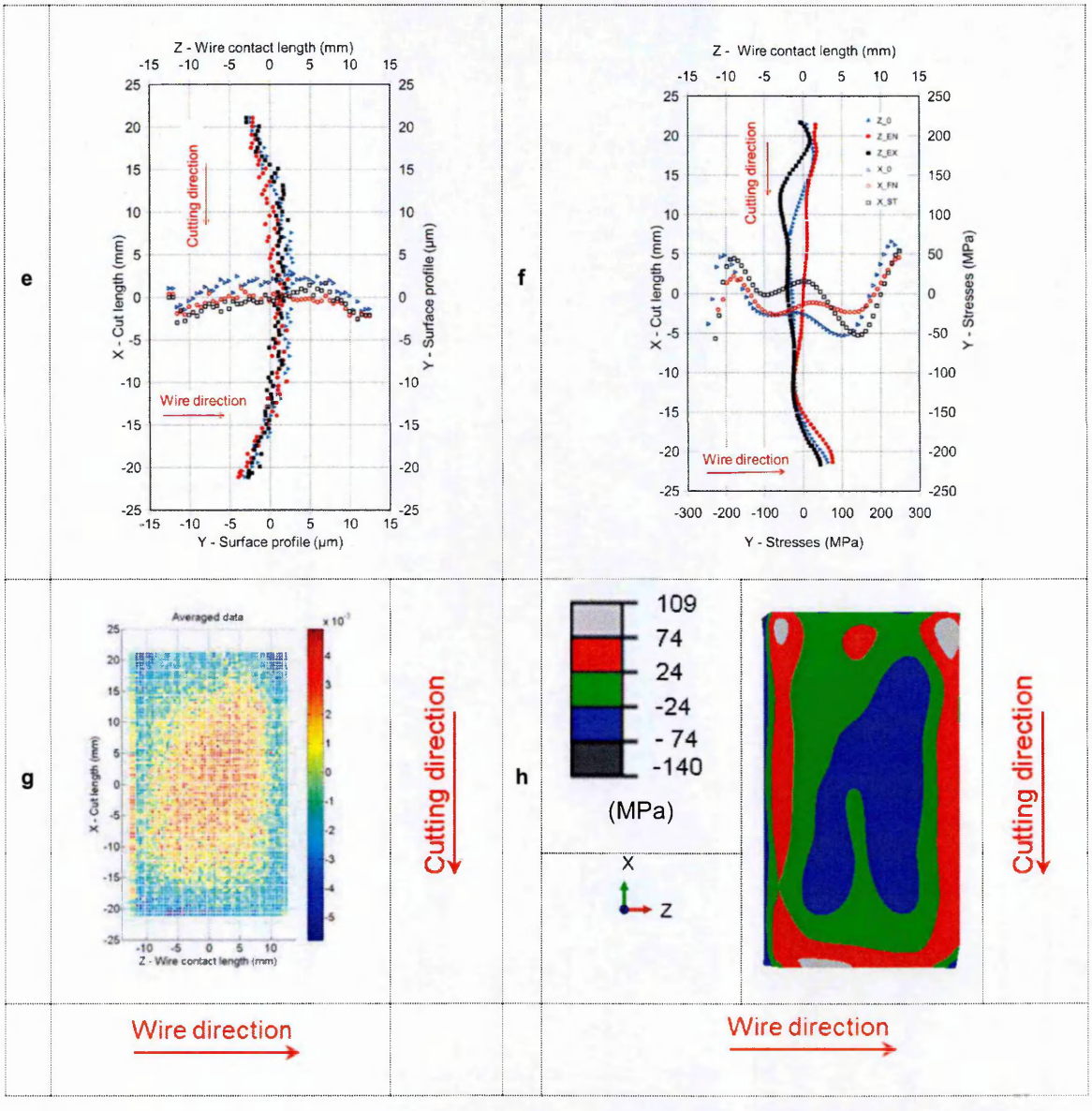

Figure 3-34 cont: The MS-D-2 cut surface quality metrics, profiles of averaged displacement (e) and stress (f), maps of averaged displacement (g) and stress (h).

Surface quality metrics										
Sample Ref.	Clamped side displacement, µm		Free side displacement, µm		Averaged displacement, µm		Stress error, MPa (% Yield strength)			
	X	Z	X	Z	X	Z	X		Z	
	Peak to valley range	Peak to valley range	Peak to valley range	Peak to valley range	Peak to valley range	Peak to valley range	min	max	min	Max
Unrestrained cut										
MS-A-1	4.5	7.5	26.0	11.0	13.0	7.0	-66(18)	124(34)	-69(19)	106(28)
MS-A-2	6.0	8.0	26.0	10.0	14.0	7.0	-76(21)	119(32)	-69(18)	91(25)
MS-A-3	6.0	7.0	20.9	8.0	11.0	7.0	-77(21)	97(26)	-55(15)	104(28)
MS-B-1	7.0	10.5	22.0	11.0	12.0	9.0	-52(14)	153(41)	-63.5(17)	157(42)
MS-B-2	7.0	10.0	22.0	9.5	13.5	9.5	-60(16)	141(38)	-82(22)	136(37)
SS-A-1	5.0	5.5	9.0	7.0	5.0	6.5	-39(16)	43(18)	-124(51)	30(12)
SS-A-2	5.5	7.0	9.0	9.0	6.0	9.5	-17(7)	54(22)	-160(66)	46(19)
SS-B-1	8.0	6.0	11.0	9.5	7.5	7.0	-73(30)	67(28)	-130(54)	22(9)
SS-B-2	7.5	4.0	10.0	8.0	7.0	5.5	-67(28)	65(26)	-80(34)	44(18)

Table 3-13: Summary comparing the quality of all the cut surfaces.

Surface quality metrics										
Sample Ref.	Clamped side displacement, µm		Free side displacement, µm		Averaged displacement, µm		Stress error, MPa (% Yield strength)			
	X	Z	X	Z	X	Z	X		Z	
	Peak to valley range	Peak to valley range	Peak to valley range	Peak to valley range	Peak to valley range	Peak to valley range	min	Max	min	max
Restrained cut										
MS-C-1	4.0	7.5	11.0	6.5	6.0	7.0	-72(19)	35(9.5)	-91(24)	83.5(22)
MS-C-2	3.5	7.0	10.0	7.0	6.0	4.0	-62(16)	40(11)	-48(13)	87(23)
MS-C-3	8.0	6.5	10.0	6.0	7.5	5.5	-88(24)	52(14)	-115(31)	69(19)
SS-C-1	4.0	5.0	5.0	7.0	3.0	4.5	-20(8)	24(10)	-122(50)	30(12)
SS-C-2	3.5	4.0	7.0	6.0	5.0	5.5	-53(22)	47(19)	-78(32)	44.5(18)
SS-C-3	4.0	5.5	6.0	5.5	4.0	6.0	-8 (3)	43(18)	-116(48)	29(12)
MS-C-4	9.0	6.0	8.8	6.8	5.2	6.0	-47(12)	36(10)	-58(15)	86(23)
SS-C-4	6.1	8.7	10.5	6.1	4.5	7.2	-53(22)	57(24)	-165(69)	34(14)
MS-B-4	6.3	6.8	16.8	5.8	8.0	5.0	-46(12)	81(22)	-71(19)	86(23)
SS-A-5	10.5	4.8	9.7	7.2	4.6	3.2	-42(17)	49(20)	-112(46)	39(16)
MS-B-5	6.1	5.3	5.3	4.8	5.3	4.3	-47(12)	31(8)	-65(17)	51(13)
MS-D-3	7.4	5.1	10	5.3	8.0	4.3	-47(12)	66(18)	-74(20)	50(13)
MS-D-1	9.3	6.1	5.7	6.2	7.8	4.7	-50(13)	44(11)	-97(26)	55(15)
MS-D-2	4.6	5.0	9.2	4.5	6.2	4.4	-36(10)	63(17)	-53(14)	66(18)

Table 3-13 cont.: Summary comparing the quality of all the cut surfaces.

Sample Ref.	Surface quality metrics										Cutting conditions
	Roughness, µm								RMS, (% Yield strength)		
	Clamped side				Free side						
	Sq	Sa	Rsm		Sq	Sa	Rsm				
			X	Z			X	Z	Displacement, µm	Stresses, MPa	
Unrestrained cut											
MS-A-1	3.4±0.16	2.6±0.08	130	150	3.7±0.44	2.9±0.39	110	130	3.0	59(16)	Cut on mild steel-Agie
MS-A-2	3.3	2.6	130	150	3.4±0.20	2.6±0.16	120	130	3.6	60(16)	Repeat cut-Agie
MS-A-3	3.3	2.5	145	130	3.3	2.5	126	134	3.5	55.5(15)	Cut in opposite direction-Agie
MS-B-1	4.5±0.11	3.5±0.10	150	140	4.6±0.22	3.6±0.19	135	150	3.0	71(19)	Cut on mild steel-Fanuc1
MS-B-2	4.5	3.5	131	164	4.5±0.14	3.5±0.14	130	150	3.6	70(19)	Repeat cut-Fanuc1
SS-A-1	3.4	2.6	120	150	3.3	2.5	130	150	2.0	33(14)	Cut on stainless steel-Agie
SS-A-2	3.5	2.7	134	125	3.3	2.6	110	170	2.3	37(15)	Repeat cut-Agie
SS-B-1	4.7	3.7	150	130	4.8	3.8	160	150	2.0	33(14)	Cut on stainless steel-Fanuc2
SS-B-2	4.4	3.5	153	155	4.8	3.7	120	150	2.0	31(13)	Repeat cut-Fanuc2

Table 3-13 cont.: Summary comparing the quality of all the cut surfaces.

Sample Ref.	Surface quality metrics										Cutting conditions
	Roughness, µm								RMS, (% Yield strength)		
	Clamped side				Free side						
	Sq	Sa	Rsm		Sq	Sa	Rsm				
			X	Z			X	Z	Displacement. µm	Stresses, MPa	
	Restrained cut										
MS-C-1	3.5	2.6	128	124	3.7	2.7	131	147	2.3	52(14.0)	Cut on mild steel-Agie-S5
MS-C-2	2.5	1.8	131	121	2.5	1.8	133	122	2.0	47(12.5)	Cut on mild steel-Agie-S3, A=0.2, TAC=0.1
MS-C-3	2.3	1.8	120	130	2.3	1.8	102	131	2.3	54(14.5)	Cut on mild steel-Agie-S3, A=0.1, TAC=0.05
SS-C-1	3.0	2.5	127	151	3.0	2.5	125	135	1.5	33(14.0)	Cut on stainless steel-Agie-S5
SS-C-2	1.9	1.5	126	129	1.9	1.5	125	116	1.9	37(15.0)	Cut on stainless steel-Agie-S3, A=0.2, TAC=0.1
SS-C-3	2.2	1.7	129	114	2.1	1.7	96	115	2.0	39 (16.0)	Cut on stainless steel-Agie-S3, A=0.1, TAC=0.05
MS-B-4	X	X	X	X	3.6	2.7	135	136	2.3	49(13.0)	Cut on mild steel-Agie-S5, 5 mm ligament length
MS-C-4	3.3	2.6	115	148	3.3	2.5	125	142	2.0	43(11.0)	Cut on mild steel-Agie-S5, Symmetric cut
SS-A-5	3.4	2.6	112	142	3.4	2.6	140	131	1.9	41(17.0)	Cut on stainless steel-Agie-S5, 5 mm ligament length
SS-C-4	3.6	2.8	121	174	3.7	3	140	150	1.8	41(17.0)	Cut on stainless steel-Agie-S5, Symmetric cut
MS-B-5	3.4	2.7	127	143	3.5	2.6	135	145	1.8	39(10.0)	After second heat treatment, cutting condition same as MS-C-4
MS-D-3	3.3	2.8	126	145	3.4	2.7	125	140	2.0	43(11.5)	After second heat treatment, cutting condition same as MS-B-5
MS-D-1	3.3	2.6	125	130	3.2	2.5	126	137	2.0	44(12.0)	After second heat treatment, cutting condition same as MS-C-1
MS-D-2	3.4	2.6	130	145	3.2	2.5	135	150	1.9	46(10.0)	After second heat treatment, cutting condition same as MS-D-1

Table 3-13 cont.: Summary comparing the quality of all the cut surfaces.

3.12.2 Incremental X-ray diffraction measurement of residual stresses

The possibility that near-surface residual stresses might be present in the specimens to an extent that affects the quality of the cut surface merits investigation. This study presents the results of X-ray diffraction measurements of the in-plane residual stresses along the longitudinal (Z-axis) and transverse (X axis) directions on the WEDM cut surface (see *Figure 3-4*). Incremental electro polishing was performed on the central region of the WEDM cut surface of the free part of the MS-A-1 cut to remove layers of material. The free part of the MS-A-1 (unrestrained) cut was selected because it showed a high value of surface displacement among all the cut results. At each increment, the depth and the surface residual stresses were measured at the newly-exposed surface at the centre of the polished region. By repeating this process several times, it was possible to incrementally remove the surface and obtain a depth profile of the surface residual stress. In the present work, a Struers Electropol-5 tool was employed for electro polishing. This allows the electro-polishing of a small rectangular region of a surface of 10 mm by 20 mm. Initially, the electro polishing parameters were set to achieve the flattest surface with the removal of a minimal depth of material. The depth and flatness of the polished surface was measured using a laser CMM. The stresses were measured using an XSTRESS 3000 X-ray diffractometer (Stresstech Oy, VALAKOSKI, Finland) with a 3 mm diameter collimator. The X-ray radiation source of Cr K-α with a wavelength of 2.2897 Å was used at 270 W power and 10 mA current. The position of the peak arising from {211} diffracting planes was at a 2θ angle of approximately 156.1° (152). The $\sin^2\psi$ technique was applied using 10 angles within a range of $-45^\circ \leq \psi \leq 45^\circ$ in order to

determine the error margins for each stress measurement. The results are shown in *Figure 3-35*.

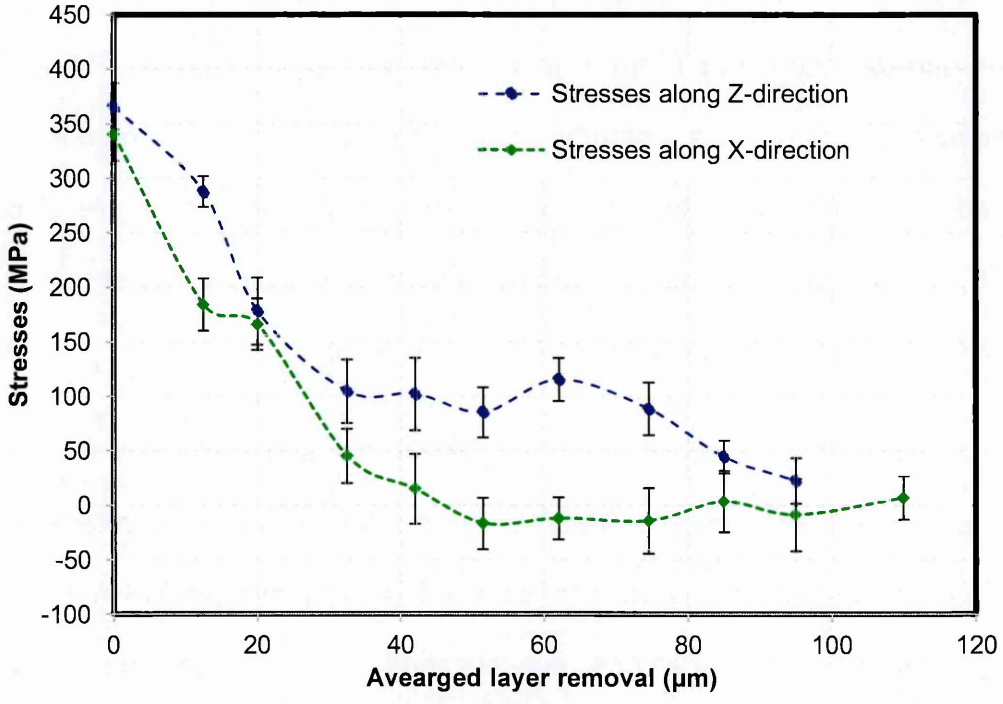

Figure 3-35: Stress measurement as a function of depth through the WEDM cut on the mild steel specimen.

The results show that high tensile stresses were present at the WEDM cut surface and these stresses must have been the result of the formation of the WEDM affected layer (see *Figure 3-35*). A significant value of tensile stresses was measured on the WEDM cut surface before the first electro polishing step. These stress values progressively decreased with depth to near zero at approximately 100 µm indicating there were no internal stresses present in the bulk of the mild steel specimen.

3.12.3 Thin section reference cut adjacent to the WEDM cut surface

The unrestrained MS-A-4 cut was performed using the same cutting conditions as MS-A-1 (*Figure 3-7)*. A reference cut was performed on the clamped side of the MS-A-4 unrestrained cut at 1 mm away from the WEDM cut surface. The test cut or reference cut approach is a standard approach used to improve contour results obtained by correcting for the curvature in the actual cut, details are given in (33,139,147). In this study this approach was used to investigate the effects of the WEDM cutting process on the quality of the cut surface.

The results of the reference cut are shown in the surface quality metrics on characterisation sheet, *Figure 3-36*. Displacement variations on the reference cut are slightly improved compared with clamped side of the cut MS-A-4 (*Figure* 3-36 *c*). However, the reference cut clamped surface side shows similar topographical features to those observed on the clamped side of the reference cut (MS-A-4-Ref.cut). For example large displacements associated "flared edges", are observed at the wire entry position, as well as at the start and end of the cut (see *Figure 3-36 d*). Thus, the reference cut results show similar features on the cut surfaces to those observed on the clamped cut surface of MS-A-4. These features must form as a result of the WEDM cutting process rather than any stress relaxation during the cutting process.

Specimen details							
Specimen reference			MS-A-4-Ref. cut				
Specimen material			Mild Steel (EN3B)				
Cut length, m, thickness, n			(50 x 25) mm				
Cantilever dimensions, p, q			(1 x 144) mm				
Specimen top and bottom surfaces were milled flat surfaces. Vacuum heat treatment performed to relieve internal stresses.							
WEDM information							
Cut date			12th Nov, 2013				
Machine type			Agie Charmillies FI440ccS				
Wire material			Brass (LT25.WIR)				
Wire diameter			0.25 mm				
Cutting technology			LT25A.TEC				
WEDM bath temperature			20 °C				
Nozzles position, pressure			0.2 mm, 1.4 MPa				
The cut was performed with a standard S5 set of parameters and no manual intervention							
WEDM cutting parameters							
EL	10	PA	6	PM	3	Offset	0.16
ST	1	M	3	S	10	V	80
FF	100	B	7	A	0.6	TAC	0.3
Aj	41	S	10	WS	12	WB	1.6
Inj	14	Rate	3.5	IAL	10		
Metrology information							
CMM			Mitutoyo Crysta plus 547 CMM				
Spacing		(0.5 x 0.5) mm		**Probe dia.**		3 mm	
Roughness instrument			Leica 3DCM				
Resolution		12		**Overlap area**		10%	
Threshold		10 %		**Z-Scan value**		200 µm	

Cut MS-A-4 was performed on same cutting conditions as MS-A-1 and then the cut (MS-A-4-Ref.cut) was performed as a reference cut on the MS-A-4 cut surface.

a

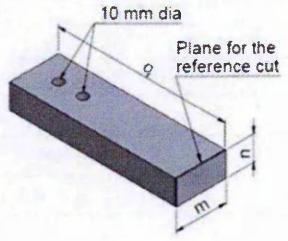

B

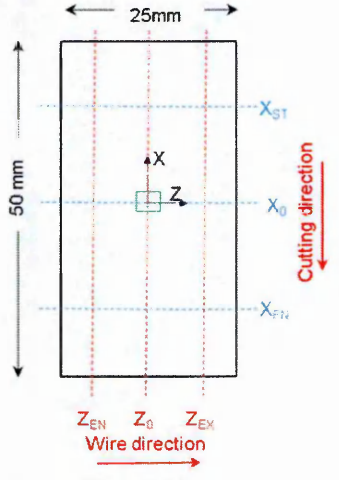

c

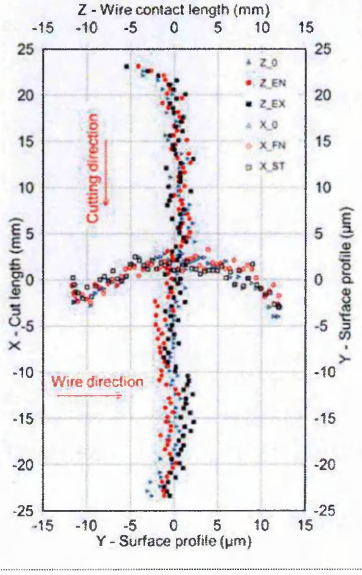

d

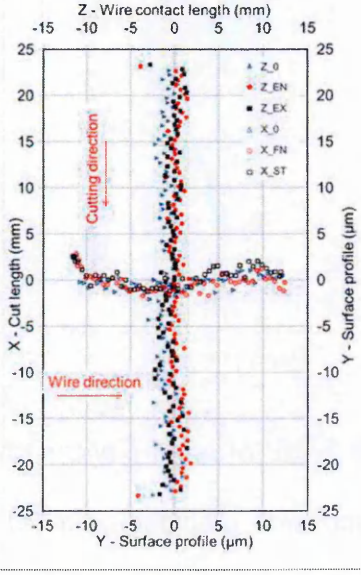

Figure 3-36: The reference cut surface data, and displacement profiles for clamped sides of MS-A-4 (c)and MS-A-4-Ref. cut (d).

Surface quality metrics				
	X (cutting direction)	Z (wire direction)	X (cutting direction)	Z (wire direction)
	MS-A-4 Clamped side displacement, Fig c, µm		MS-A-4-Ref. cut Clamped side displacement, Fig d, µm	
Min	-5.5	-4.0	-3.7	-2.0
Max	2.0	3.0	1.0	2.6
	Averaged displacement, Fig e, µm		Averaged displacement, Fig g, µm	
RMS	2.0		1.6	
	Stress error, Fig f, MPa (%yield)		Stress error, Fig h, MPa (%yield)	
RMS	49.0 (13.0)		43.0 (11.0)	

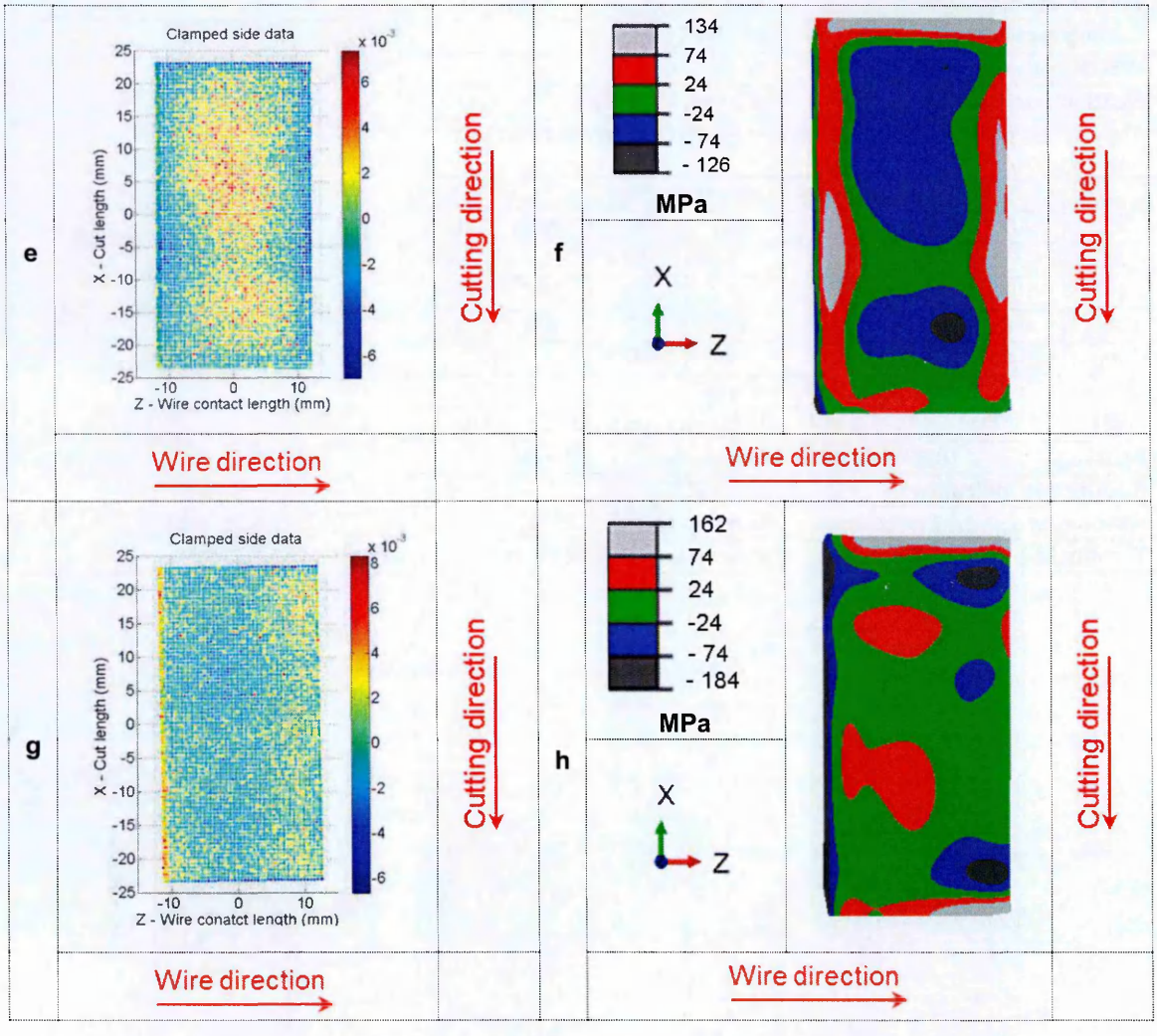

Figure 3-36*: MS-A-4-Ref cut surface quality metrics (top table), maps of MS-A-4 clamped side displacement (e) and stress (f), maps of MS-A-4-Ref cut clamped side displacement (g) and stress (h).*

3.13 Discussion on benchmark study results

On the topography of the cut surfaces, noticeable cutting features are present on both sides of the cut, a bowed form of profile and flared edge effects. It has been identified that all these features formed as a result of the WEDM cutting process.

In the study, the symmetric features on the surfaces of both sides of the cut were improved by providing a restraint along the plane of the cut. Two ligament lengths (1.6 mm and 5 mm) were tested to provide restraint during the cutting process. It would be worthwhile to further investigate the cutting process whilst providing extra restraint. A bowed form of cut surface occurred in all the cuts on both sides. This study found that this cutting artefact is influenced by the material type (convex in mild steel and concave in stainless steel) as well as the electrical parameters of WEDM. Two electrical parameters (A and TAC) related to the energy of the spark were tested. An improvement in the quality of the cut surface was achieved for the mild steel case by successively reducing these electrical parameters; this is thought to be associated with a reduction of electro-magnetic effects. It would be worthwhile to investigate the other electrical parameters that characterise the spark such as IAL (spark ignition intensity) and V (applied voltage). A list of all the electrical parameters of WEDM is given at the end of the thesis in Appendix Table A - 1. The severity of bowed feature is greater in the mild steel specimen (convex) and in an opposite direction compared to the stainless steel specimen (concave). This study suggests that the magnetic properties of mild steel affected the quality of the cut surface. It would be worthwhile to use a

demagnetising (157) treatment for the mild steel specimens prior to WEDM cutting (155) and then investigate the quality of the cut surface. High values of displacement approaching the edges of the cut surfaces were commonly observed for all the cuts for both on mild steel and stainless steel. These surface displacement errors arise in consequence of edge effects during WEDM cutting process. The edge effects can be reduced by placing sacrificial layers (143) along the plane of the cut at the wire entry and wire exit sides, and at the start and end of the cut where the wire WEDM cutting artefacts must be avoided. The merits of using a thinner wire diameter of 0.1 mm were investigated in this study. The study revealed that a better quality of surface finish with lower surface roughness is achieved when a thinner wire diameter was used. It would be worthwhile to investigate systematically the use of thinner wire diameters and their effect on the quality of the WEDM cut surfaces.

For the study nominally stress free specimens were tested. The cut in a stress-free body should produce perfect flat mating surfaces. During the study it was observed that machining a perfectly flat cut surface is not an easy task to be achieved due to the many variables involved in the cutting process. It might be worthwhile to investigate the quality of WEDM cut surfaces using specimens with a known distribution of residual stress.

Characterisation sheets have been designed with intention of recording sufficient details relating to the quality of cut surfaces for contour measurements. The most important parameters indicating the quality of the cut surfaces are *Sa, RSm, RMS displacement and RMS stress*. The maximum/minimum displacements are more a measure of the edge artefacts.

3.14 Conclusions

The following conclusions are drawn from the work carried out in this chapter.

1. A benchmark test specimen design for contour method cutting trials has been developed (see *Figure 3-37*). A stress-free rectangular specimen with dimensions 245 mm long, 50 mm wide and 25 mm thick allows multiple trial cuts to be performed in the same set up. During WEDM cutting, one end of the specimen will be bolted to the bed of the WEDM machine, whilst 25 mm thick slices are removed from the free end. "Restrained" cutting conditions can be simulated by starting cuts from a pilot hole (1.8 mm diameter) situated 2.5 millimetres away from the side of the beam (leaving a ligament of 1.6 mm) to provide constraint whilst cutting. The cut will be stopped 2.5 mm away from the opposite side of the specimen giving a cut length of 45 mm and a wire contact length of 25 mm.

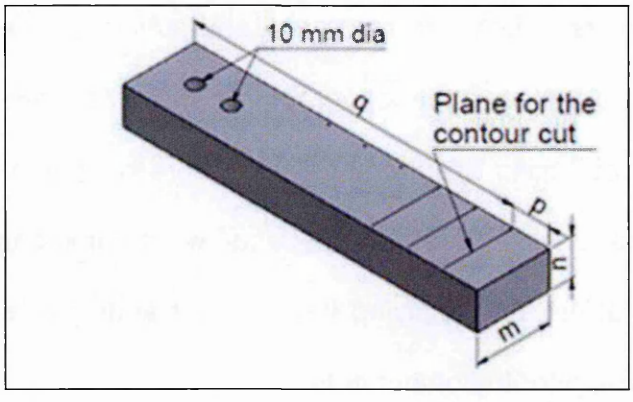

Figure 3-37: The proposed geometry for the benchmark specimen.

2. Parameters that characterise and quantify the quality of cut surfaces for contour method evaluation have been developed and characterisation data sheets have also been developed. These 'surface quality parameters' are:

- The maximum and minimum values of mean surface displacements along the cutting and wire direction.
- The maximum and minimum values of mean apparent stresses along the cutting and wire direction calculated using the contour method.
- Three dimensional surface roughness parameters *Sa, Sq* and *RSm.*
- Root mean square variations for displacement and stress across the cut surface.

3. The study has confirmed the reproducibility of surface profiles for contour measurement for each of three different types of wire electro discharge machine.
4. This study showed that the Agie Charmilles FI 440 CCS WEDM gave better cut surfaces for contour measurements than a Fanuc Robocut α-C600iA WEDM and Fanuc OiB5 WEDM.
5. A thinner wire diameter gave a better quality of surface finish (lower roughness) for cuts in both the mild steel and stainless steel test specimens, but made little difference to the topographical artefacts (bowing, wire start and flared edges) contributing to apparent stress errors in a contour analysis.
6. In all cut surface results, "flared edge effects" were commonly found along the wire entry side of the cuts implying the need for adding a "sacrificial" layer at the wire entry side prior to contour cuts.
7. Wire start topographic artefacts were observed in all cuts, again implying the need for adding a "sacrificial" material at the wire start face of a contour cut.
8. In unrestrained cuts, a *convex* bowed form of the cut surfaces was found in mild steel specimens, whereas a *concave* bowed form of the cut surfaces was

observed in stainless steel specimens. The severity of the bowing was greater in the mild steel specimens than in the stainless steel. The origin of these "bowed" features is uncertain.

9. The quality of the cut surfaces for both material types, mild steel and stainless steel specimens, was improved by providing a restraint along the plane of the cut. In particular bowing of the free side of the cuts was reduced resulting in improved averaged displacement variations.

Chapter 4 : Data analysis parameters for the contour method

4.1 Introduction

In residual stress measurement using the contour method, deformation data defining the "contour" of the cut surface profile is applied to a finite element (FE) model of the cut component, and a linear elastic mechanical FE analysis is carried out to determine the residual stresses released by the cut. The following data collection and analysis parameters are important in this process:

- The deformation measurement spacing of the cut face.
- The data smoothing (for example the 'knot spacing' in cubic spline smoothing).
- The size and type of element employed in the FE stress analysis.

A suitable choice of these parameters is essential, especially where the residual stress distribution varies over short distances.

In this chapter the choice of parameters is studied by considering an idealised surface deformation profile and assessing how effectively the profile is captured using different sets of linear and cubic spline knot spacing intervals. The quality of fit is calculated from the error relative to the idealised profile. On the basis of this investigation, guidelines are provided to help contour method measurement practitioners select a suitable surface measurement density, knot spacing to smooth the deformation data and FE mesh size for the contour method data

collection and analysis. The results of the study will be applied later in this thesis when the contour method is applied to measure rapidly changing residual stresses.

4.2 Idealised deformation profile

A cosine distribution of direct stress acting across a large plate is self-balancing and can therefore be taken to represent an idealised residual stress distribution. Consider a cosine displacement profile applied normal to the edge of a wide plate having a wavelength w, and peak amplitude M. The stress distribution at the surface is calculated for this case using a finite element (FE) stress analysis, for example with w = *6.28* mm and M = *0.2 μm*, using symmetric boundary conditions and assuming plane strain conditions. The elastic material properties (Young's modulus, E = 210 GPa and Poisson's ratio, ϑ = 0.3) are defined to obtain the residual stress distribution. *Figure 4-1* represents the FE model dimensions and boundary conditions. The FE stress results show that in the result of applied cosine displacement profile, the stress profile along the edge has a similar cosine form (see *Figure 4-2*). The following empirical formula (see in Eq 4-1) can be derived from the FE results.

$$\sigma\left(\frac{x}{w}\right) = 3.45\, E \left(\frac{M}{W}\right) cos\left(\frac{2\pi x}{w}\right) \qquad \text{Eq 4-1}$$

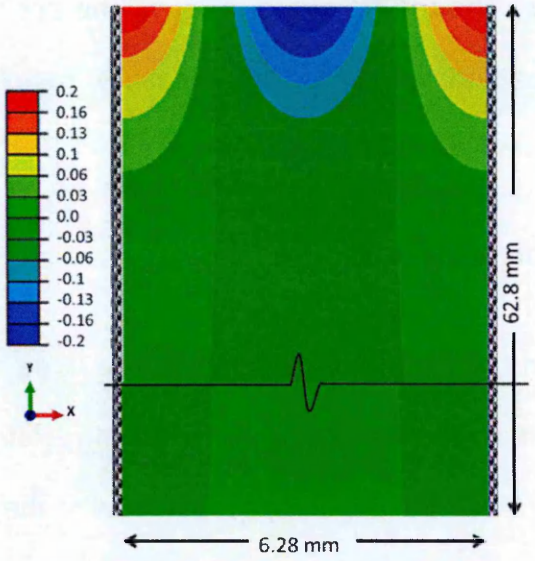

Figure 4-1: Finite element model, the boundary conditions and applied normal displacement (M = 0.2 microns) along the edge of a semi-infinite plate.

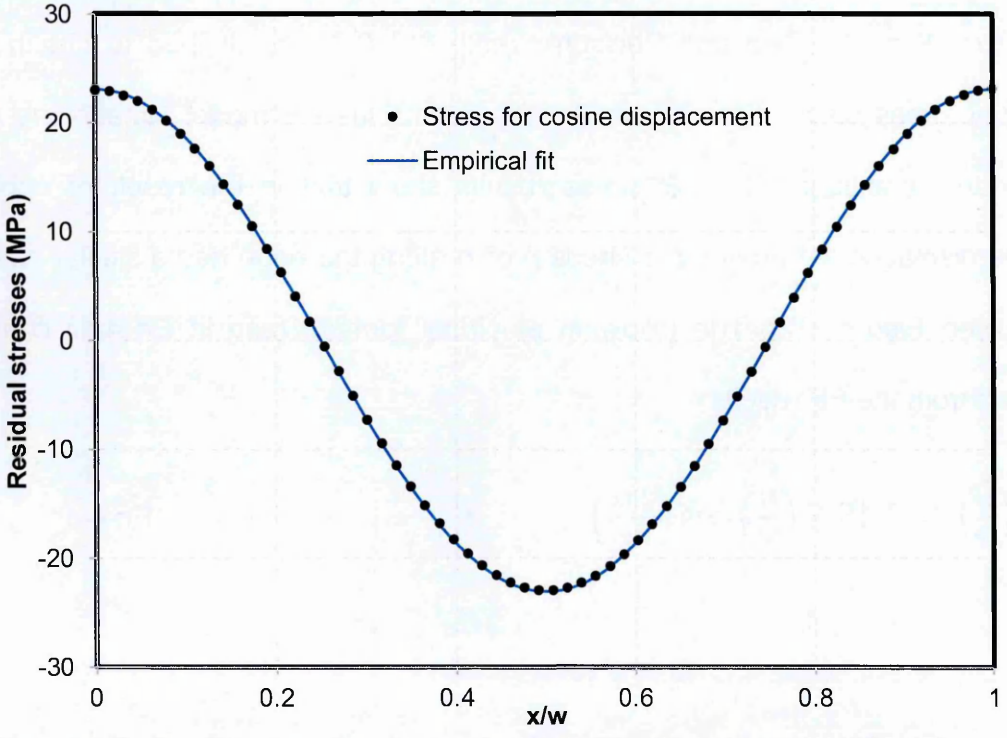

Figure 4-2: Predicted cosine form of self-equilibrated stress profile influence by a cosine displacement profile.

The above study shows that an idealised one dimensional cosine surface deformation profile (see *Figure 4-3*) defined by Eq 4-2, can be used for simplified data analysis investigations.

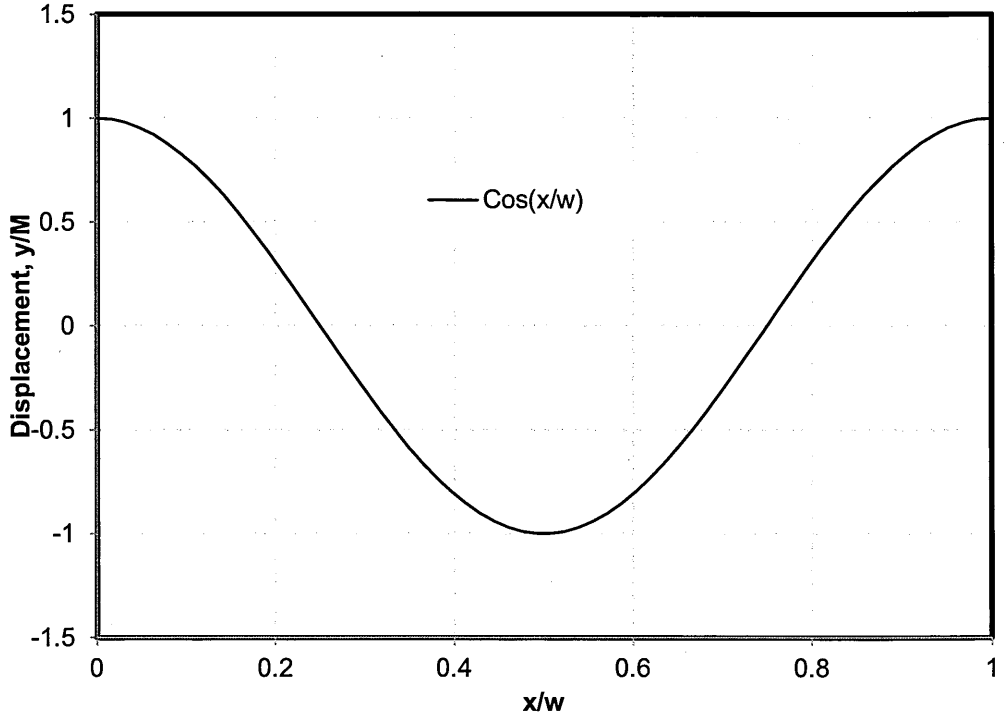

Figure 4-3: Idealised cosine displacement profile as a function of x/w.

$$y(x) = M\,cos(n\emptyset) \qquad \text{Eq 4-2}$$

Where, $y(x)$ represents the surface deformation profile, M the maximum amplitude, and n is the order of the function and $\emptyset = \frac{2\pi x}{w}$, where w is the wavelength of the surface profile distribution.

For a simple case where M and n have values of *1,* the cosine distribution $y(x)$ has a period of 2π, giving Eq 4-3.

$$y(x) = \cos(\frac{2\pi x}{w})$$ Eq 4-3

4.3 Piece-wise linear fit to cosine deformation profile

The accuracy of piece-wise linear fits to a cosine displacement profile over different sets of spacings, *a*, ranging from *a/w* = 0.33 to 0.071 (i.e. *a* = *w/3* to *w/14)* are considered.

Figure 4-4 shows an example where five equally spaced sampling points are used, that is $a = w/4$ for a cosine distribution. The plot also represents the piece-wise linear fit to sample points. Note that for this case sampling points start at $x/w = 0$.

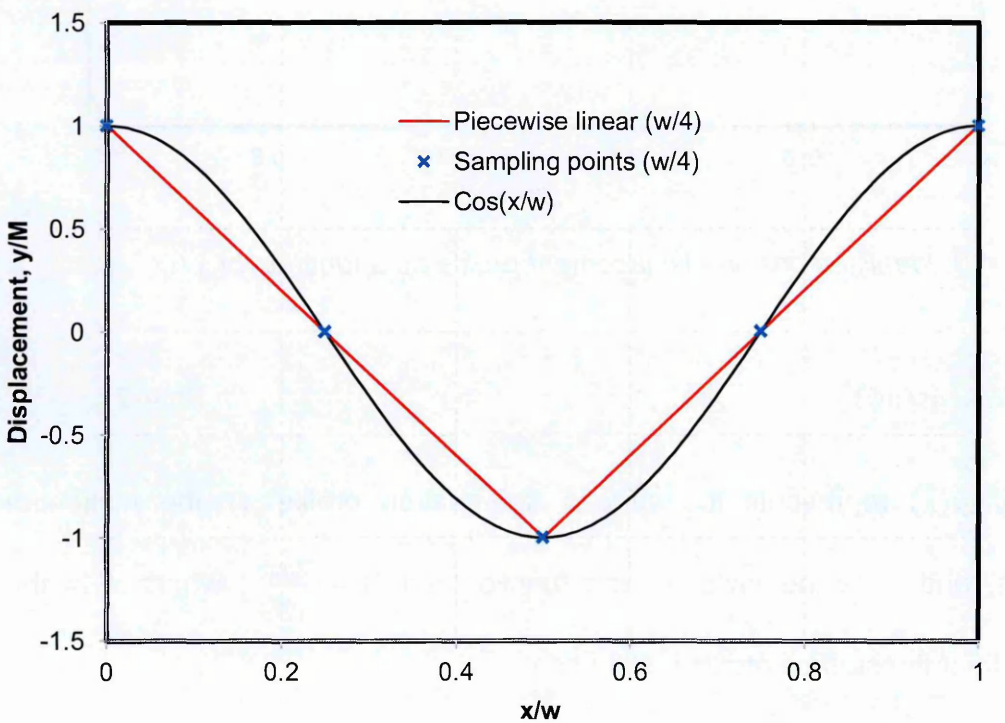

Figure 4-4: Piece-wise linear fit to sampling points spaced w/4 apart on a cosine displacement profile.

The equation of a straight-line can give the piece-wise linear intermediate y values between two consecutive sampling points of each fit. Eq 4-4 represents the general equation for a straight-line.

$$(y - y_1) = m\,(x - x_1) \qquad \text{Eq 4-4}$$

Where,

$$m = \frac{(y_2 - y_1)}{(x_2 - x_1)}$$

x and y represent the coordinate and ordinate respectively of the intermediate points between the two points (x_1, y_1) and (x_2, y_2), and m represents the gradient of the line.

Eq 4-4 is used to calculate the values of the y coordinate along the piecewise linear fit. The deviations (errors) of each piecewise linear fit to the idealised cosine displacement profile are then readily calculated. The modulus of deviations for each fit are determined and used to calculate the overall maximum deviation error, the mean deviation error and the root mean square (RMS) deviation error. The overall maximum deviation error is found directly by considering the largest value of the maximum deviations. The mean deviation error value is calculated by taking the mean of all the maximum deviation values of each fit. The RMS deviation error is calculated using Eq 4-5.

$$RMSE = \sqrt{\frac{\sum_{i=1}^{N}(y_i - \hat{y}_i)^2}{N}} \qquad \text{Eq 4-5}$$

Where: y_i is the y coordinate of the cosine profile at point i and $\hat{y}_i$ is the y

coordinate of the piecewise linear fit at point i. $y_{i-}\widehat{y_i}$ are the maximum values of the deviations of each piecewise linear fit. N is the number of intervals.

Then, the non-dimensional form of the maximum, mean and RMS error is calculated by normalising the maximum, mean and RMS errors to the idealised cosine displacement function. The normalized maximum, mean and root-mean square (NRMS) errors are defined in Eq 4-6.

$$N.max\ or\ N.mean\ or\ NRMS\ = \frac{\max or\ mean\ or\ RMS}{y_{i(Max)} - y_{i(Min)}} \qquad \text{Eq 4-6}$$

$y_{i(Max)}$ and $y_{i(Min)}$ are defined by the maximum and minimum values of the cosine displacement function. The normalised maximum, mean and RMS values are represented as percentage errors (normalised mean and NRMS are multiplied by 100%). This procedure is repeated for the error calculations for all sets of spacing intervals.

Figure 4-5 demonstrates that the form of a cosine displacement distribution can be captured in a piece-wise linear manner with increasing error for $a/w > 0.1$ (i-e $a > w/10$). The maximum deviation error values vary from 2.3 % to 25 % and normalised mean and RMS deviation error values vary from 2 % to 18 %. For $a/w = 0.1$, the maximum deviation is < 2.5 %, and the normalised mean and RMS deviations are < 2 %; for $a/w \leq 0.083$ ($a \leq w/12$) the maximum deviations are < 2 %, and normalised mean and RMS deviations are ~ 1 %. Taking ~ 1 % as an acceptable NRMS error, it can be defined that a minimum of 12 equally spaced intervals must be selected ($a/w \leq 0.083$).

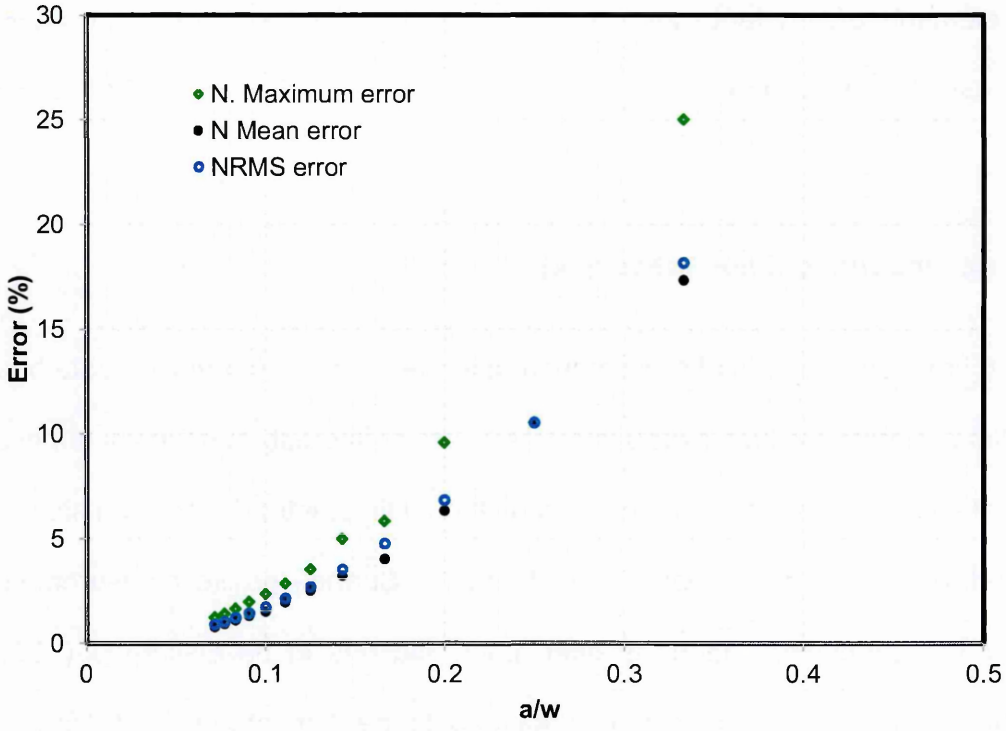

Figure 4-5: Error in piece-wise linear fits to cosine distribution as a function of spacing intervals a/w.

4.4 Data analysis parameters for the contour method

4.4.1 Element mesh size *(s)* for contour stress analysis

A regular array of first order, linear hexahedral 8-node brick finite elements is commonly used to mesh the cut face of the finite element model in a contour measurement. First order brick elements of this kind represent constant stress in each element and have linear shape functions (158).

The errors introduced by idealising a simple cosine displacement function using first order elements (with linear variation in displacement from node to node) can be assessed using the errors analysis presented above (section 4.3). Thus, at

least 12 elements of constant size,s, are required to capture a cosine deformation profile of wavelength, w, *that is* $s \leq w/12 (s/w \leq 0.083)$ to ensure the NRMS error ≤ 1 %.

4.4.2 Data smoothing (knot spacing, k)

In contour measurements of real components, the surface deformation data has contributions from the relaxed residual stress field of interest, surface roughness features of varying length-scale introduced by the cutting method, and from scatter associated with the surface measurement device. Surface profile measurement data near the component edges is often poor and has to be discarded (130). Generally the measured deformation data has to be "smoothed" (130,159) to remove the unwanted contributions that are not associated with residual stresses.

For smoothing the surface data, "cubic smoothing splines" (39) across an array of 'knots' after data cleaning, averaging and flattening are commonly used. All these data process steps allow interpolation at the exact positions of surface nodes on the finite element model, and extrapolation to the boundary of the component, where measured data can be sparse. A cubic spline is constructed by using a piece-wise cubic (third-order) polynomial curves (160). The points where the polynomials are joined are called knots (130). The knot-spacing, k, is a user specified variable and often chosen on the basis of user experience or sensitivity studies. Having a too large spacing can over-smooth the data, whereas too short a spacing can result in over-fitting the data. The convergence approach of Prime et al. (130) can successfully be applied to identify an optimum knot spacing. Details of standard contour data analysis steps are given in section 2.8 of chapter 2.

In order to investigate the best choice for knot spacing to smooth the measured surface deformation data, errors associated with fitting an idealised function can be quantified in a similar way to the element mesh size study presented in section 4.4.1. Cubic splines can be used to fit the idealised cosine displacement profile over different sets of knot spacing ranging from k/w 0.33 to 0.071 (i.e. k = $w/3$ to $w/14$). In order to investigate the deviation between each spline fit and the original cosine displacement profile, the root-mean-squared (RMS), maximum and mean errors are calculated for each set of knot spacing *(k)*.

Figure 4-6 shows an example where 5 knots are used, that is k = $w/4$ (k/w =0.25) to capture a cosine distribution. The plot also represents the spline fit between the knots.

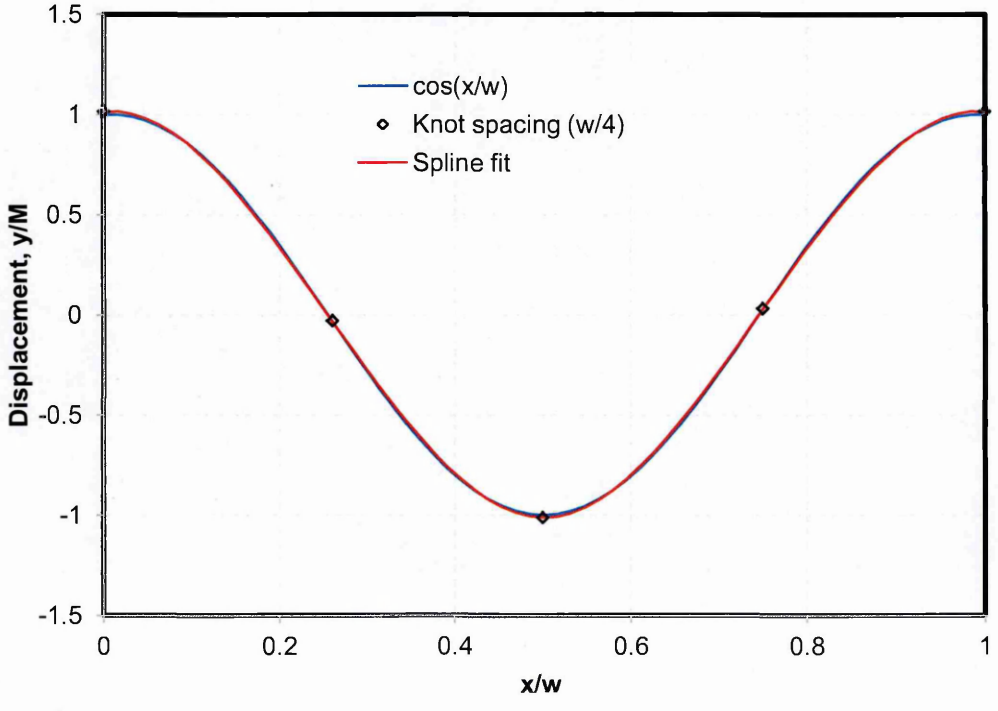

Figure 4-6: Spline fit to w/4 knot spacing on a cosine displacement profile.

The root mean squared error (deviation) function is defined by Eq 4-5, but noting that here y_i are the y coordinates of the cosine profile representing the measurement data points, $\hat{y}_i$ are the cubic spline fit data points and N is the total number of data points for each knot spacing interval. The maximum deviation error is found directly by considering the largest value of deviations. The mean deviation error value is calculated by taking the mean of all the deviation values of each fit.

The non-dimensional form of the RMS, maximum and mean errors are then calculated using Eq 4-6 given earlier, where $y_{i(Max)}$ is the maximum displacement value taking from the idealised cosine distribution function, and $y_{i(Min)}$ is the minimum displacement value taking from an idealised cosine distribution function.

As previously the NRMS values are represented as percentage errors. This error is repeated for each set of knot spacings.

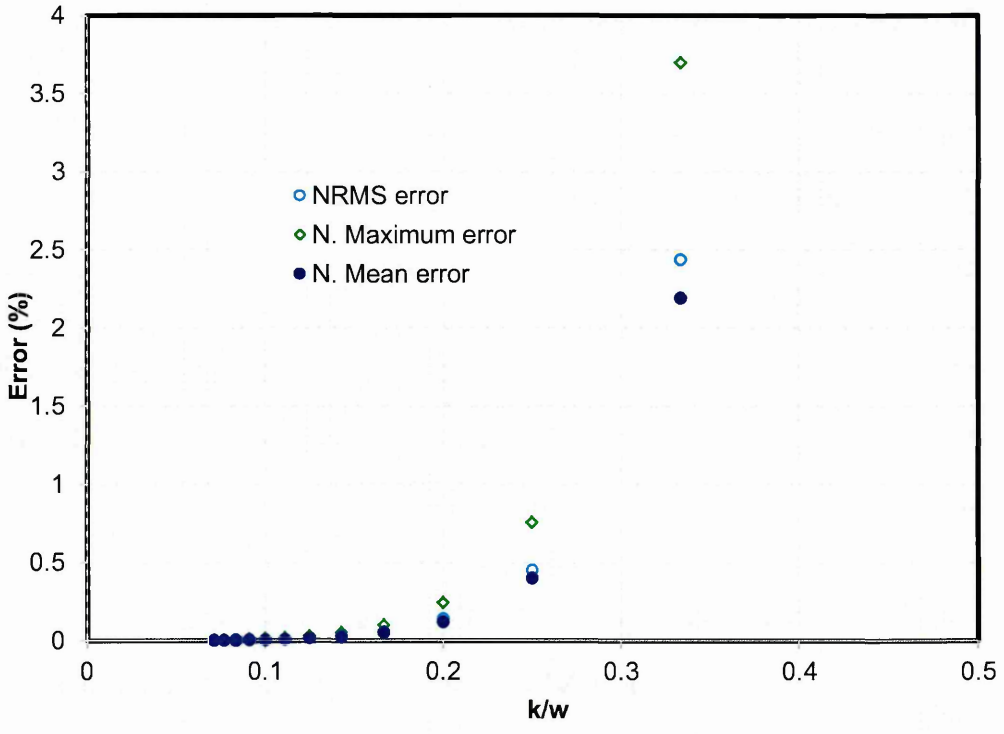

Figure 4-7: Error in cubic spline fits to a cosine distribution as a function of knot spacing interval (k/w).

Figure 4-7 represents the error values versus knot spacing for the range of k intervals from k/w= 0.33 to 0.071 ($k = w/3$ to $w/14$). *Figure 4-7* shows that the percentage error increases with increase in the knot spacing. However, the errors are small because the spline fits efficiently capture the idealised cosine profile.

From *Figure 4-7* it is evident that knot spacings $k/w \leq 0.25$ ($k \leq w/4$) give a NRMS error, normalised mean error and normalised maximum error < 1 %. However, as the knot spacing increases the error begins to ramp up (for example for k/w = 0.33). This evidence shows that 4 knot intervals can capture the idealised cosine displacement profile of wavelength, *w* with a NRMS error < 1 %.

4.4.3 Surface deformation measurement spacing (d)

In order to acquire a good spline fit to the surface deformation profile introduced by the relaxed residual stress field a suitable surface measurement spacing d is required.

The surface deformation of the cut face of a component in a contour measurement is usually measured in a regular grid of point spacing (d) in both x and y directions as shown in *Figure 4-8.*

For laser CMM measurements, each measured point is averaged over the laser beam diameter. For touch probe CMM measurements each measurement point represents the height of the surface area at which the probe makes the contact.

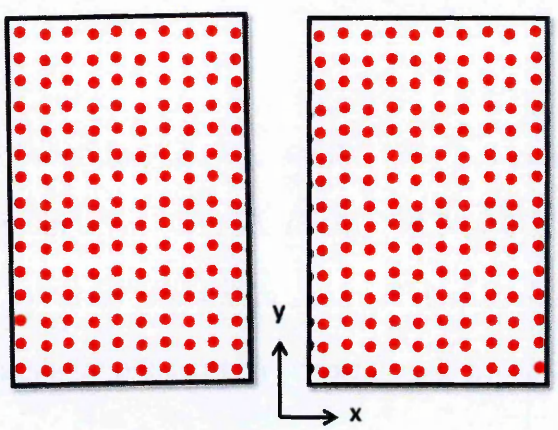

Figure 4-8: Schematic drawing showing a regular grid of surface deformation sampling points for the mating cut surfaces.

It can be intuitively argued that the measurement spacing,d , should be less than or equal to the linear element mesh size used to idealise the smoothed profile, that is $d \leq s$, where $s \leq w/12$. But ideally the measurement spacing should

be as small as possible as several data points are required for cubic spline smoothing of noisy data between knots, that is $d<<k$.

4.5 Residual stress wavelength, *w*

The residual stress wavelengths of interest have to be defined in order to apply the simple criteria developed above. A rigorous way of identifying the dominant cosine form wavelengths present in a residual stress field is to carry out a fourier series analysis (161). But preliminary knowledge of the full residual stress field may not be available. Often the reason why a contour measurement is done is to actually quantify the residual stress field.

It is more difficult to measure short wavelength residual stress distributions because very fine surface deformations must be resolved as shown in Eq 4-1. The shortest residual stress length scale that can be resolved in a conventional contour method measurement can be inferred from the characteristic length scale of the surface roughness created by the WEDM process. *RSm*, the mean spacing between the profile peaks, is an important surface roughness parameter as it provides a measure of the mean length scale of noise introduced by the cutting process. It has been estimated that the contour method is unlikely to be able to resolve variations in displacement across a length less than about five times *RSm* (129). The experimental results in chapter 3 show that, *RSm* is ≈ 0.15 mm for a typical 0.25 mm diameter WEDM contour cut. Thus for this case the minimum residual stress length scale that can be practically measured by contour method is of order 0.5 to 1 mm.

More generally residual stress wavelengths likely to be present can be estimated using the following information:

- Prior knowledge: residual stress measurement results from other techniques, from prediction or/and published data from a similar component.
- Component dimensions (gives maximum wavelengths)
- Expert judgment

4.6 Discussion

The criteria developed in this simple study can be used for choosing the measurement spacing *d*, cubic spline knot spacing *k* and finite element mesh size *s* for the contour method data analysis, providing the residual stress wavelengths of interest are known or can be estimated.

An appropriate estimation of the residual stress wavelengths of interest is essential because it has a great influence on establishing suitable choices for data analysis parameters.

The developed criteria are based on a one dimensional idealised cosine displacement function of fixed wavelength and a simple estimation of errors. In practice, the contour method provides a two dimensional map of stress using surface deformation data measured across a two dimensional plane. Two dimensional cubic splines are used to smooth the deformation data and can provide better accuracy in the stress results. But of course the deformation field

usually comprises a mixture of wavelengths including unwanted noise for which a more robust analysis is desirable.

A further consideration is that deformation data are difficult to capture close to the edges of the specimen especially using a touch probe CMM (130). But the edge effects have not been considered in the above study and again there is a scope for improving the criteria.

The importance of selecting appropriate data analysis parameters becomes very high where short length scale residual stresses are of interest. But in order to resolve short length scale residual stresses, a very fine surface deformation measurement density is required for which an improved surface finish (lower roughness) is desirable to reduce 'noise' levels. In addition, the cut surface should be free from cutting effects. Therefore, a good quality of cut surface is essential for achieving a better resolution and accuracy in contour method residual stress results together with the suitable gauge size for data collection and data analysis parameters.

The gauge size for the contour method depends upon the spacing for the surface deformation measurements, the optimum knot spacing used to smooth the deformation data, and the element size used in the finite element stress analysis. The deformation of the cut surface should be measured using a suitable measurement spacing (which is usually smaller than the FE mesh size), and then the optimum knot spacing should be selected so that the associated cubic spline is best fitted to the displacement data. Then finally, first order elements are used to mesh the cut face of the finite element model for stress analysis. First order

elements have linear shape function and provide constant stresses for each element. Thus, if first order elements are used the element size used at the cut surface gives a measure of the effective gauge size. Therefore, the effective 'top-hat' gauge size for the contour method can be controlled by FE element mesh size.

The following procedure is proposed to improve the reliability of contour residual stress measurements, especially where short length scale stress fields are of interest.

Step 1: Compile specimen geometry data and material mechanical properties including Young's modulus, Poisson's ratio and the material yield stress.

Step 2: Estimate the residual stress profile across the measurement plane from which the residual stress wavelengths *w*, of interest that best characterise the expected stress field can be identified. This can be obtained from other measurement techniques, from prediction or/and published data from a similar component.

Step 3: Perform WEDM contour cut using cutting conditions suggested in chapter 3. For short length scale residual stress variations, cutting conditions giving a fine surface finish should be chosen.

Step 4: Define the contour surface measurement density based upon the developed criteria; that is $d \leq w/12$ and $d<<k$ noting that the finer the spacing the better.

Step 5: Measure the cut surface with defined sampling density.

Step 6: Perform data analysis steps detailed in chapter 2.

Step 7: Choose the initial knot spacing for cubic spline smoothing based upon the wavelength analysis; that is $k \leq w/4$.

Step 8: Select the finite element mesh size based upon the wavelength analysis; that is $s \leq w/12$.

Step 9: Then, optimise the knot spacing using the uncertainty approach of Prime (3), by examining the different k spacings across the initial k value and calculate the stresses for each k increment. Estimate the averaged stress uncertainty for each k increment. The final k value is selected by minimising average uncertainty in the calculated stresses.

Step 10: Perform final FE analysis to calculate stress results.

All above steps are summarised in the flowchart shown in *Figure 4-9*.

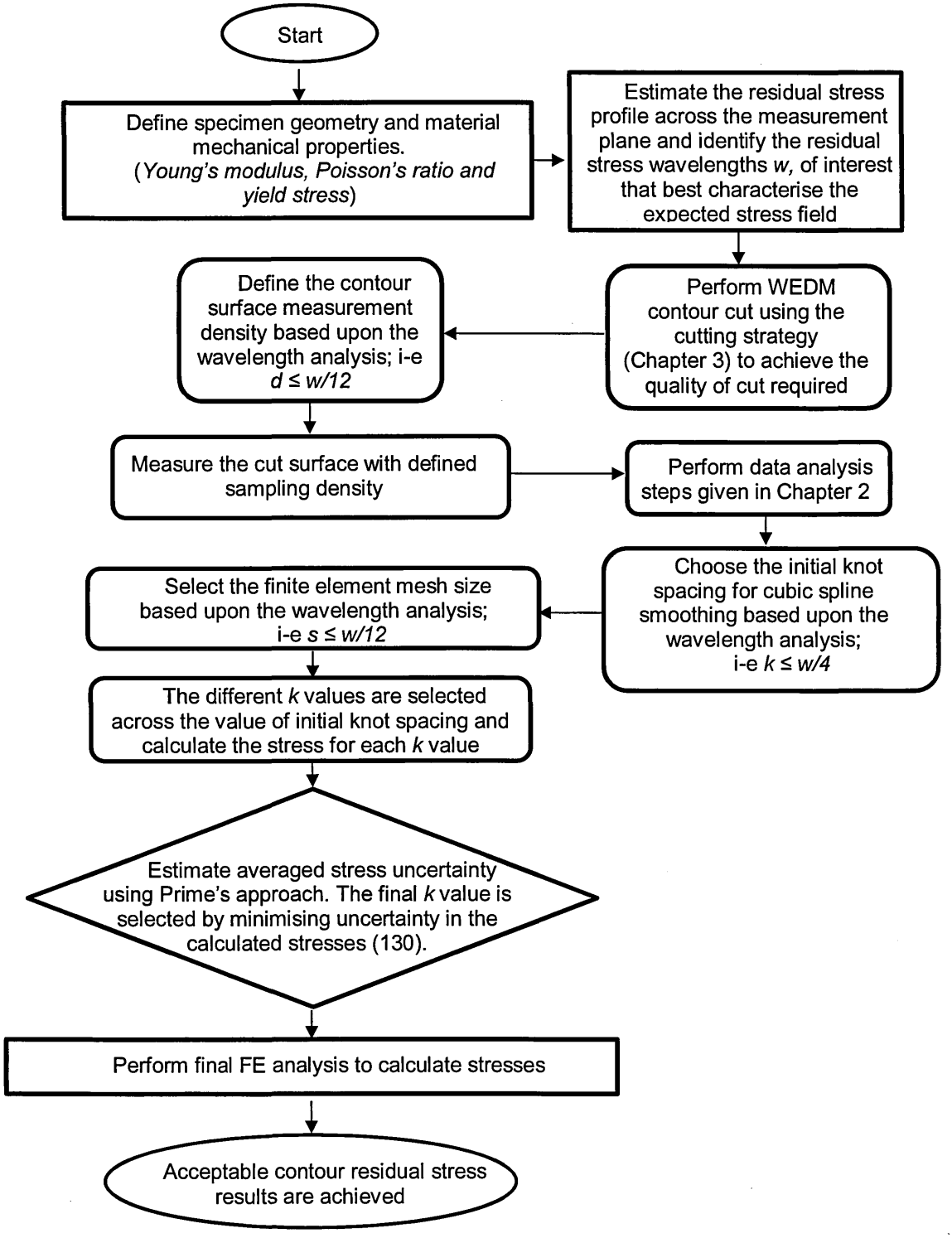

Figure 4-9: Flowchart illustrating the proposed contour method data analysis procedure to improve the robustness of the calculated results.

4.7 Conclusions

1. Three deformation data collection and analysis parameters have a major influence on the contour method residual stress results: the surface deformation measurements spacing,d, the cubic spline knot spacing,k, chosen to smooth the measured deformation and the finite element mesh size, s.
2. The contour method data collecting and analysis parameters have been investigated by considering a one dimensional idealised cosine function. The quality of piece-wise linear and cubic spline fits to the idealised profile have been evaluated by calculating the fitting errors. Threshold acceptable errors are defined which inform the choice of these parameters.
   - The residual stress wavelength,w, likely to be present in the specimen is first needed to apply the simple developed criteria.
   - For the measurement spacing, select $d \leq w/12$ $(d/w \leq 0.083)$ and $d<<k$ noting, the finer the spacing the better.
   - For the knot spacing, select $k \leq w/4 (k/w \leq 0.25)$.
   - For the finite element mesh size, select $s \leq w/12 (s/w \leq 0.083)$.

Chapter 5 : Residual stress measurements

5.1 Introduction

In this chapter, residual stresses are evaluated in three welded components using special measures to perform the contour cut and applying the criteria developed in chapter 4 in making suitable choices for deformation data sampling and analysis parameters. The three welded components include:

1. an electron beam (EB) butt-welded P91 ferritic-martensitic steel plate,
2. a dissimilar metal (AISI Type 316LN stainless steel and P91 modified 9Cr-1Mo steel) EB butt-welded plate, and
3. a stainless steel clad ferritic steel plate.

The challenges associated with the residual stress measurement related to EB welded and overlay cladded plates have been discussed in detail in section 2.5 of chapter 2. The present studies demonstrate that by applying the developed data analysis criteria, detailed characteristics of residual stress distributions having a short length scale can be successfully captured thus showing that the spatial resolution of the contour method can be improved. The success of the developed approach is evaluated by comparing the new contour measurement residual stress results with conventional contour measurements and with other stress measurement techniques results.

5.2 Case study 1: P91 electron beam welded plate

An EB butt-welded P91 steel plate for which neutron diffraction residual stress measurements were available was selected for the contour measurement studies. Firstly, residual stress measurements were conducted using a conventional contour method. Then, special measures were applied in the cutting and data analysis steps to improve the spatial resolution of the contour method. The success of the improvements implemented is assessed by comparing the new measurements with conventional contour method results and published neutron diffraction results.

5.2.1 Specimen details

The chemical composition for the base material of the EB welded P91 steel plate used for the present investigation is given in Table 5-1 (112). The test specimen was fabricated from a hot rolled plate material. As a first step of specimen preparation, the hot rolled plate material was normalized at 1050 $^{\circ}$C for 1 min mm^{-1} thickness. Then, it was tempered at 770 $^{\circ}$C for 3 min mm^{-1} followed by cooling in air. Then, the tempered material was machined to create plates of dimensions 290 mm long by 75 mm wide by 10 mm thick. Finally, the top and bottom surfaces of the sample plates were ground to get flat parallel surfaces by removing the surface waviness caused by the hot rolling fabrication process. A final plate thickness of ~9 mm was achieved (112). Pairs of prepared plates were then butt welded along the 290 mm edge by an electron beam process. The recorded welding parameters are given in Table 5-2. The final dimensions of the test plate obtained were 290 mm length, 150 mm width and ~ 9 mm thick.

C	Mn	Zr	Si	P	S	Cr	Mo
0.106	0.443	0.005	0.221	0.018	0.0008	8.965	0.901
Ni	Cu	Al	N	Nb	Ti	V	
0.212	0.045	0.010	0.0464	0.073	0.004	0.194	

Table 5-1: The chemical composition of the Mod.9Cr-1Mo steel (remaining Fe) (112).

Welding parameters	
Beam current (mA)	70
Gun voltage (kV)	60
Travel speed (m/min)	1
Pre-heat (°C)	No

Table 5-2: The welding parameters for the EB welded P91 steel plate (112,162).

As-welded residual stresses in the plate were measured using the contour method. The contour surface deformation data were analysed using a bulk Young's modulus of 218 GPa and a Poisson's ratio of 0.3 for both the P91 base metal and the fusion zone.

5.2.2 First contour measurement

The first contour residual stress measurement was carried out using a conventional contour cutting and analysis method. In order to determine the longitudinal residual stress, the first contour cut was performed across the mid-length of the plate, in the direction perpendicular to the weld as shown in *Figure* 5-1. Before specimen cutting, sacrificial layers were attached to both the top and bottom of the plate along the plane of the cut. They help to avoid undesirable wire

entry and exit effects (143). These were made up of carbon steel having a cross-section of 5 mm x 10 mm. An Agie Charmilles FI 440 CCS Wire Electro Discharge Machine (EDM) was used to perform the cut. A 0.25 mm diameter brass wire was chosen to perform the cut. This limits the surface finish achievable and thereby the stress resolution length-scale (see chapter 4). The deformation contours of the created cut surfaces were measured using a Mitutoyo Crysta Plus 547 CMM. For this measurement, a 4 mm diameter Renishaw PH10M touch trigger probe was used. The three spatial coordinates of each point on a 0.5 mm square grid pattern on the cut surfaces were measured. The contour cut surface data were processed into a suitable form using standard contour routines coded in MATLAB 7.10. Basic steps for data processing were used, such as alignment of the two data sets with one another by translating and rotating the data in the cut x-y plane, removing of noise and outliers in the raw data of the surface contours, averaging of the measurements points from the pair of cut halves and smoothing by fitting cubic spline functions, with a 1 mm x 1 mm knot spacing (112). The data analysis steps are discussed in detail in (39,130). Finally, the linear elastic finite element analysis was performed using ABAQUS. For building the 3D model, one half of the plate was built by extruding the measured shape of the perimeter at the cut interface. The measured displacements on the cut surface were very small and the analysis is elastic. Therefore the created cut surface was modelled as a flat surface. The cut face was meshed using 0.5 mm size first order elements. The processed surface contour data were applied as boundary conditions, with reverse sign at the cut face nodes of the FE model. The elastic material properties (112) (Young's modulus, E = 218 GPa and Poisson's ratio, ϑ = 0.3) of the specimen were defined

and the elastic FE analysis conducted to determine the released residual stress distribution across the created cut surface.

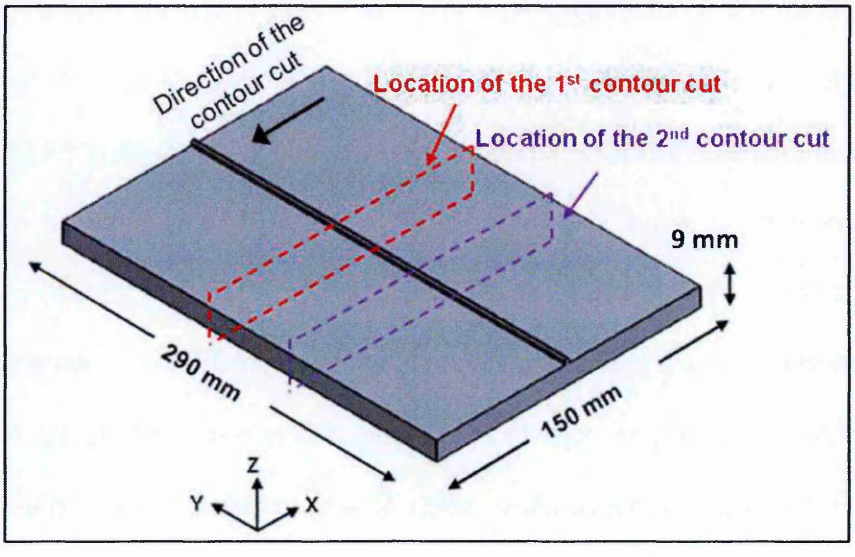

Figure 5-1: Sketch of the EB-welded P91 plate showing the locations of the contour cuts.

A map of the longitudinal residual stresses from the first cut measured using the conventional contour method (112) is represented in *Figure 5-2*. The conventional contour stress results are compared with published neutron diffraction measurements (112,162) along a line 1.5 mm below the top surface of the plate in *Figure 5-3*.

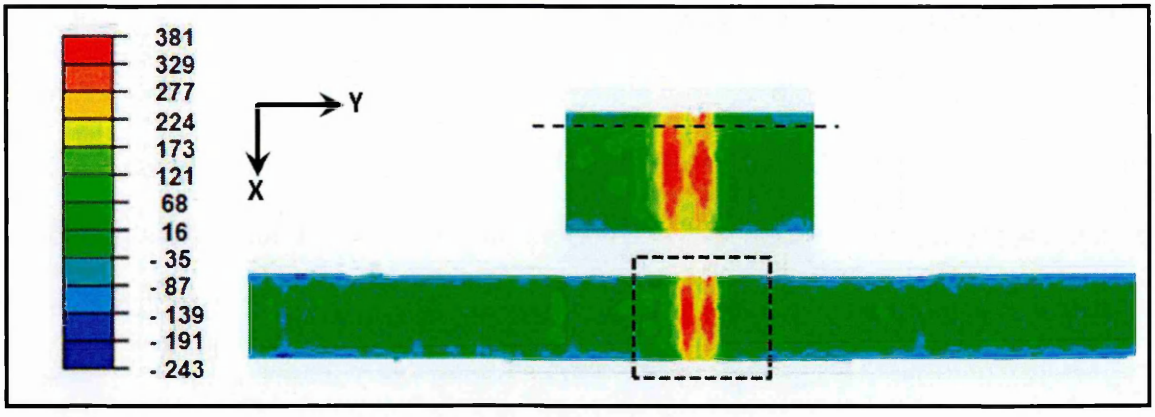

Figure 5-2: Map of the longitudinal stress measured using the conventional contour method (112). Units are in MPa.

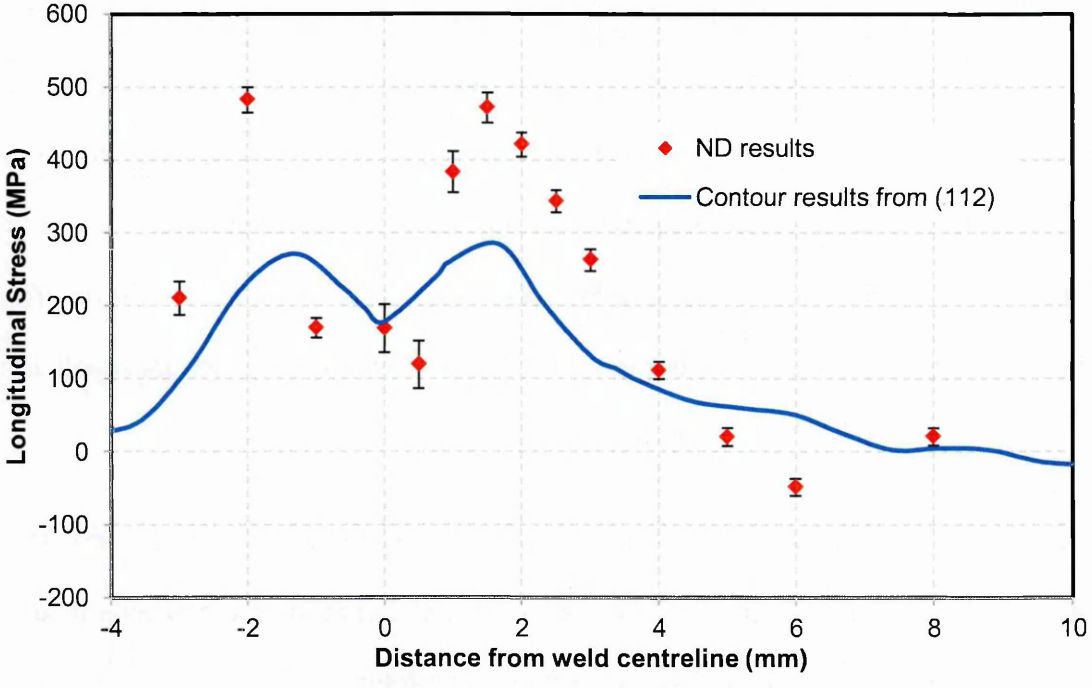

Figure 5-3: Comparison of the conventional contour method measurement with neutron diffraction measurements (112,162) for a line profile at 1.5 mm below the top surface of the EB butt-welded P91 plate.

Neutron diffraction measurements were conducted to measure the residual stresses at the mid length of the plate on a transverse plane relative to the direction of the EB weld as reported in (112,162). The longitudinal residual stress profile measured by neutron diffraction had an 'M' shaped stress distribution across the weld centre line at 1.5 mm below the top surface of the plate, see *Figure 5-3*. In these results, high tensile stress peaks were observed on both sides of the weld centre line beyond the heat affected zone (HAZ) to parent material boundary. The tensile peaks of this stress distribution are spread across a very short length, that is within ~3 mm spanning the 1 mm wide fusion zone (as shown in *Figure 5-3*). The conventional contour measurement was conducted at the same mid-length location as the neutron diffraction measurements. Overall, the residual stress results measured from both methods show the same M-shaped trend. However, the contour method measurement has not captured the maximum tensile stress peaks on both sides of the weld centre line observed in the neutron diffraction results (112,162). This evidence illustrates the limited spatial resolution of the contour method measurement approach used.

Table 5-3 summarises the cutting conditions, deformation collection and data analysis parameters used for this "conventional" contour measurement and compares them with the guidelines presented in chapter 4. Note that the minimum residual stress wavelength, *w*, of interest is defined here by the distance between the peak tensile stresses observed in the measurements.

Case	Cutting wire Diameter (mm)	Deformation spacing, *d* (mm)	Knot spacing, *k* (mm)	FE mesh size, *s* (mm)	Residual stress wavelength, *w* (mm)
Conventional	0.25	0.5	1.0	0.5	3
Criteria	0.25	$<< k, \leq w/12$	$\leq w/4$	$\geq d, \leq w/12$	w
Met	Yes	No	No	No	-
Required	0.25	$<< 0.75, \leq 0.25$	≤ 0.75	≤ 0.25	3

Table 5-3: Cutting conditions, deformation collection and data analysis parameters for the first "conventional" contour measurement.

In the next section, a second contour cut performed on the same plate is described where attempts were made to improve the measurement spatial resolution.

5.2.3 Second contour measurement

A second contour cut was conducted with the aim to improve the spatial resolution of the contour method. The location of the second contour cut in one of the half-plates remaining from the first cut (145 mm long and 150 mm wide) is indicated in *Figure 5-1*. The second cut was made 60 mm away from the first contour cut plane as shown in *Figure 5-4*. The following sub-sections describe the details of the special measures taken in the cutting and data analysis steps to improve the quality of the contour measurement results.

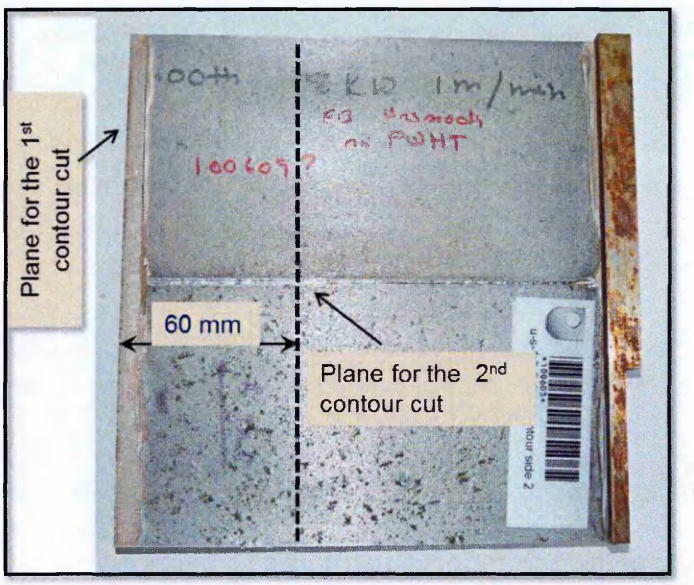

Figure 5-4: Photo of one half of the EB welded P91 plate after the 1st contour measurement showing the location of the 2nd contour measurement cut.

Wire EDM cutting

Sacrificial layers 5 mm thick were attached on the top and bottom faces of the plate along the plane of the cut to avoid wire entry and exit artefacts (143). A 1.8 mm diameter start pilot hole was drilled at 10 mm from one end of the plate. This provided an embedded cutting configuration giving self-restraint during cutting (116). Finger clamping tools were used to provide support and to stop any movement of the test component on the WEDM bed table. The test component and the fixture were left to reach thermal equilibrium conditions within the WEDM deionised water tank before clamping to prevent any thermal stresses. It also helps to produce the cut surface with better precision and fine surface finish by minimising any recast layer and cutting induced stresses (131). An Agie Charmilles FI 440 CCS Wire Electro Discharge Machine (WEDM) was used to

perform the cut. In order to improve the cut surface finish quality, the WEDM wire diameter was reduced for the second cut from 0.25 mm to 0.1 mm (38). The set of WEDM cutting parameters were selected as a result of the benchmark studies to characterise the WEDM cut given in chapter 3. The cut was performed using the S3 (designated on the machine) set of cutting parameters with the 'A' value of 0.2 µs and 'TAC' value of 0.1 µs (A and TAC cutting parameters were discussed in chapter 3). After cutting, the cut length was reduced by 20 mm from both sides in order to remove cut start and stop effects (the first contour measurement showed that significant residual stresses associated with the EB weld did not extend this far). *Figure 5-5* shows both parts of the sample after the second contour cut.

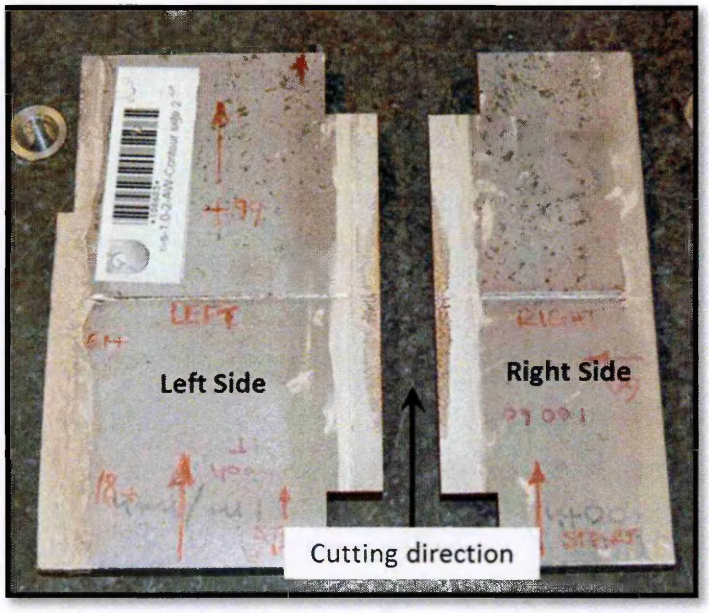

Figure 5-5: The P91 EB butt-welded plate after the second contour cut and removal of 20 mm from the wire cut start and stop edges.

Surface contour measurement

The thin cutting wire diameter (0.1 mm compared with 0.25 mm diameter for the first contour cut) produced a finer surface finish. Two further measures were taken to help improve the resolution of the short length-scale (w = 3 mm) residual stresses in the plate. A 1 mm diameter Renishaw PH10M touch trigger probe (i.e. smaller than the 4 mm diameter probe used for the first cut) was used to measure the surface profiles of the cut parts in the CMM (a Mitutoyo Crysta Plus 547). Also the measurement spacing was reduced from 0.5 mm to 0.125 mm (meeting the criteria of chapter 4).

Data processing and FE simulation

The surface deformation data from the second contour cut were processed using standard contour routines coded in MATLAB 7.10. as described in (39,130). *Figure 5-6* shows the map of the averaged surface displacement measurements across the transverse cut plane. The maximum peak to valley deformation is about 32 μm in the region of the weld.

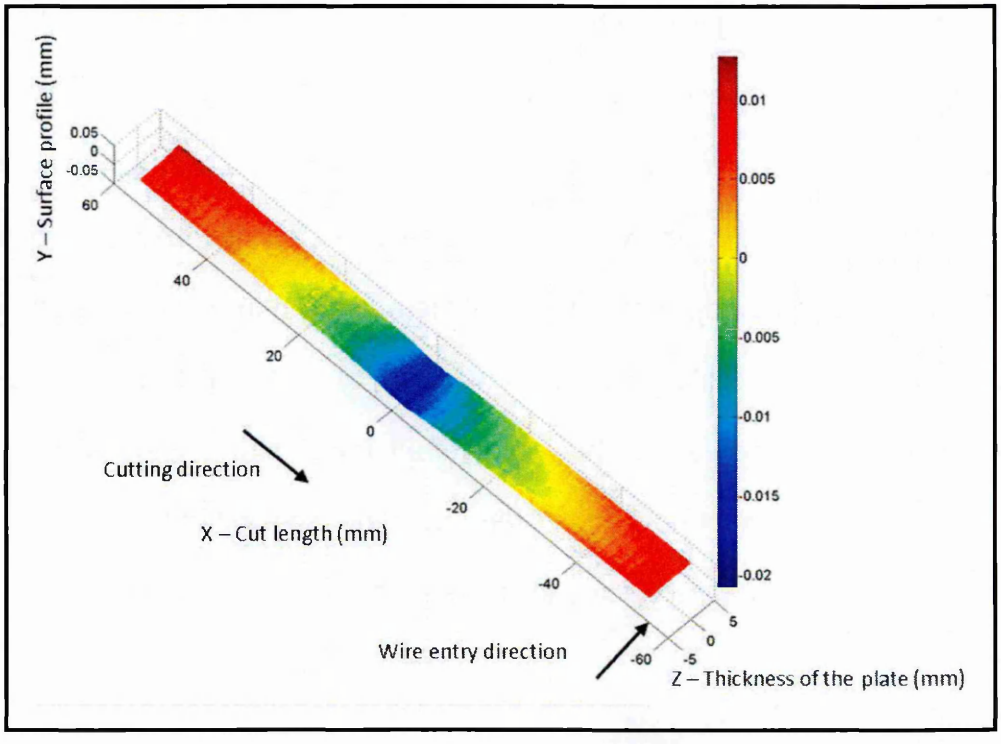

Figure 5-6: Map of averaged surface displacement measurements across the transverse cut plane (2nd contour cut) for the EB welded P91 steel plate (scale is mm)

Then, the measured contour data were smoothed by fitting a cubic spline function, with suitable knot spacing. The criteria given in chapter 4 were applied to make the best choices for suitable knot spacing (k) and finite element mesh size (s), based upon a residual stress wavelength (w) estimated from the neutron diffraction measurements conducted on the same plate (112,162). Taking the minimum wavelength as $w = 3$ mm, an initial knot spacing $k \leq w/4$, that is $k \leq 0.75$ mm, should be selected and the finite element mesh size $\leq w/12$, that is $s \leq 0.25$ mm, should be chosen.

Then, the knot spacing was optimised using the uncertainty approach of Prime (130), by examining spacings ranging from 1 mm to 0.3 mm with 0.1 mm increments. Stresses were calculated for each k value using finite element analysis. A 0.25 mm mesh size was used for the cut face (within 7 mm across the centre of the weld) and adjacent to the cut face as shown in *Figure 5-7*. The knot spacing was selected which minimised uncertainty in the calculated stresses (130). *Figure 5-8* illustrates that the minimum averaged stress uncertainty in the calculated stresses was found to be 17 MPa at a knot spacing of 0.4 mm. Thus, a knot spacing of 0.4 mm was selected to smooth the surface deformation data.

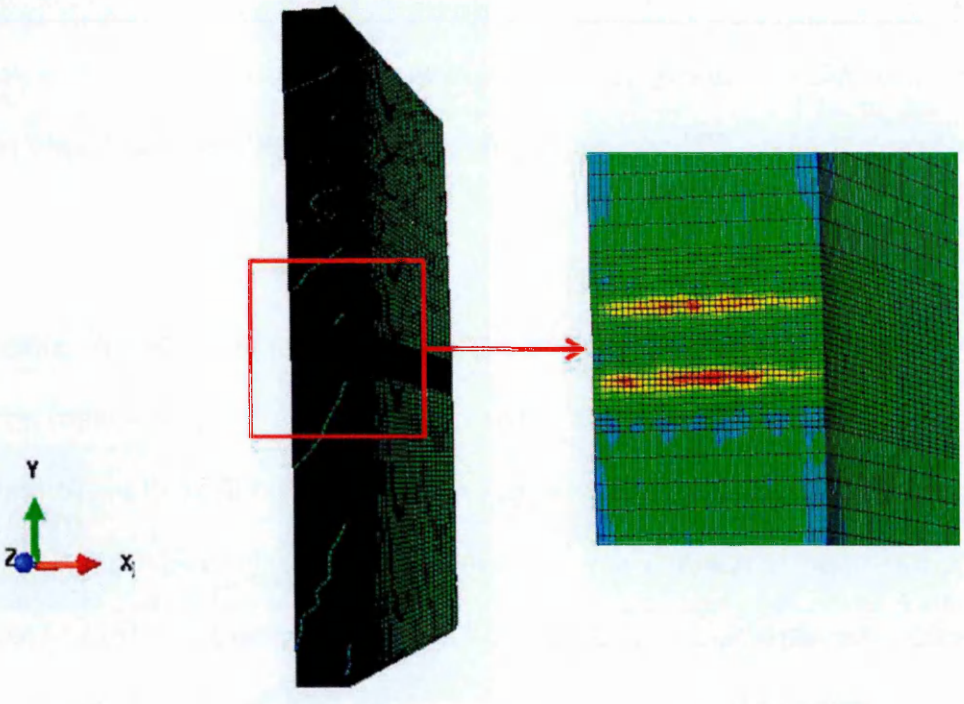

Figure 5-7: Mesh used for the EB welded P91 plate with close up view.

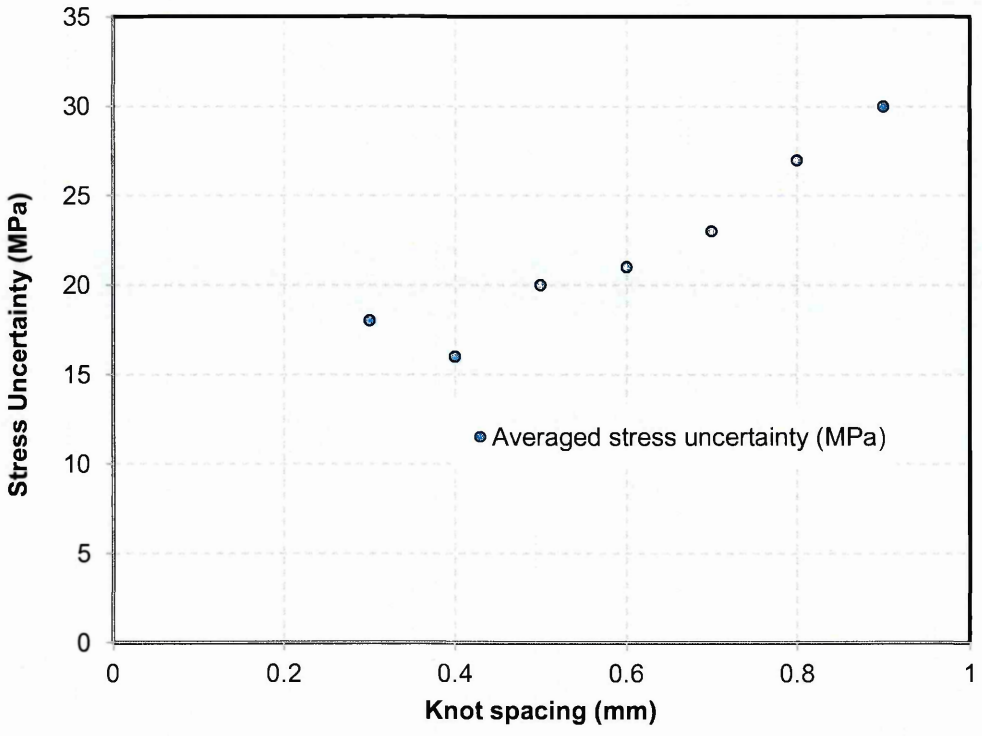

Figure 5-8: Optimal knot spacing indicated by minimising the averaged uncertainty in calculated stresses for the 2nd contour measurement of the EB P91 butt-welded plate.

The processed contour data were then used to perform a final linear elastic finite element analysis as explained in section 5.2.2 of chapter 5 with the 0.25 mm mesh size. The elastic constants used in the analysis were a Young's modulus of 218 GPa and Poisson ratio 0.3 (112).

A map of the longitudinal residual stress measured using the improved contour approach is presented in *Figure 5-9*. The new results are compared with results from the first conventional contour measurement and the neutron diffraction measurements along a line 1.5 mm below the top surface of the plate in *Figure* 5-10.

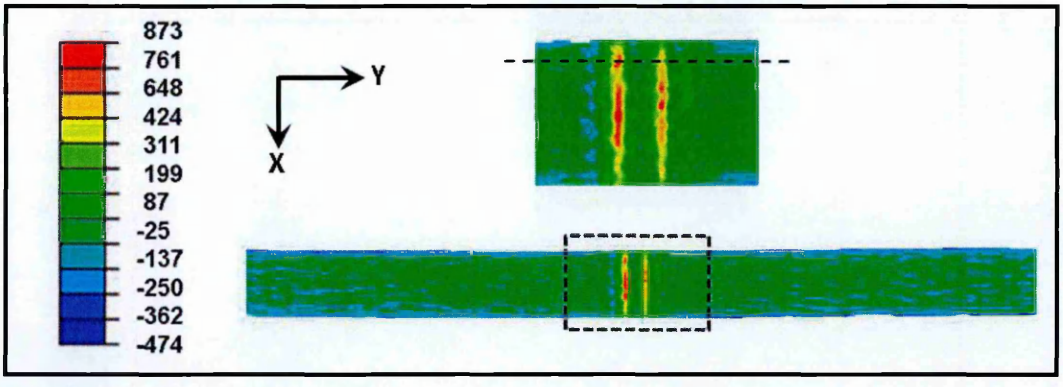

Figure 5-9: Map of the longitudinal stresses from the improved (2nd cut) contour measurement. (Units are in MPa).

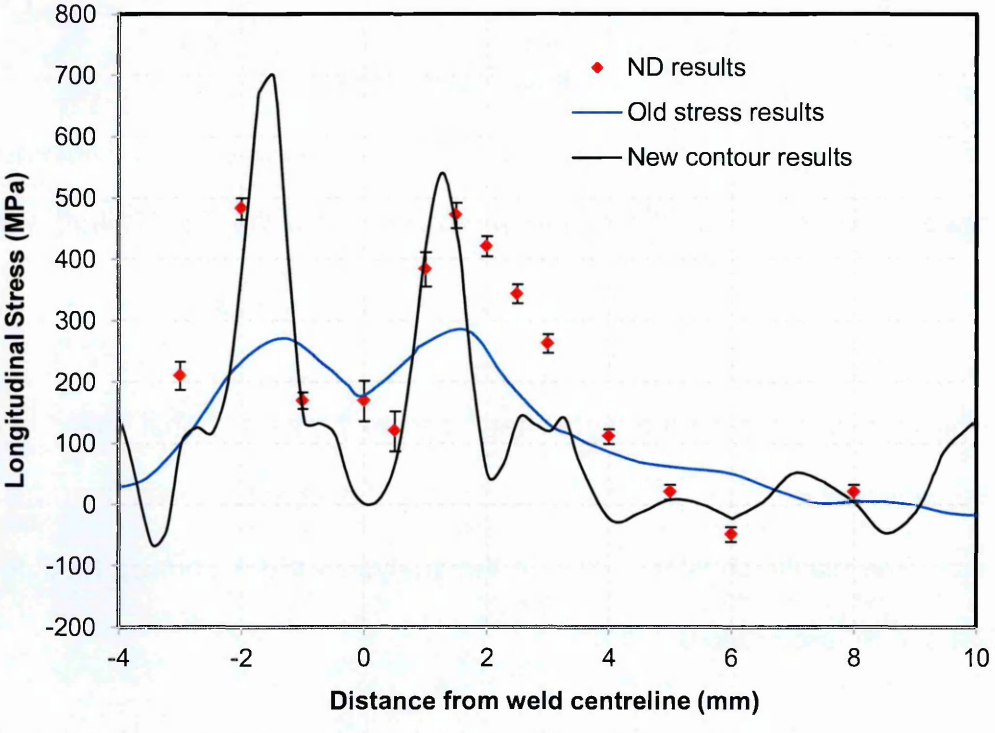

Figure 5-10: Comparison of the improved and original contour measurements with neutron diffraction measurements (112,162) for a line profile at 1.5 mm below the top surface of the EB butt-welded P91 plate.

5.2.4 Surface roughness measurement for the EB welded P91 plate

Surface roughness profiles over the first and second contour cuts were measured to investigate the quality of the cut surfaces using a confocal microscope with the instrumental configurations given in Table 5-4. Profiles were measured over a 15 mm region across the EB weld centre covering the whole thickness of the plate.

Roughness instrument			
Objective	10 X	**Resolution**	12µm
Overlap area	10%	**Threshold**	10%
Z-Scan value	200µm		

Table 5-4: Confocal microscope parameters used for 3D roughness measurements.

For the first cut, a S_q (the root-mean square) value of *2.9 µm* and S_a (the arithmetic mean of the absolute height) value of *2.2 µm* were measured. For the second cut a S_q value of *2.3 µm* and S_a value of *1.8 µm* were measured. Thus, the quality (roughness) of the second contour cut surface was improved by using a thinner wire diameter.

5.2.5 Results and discussion for the EB welded P91 plate

An electron beam welded joint forms a narrow weld fusion zone that introduces short length scale residual stresses. For the EB welded P91 plate additional local stress variations arising from martensitic phase transformation were seen in

neutron diffraction measurements (112,162). But the initial conventional contour method measurement was unable to resolve the tensile stress peaks in the HAZs adjacent to the weld fusion zone.

The second contour cut used a smaller diameter wire to achieve a better surface roughness and implemented the criteria developed in chapter 4 as summarised in Table 5-5 below.

Case	Cutting wire Diameter (mm)	Deformation spacing, *d* (mm)	Knot spacing, *k* (mm)	FE mesh size, *s* (mm)	Residual stress wavelength, *w* (mm)
Improved Contour	0.15	0.125	0.4	0.25	3
Criteria	0.25	$<< k$, $\leq w/12$	$\leq w/4$	$\geq d$, $\leq w/12$	w
Met	Yes	Yes	Yes	Yes	-

Table 5-5: Cutting conditions, deformation collection and data analysis parameters for the second "improved" contour measurement.

A knot spacing of 0.4 mm (smaller than *w*/4) was adopted on the basis of the uncertainties analysis described earlier (see *Figure 5-8*). Sensitivity studies were carried for mesh size 0.25 mm and the effect of different knot spacings was observed. It can be seen that in *Figure 5-11* that the large knot spacing failed to capture the dip in stresses at the weld centre arising from martensitic phase transformation. On the other hand, the small knot spacings more precisely captured the stress distribution at and around the weld region.

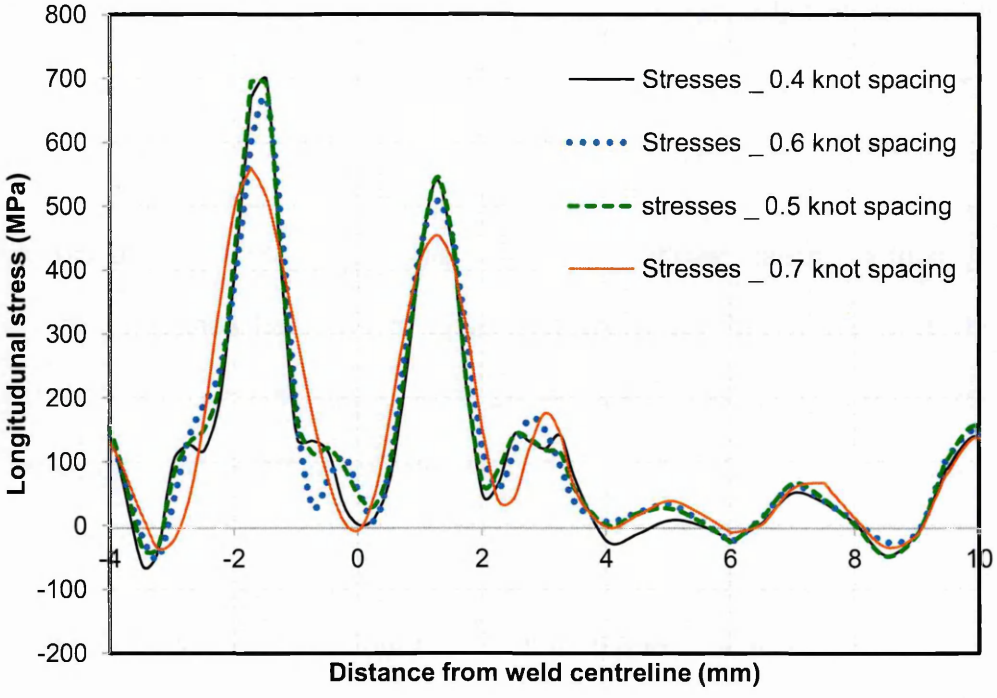

Figure 5-11: Showing the effect of change in knot spacing for element mesh size (0.25 mm).

The second contour measurement residual stresses are much closer to the neutron diffraction results as shown in *Figure 5-10* along the line 1.5 mm below the top surface, although the neutron data are sparse in the weld region of interest. The tensile stress peaks and approaching steep gradients have been successfully captured on both sides of the weld centre line. The contour method tensile stress peaks are situated 2.6 mm apart.

Sharp stress variations are also found in the contour results away from the peak tensile stress region. This is most likely to be because of over fitting of the surface displacement data away from the weld region. This problem can be resolved by controlling the knot spacing along the cut length. Finer knot spacing can be used

for a highly concentrated stress region with a short residual stress length-scale and for the rest of the cut length relatively coarser knot spacing can be used where the wavelength of this stress field is much larger.

The new contour stress results within the weld region and HAZ are closely aligned with the neutron diffraction results except at the weld centre where the contour measurement indicates a dip to zero stress. This reduction is plausible owing to martensitic solid state face transformation during the weld fusion zone cooling process (163,164).

The differences in the location and magnitude of both the tensile stress peaks in the new contour method results and neutron diffraction results are mainly because both the methods are executed using different gauge sizes. The neutron diffraction measurements were conducted using (1 x 1 x 1) mm gauge size. For the contour method it can be argued that the first order finite element mesh size, *s*, represents the gauge size providing an appropriate knot size has been used with sufficient measurement density. Thus, the new contour measurement had an effective "gauge area" of 0.25 mm and therefore this captured the stress field near to the weld more precisely.

5.3 Case study 2: dissimilar metal electron beam welded plate

In this second case study, contour residual stress measurements were conducted on an EB dissimilar metal weld joining AISI Type 316LN stainless steel and P91 modified 9Cr-1Mo steel as shown in *Figure 5-12*. The test component was supplied by the Indira Gandhi Centre for Atomic Research (IGCAR), India, in

the as-welded condition. The results of this study show how the contour method can be magnificently applied to map longitudinal residual stresses across a dissimilar metal weld with high spatial resolution.

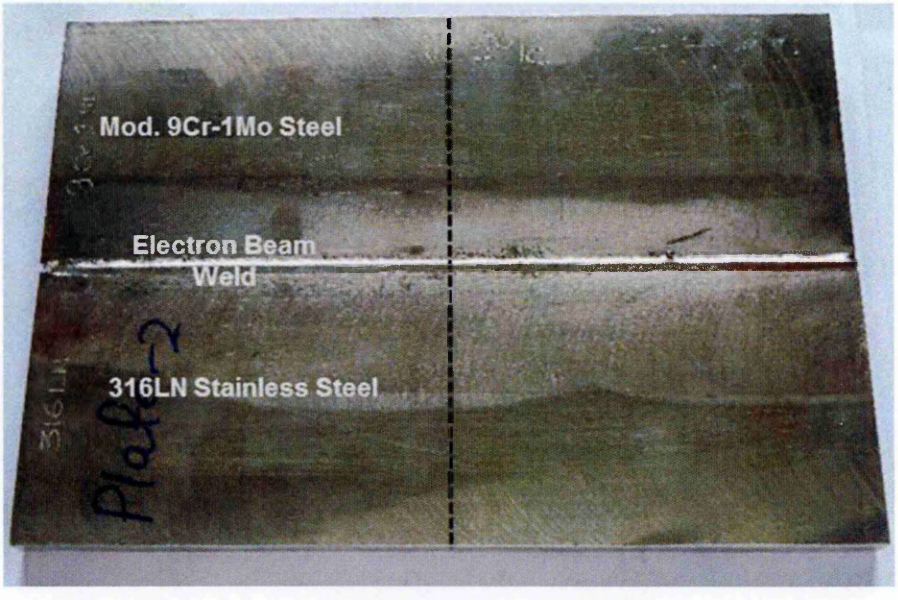

Figure 5-12: Photograph illustrates the P91:316LN EB welded plate.

5.3.1 Specimen details

The test component used for this study joined two dissimilar metals, an austenitic stainless steel (AISI Type 316 LN) to a ferritic-martensitic steel (modified 9Cr-1Mo P91), using EB welding with no filler material. The square butt joint configuration used for the EB welded plate is illustrated in *Figure 5-13*. The recorded welding parameters are given in Table 5-6. The test component had final dimensions of 250 mm long, 155 mm wide and 11 mm thick in the as-welded condition.

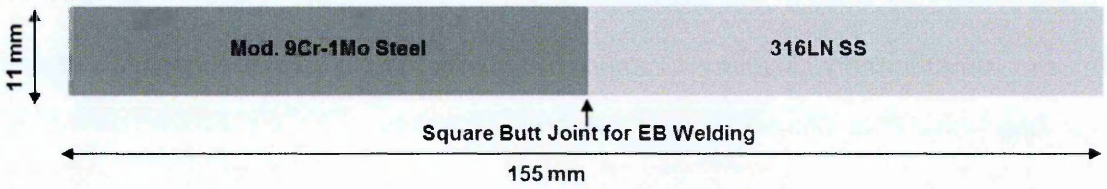

Figure 5-13: The electron beam weld joint configuration for the P91:316LN plate.

Welding Parameters	
Beam current (mA)	48
Gun voltage (kV)	120
Travel speed (mm/min)	500

Table 5-6: The recorded welding parameters used for the P91:316LN plate.

5.3.2 Contour measurement

Wire EDM cutting

The cut was performed along a transverse plane at mid-length of the plate to measure the distribution of longitudinal (welding direction) residual stress as shown in *Figure 5-12*. The stress distribution was expected to vary in magnitude over a length-scale of a few millimetres giving very sharp stress gradients. Therefore, the following approach to cutting the component was implemented. First, 5 mm wide by 3 mm thick sacrificial carbon steel layers were attached to the top and bottom faces of the plate using conductive adhesive along the plane of the cut to protect the cut faces from unintended WEDM cutting artefacts (143), see *Figure 5-14*. Secondly, a 3 mm diameter small hole was drilled at 20 mm from the edge of the plate to start the WEDM cut. This provides an embedded cutting

configuration and self-restraint during cutting (116), see *Figure 5-14*. Third, a 50 microns diameter wire was used for the WEDM cut in order to achieve a surface finish finer than for the Case 1 EB weld study. The intention here was to reduce "noise" in the surface deformation data by achieving a better surface finish (lower roughness) and thereby improve the spatial resolution of the stress measurement. After WEDM cutting the test component was removed immediately from the WEDM bath to minimise the risk of corrosion. *Figure 5-15* shows the WEDM cut surfaces for the P91:316SS electron beam welded plate and marks various undesirable surface topographic features that resulted from cutting problems with the fine wire size.

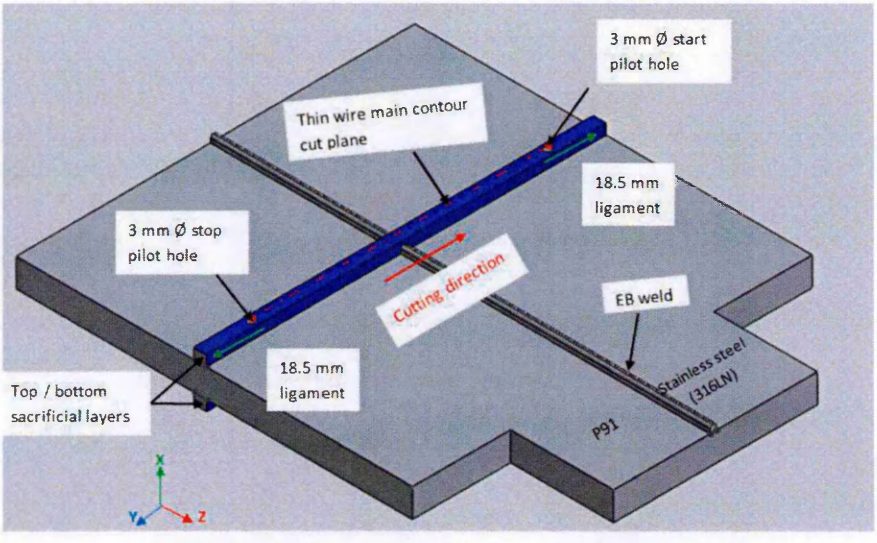

Figure 5-14: Schematic drawing of the P91:316SS electron beam welded plate (250 mm x 155 mm x 11 mm) showing the embedded cutting configuration using start and end pilot holes and cutting direction, with protective strips attached at the plane to be cut (note length reduced to 194 mm).

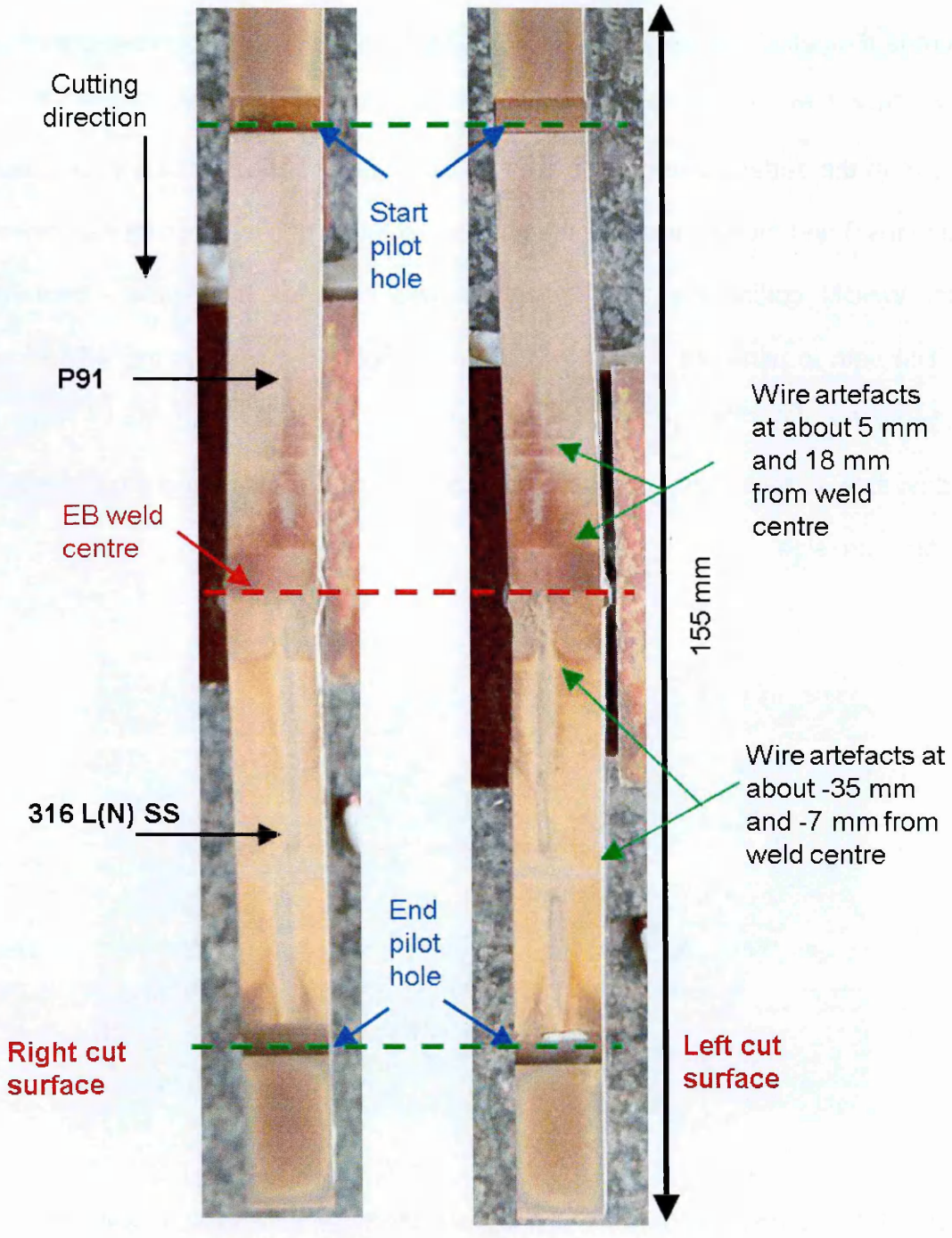

Figure 5-15: Photograph showing the WEDM cut surfaces for the P91:316SS electron beam welded plate.

Surface contour measurement

The profiles of both the cut parts were measured using a Mitutoyo Crysta plus 547 CMM with a 1 mm diameter Renishaw PH10M touch trigger probe. A finer probe size and measurement pitch of 0.125 mm was used, to try to capture detail in the expected short length-scale of the surface displacement variations.

Data analysis and finite element analysis

The measured surface deformation contour data were processed using standard contour analysis routines coded in MATLAB 7.10, as given in (39,130). *Figure 5-16* shows a map of the averaged surface displacement measurements across the transverse cut plane for the plate. The maximum peak to valley deformation is about 35 μm in the region of the weld.

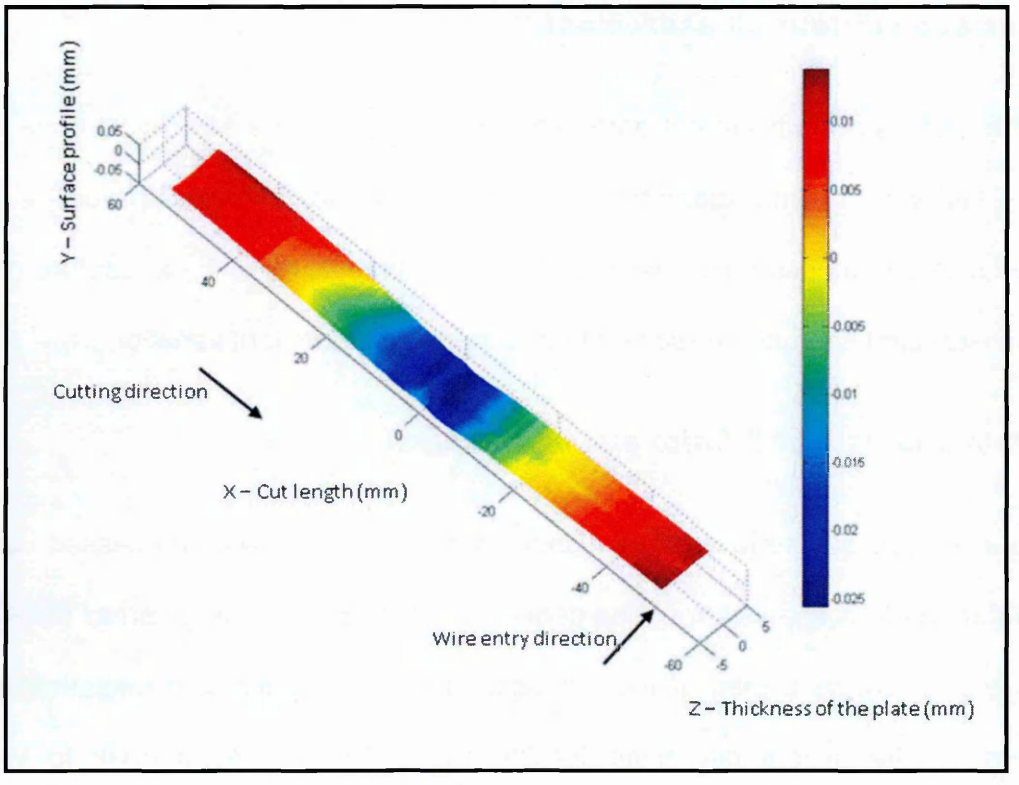

Figure 5-16: Map of the averaged surface displacement measurements across the transverse cut plane for the P91:316SS electron beam welded plate.

Then, the next step is to smooth the deformation data by fitting cubic spline functions, with suitable knot spacing. The criteria developed in chapter 4 were applied to estimate the suitable knot spacing (k) and finite element mesh size (s). The case study described in section 5.2 for an EB weld in a 9 mm thick P91 plate shows how the EB welding process forms a very narrow weld fusion and heat affected zone, and introduces residual stresses with a ~3 mm peak to peak wavelength across the weld centre line. The Case 2 study test component is made from the same material (on one side), has a similar thickness (11 mm) and is also welded using a similar EB welding process. Therefore, the minimum residual stress wavelength (w) might be expected to be of the order ~ 3 mm. Applying the

simplistic criteria developed in chapter 4, and successfully used for the Case 1 study, an initial knot spacing $k \leq 0.75\ mm$ $(k \leq w/4)$ and FE mesh size $s \leq 0.25\ mm$ $(s \leq w/12)$ was chosen.

The knot spacing was then optimised by considering a range of spacings from 0.9 mm to 0.4 mm with 0.1 mm increment.

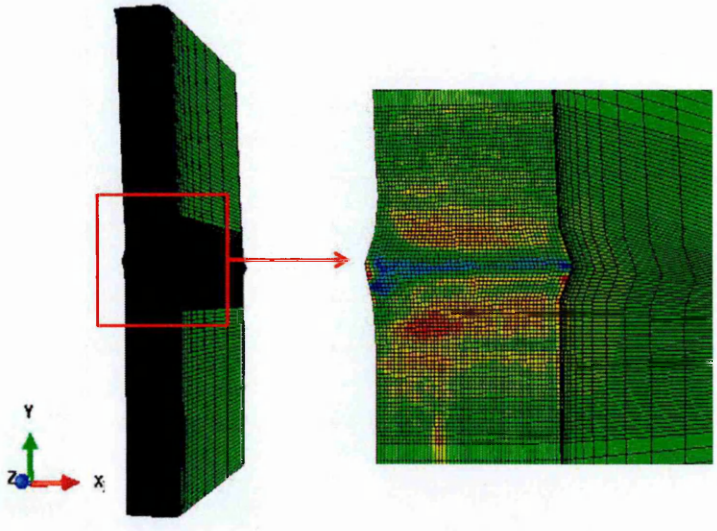

Figure 5-17: Mesh used for the P91:316 SS welded plate with close up view.

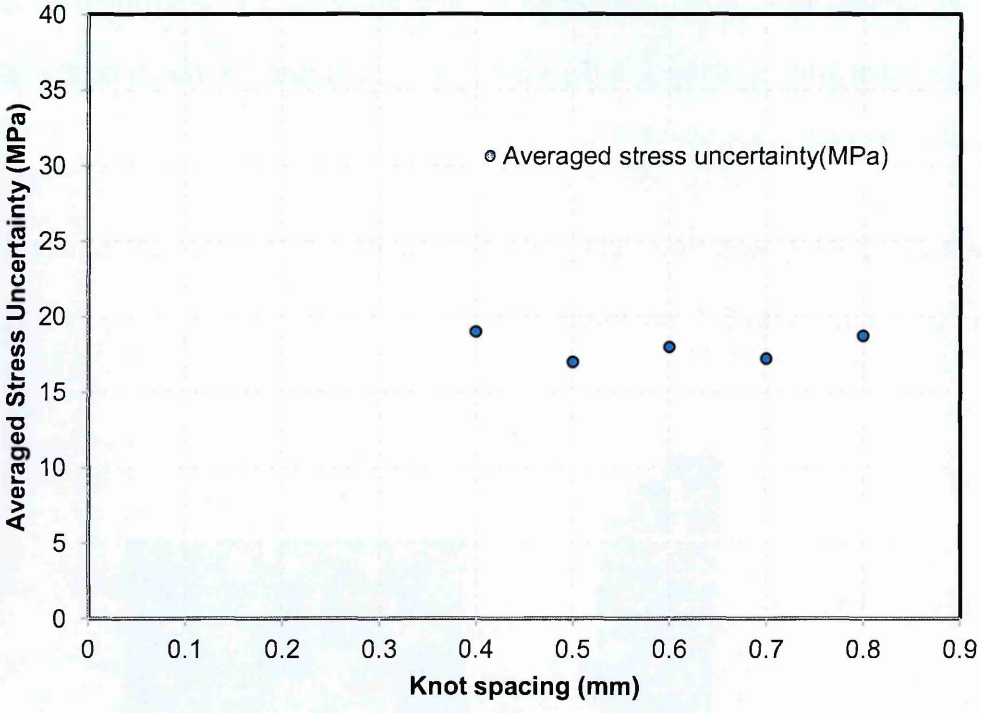

Figure 5-18: The averaged uncertainty in calculated stresses versus knot spacing for the P91:316 SS EB welded plate.

Stresses for each knot spacing were calculated with a FE mesh size, s = 0.25 mm as shown in *Figure 5-17*. The same material properties were applied for the austenitic stainless steel and the ferritic-martensitic steel to avoid complexities during the analysis (that is E = 210 GPa and $\vartheta = 0.3$). The trend in averaged uncertainty for these calculated stresses (130) is then examined, see *Figure 5-18*. The variation in uncertainty across the knot spacing range examined was small. A 0.5 mm knot spacing was chosen as this gave a minimum value of averaged uncertainty of about 17 MPa.

Finally, the processed deformation contour data were applied as surface boundary conditions in a linear elastic finite element analysis of the cut

component. However, the deformation data of the cut length beyond the pilot holes were discarded in order to reduce the cut length. Significant levels of residual stress associated with the electron beam weld were judged not extend this far. The material properties (E = 210 GPa and $\vartheta = 0.3$ and E = 180 GPa and $\vartheta = 0.3$) were used for ferritic P91 material and 316 L(N) stainless steel respectively for the final FE analysis. The cut surface was meshed with 0.25 mm × 0.25 mm linear hexahedral elements (ABAQUS type C3D8R) 20 mm across and adjacent to the weld region. Finally, the elastic FE analysis was performed as explained in section 5.2.2 of chapter 5 to determine the residual stress distribution.

A map of the longitudinal residual stress measured is presented in *Figure 5-19* and a line profile at 5.5 mm below the top surface of the plate is shown in *Figure* 5-20. The line profile clearly shows how cutting artefacts can influence the results when a fine length-scale analysis is used.

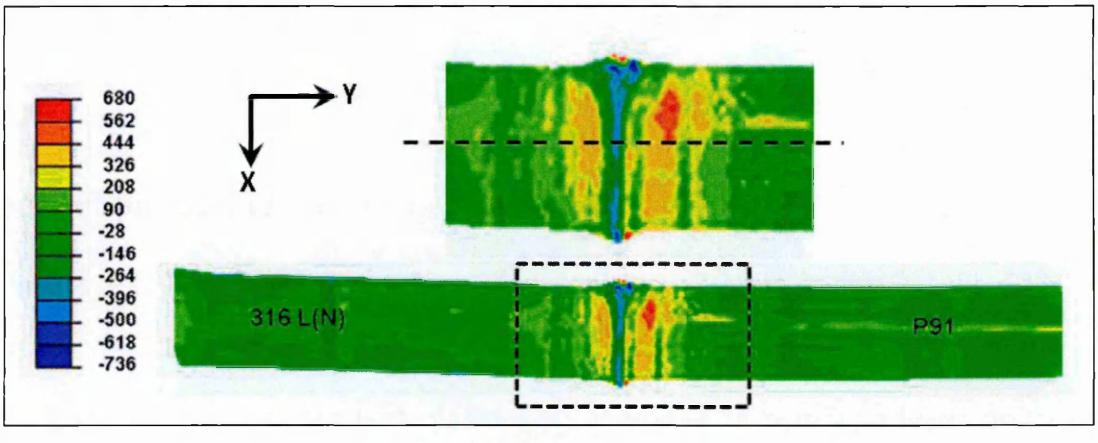

Figure 5-19: Map of the measured residual stresses for the P91:316LN SS electron beam welded plate (units in MPa).

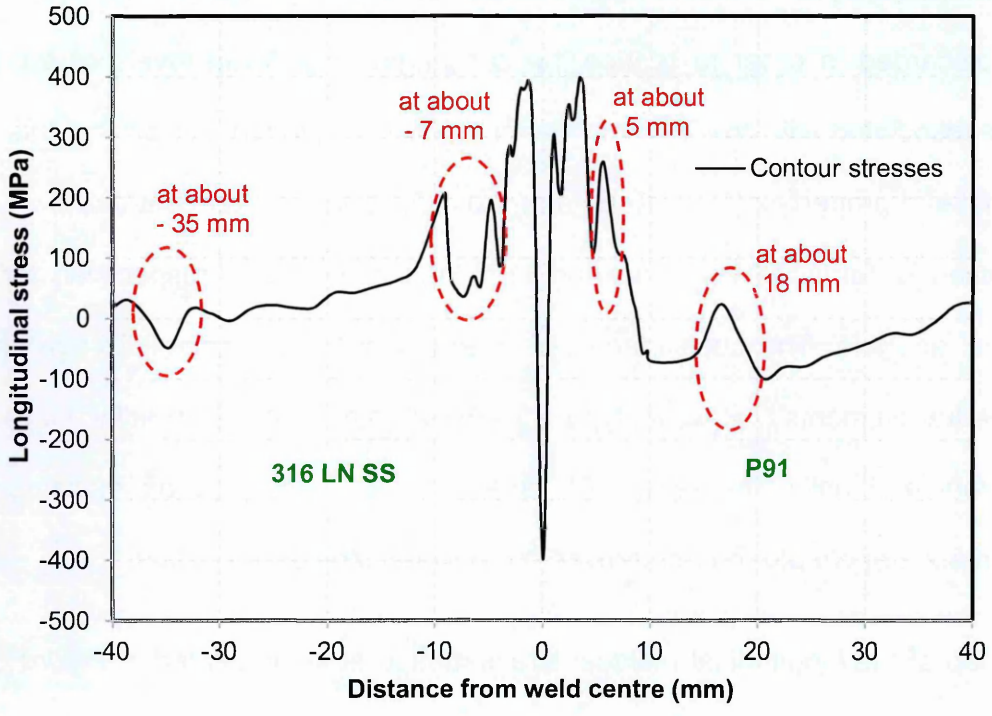

Figure 5-20: Residual stress line profile across the P91:316 SS weld at mid-thickness 5.5 mm below from the top face of the plate. The regions of influence of the cutting artefacts are also marked.

5.3.3 Other measurement results

Neutron diffraction (ND) measurements were conducted to measure residual stresses in the mid-plane of the dissimilar metals EB welded plate by the University of Bristol (165) at the ENGIN-X instrument. These preliminary neutron diffraction results (shown in *Figure 5-21)* indicate that the residual stresses are compressive at the weld centre line (- 442 MPa) and rise rapidly to tension within the HAZ on either side of the welded joint to an apparent magnitude of about 881 MPa at -0.5 mm on the 316L(N) stainless steel side and about 481 MPa at 2.5 mm on the modified 9Cr-1Mo steel side of the weld centre line. However, there are

significant uncertainties associated with the data analysis for the neutron diffraction measurements in the weld region where the 316L(N) stainless steel and the modified 9Cr-1Mo steel materials were mixed together.

Incremental centre-hole drilling (ICHD) measurements were also conducted to measure residual stresses of the dissimilar metals EB welded plate by the University of Bristol (165). In *Figure 5-21* the average of the ICHD measurement results are compared with the neutron diffraction and contour results.

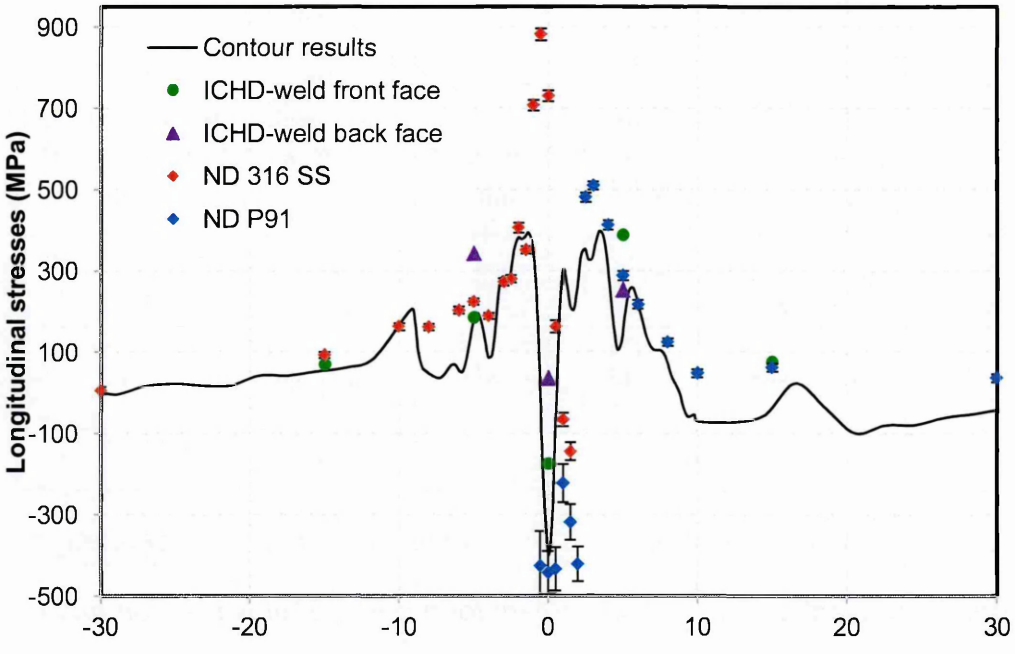

Figure 5-21: Contour method residual stress measurement compared with neutron diffraction and iCHD measurements from (165) at mid thickness 5.5 mm below the top face of the plate.

5.3.4 Results and discussion for the dissimilar metal EB welded plate

The P91:316LN EB welded plate was used to measure the distribution of longitudinal (welding direction) residual stress using the new contour measurement approach. The P91:316LN electron beam welded joint forms a narrow fusion zone and introduces short length scale residual stresses with steep stress gradients. A smaller diameter of WEDM wire (50 μm) was chosen to perform the contour cut in order to achieve a better surface roughness and the deformation sampling and analysis criteria developed in chapter 4 implemented as summarised in Table 5-7.

Case	Cutting wire Diameter (mm)	Deformation spacing, *d* (mm)	Knot spacing, *k* (mm)	FE mesh size, *s* (mm)	Residual stress wavelength, *w* (mm)
Improved Contour	0.05	0.125	0.5	0.25	3
Criteria	0.25	$<< k$, $\leq w/12$	$\leq w/4$	$\geq d$, $\leq w/12$	w
Met	Yes	Yes	Yes	Yes	-

Table 5-7: Cutting conditions, deformation collection and data analysis parameters for the second "improved" contour measurement for the P91:316LN electron beam welded plate.

Slight variations were observed in the calculated stresses using different knot spacings for a 0.25 mm mesh size (as shown in *Figure 5-22*). As a result, a small variation in stress uncertainty was observed across the knot spacing range as shown in *Figure 5-18*. This is likely to be because a better surface finish was

achieved as a result of using a smaller wire diameter to perform the contour cut. A knot spacing of 0.5 mm (smaller than $w/4$) was adopted to calculate the final stress results on the basis of the marginally smaller averaged stress uncertainty as shown in *Figure 5-18*.

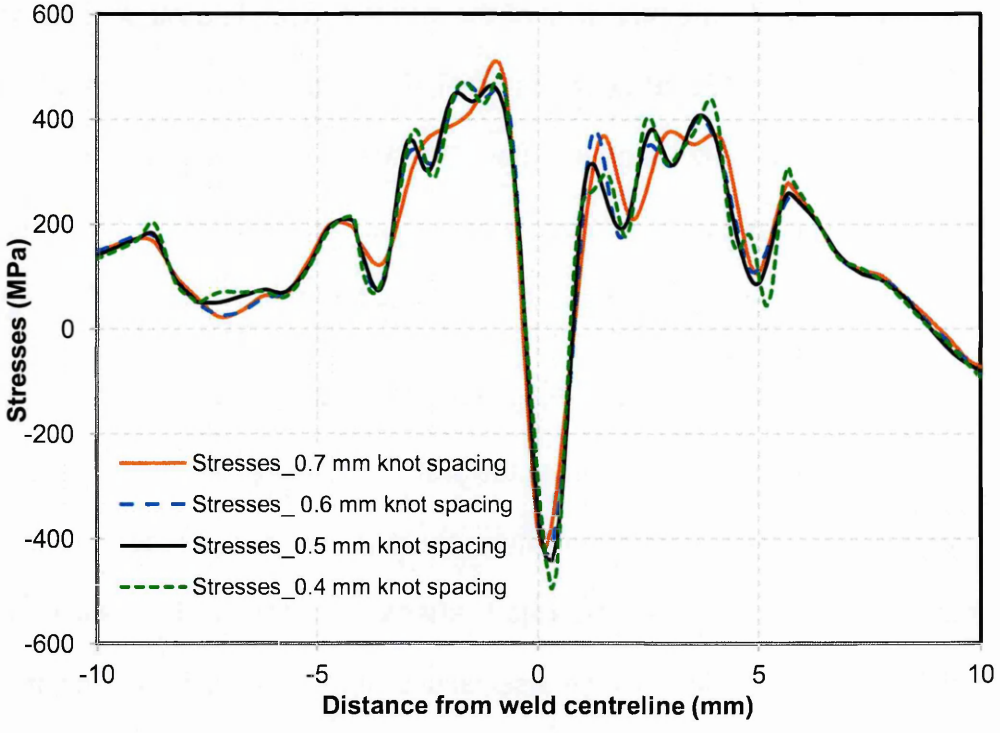

Figure 5-22: Showing the effect of change in knot spacing for 0.25 mm element mesh size.

Two high tensile stress regions are present in the measured stress field (see *Figure 5-19*) flanking the weld centre line. But the regions have several spikes potentially associated with the quality of the cut surface. The line profile of *Figure* 5-20 shows how steep stress gradients on both sides of the weld centre line have been resolved by the contour measurement. The maximum tensile stress peaks are situated just 2.3 mm apart within the weld region. To the author's knowledge

this is a shorter residual stress length scale than previously measured by the contour method.

The line profile from the contour measurement also shows that the residual stresses are compressive at the weld centre line (- 400 MPa) rising rapidly to tension within the HAZ on either side of the welded joint. The magnitude of the tensile stresses in the 316L(N) stainless steel side of the weld is about 400 MPa and in the modified 9Cr-1Mo steel is about 300 MPa. High compressive residual stresses in the weld region are most likely to be due to phase transformation effects counteracting tensile stresses introduced by thermal shrinkage (163,164).

The line profile of stresses also indicates sharp stress variations across the weld region, - 10 mm to + 10 mm from the weld centre line. A thin wire diameter (50 microns) was used to perform the contour cut but surface roughness measurements could not be performed afterwards (the plate was required elsewhere). However, surface roughness results are available for a similar plate on which a contour cut was performed using same wire diameter on the same wire EDM. The results indicate an averaged *Sa* value of less than of 1 µm between the pilot holes using the 50 micron wire diameter. As expected the thinner wire diameter gave a better surface roughness. However, the choice of the thinner wire diameter increases the risk of the wire breakage and other cutting artefacts. During the cutting the WEDM wire broke at four different locations along the cut length and formed marks on both the cut parts as shown *Figure 5-15*. These cutting artefacts are symmetric in nature and they are not canceled out by averaging the deformation data of both the cut parts (see in *Figure 5-16*).

Therefore, the cutting effects associated with these lines and marks are found in the resulting stress map (see in *Figure 5-19*) at about 5 mm, 18 mm, -7 mm and -35 mm from the weld centre line. The sharp stress variations associated with these cutting effects can also be seen in the stress line profile in *Figure 5-20*. This study demonstrates that a smaller wire diameter such as 50 μm gives better surface finish compared to the 0.15 mm wire diameter but at the expense of increasing cutting artefacts. As Case Study 1 managed to resolve a residual stress wavelength of the order of 3 mm with a 0.15 mm wire diameter, it might be argued that use of a smaller diameter wire is not necessary.

The neutron diffraction results discussed earlier in section 5.3.3 also show high compressive stress values within weld and tensile peaks in the adjacent HAZs. But these stresses may not reflect the actual bulk residual stress levels present as there is a mixture of materials in the weld region. Significant uncertainties were reported in the stress results within the weld region because of difficulties in determining reliable stress free lattice parameter reference measurements and dealing with the mixture of materials (165). The incremental centre-hole drilling (ICHD) measurements and neutron diffraction measurements 3 mm or more away from the weld centre line are in reasonable agreement with the contour results. Also both the contour and neutron diffraction measurements indicate deep compression at the weld centre line. Thus, the new contour method measurement approach has been successfully applied to map short length scale longitudinal residual stresses in the dissimilar metal EB welded plate.

5.4 Case study 3: stainless steel clad ferritic plate

In this third case study, manufacturing residual stresses in a thick section ferritic steel plate clad with several layers of austenitic stainless steel weld metal (see *Figure 5-23*) are measured using the contour method. Peak tensile residual stresses are known to normally occur in the cladding layer of this type of component (89). But there is also a possibility of phase transformation in the ferritic base material adjacent to the clad interface that can result in sharp variations of residual stresses within a short length scale and this can contribute to the development of under clad cracking (45). This study aimed to capture residual stress variations from these local phase transformation effects by implementing the new contour measurement approach developed in chapter 4. The accuracy of the new contour measurement results presented here is assessed by comparing them with published data for the same component obtained from a previous conventional contour method measurement conducted by the author (89), and incremental deep hole drilling measurements (90) and neutron diffraction measurements performed elsewhere (95).

Figure 5-23: Photograph of the clad ferritic steel plate.

5.4.1 Specimen details

The clad test component for the present study was supplied by Rolls-Royce. The test specimen was fabricated from a 300 mm long by 180 mm wide by 50 mm thick ferritic base plate of SA508 Grade 3 steel. Three layers (totalling ~ 9 mm thick) of austenitic stainless steel weld metal cladding were deposited on the top surface as shown in *Figure 5-24*. The first clad layer was 309L stainless steel to minimise dilution effects and the final two layers were 308L stainless steel. A mechanical hot wire TIG welding clad process was used with stringer beads having an approximately 50% overlap. The welding parameters recorded are given in Table 5-8.

The welding procedure for the clad plate specimen included a hydrogen bake-out phase after completion of welding. The specimen was held at the pre-heat

temperature of 170 ºC for a minimum of four hours. This procedure was done to minimise the risk of hydrogen cracking in the heat affected zone. There was no post weld heat treatment applied for the specimen, thus the specimen supplied for measurement was in the as-welded condition.

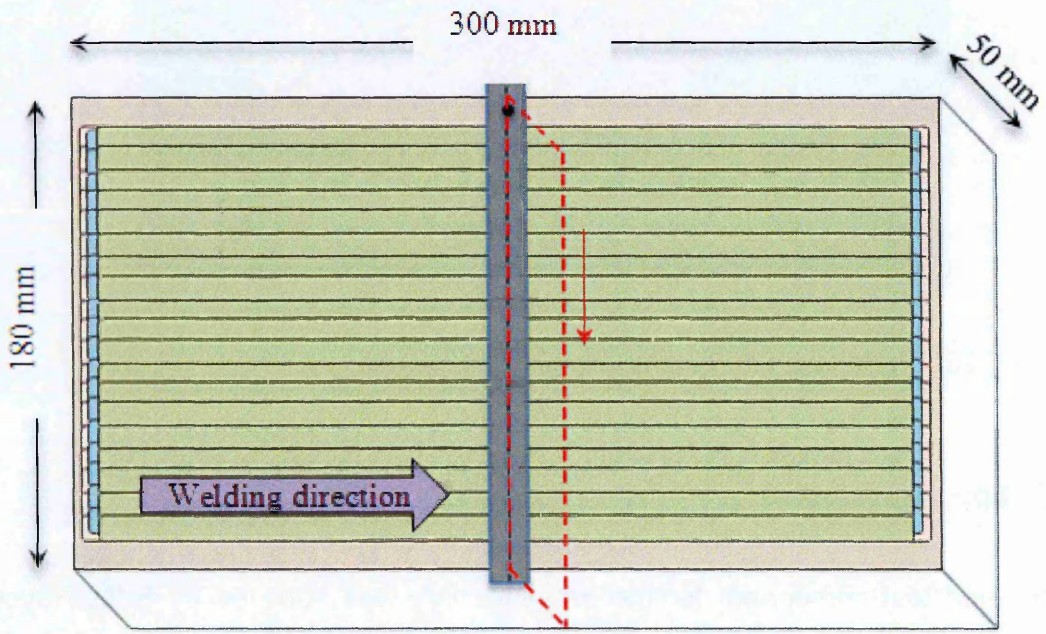

Figure 5-24: Schematic image of the clad plate showing the dimensions, direction of clad welding, cross-section of contour method measurement (red chained line), pilot start hole for WEDM cut and sacrificial strip applied to the clad surface.

		Layer 1	Layer 2	Layer 3
Material of the band electrode		Type 309L	Type 308L	Type 308L
Current (A)	**Primary**	315	315	315
	Background	180	180	180
Voltage (V)		12	12	12
Inter pass Temperature (ºC)		250	250	250

Pre-heat (°C)	170	170	170
Travel speed (mm/min)	150	150	150
Number of passes	19	19	19

Table 5-8: Clad welding conditions (95).

5.4.2 Wire EDM cutting

In order to determine the longitudinal (welding direction) stresses, a contour cut was performed along a transverse plane at mid-length of the plate, that is in a direction perpendicular to the weld beads. Before specimen cutting, a 1.5 mm diameter pilot hole was introduced 5 mm from the edge of the plate in the plane of the cut. This provided self-restraint and edge clamping of the plate during cutting (116). Finger clamping tools were used to provide support and to stop any bulk movement of the test component on the WEDM bed table. An Agie Charmilles FI 440 CCS WEDM was used to perform the cut. The running of cutting trials was impossible for this sample case because there was no stress free material available exactly similar to the clad specimen. Therefore, cutting parameters were chosen based on past experience. The first attempt at cutting was carried out using 0.15 mm diameter brass wire. Stable cutting conditions for this component could not be achieved with this wire size resulting in wire breakage at the start of the cut. Therefore, a thicker wire (0.25 mm diameter brass wire) was chosen to perform the cut. To avoid wire entry, wire exit, and the cut start and end effects, sacrificial layers were placed around the perimeter of the intended cut section (143). These were of carbon steel having a cross-section of 5 mm x 10 mm (see *Figure 5-25*). They were placed at the top and bottom of the

plate along the plane of the cut and at the start and end of the cut. Special consideration was given to obtain a close fit between the wavy clad surface and the attached layer, by using silver-loaded epoxy resin to fill the gaps.

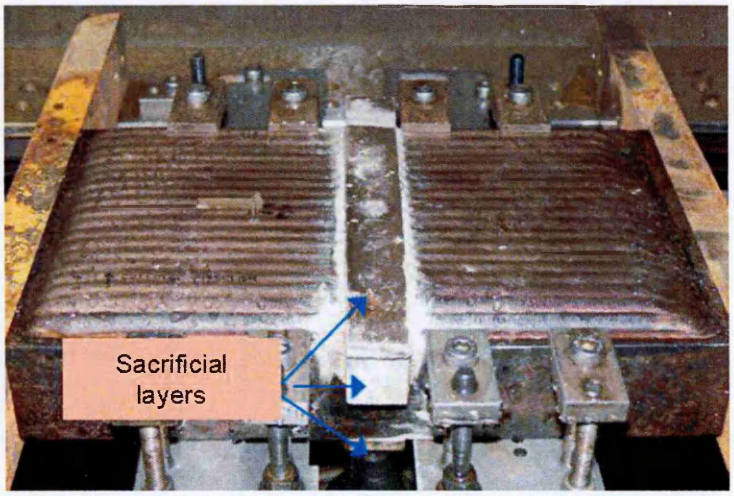

Figure 5-25: The clad plate mounted on the WEDM table showing sacrificial plates attached to the component and the clamping arrangement.

The clad specimen was a combination of two different materials; therefore, to avoid introducing thermal expansion errors, the deformation of the cut surface was measured in a temperature controlled room, held at the cutting bath temperature of 20 ºC. After completion of the WEDM cutting, the cut surfaces were inspected by eye for any obvious cutting artefacts and the sacrificial layers were removed.

5.4.3 Surface contour measurements

During the WEDM cutting, debris, in the form of tiny particles of metal, was formed and deposited onto the cut surfaces. The thickness of the debris layer was a few microns and if left in place can affect the contour measurement. The cut

surface should be free from these dust deposits. Removal of these deposits was done using a rubber eraser (see *Figure 5-26*). The cut surfaces were measured using a hybrid laser-CMM system with fine measurement pitch, that is a 0.125 mm x 0.125 mm point spacing with 2 mm s^{-1} measuring speed. The laser CMM system comprises a Zeiss Eclipse CMM to which a Micro-Epsilon triangulating laser probe was fitted.

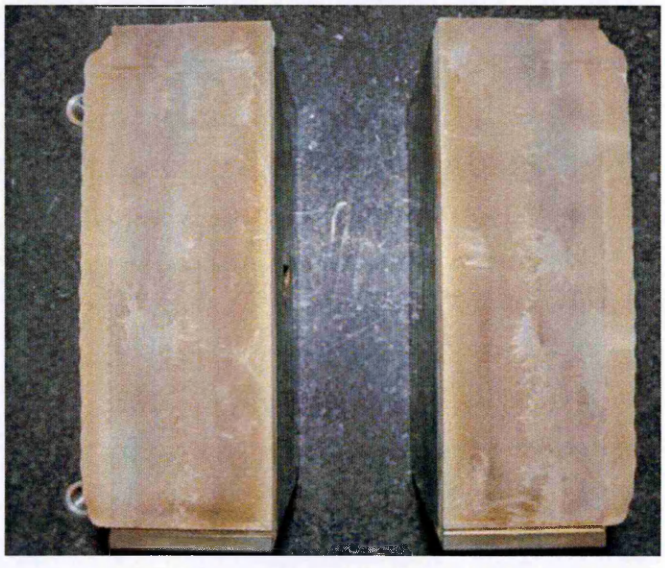

Figure 5-26: WEDM cut after cleaning with rubber eraser.

5.4.4 Conventional contour method approach for data analysis

The set of measured surface deformation data were initially analysed using a conventional data analysis approach as described in (39,130). The processed data were then fitted with cubic splines using 7 mm x 7 mm knot spacing. Residual stresses were calculated using an ABAQUS FE linear elastic analysis with a 1 mm × 1 mm linear hexahedral element (type C3D8R) mesh within the clad material and up to 10 mm below the clad interface. The rest of the plate cut face

was meshed with 3 mm × 3 mm sized elements. The material properties (E = 209 GPa and $\vartheta = 0.3$ and E = 171 GPa and $\vartheta = 0.3$) were used for ferritic base plate and stainless steel weld metal cladding, respectively.

The measured map of longitudinal residual stresses obtained using the conventional contour method data analysis approach (89) described above is shown in *Figure 5-27*. Residual stress line profile along mid thickness from bottom to top for the clad plate is shown in *Figure 5-28*. The stresses are tensile in the clad itself but rapidly reduce to compression in the ferritic base metal before rising to tension towards the bottom surface. The maximum tensile stress of 330 MPa in the clad near to the clad/parent material interface and maximum compressive stress of -250 MPa are located at approximately 50 mm and 34 mm from the bottom, respectively.

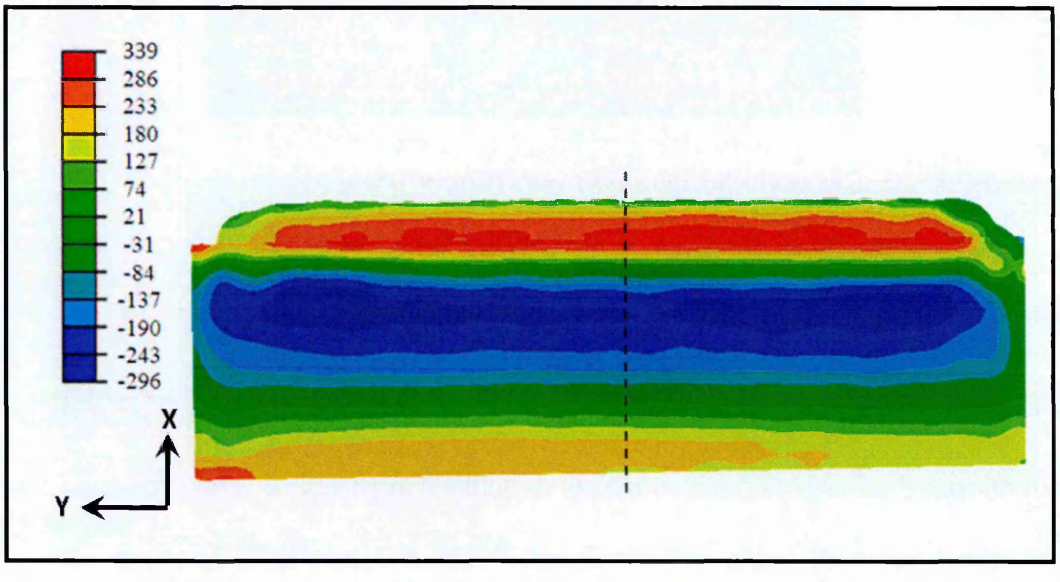

Figure 5-27: Map of the longitudinal residual stresses measured using a conventional contour method data analysis approach (89) (stresses are in MPa).

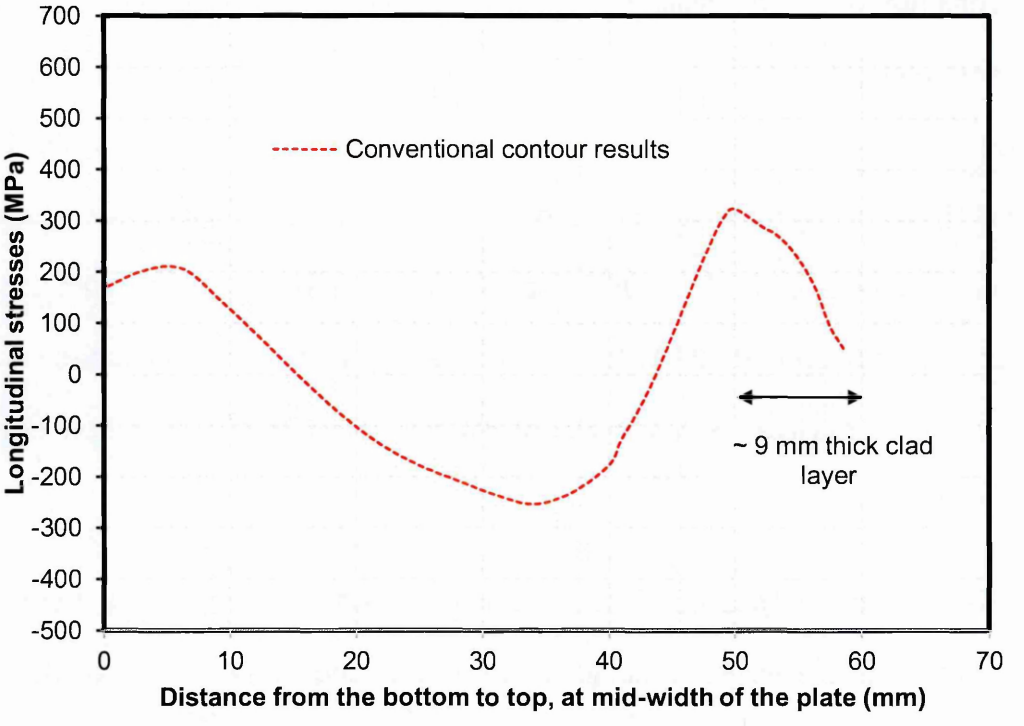

Figure 5-28: Residual stress line profile along mid thickness from bottom to top for the clad plate (89).

5.4.5 Other residual stress measurement techniques results

Neutron diffraction measurements were conducted on a nominally identical plate that was manufactured under the same conditions (90). These were carried out using a 3 mm x 3.4 mm x 5.8 mm diffracting gauge volume by researchers from Manchester University and Rolls Royce (95) at the ENGIN-X instrument at ISIS. A rectangular window was cut in the underside of the plate to reduce the beam path length and count time. The neutron diffraction results show that a tensile stress of around 400 MPa was present at the clad/parent interface and a peak compressive stress of -300 MPa within the ferritic base plate at a location of 36 mm from bottom of the plate.

Incremental deep hole drilling (iDHD) measurements were also undertaken on the same plate that was studied by neutron diffraction. The measurements were carried out at the longitudinal centre-line of the plate perpendicular to the weld beads. These measurements were performed using a 1.5 mm reference hole with a 5 mm diameter core. The iDHD measurements showed a maximum tensile residual stress of around 600 MPa at the clad/ferritic base material interface and a maximum compressive residual stress of around -200 MPa at 40 mm from bottom of the plate (90).

Finite element analysis was also performed to predict welding residual stresses in the clad plate. This FE simulation of the cladding process was carried out without considering phase transformation effects. The FE simulation predicted a tensile residual stress of around 400 MPa at the clad/ferritic base material interface and a maximum compressive residual stress of around -325 MPa to about 34.5 mm depth from bottom of the plate (90).

Figure 5-29 shows a comparison of the longitudinal residual stress distributions in the clad plate obtained by the conventional contour measurement (39), neutron diffraction, iDHD and FE techniques. The stress distribution is plotted along a line located at the 90 mm mid-width of the plate, extending from the bottom of the ferritic plate to the top of the cladding. It can be seen that the residual stress distributions from all the techniques follow a similar trend to one another. However, these profiles give no indication of any short length scale stress fluctuations in the ferritic base material adjacent to the clad interface. This is most likely to be because the inherent gauge size of the techniques used was too large. Further

investigation to capture any phase transformation effects therefore requires applying a measurement technique with a finer spatial resolution capability.

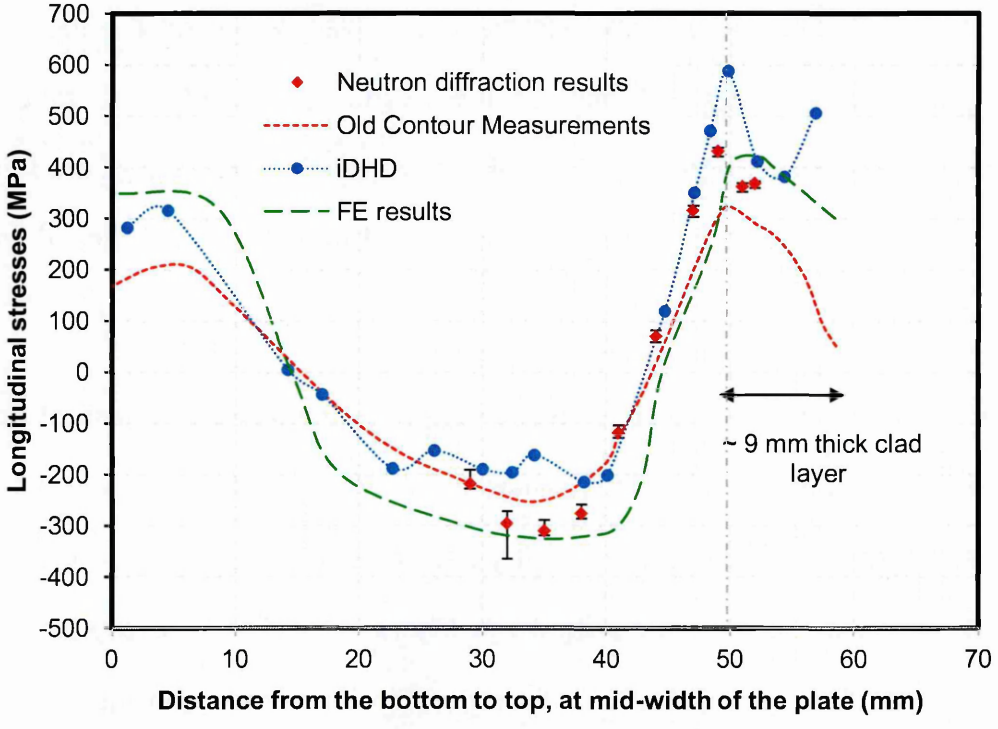

Figure 5-29: Comparison of measured and predicted residual stresses along a through-thickness line at mid-width of the clad ferritic plate.

In the next section, the surface contour deformation data were re-analysed using the developed criteria described in chapter 4 to improve the contour measurement spatial resolution.

5.4.6 New contour method approach for data analysis

The set of measured surface deformation data were re-analysed using a careful selection of data analysis parameters, as described in chapter 4. The knot spacing

and finite element mesh size for the revised analysis were based on a residual stress wavelength *(w)* estimated from a hardness measurement profile. Hardness measurements were conducted on one of the contour cut surfaces (details are given below in section 5.4.8). The hardness results show (see in *Figure 5-36*) that rapid hardness variations occurred just below the clad region (at the top of the ferritic base plate) within ~ 3 mm of the interface, probably due to phase transformation effects. Therefore, the minimum wavelength was considered to be w = 3 mm giving an initial knot spacing $k \leq 0.75\ mm$ $(k \leq w/4)$ and FE mesh size $s \leq 0.25\ mm$ $(s \leq w/12)$.

Then, the knot spacing was optimised using the uncertainty approach of Prime (130) by examining the range of spacings from 1.7 mm to 0.7 mm with 0.1 mm increment. Stresses for each knot spacing were calculated using FE analysis with a mesh size of s = 0.25 mm as shown in *Figure 5-30*. For simplicity the same material properties were used for both the ferritic base plate and the austenitic stainless steel clad portion for knot spacing optimisation. *Figure 5-31* illustrates how the minimum averaged uncertainty in the calculated stresses was found to be 28 MPa at a knot spacing of 1.4 mm.

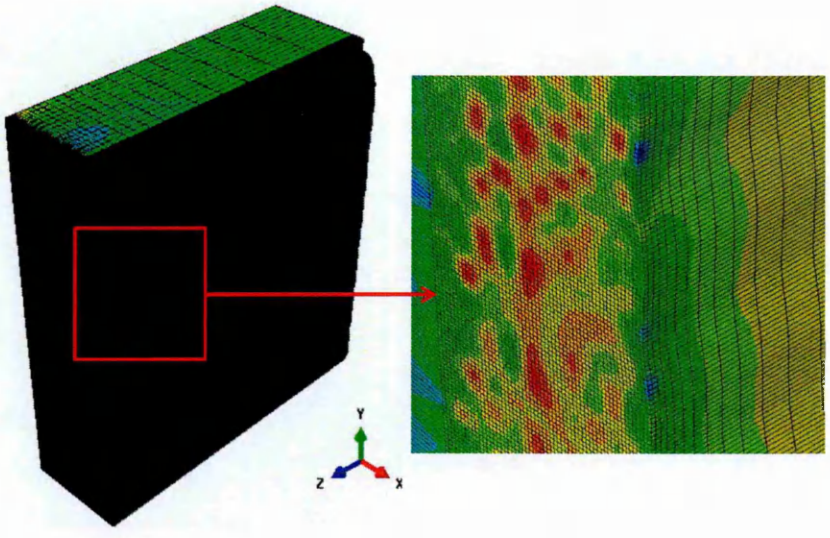

Figure 5-30: Mesh used for the clad plate with close up view.

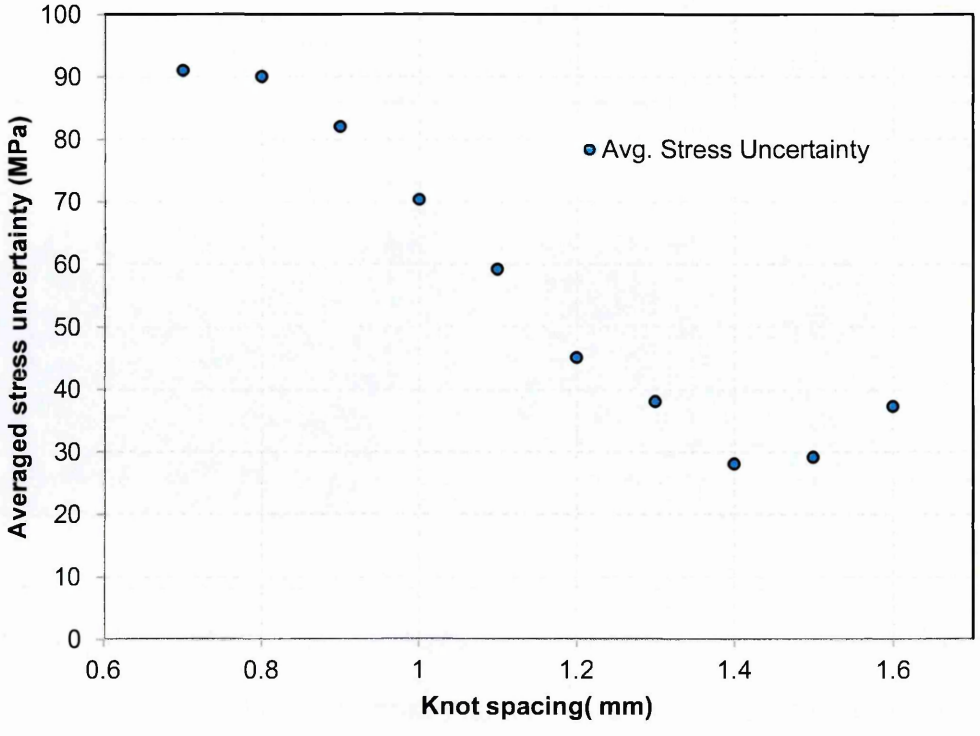

Figure 5-31: The best suitable knot spacing was determined by minimising the averaged uncertainty in the calculated stresses.

Finally, the processed deformation contour data were applied as surface boundary conditions in a linear elastic FE analysis of the cut component. The deformation data of the cut length beyond the pilot holes were determined by linear interpolation. The material properties (E = 209 GPa and $\vartheta = 0.3$ and E = 171 GPa and $\vartheta = 0.3$) were used for a ferritic material and stainless steel respectively for the final FE analysis. The cut surface was meshed with s = 0.25 mm linear hexahedral elements (type C3D8R) across and adjacent to the clad region.

A map of the measured longitudinal residual stress based on the refined analysis is presented in *Figure 5-32*. The line profile at mid-width from bottom to top of the plate is shown in *Figure 5-33*.

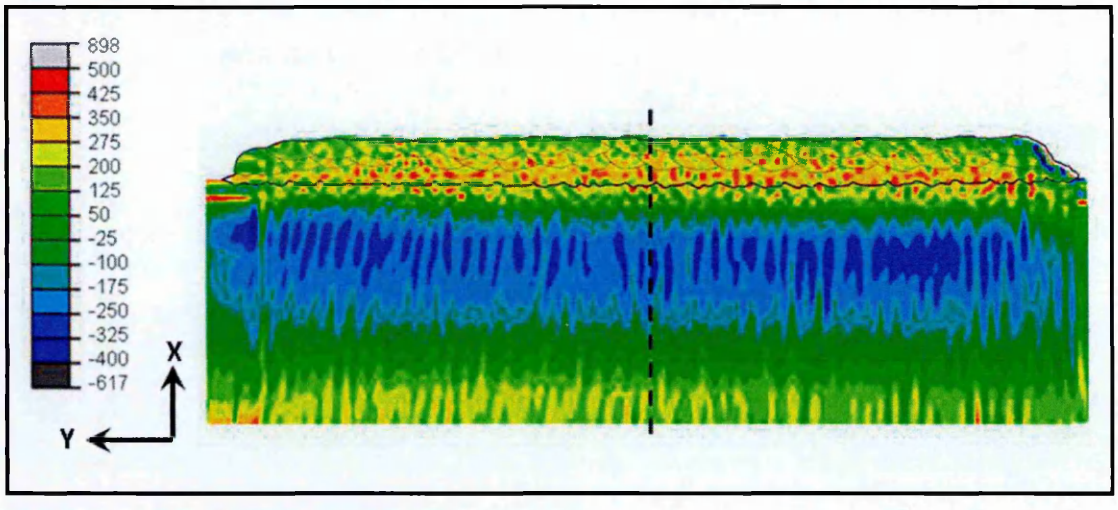

Figure 5-32: Map of measured residual stresses for the clad plate from the improved contour measurement analysis approach (units in MPa).

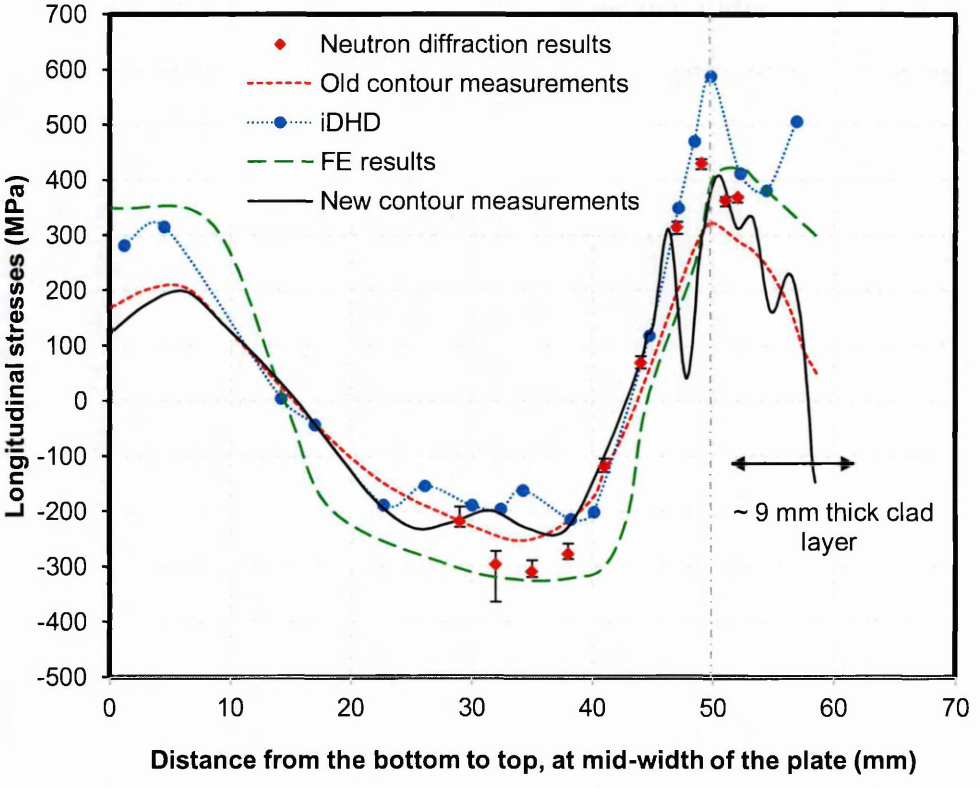

Figure 5-33: New contour method residual stress measurement compared with the old contour measurement, iDHD measurement, neutron diffraction measurements and an FE prediction for a through-thickness line at mid-width of the plate.

5.4.7 Metallography for the clad plate

Metallographic analysis was performed to observe the macrostructure of the clad plate. A slice 10 mm thick was extracted from the WEDM cut surface created for the contour cut. The slice was first ground using 500 to 4000 grit grade papers and later, mechanically polished to a 0.05 μm surface finish. Then, the austenitic stainless steel clad portion was etched with 10 % oxalic acid for 6 minutes and the ferritic portion etched with 2 % nitrite for 8 minutes. Finally the macrostructure was observed under an optical microscope and digital images were captured along the

cut face and covering different metallurgical zones that were produced as a result of the deposition of the clad layers. *Figure 5-34* illustrates the macrostructure of the clad plate.

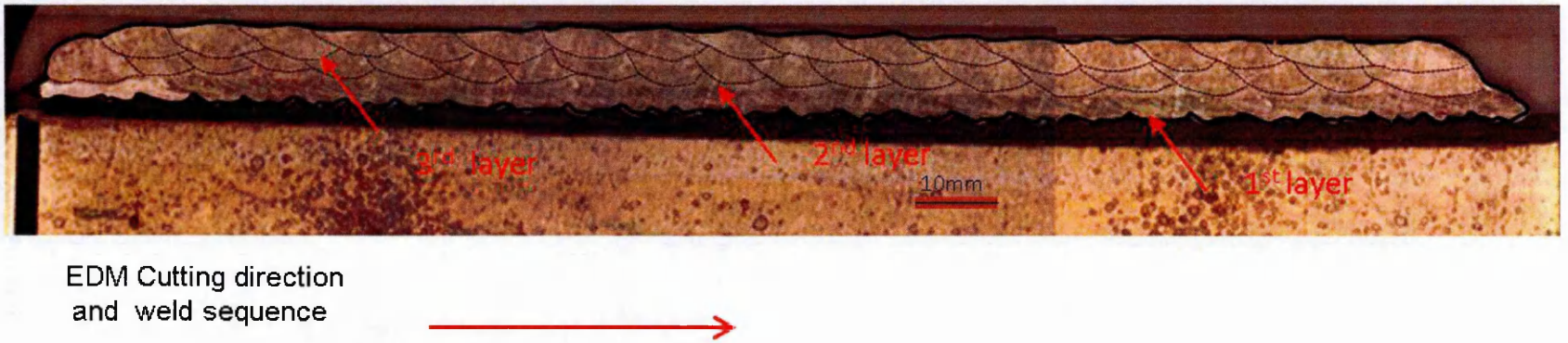

Figure 5-34: Macrograph showing the regions of three clad layers and HAZ for the clad plate.

5.4.8 Hardness testing

A hardness survey was undertaken to investigate whether the clad welding process had introduced a hardened region beneath the cladding owing to local martensitic phase transformation in the HAZ. If present such a region could characterise the length scale of associated residual stress perturbations. A Vickers hardness survey was conducted on the prepared macrograph slice using a 0.625 mm spacing with a 5 kgf load. The hardness survey was carried out at the mid-width of the cut face from the top of the clad down to the bottom of the ferritic base plate. *Figure 5-35* shows Vickers Hardness indentations from base to top of the plate, and highlighting the position of the indentation corresponding to the maximum hardness on the centre line. *Figure 5-36* illustrates the hardness profile measured.

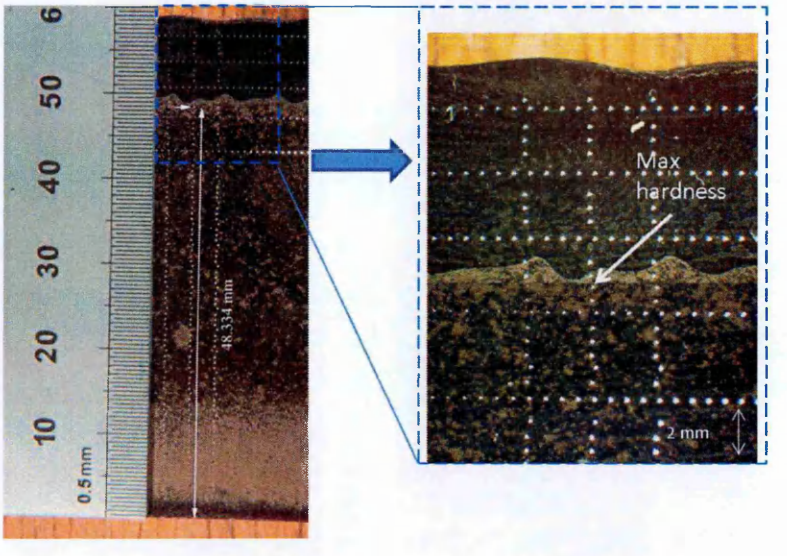

Figure 5-35: Stainless Steel Welds (clad) on SA508 Plate, shows Vickers Hardness indentations from base to top of the plate, and highlighting the position of the indentation corresponding to the maximum hardness on the centre line.

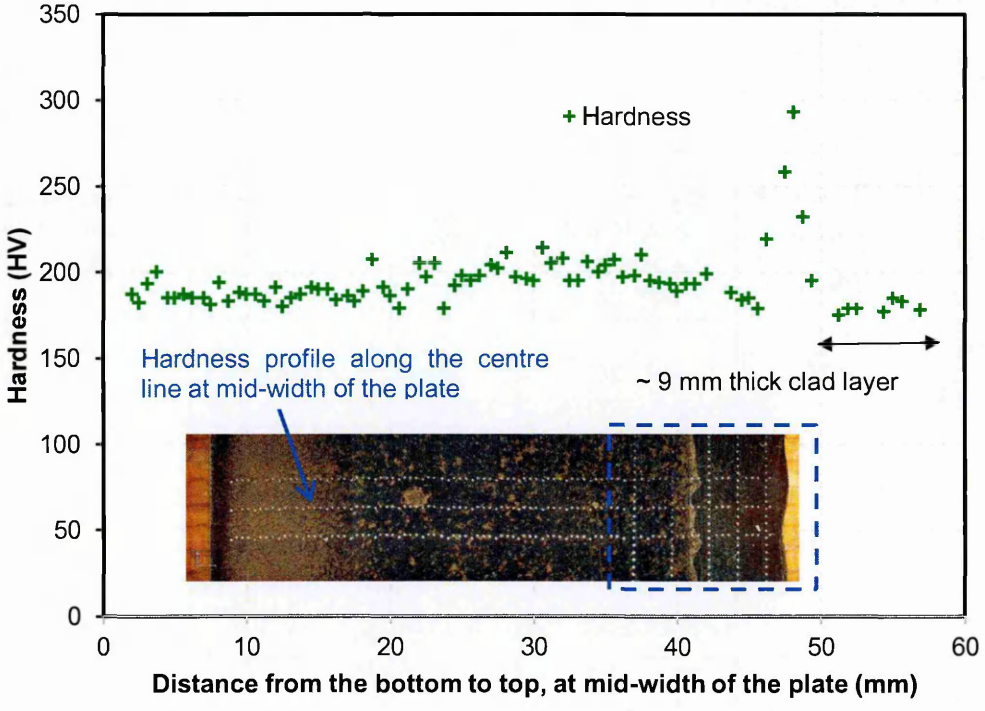

Figure 5-36: Hardness measurement profile from bottom of the plate to the top of the clad layer at mid-width of the component.

5.4.9 Results and discussion for the clad plate

The conventional contour method captured the long length scale residual stress field but, like the other measurement methods, was unable to pick up information of any local stress fluctuations in the ferritic base material adjacent to the clad interface, see *Figure 5-29.*

The improved contour stress measurement results were calculated using the criteria developed in chapter 4 for data analysis parameters. Table 5-9 summarises the cutting conditions, deformation collection and data analysis

parameters used for the old contour results and improved contour results, and compares them with the guidelines presented in chapter 4.

Case	Cutting wire Diameter (mm)	Deformation spacing, *d* (mm)	Knot spacing, *k* (mm)	FE mesh size, *s* (mm)	Residual stress wavelength, *w* (mm)
Old contour measurement	0.25	0.125	7	1	-
Criteria	0.25	<< *k*, ≤ *w*/12	≤ *w*/4	≥ *d*, ≤ *w*/12	*w*
Met (old measurement)	Yes	No	No	No	-
Required	0.25	<< 0.75, ≤ 0.25	≤ 0.75	≤ 0.25	3
Improved contour measurement	0.25	0.125	1.4	0.25	3
Met (improved measurement)	Yes	Yes	No	Yes	-

Table 5-9: Cutting conditions, deformation collection and data analysis parameters for the old and second "improved" contour measurement for the clad plate.

The sensitivity studies carried out examining the effect of different knot spacings (with a mesh size of 0.25 mm) are illustrated in *Figure 5-37.* It is seen that the small knot spacings over fitted the contour deformation data compared to the large knot spacing. A knot spacing of 1.4 mm was adopted on the basis of the uncertainties analysis (results are shown in *Figure 5-31*).

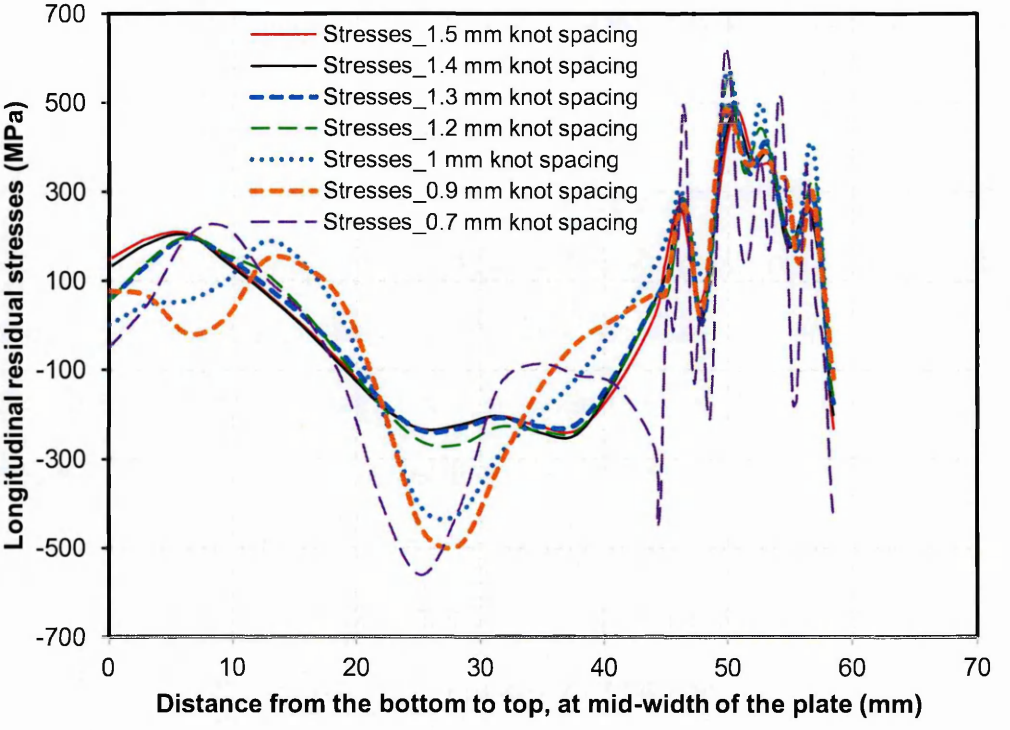

Figure 5-37: Showing the effect of change in knot spacing for element mesh size (s = 0.25 mm).

In this study, a knot spacing of k = 1.4 mm (that is $k \geq w/4$) gave a minimum averaged stress uncertainty value. For the clad plate, the contour cut was performed using a 0.25 mm wire diameter. Although this limited the cut surface finish quality, short length scale stress variations of the order of 3 mm were resolved. However, small knot spacings over fitted the surface data giving large average stress uncertainties. This perhaps demonstrates the importance of trying to achieve a good contour surface finish when applying the criteria given in chapter 4.

The new contour measurement on the clad plate exhibits a significant improvement in the residual stress measurement resolution compared to the old contour results, for example compare the new contour measurement results with

the old contour method and other measurement techniques results shown in *Figure 5-33.*

A map of the measured longitudinal residual stress using the new contour approach is shown in *Figure 5-32.* Longitudinal stresses normal to the cut plane (at mid length of the clad plate) are tensile in the cladding region. The macrograph for the clad portion confirms the presence of the three clad layers in *Figure 5-34.* In the new contour measurement results three tensile stress peaks appear to correspond with three weld beads with in the clad region. This is in contrast to the conventional contour measurement and other measurement techniques results shown in *Figure 5-29* . The highest value of tensile stresses is reported within the first clad layer (just above the ferritic base plate) and the stress magnitude reduces towards approaching the last layer (at the top) of the plate. The maximum tensile stress peak with the magnitude of 410 MPa is found within the first clad layer (at clad/parent interface), and the stresses reduce down to the value of 330 MPa and 230 MPa for the second and third layers respectively. The new contour measurement results resolve a dip in the tensile stress profile below the nominal clad/ferritic baseplate interface. The dip in the tensile stresses coincides with the maximum hardness value at the same location as shown in *Figure 5-38.* The highest value of hardness 293 HV is found at the same location, where the measured value of tensile stress is smallest (about 41 MPa). The exact location of this point is shown in *Figure 5-35,* that is 0.625 mm below the local fusion boundary. This evidence confirms that the new contour measurement analysis approach has successfully picked up martensitic transformation residual stress effects in the ferritic material just below the cladding fusion boundary.

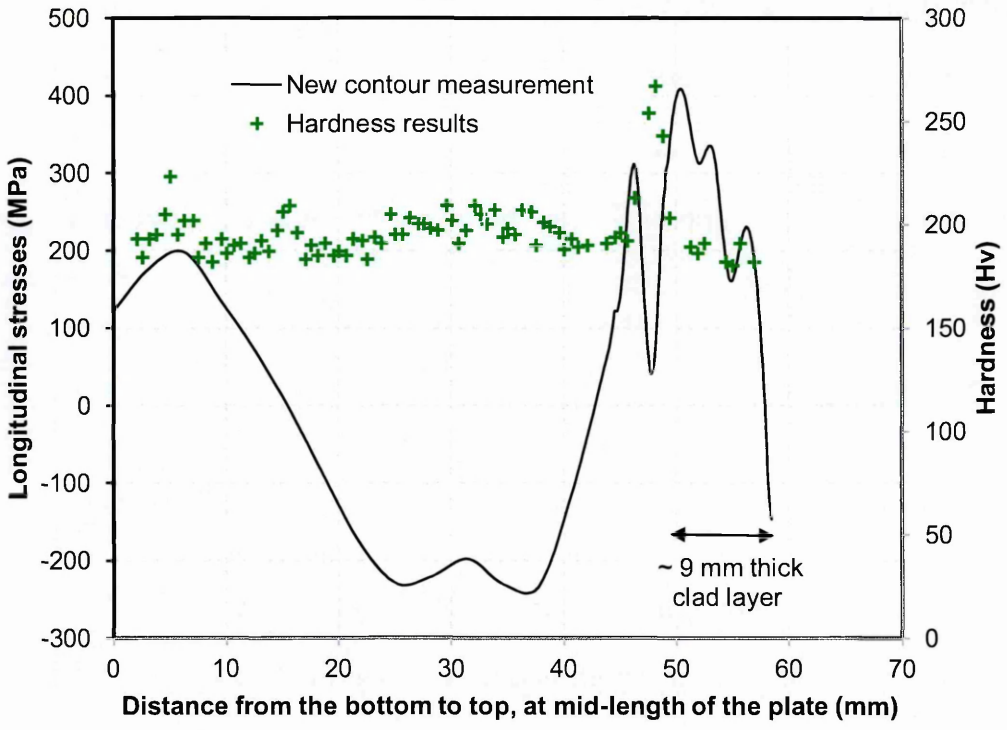

Figure 5-38: New contour method residual stress measurement compared with the hardness measurement profile along a through-thickness line at mid-width of the plate.

None of the residual stress measurements discussed earlier in section 5.4.5 could capture the short length scale stress variations expected to be present in the region of phase transformation near to the clad/parent material interface. The neutron diffraction measurement were carried out using a 3 mm x 3.4 mm x 5.8 mm diffracting gauge volume (12). The iDHD measurements were conducted using a 5 mm diameter core. The FE simulation was performed for the clad plate to predict the residual stress distribution without consideration of phase transformation. Hence, all of the residual stress measurements techniques involved using a limited gauge size. In contrast, the new contour measurement

analysis approach has used an "effective gauge size" of 0.25 mm which has successfully captured evidence of a phase transformation effect that correlates with hardness measurements. Thus, these results confirm that the new contour measurement analysis approach can be used for detailed characterisation of rapidly varying stresses.

5.5 Conclusions

The following conclusions can be drawn from the present case studies.

1. The contour method, as conventionally applied, failed to provide a detailed characterisation of the short length scale residual stress distributions that can be formed as a result of advance welding techniques such as high power density electron beam welds, and as a result of underclad phase transformation effects.
2. The criteria developed in chapter 4, informing choices for contour method data analysis parameters, can be successfully applied to capture short length scale residual stress variations (2 to 3 mm peak to peak) if the wavelength of such variations can be estimated.
3. Contour method measurements can be significantly improved by careful execution of the cutting process, surface measurement steps, and suitable selection of data analysis parameters.
4. The quality of the contour cut surfaces can be improved by undertaking following measures.
    - Use of thinner WEDM wire diameters.
    - Careful selection of wire WEDM cutting parameters.

- Use of sacrificial layers at the top and bottom faces of the plate along the plane of the contour, and at the start and end of the cut.
- Use of embedded cutting configuration.

5. Improved quality of the contour cut surfaces allows a finer deformation measurement spacing to be used that can help to capture the underlying short length scale surface features.
6. A smaller wire diameter produces a better surface finish and can give smaller variations in stress uncertainties providing no cutting artefacts are introduced (for example from wire breakage).
7. In this study, In order to capture the short length scale stress variations fine knot spacings were used. This caused the problem of unrealistic sharp stress variations appearing away from the peak tensile stress region. This is most likely to be because of the over fitting of the surface displacement data away from the weld region. This problem can be resolved by controlling the knot spacing along the cut length. Finer knot spacing can be used for highly concentrated stress region and short residual stress length-scale and for the rest of the cut length relatively coarser knot spacing can be used where the wavelength of this stress field is much larger.

Chapter 6 : Discussion and conclusions

This chapter provides a general discussion of the research presented in this thesis, draws overall conclusions and also covers ideas to take forward the work.

6.1 General discussion

The contour method is a powerful technique to evaluate residual stresses (33). It is of paramount importance that all steps to execute the contour method should be carefully planned so as to improve the quality of the stress results that can be achieved and to minimise the associated errors. The method comprises four basic steps: specimen cutting, topographic measurement of the cut surface, data analysis and finite element simulation. In order to achieve high-precision measurement results, each of the steps has to be controlled as demonstrated by the present research.

Specimen cutting is the first and most crucial step. Undesirable geometric features on the cut surfaces can arise from the cutting process. These features intrude upon the quality of the contour cut surface, and cause errors and uncertainty in stress results (38). In order to minimise such errors, cutting conditions can be optimised by performing trial cuts on a stress free part of the test component (117,135,143) , or on another piece of similar stress free material (38,139). However, prior to this research there has been no systematic approach applied to performing cutting trials and assessing the quality of the cut. Here a benchmark specimen geometry has been designed that can be used for developing a cutting strategy for the contour cuts. An accompanying

characterisation record sheet has been devised to quantify the benchmark cut surface quality and features that can introduce errors in contour measurements. The metrics of particular interest are the areal surface roughness, Sa, the roughness characteristic periodicity, RSm, and areal *RMS displacement* and areal *RMS apparent stress*. These metrics can be used to rank the quality of cutting conditions and thereby optimise cutting procedures for contour measurements. The characterisation sheets record the displacement errors introduced by cutting artefacts, most notably "bowing" features spanning across the cut faces (convex in ferritic steel and concave in stainless steel) and local edge effects. It is shown that these features could introduce errors in the order of 40 MPa to 50 MPa in contour residual stress measurements of the benchmark beams. This level of error (10 – 15 % of the material yield stress) is larger than desirable for a residual stress measurement technique. This emphasizes the importance of carrying out systematic cutting trials of the type developed in this thesis in order to minimise cutting errors for contour measurements, and in applying suitable mitigation measures (e.g. application of sacrificial layers to the specimen surfaces).

This study was limited to two material types, mild steel and stainless steel as well as one material thickness (25 mm). But the benchmark design and characterisation sheet can be used for any metallic material. The benchmark specimen design could also be usefully extended to study different specimen geometries (e.g. larger thicknesses and variable geometry). Clearly the setting of WEDM cutting parameters will change according to the material type and geometry of the specimens and this will change their effects on the quality of the cut surfaces.

The WEDM cutting technique works with a large number of electrical parameters. All of these parameters have their own effects on the quality of the cut surfaces. Small changes in each of the parameters can make the quality of the cut worse and unacceptable for the contour measurements. A good understanding of each of the WEDM parameters and their effects on the quality of the cuts is essential.

In this thesis, a procedure has been identified to quantify the quality of the cut surfaces and important parameters identified that can describe the quality of the cut surface. The characterisation record sheet is a very useful means to identify the quality of the individual cut and to allow comparison of cut surfaces with one and other. It will provide a means of capturing the knowledge and expertise of WEDM technicians as well as the characteristics of specific WEDM machines. Once a databank of records of cutting trials has been fully developed for different materials and geometries, this will provide tremendous help to contour method practitioners to improve residual stress measurement results. Future measurements will consume less material (dispensing the need for trials) and take less time.

The present research has also addressed the gap in published guidance for choosing surface deformation measurement spacings and deformation data analysis parameters for contour residual stress measurements. The contour cut surface should be measured using an appropriate measurement density that captures all of the surface features resulting from stress relaxation. In addition to this, the careful selection for data analysis parameters such as knot spacing for

data smoothing (130) and finite element mesh size are also very important in order to minimise error and uncertainty in calculated stress results.

A simple investigation of data analysis parameters for the contour method has been conducted in this thesis based on an idealised cosine displacement function (giving a self-equilibrated one-dimensional residual stress profile). A set of guidelines is proposed (see *Figure 4-9* in chapter 4) for making a suitable selection of cubic spline knot spacing, FE mesh size and deformation measurements spacing based on the wavelength of the residual stress distribution. This requires some prior knowledge (or estimate) of the residual stresses present in the component of interest. These guidelines have been successively applied to characterise rapidly varying (small length scale) residual stresses in three welded components: an EB butt welded P91 plate, an EB butt welded P91 to 316 stainless steel plate and a stainless steel clad ferritic plate. The author believes that the resolution in residual stress length-scale (peak to peak of 2 to 3 mm) in these components is the best achieved to date in contour measurements; for example the author is unaware of published work indicating the influence of martensitic transformation effects below stainless steel cladding on SA508 ferritic steel plate material.

Short length scale residual stress measurements are more sensitive to the surface roughness of the contour cut surface because the variations in displacement across a short span length can be very small (see Eq 4-1 in chapter 4); that is the "noise" associated with the roughness makes the underlying residual stress deformation more difficult to resolve. A thinner wire diameter was found to produce

cut surfaces with smaller surface roughness; for example in some of the benchmark cuts and for the two EB welded plate examples described in chapter 5. However, the thinner wire diameter increases the risk of wire breakages during the cutting process (as found for the dissimilar metal EB weld discussed in chapter 5) which is undesirable. Further work is required to determine the maximum acceptable surface roughness for resolving stresses of a specified minimum wavelength. Another consideration is that the cubic spline knot spacing chosen must be significantly larger than the surface roughness wavelength *RSm* to minimise the influence of surface roughness in the residual stress results. More work to investigate minimum limits for the developed data analysis criteria is needed.

6.2 Conclusions

The following conclusions are drawn from the work carried out in this thesis.

6.2.1 Benchmark study to characterise the wire EDM contour cut

1. A benchmark test specimen design for contour method cutting trials has been developed. A stress-free rectangular specimen with dimensions 245 mm long, 50 mm wide and 25 mm thick allows multiple trial cuts to be performed in the same set up. During WEDM cutting, one end of the specimen will be bolted to the bed of the WEDM machine, whilst 25 mm thick slices are removed from the free end. "Restrained" cutting conditions can be simulated by starting cuts from a pilot hole (1.8 mm diameter) situated 2.5 millimetres away from the side of the beam (leaving a ligament

of 1.6 mm) to provide constraint whilst cutting. The cut is stopped 2.5 mm away from the opposite side of the specimen giving a cut length of 45 mm and a wire contact length of 25 mm. The proposed geometry of the benchmark test specimen design is shown in *Figure 3-37* in chapter 3.

2. Parameters that characterise and quantify the quality of cut surfaces for contour method evaluation have been developed and characterisation data sheets developed. These 'surface quality parameters' are:
    - The maximum and minimum values of mean surface displacements along the cutting and wire direction
    - The maximum and minimum values of mean apparent stresses along the cutting and wire direction calculated using the contour method.
    - Three dimensional surface roughness parameters Sa, Sq and RSm.
    - Root mean square variations for displacement and stress across the cut surface.
3. The most important parameters to efficiently demonstrate the quality of the cut surfaces are Sa, RSm, *RMS displacement* and *RMS stress*. The maximum/minimum displacements are more a measure of the edge artefacts.
4. The study has confirmed the reproducibility of surface profiles for contour measurement for each of three different types of wire electro discharge machines tested.
5. This study showed that out of the machines installed at the Open University workshop, an Agie Charmilles FI 440 CCS WEDM gave better cut surfaces

for contour measurements than a Fanuc Robocut α-C600iA WEDM and Fanuc OiB5 WEDM.

6. A thinner wire diameter gave a better quality of surface finish (lower roughness) for cuts in both the mild steel and stainless steel test specimens, but made little difference to the topographical artefacts (bowing, wire start and flared edges) contributing to apparent stress errors in a contour analysis.
7. In all cut surface results, "flared edge effects" were commonly found along the wire entry side of the cuts implying the need for adding a "sacrificial" layer at the wire entry side prior to contour cuts.
8. Wire start topographic artefacts were observed in all cuts, again implying the need for adding a "sacrificial" material at the wire start face of a contour cut.
9. In unrestrained cuts, a *convex* bowed form of the cut surfaces was found in mild steel specimens, whereas a *concave* bowed form of the cut surfaces was observed in stainless steel specimens. The severity of the bowing was greater in the mild steel specimens than in the stainless steel. The origin of these "bowed" features is uncertain.
10. The quality of the cut surfaces for both material types, mild steel and stainless steel specimens was improved by providing a restraint along the plane of the cut. In particular bowing of the free side of the cuts was reduced resulting in improved averaged displacement variations.

6.2.2 Data analysis parameters for the contour method

Three data analysis parameters of the contour method; the size of deformation measurement density 'd' to measure the contour cut surface, the knot spacing 'k ' to smooth the measured contour cut surface data and the finite element mesh size 's' have a major influence on the contour method residual stress results. These parameters have been studied by considering a one dimensional idealised cosine function. The quality of piece-wise linear and cubic spline fits to the idealised profile have been evaluated by calculating the fitting errors and threshold acceptable errors defined to help inform the choice of the parameters.

1. The expected residual stress wavelength 'w 'has been identified as an important initial input.
2. For the measurement spacing, select $d \leq w/12 (d/w \leq 0.083)$ and $d<<k$ noting that the finer the spacing the better.
3. For the knot spacing (initial analysis), select $k \leq w/4 (k/w \leq 0.25)$.
4. For the finite element mesh size, select $s \leq w/12 (s/w \leq 0.083)$.

6.2.3 Guidelines for improving the spatial resolution of contour results

A detailed procedure is proposed in chapter 4 (flowchart shown in *Figure 4-9*) to improve the reliability of contour residual stress measurements, especially where short length scale stress fields are of interest. It includes, perform a precise wire WEDM contour cut using cutting conditions suggested in chapter 3 and chapter 5. Then, measure the contour of the cut surfaces and analyse the measured surface data according to the criteria proposed in chapter 4. The most

important input to implement the simplistic criteria developed in chapter 4 is an appropriate estimation of the residual stress wavelengths (w) of interest.

6.2.4 Residual stress measurements

1. The contour method, as conventionally applied, failed to provide a detailed characterisation of the short length scale residual stress distributions that can be formed as a result of advanced welding techniques such as high power density electron beam, and as a result of underclad phase transformation effects.
2. The criteria developed in chapter 4 informing choices for contour method data analysis parameters can be successfully applied to capture short length scale residual stress variations (2 to 3 mm peak to peak) if the wavelength of such variations can be estimated.
3. Contour method measurements can be significantly improved by careful execution of the cutting process, surface measurement steps, and suitable selection of data analysis parameters.
4. The quality of the contour cut surfaces can be improved by undertaking following measures.
    - Use of thinner WEDM wire diameters.
    - Careful selection of WEDM cutting parameters.
    - Use of sacrificial layers at the top and bottom faces of the plate along the plane of the contour, and at the start and end of the cut.
    - Use of embedded cutting configuration.

5. Improved quality of the contour cut surfaces allows a finer deformation measurement spacing to be used which is essential for capturing of all of the underlying short length scale surface features.
6. A smaller wire diameter produces a better surface finish and can give smaller variations in stress uncertainties providing no cutting artefacts are introduced (for example from wire breakage).

6.3 Suggested future work

This research has covered several aspects of the topic of interest. However, some important issues remain and need to be studied in the future.

- A benchmark specimen has been designed that can be used to perform trial cuts to optimise WEDM cutting conditions for contour residual stress measurement. Many issues related to the quality of the cut have been identified in chapter 3. It would be rewarding to continue this work for testing and evaluating different types of material and varying the cutting conditions systematically. Similar designs of benchmark specimen with larger cross-section dimensions could be used to examine the influence of size (wire contact length and cut length). Once the best operational parameters for WEDM cutting have been well established for different material types and geometries, WEDM cutting guidelines for contour residual stress measurements can be developed to improve the accuracy and reliability of the contour method.
- The contour method is being rapidly adopted for new applications including non-uniform shapes and complex multi-material welds. In this thesis, sacrificial

layers have been successfully applied to mitigate wire entry effects (flared edges) arising from cutting. It would be good to establish a technique to make the sacrificial layers locally according to required shapes. For this purpose a low melting alloy might be used to form a particular shape.

- In this thesis, it was found that a fine knot spacing was required to capture the true short wavelength stress variations. But this caused the problem of over fitting the surface deformation data away from the highly concentrated stress region. Further investigation is required for these cases to control the knot spacing to smooth the surface data to an appropriate level along the cut length according to the local expected residual stress length scale.
- The accuracy of the contour method can be improved by preserving the contour cut surface from all unwanted effects resulting from the machining process. Investigation and development of other advance cutting techniques that can minimise these effects is desirable. There are some techniques available for materials cutting that have been used successfully for residual stress measurement in other strain relief methods. These cutting techniques include focused ion beam (FIB) milling (166,167), laser ablation (168,169) and waterjet cutting (172). Limited reporting on the use of these cutting techniques for contour method measurements opens up a wide field of possibilities for developing a novel cutting approach with an improved surface finish.

Appendix A - Wire EDM Parameters

Parameter	Explanation	Units	Set
EL	Agie parameter		S
Pa	Agie parameter		S
Pm	Agie parameter		S
ST	Strategy		S
M	Sparking mode		S
E	Agie parameter		S
V	Machining voltage	V	S
IAL	Spark ignition intensity (see *Figure A - 1*), × 0.5	A	S
FF	Pulse Frequency	S	
B	Pulse period (see *Figure A - 1*)	µs	S
A	Pulse rise time (duration of material removal phase), (see *Figure A - 1*)	µs	S
TAC	Reduced pulse rise time A for difficult cutting conditions	µs	S
Aj	Machining voltage setting	V	S
S	Cutting speed (× 7.42)	mm min^{-1}	S
WS	Wire speed	mm min^{-1}	S
WB	Wire tension	S	
Inj	Flushing water injection pressure	S	
mm/min	Speed of cut	mm min^{-1}	M
Cut time	Total duration of cut	hh:mm:ss	M

Table A - 1: Explanation of terms used for an Agie Charmilles WEDM machine (156).

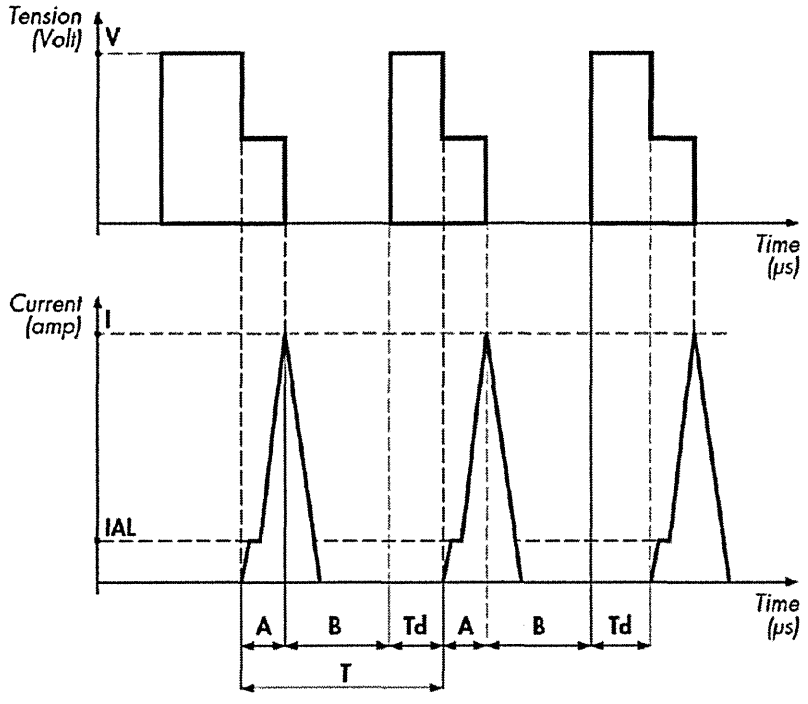

Figure A - 1: The diagram presents the phenomenon of spark generation with the simultaneous trends of the voltage and current (156).

References

1. Masubuchi K. Analysis of Welded Structures: Residual Stresses, Distortion, and Their Consequences. Elsevier; 2013. 655 p.

2. Withers PJ. Residual stress and its role in failure. Rep Prog Phys. 2007;70(12):2211.

3. Totten G, Inoue T, Howes M. Handbook of Residual Stress and Deformation of Steel. Materials Park, Ohio: ASM International; 2001. 550 p.

4. Withers PJ, Bhadeshia H. Residual stress. Part 2–Nature and origins. Mater Sci Technol. 2001;17(4):366–75.

5. Rossini N, Dassisti M, Benyounis K, Olabi A. Methods of measuring residual stresses in components. Mater Des. 2012;35:572–88.

6. Gary SS, Clayton OR. Overview of resdual stresses and their measurement. In: Practical Residual Stress Measurement Methods. John Wiley & Sons, Ltd; 2013. p. 1–27.

7. Sharpe WN. Springer Handbook of Experimental Solid Mechanics. Springer Science & Business Media; 2008. 1100 p.

8. Withers PJ, Bhadeshia HKDH. Residual stress. Part 1 – Measurement techniques. Mater Sci Technol. 2001 Apr 1;17(4):355–65.

9. Bouchard P. Section II.7 Treatment of weld residual stresses. In: Budden PJ. In: Assessment of the integrity of structures containing defects. R6 Revision 4. Gloucester , UK: British Energy Generation Ltd; 2004.

10. Khan MI. Welding Science and Technology. New Age International; 2007. 12 p.

11. Cerjak H. The role of welding in the power generation industry. In: Proc IIW Int Conf on "Safety and reliability of welded components in energy and processing industry", Graz, Austria. 2008. p. 17–27.

12. Colegrove P, Ikeagu C, Thistlethwaite A, Williams S, Nagy T, Suder W, et al. Welding process impact on residual stress and distortion. Sci Technol Weld Join. 2009 Nov;14(8):717–25.

13. Schultz H. Electron Beam Welding. Elsevier; 1994. 245 p.

14. Katsuyama J, Udagawa M, Nishikawa H. Evaluation of weld residual stress near the cladding and J-weld in reactor pressure vessel head for the assessment of PWSCC behavior. 2010;

15. Giedt WH, Tallerico LN. Prediction of electron beam depth of penetration. Weld J. 1988;67(12):299–305.

16. Lancaster JF. Handbook of Structural Welding: Processes, Materials and Methods Used in the Welding of Major Structures, Pipelines and Process Plant. Elsevier; 1997. 445 p.

17. Joseph B, Katherasan D, Sathiya P, Murthy CS. Weld metal characterization of 316L (N) austenitic stainless steel by electron beam welding process. Int J Eng Sci Technol. 2012;4(2):169–76.

18. Stone HJ, Withers PJ, Roberts SM, Reed RC, Holden TM. Comparison of three different techniques for measuring the residual stresses in an electron beam-welded plate of WASPALOY. Metall Mater Trans A. 1999;30(7):1797–808.

19. British Standard - BS 7910. Guide to methods for assessing the acceptability of flaws in metallic structures. 2005.

20. Bouchard PJ. Code characterisation of weld residual stress levels and the problem of innate scatter. Int J Press Vessels Pip. 2008 Mar;85(3):152–65.

21. Bouchard PJ. Identification of residual stress length scales in welds for fracture assessment. In: Residual Stress and Its Effects on Fatigue and Fracture. Springer; 2006. p. 163–76.

22. Bouchard P j., Withers P j. The Appropriateness of Residual Stress Length Scales in Structural Integrity. J Neutron Res. 2004 Jan;12(1-3):81–91.

23. Schajer GS, Ruud CO. Overview of Residual Stresses and Their Measurement. Pract Residual Stress Meas Methods. 2013;1–27.

24. Krawitz AD, Winholtz RA. Use of position-dependent stress-free standards for diffraction stress measurements. Mater Sci Eng A. 1994 Sep 15;185(1–2):123–30.

25. Clapham L, Abdullah K, Jeswiet JJ, Wild PM, Rogge R. Neutron diffraction residual stress mapping in same gauge and differential gauge tailor-welded blanks. J Mater Process Technol. 2004 May 15;148(2):177–85.

26. Fitzpatrick ME, Lodini A. Analysis of Residual Stress by Diffraction using Neutron and Synchrotron Radiation. CRC Press; 2003. 367 p.

27. Withers PJ, Preuss M, Steuwer A, Pang JWL. Methods for obtaining the strain-free lattice parameter when using diffraction to determine residual stress. J Appl Crystallogr. 2007 Oct 1;40(5):891–904.

28. Grant PV, Lord JD, Whitehead P. The measurement of residual stresses by the incremental hole drilling technique–Issue 2. NPL Good Pract Guide. 2006;(53).

29. Leggatt RH, Smith DJ, Smith SD, Faure F. Development and experimental validation of the deep hole method for residual stress measurement. J Strain Anal Eng Des. 1996;31(3):177–86.

30. Kingston E, Stefanescu D, Mahmoudi A, Truman C, Smith D. Novel Applications of the Deep-Hole Drilling Technique for Measuring Through-Thickness Residual Stress Distributions. J ASTM Int. 2006;3(4):12568.

31. Su B, Hossainzadeh F, Truman C, Smith D. Residual stresses in machined and shrink-fitted assemblies. JCPDS-Int Cent Diffr Data Adv X-Ray Anal. 2008;52:675–82.

32. Skouras A, Pavier MJ, Shterenlikht A. A Spatial Resolution of Residual Stress Measurements Using the Deep Hole Drilling Technique. In: ASME 2010 Pressure Vessels and Piping Division/K-PVP Conference. American Society of Mechanical Engineers; 2010. p. 1477–82.

33. Prime MB. Cross-Sectional Mapping of Residual Stresses by Measuring the Surface Contour After a Cut. J Eng Mater Technol. 2000 Nov 3;123(2):162–8.

34. Schajer GS. Practical Residual Stress Measurement Methods. Wiley; 2013. 330 p.

35. P. Pagliaro MBP. Measuring Multiple Residual-Stress Components using the Contour Method and Multiple Cuts. Exp Mech. 2010;50(2):187–94.

36. Prime MB, Newborn MA, Balog JA. Quenching and Cold-Work Residual Stresses in Aluminum Hand Forgings: Contour Method Measurement and FEM Prediction. Mater Sci Forum. 2003;426-432:435–40.

37. Pagliaro P. Mapping Multiple Residual Stress Components Using the Contour Method and Superposition. Universitá degli Studi di Palermo, Palermo.; 2008.

38. Prime MB, Kastengren AL. The contour method cutting assumption: error minimization and correction. In: Experimental and Applied Mechanics, Volume 6. Springer; 2011. p. 233–50.

39. Hosseinzadeh F, Kowal J, Bouchard PJ. Towards good practice guidelines for the contour method of residual stress measurement. J Eng. 2014;Online – only.

40. Bouchard P. Treatment of weld residual stresses. In: Budden PJ. R6 Revision 4. Gloucester , UK: British Energy Generation Ltd; 2004.

41. Lu J. Handbook of measurement of residual stresses. Society for Experimental Mechanics; 1995. 238 p.

42. R. J. Katemi JE. Investigations of residual stress distributions in retained austenite and martensite after carbonitriding of low alloy steel. In: Advanced Materials Research. UTT-France; 2014.

43. Branch TS-P. On the influence of the process of carbonitriding in smouldering discharge on the properties of 25CrMnSiNiMo steel. Ann Fac Eng Hunedoara. 2006;Tome IV(Fascicole 3):ISSN 1584–2673.

44. Grondin GY, Elwi AE, Cheng JJR. Buckling of stiffened steel plates—a parametric study. J Constr Steel Res. 1999 May;50(2):151–75.

45. Katsuyama J, Udagawa M, Nishikawa H, Nakamura M, Onizawa K. Evaluation of Weld Residual Stress near the Cladding and J-weld in Reactor Pressure Vessel Head for the assessment of PWSCC Behavior. EJ Adv Maint. 2010;2:55–64.

46. Schajer GS. Relaxation methods for measuring residual stresses: techniques and opportunities. Exp Mech. 2010;50(8):1117–27.

47. Kudryavtsev YF. Residual Stress. In: Prof WNSJ, editor. Springer Handbook of Experimental Solid Mechanics. Springer US; 2008. p. 371–88.

48. Altpeter I, Dobmann G, Kröning M, Rabung M, Szielasko S. Micro-magnetic evaluation of micro residual stresses of the IInd and IIIrd order. NDT E Int. 2009 Jun;42(4):283–90.

49. Belahcene F, Lu J. Study of residual stress induced in welded steel by surface longitudinal ultrasonic method. In: Society for Experimental Mechanics, Inc, Proceedings of the SEM Annual Conference on Theoretical, Experimental and Computational Mechanics(USA),. 1999. p. 331–4.

50. Hauk V. Structural and Residual Stress Analysis by Nondestructive Methods: Evaluation - Application - Assessment. Elsevier; 1997. 655 p.

51. Ruud CO. A review of selected non-destructive methods for residual stress measurement. NDT Int. 1982 Feb;15(1):15–23.

52. Michael B Prime MLS. Beyond the Streetlight Effect: A United Future for Relaxation and Diffraction Methods for Residual Stress Measurement. Adv Mater Res. 2014;996:234–42.

53. Withers PJ, Turski M, Edwards L, Bouchard PJ, Buttle DJ. Recent advances in residual stress measurement. Int J Press Vessels Pip. 2008 Mar;85(3):118–27.

54. Leggatt RH, Smith DJ, Smith SD, Faure F. Development and experimental validation of the deep hole method for residual stress measurement. J Strain Anal Eng Des. 1996 May 1;31(3):177–86.

55. Mahmoudi AH, Zheng G, Smith DJ. A Procedure to Measure Biaxial Near Yield Residual Stresses Using the Deep Hole Drilling Technique. Exp Mech-9 Doi101007s11340-013-9729-2. 2013;53:1223–31.

56. Mahmoudi AH, Smith DJ. The effect of plasticity on the ability of the deep hole drilling technique to measure axisymmetric residual stress. Int J Mech Sci. 2011;53(11):978–88.

57. Goudar DM, Truman CE, Smith DJ. Evaluating Uncertainty in Residual Stress Measured Using the Deep-Hole Drilling Technique. Strain. 2011 Feb;47(1):62–74.

58. Veqter. Residual stress measurement techniques. Available: http://www.veqter.co.uk/. Last accessed 03rd Aug 2015. 2013.

59. Kitano H, Okano S, Mochizuki M. A study for high accuracy measurement of residual stress by deep hole drilling technique. In: Journal of Physics: Conference Series. IOP Publishing; 2012. p. 012049.

60. Smith DJ, Bouchard PJ, George D. Measurement and prediction of residual stresses in thick-section steel welds. J Strain Anal Eng Des. 2000 Jan 1;35(4):287–305.

61. Bateman MG, Miller OH, Palmer TJ, Breen CEP, Kingston EJ, Smith DJ, et al. Measurement of residual stress in thick section composite laminates using the deep-hole method. Int J Mech Sci. 2005;47(11):1718–39.

62. Zheng G, Smith D. A New Procedure for Measuring Residual Stresses in Electron Beam Welds Using the Deep Hole Drilling Technique. In: The society for Experimental Mechanics series 2011. 2011. p. 75–84.

63. Hutchings MT, Withers PJ, Holden TM, Lorentzen T. Introduction to the Characterization of Residual Stress by Neutron Diffraction. CRC Press; 2005. 383 p.

64. Stacey A, MacGillivary HJ, Webster GA, Webster PJ, Ziebeck KRA. Measurement of residual stresses by neutron diffraction. J Strain Anal Eng Des. 1985 Apr 1;20(2):93–100.

65. Webster GA, Wimpory RW. Polycrystalline materials: determination of residual stresses by neutron diffraction. European Commission, Joint Research Centre, Institute for Energy; 2002.

66. British Standard Institute Staff. Non-destructive testing - Standard test method for determining residual stresses by neutron diffraction. 2005.

67. Daymond MR, Bourke MAM, Von Dreele RB. Use of Rietveld refinement for elastic macrostrain determination and for evaluation of plastic strain history from diffraction spectra. 1997;82(4).

68. Residual stress measurement by X-ray diffraction. Warrendale, PA: SAE, Society of Automative Engineering Handbook Supplement; 2003.

69. M.E. F. Measurement Good practice Guide No.52. Determination of residual stresses by X-ray diffraction-Issue 2. 2005.

70. Prevey P. Current applications of X-ray diffraction residual stress. Dev Mater Characterisation Technol. 1996;103–10.

71. Holden TM, Suzuki H, Carr DG, Ripley MI, Clausen B. Stress measurements in welds: Problem areas. Mater Sci Eng A. 2006 Nov 10;437(1):33–7.

72. Klueh RL. Elevated temperature ferritic and martensitic steels and their application to future nuclear reactors. Int Mater Rev. 2005;50(5):287–310.

73. Abe F, Tabuchi M. Microstructure and creep strength of welds in advanced ferritic power plant steels. Sci Technol Weld Join. 2004 Jan;9(1):22–30.

74. Francis J, Mazur W, Bhadeshia H. Type IV cracking in ferritic power plant steels. Mater Sci Technol. 2006;22(12):1387–95.

75. Coleman KK, Newell WF. P91 and Beyond. Weld J-N Y. 2007;86(8):29.

76. Tabuchi M, Watanabe T, Kubo K, Matsui M, Kinugawa J, Abe F. Creep crack growth behavior in the HAZ of weldments of W containing high Cr steel. Int J Press Vessels Pip. 2001 Nov 12;78(11–12):779–84.

77. Spigarelli S, Quadrini E. Analysis of the creep behaviour of modified P91 (9Cr–1Mo–NbV) welds. Mater Des. 2002 Sep;23(6):547–52.

78. Paddea S, Francis JA, Paradowska AM, Bouchard PJ, Shibli IA. Residual stress distributions in a P91 steel-pipe girth weld before and after post weld heat treatment. Mater Sci Eng A. 2012 Feb;534:663–72.

79. Albert SK, Tabuchi M, Hongo H, Watanabe T, Kubo K, Matsui M. Effect of welding process and groove angle on type IV cracking behaviour of weld joints of a ferritic steel. Sci Technol Weld Join. 2005;10(2):149–57.

80. Sun Z. Feasibility of producing ferritic/austenitic dissimilar metal joints by high energy density laser beam process. Int J Press Vessels Pip. 1996;68(2):153–60.

81. Pan C, Zhang Z. Morphologies of the transition region in dissimilar austenitic-ferritic welds. Mater Charact. 1996;36(1):5–10.

82. Celik A, Alsaran A. Mechanical and Structural Properties of Similar and Dissimilar Steel Joints. Mater Charact. 1999 Nov;43(5):311–8.

83. Smith RE, Hanford R, Cheng SC. Pressure vessel nozzle repair. Nucl Eng Des. 1990 Nov;124(1–2):79–89.

84. Venkata Ramana P, Madhusudhan Reddy G, Mohandas T, Gupta A. Microstructure and residual stress distribution of similar and dissimilar electron beam welds–Maraging steel to medium alloy medium carbon steel. Mater Des. 2010;31(2):749–60.

85. Sun Z, Karppi R. The application of electron beam welding for the joining of dissimilar metals: an overview. J Mater Process Technol. 1996;59(3):257–67.

86. Arivazhagan N, Singh S, Prakash S, Reddy GM. Investigation on AISI 304 austenitic stainless steel to AISI 4140 low alloy steel dissimilar joints by gas tungsten arc, electron beam and friction welding. Mater Des. 2011;32(5):3036–50.

87. Chaudhari R, Parekh R, Ingle A. Reliability of dissimilar metal joints using fusion welding: A Review. In: International Conference on Machine Learning, Electrical and Mechanical Engineering (ICMLEME'2014). Dubai(UAE); 2014. p. 98–104.

88. Liu C, Wu B, Zhang JX. Numerical investigation of residual stress in thick titanium alloy plate joined with electron beam welding. Metall Mater Trans B. 2010;41(5):1129–38.

89. Naveed N, Hosseinzadeh F, Kowal J. Residual Stress Measurement in a Stainless Steel Clad Ferritic Plate Using the Contour Method. In: ASME 2013 Pressure Vessels and Piping Conference - Materials and Fabrication. Paris, France: American Society of Mechanical Engineers; 2013. p. V005T11A006.

90. Serasli K, Coules H, Smith D. Residual stresses in clad nuclear reactor pressure vessel steels; prediction, measurement and reconstruction. In: ASME 2015 Pressure Vessels & Piping Conference. Boston, Massachusetts, USA: American Society of Mechanical Engineers; 2015. p. PVP2015–45224.

91. Sattari-Far I, Andersson M. Cladding effects on structural integrity of nuclear components. Swedish Nuclear Power Inspectorate, Stockholm (Sweden); 2006 p. SKI Report 2006:23.

92. Parma C, Gill C, Hurrell P, Pellereau B. Simulation of a Multi-pass Groove Weld and Clad Plate Using Abaqus 2D Weld GUI and Comparison with Measurements. Rolls-Royce plc; 2014.

94. Brown DW, Holden TM, Clausen B, Prime MB, Sisneros TA, Swenson H, et al. Critical comparison of two independent measurements of residual stress in an electron-beam welded uranium cylinder: neutron diffraction and the contour method. Acta Mater. 2011;59(3):864–73.

95. Manchester University, Rolls Royce. Residual stress measurements in a stainless steel clad ferritic plate using the neutron diffraction technique. Private communication; 2013.

96. Prime M, DeWald AT. The Contour Method. In: Practical Residual Stress Measurement Methods. John Wiley & Sons, Ltd; 2013. p. 109–38.

97. Prime M, Hill M, DeWald A, Sebring R, Dave V, Cola M. Residual stress mapping in welds using the contour method. In: the 6th International Conference. Pine Mountain, Georgia: ASM International; 2002. p. 891–6.

98. Traore Y, Paddea S, Bouchard PJ, Gharghouri MA. Measurement of the residual stress tensor in a compact tension weld specimen. Exp Mech. 2013;53(4):605–18.

99. Hosseinzadeh F, Toparli MB, Bouchard PJ. Slitting and contour method residual stress measurements in an edge welded beam. J Press Vessel Technol. 2012;134(1):011402–6.

100. DeWald AT, Hill MR. Eigenstrain-based model for prediction of laser peening residual stresses in arbitrary three-dimensional bodies Part 1: Model description. J Strain Anal Eng Des. 2009 Jan 1;44(1):1–11.

101. Evans A, Johnson G, King A, Withers PJ. Characterization of laser peening residual stresses in Al 7075 by synchrotron diffraction and the contour method. J Neutron Res. 2007 Jun;15(2):147–54.

102. Zhang Y, Ganguly S, Stelmukh V, Fitzpatrick ME, Edwards L. Validation of the Contour Method of Residual Stress Measurement in a MIG 2024 Weld by Neutron and Synchrotron X-ray Diffraction. J Neutron Res. 2003 Dec;11(4):181–5.

103. Richter-Trummer V, Tavares SM, Moreira PM, de Figueiredo MA, de Castro PM. Residual stress measurement using the contour and the sectioning methods in a MIG weld: Effects on the stress intensity factor. Ciênc Tecnol Mater. 2008;20(1-2):114–9.

104. Prime MB, Gnäupel-Herold T, Baumann JA, Lederich RJ, Bowden DM, Sebring RJ. Residual stress measurements in a thick, dissimilar aluminum alloy friction stir weld. Acta Mater. 2006 Sep;54(15):4013–21.

105. Frankel P, Preuss M, Steuwer A, Withers PJ, Bray S. Comparison of residual stresses in Ti–6Al–4V and Ti–6Al–2Sn–4Zr–2Mo linear friction welds. Mater Sci Technol. 2009;25(5):640–50.

106. Turski M, Edwards L. Residual stress measurement of a 316L stainless steel bead-on-plate specimen utilising the contour method. Int J Press Vessels Pip. 2009;86(1):126–31.

107. Hacini L, Lê NV, Bocher P. Evaluation of Residual Stresses Induced by Robotized Hammer Peening by the Contour Method. Exp Mech. 2008 Dec 16;49(6):775–83.

108. DeWald AT, Rankin JE, Hill MR, Lee MJ, Chen H-L. Assessment of tensile residual stress mitigation in Alloy 22 welds due to laser peening. J Eng Mater Technol. 2004;126(4):465–73.

109. Hatamleh O, Lyons J, Forman R. Laser peening and shot peening effects on fatigue life and surface roughness of friction stir welded 7075-T7351 aluminum. Fatigue Fract Eng Mater Struct. 2007;30(2):115–30.

110. Hatamleh O. Effects of peening on mechanical properties in friction stir welded 2195 aluminum alloy joints. Mater Sci Eng A. 2008;492(1):168–76.

111. Zhang Y, Fitzpatrick ME, Edwards L. Measurement of the residual stresses around a cold expanded hole in an EN8 steel plate using the contour method. In: Materials science forum. Trans Tech Publ; 2002. p. 527–34.

112. Kundu A, Bouchard PJ, Kumar S, Venkata KA, Francis JA, Paradowska A, et al. Residual stresses in P91 steel electron beam welds. Sci Technol Weld Join. 2013 Jan;18(1):70–5.

113. Bueckner HF. The propagation of cracks and the energy of elastic deformation. Trans ASME. 1958;80:1228–30.

114. Shin SH. FEM analysis of plasticity-induced error on measurement of welding residual stress by the contour method. J Mech Sci Technol. 2005;19(10):1885–90.

115. Dennis RJ, Bray DP, Leggatt NA, Turski M. Assessment of the influence of plasticity and constraint on measured residual stresses using the contour method. In: ASME 2008 Pressure Vessels and Piping Conference. American Society of Mechanical Engineers; 2008. p. 477–85.

116. Traore Y. Controlling Plasticity in the Contour Method of Residual Stress Measurement (PhD thesis). Materials Science & Engineering, The Open University; 2013.

117. Hosseinzadeh F, Bouchard PJ. Mapping Multiple Components of the Residual Stress Tensor in a Large P91 Steel Pipe Girth Weld Using a Single Contour Cut. Exp Mech. 2012 May 23;53(2):171–81.

118. Traore Y, Bouchard PJ, Francis J, Hosseinzadeh F. A Novel Cutting Strategy for Reducing Plasticity Induced Errors in Residual Stress Measurements Made With the Contour Method. In: ASME 2011 Pressure Vessels and Piping Conference - Materials and Fabrication. Baltimore, Maryland, USA: American Society of Mechanical Engineers; 2011. p. 1201–12.

119. Kunieda M, Lauwers B, Rajurkar KP, Schumacher BM. Advancing EDM through Fundamental Insight into the Process. CIRP Ann - Manuf Technol. 2005;54(2):64–87.

120. Spedding TA, Wang ZQ. Parametric optimization and surface characterization of wire electrical discharge machining process. Precis Eng. 1997 Jan;20(1):5–15.

121. Ho KH, Newman ST. State of the art electrical discharge machining (EDM). Int J Mach Tools Manuf. 2003 Oct;43(13):1287–300.

122. Hargrove SK, Duowen Ding. Determining cutting parameters in wire EDM based on workpiece surface temperature distribution. Int J Adv Manuf Technol. 2007 Aug 15;34(3/4):295–9.

123. Iqbal AA, Khan AA. Influence of process parameters on electrical discharge machined job surface integrity. Am J Eng Appl Sci. 2010;3(2):396–402.

124. Wang C-C, Chow H-M, Yang L-D, Lu C-T. Recast layer removal after electrical discharge machining via Taguchi analysis: A feasibility study. J Mater Process Technol. 2009 Apr 21;209(8):4134–40.

125. Cusanelli G, Hessler-Wyser A, Bobard F, Demellayer R, Perez R, Flükiger R. Microstructure at submicron scale of the white layer produced by EDM technique. J Mater Process Technol. 2004 Jun 10;149(1–3):289–95.

126. Ali S. Probing system characteristics in coordinate metrology. Meas Sci Rev. 2010;10(4):120–9.

127. Hocken RJ, Pereira PH. Coordinate Measuring Machines and Systems, Second Edition. CRC Press; 2011. 586 p.

128. Flack D. CMM probing-Issue 2. A National Measurement Good Practice Guide, No 43. 2014.

129. Hosseinzadeh F. Surface profile measurement for the contour method. The Open University; Report No.: OU/MatsEng/019, Issue 1.

130. Prime MB, Sebring RJ, Edwards JM, Hughes DJ, Webster PJ. Laser surface-contouring and spline data-smoothing for residual stress measurement. Exp Mech. 2004 Apr 1;44(2):176–84.

131. Prime MB, Gnäupel-Herold T, Baumann JA, Lederich RJ, Bowden DM, Sebring RJ. Residual stress measurements in a thick, dissimilar aluminum alloy friction stir weld. Acta Mater. 2006;54(15):4013–21.

132. Bouchard PJ, Turski M, Smith MC. Residual Stress Concentrations in a Stainless Steel Slot-Weld Measured by the Contour Method and Neutron Diffraction. 2009 Jan 1;335–45.

133. Kartal M, Turski M, Johnson G, Fitzpatrick ME, Gungor S, Withers PJ, et al. Residual stress measurements in single and multi-pass groove weld specimens using neutron diffraction and the contour method. In: Materials Science Forum. Trans Tech Publ; 2006. p. 671–6.

134. Prime MB, Hughes DJ, Webster PJ. Weld application of a new method for cross-sectional residual stress mapping. In: 2001 SEM Annual Conf on Experimental and Applied Mechanics, Portland, OR. 2001. p. 608–11.

135. Bouchard PJ, Ledgard P, Hiller S, Hosseinzadh Torknezhad F. Making the cut for the contour method. In Porto, Portugal; 2012.

136. Leach R, Brown L, Jiang X. Guide to the measurement of smooth surface topography using coherence scanning interferometry-Issue 1368-6550. A National Measurement Good Practice Guide, No. 108; 2008.

137. Leach R. The measurement of surface texture using Stylus Instruments. Measurement good practice guide No. 37. National Physical Laboratory, Middlesex, UK; 2011.

138. Savaria V, Hoseini M, Bridier F, Bocher P, Arkinson P. On the measurement of residual stress in induction hardened parts. In: Materials Science Forum. Trans Tech Publ; 2011. p. 431–6.

139. Pagliaro P, Prime MB, Clausen B, Lovato ML, Zuccarello B. Known residual stress specimens using opposed indentation. J Eng Mater Technol. 2009;131(3):031002.

140. Olson MD, DeWald AT, Prime MB, Hill MR. Estimation of Uncertainty for Contour Method Residual Stress Measurements. Exp Mech. 2014;1–9.

141. Akaslan S, others. The effect of machining parameters on tool electrode edge wear and machining performance in electric discharge machining (EDM). KSME Int J. 2002;16(1):46–59.

142. Tsai YY, Lu CT. Influence of current impulse on machining characteristics in EDM. J Mech Sci Technol. 2007;21(10):1617–21.

143. Hosseinzadeh F, Ledgard P, Bouchard PJ. Controlling the cut in contour residual stress measurements of electron beam welded Ti-6Al-4V alloy plates. Exp Mech. 2013;53(5):829–39.

144. Hosseinzadeh F, Bouchard PJ. Residual Stress Measurement of a Hipped Bonded Valve Seat Using the Contour Method. In: ASME 2013 Pressure Vessels and Piping Conference. American Society of Mechanical Engineers; 2013. p. V06BT06A083.

145. Puri AB, Bhattacharyya B. An analysis and optimisation of the geometrical inaccuracy due to wire lag phenomenon in WEDM. Int J Mach Tools Manuf. 2003 Jan;43(2):151–9.

146. Olson MD, DeWald AT, Prime MB, Hill MR. Estimation of Uncertainty for Contour Method Residual Stress Measurements. Exp Mech. 2014;1–9.

147. DeWald AT, Hill MR. Eigenstrain-based model for prediction of laser peening residual stresses in arbitrary three-dimensional bodies Part 1: Model description. J Strain Anal Eng Des. 2009 Jan 1;44(1):1–11.

148. Prime MB. System and method for measuring residual stress. United States: Los Alamos National Laboratory (LANL), Los Alamos, NM; 2002. Report No.: US 6470756.

149. Hosseinzadeh F, Naveed N. Residual stress measurement in three pass groove welded plate using the contour method. The Open University, Milton Keynes, UK; 2013. Report No.: OU/MatsEng/042, Issue 1.

150. British Iron and Steel Research Association, Steel User Section, Woolman J, Mottram RA, British Iron and Steel Research Association, Steel User Service. The mechanical and physical properties of the British Standard En steels (B.S. 970-1955). Oxford; New York: Pergamon Press; 1964.

151. ASM International, Handbook Committee. Properties and selection-- irons, steels, and high-performance alloys. Materials Park, OH: ASM International; 1990.

152. Fitzpatric ME, Fry AT, Holdway P, Kandil FA, Shackleton J, Suominen L. Determination of Residual Stresses by X-Ray Diffraction–Issue 2. Natl Meas Good Pract Guide. (52).

153. Tomura S, Kunieda M. Analysis of electromagnetic force in wire-EDM. Precis Eng. 2009 Jul;33(3):255–62.

154. Herrero A, Azcarate S, Rees A, Gehringer A, Schoth A, Sanchez JA. Influence of force components on thin wire EDM. In: Multi-material micro manufacture Cardiff University, Cardiff. 2008.

155. Practical Machinist. Demagnetize prior to or after WEDM cutting. Available: http://www.practicalmachinist.com/vb/edm-machining/demagnetize-prior-after-wedm-cutting-165978/. Last accessed 03rd Aug 2015. 2008.

156. Reference Manual. GF AgieCharmilles 205 971 120/en/11.10.2007. 2007.

157. Techknow. Magnetization and Demagnetization - TecHKnow Wiki. Available: http://www.techknow.org.uk/wiki/index.php?title=Magnetization_and_Demagnetization. Last accessed 03rd Aug 2015. 2010.

158. Cook RD, Malkus DS, Plesha ME, Witt RJ. Concepts and Applications of Finite Element Analysis. 4th ed. New York, NY: John Wiley & Sons; 2001. 736 p.

159. Hill MR, Lin W-Y. Residual Stress Measurement in a Ceramic-Metallic Graded Material. J Eng Mater Technol. 2002 Mar 26;124(2):185–91.

160. WolframMathWorld. Cubic Spline -- from Wolfram MathWorld. Available: http://mathworld.wolfram.com/CubicSpline.html. Last accessed 07 August 2015. 2000.

161. Bouchard PJ, Budden PJ, Withers PJ. Fourier basis for the engineering assessment of cracks in residual stress fields. Eng Fract Mech. 2012 Sep;91:37–50.

162. Kundu A, Bouchard PJ, Kumar S, Dey GK. Characterisation of Residual Stress in Electron Beam Welded P91 Plates by Neutron Diffraction. Int J Metall Eng. 2013;2(1):79–84.

163. Francis JA, Turski M, Withers PJ. Measured residual stress distributions for low and high heat input single weld beads deposited on to SA508 steel. Mater Sci Technol. 2009;25(3):325–34.

164. Dai H, Francis JA, Withers PJ. Prediction of residual stress distributions for single weld beads deposited on to SA508 steel including phase transformation effects. Mater Sci Technol. 2010;26(8):940–9.

165. Hossain S. Dissimilar metal weld -creep summary report. University of Bristol; 2014.

166. McCarthy J, Pei Z, Becker M, Atteridge D. FIB micromachined submicron thickness cantilevers for the study of thin film properties. Thin Solid Films. 2000 Jan 10;358(1):146–51.

167. Sabaté N, Vogel D, Keller J, Gollhardt A, Marcos J, Gràcia I, et al. FIB-based technique for stress characterization on thin films for reliability purposes. Microelectron Eng. 2007;84(5):1783–7.

168. Schaaf P, editor. Laser Processing of Materials. Berlin, Heidelberg: Springer Berlin Heidelberg; 2010. 231 p.

169. Janne Lämsä KM. Methods for Determination of Residual Stress of a Formed Plate Using Laser Ablation, Wire EDM and Milling. Key Eng Mater. 2011;473:368–75.

170. Waterjets.org. waterjets.org. Available: http://www.waterjets.org. Last accessed 07 August 2015. 2013.